Imperial College London

iTFM: Improved Travelling Fires Methodology for Structural Design and the Effects on Steel Framed Buildings

A thesis submitted in partial fulfilment of the
requirements for the degree of

Doctor of Philosophy

in

Mechanical Engineering

by

Egle Rackauskaite

2017

Supervised by Dr Guillermo Rein

Declaration of Originality

I declare that this thesis and the work described within have been completed solely by myself under the supervision of Dr Guillermo Rein. Where others have contributed or other sources are quoted, full references are given.

Egle Rackauskaite

2017

Copyright Declaration

The copyright of this thesis rests with Egle Rackauskaite and is made available under a Creative Commons Attribution Non-Commercial No Derivatives licence. Researchers are free to copy, distribute or transmit the thesis on the condition that they attribute it, that they do not use it for commercial purposes and that they do not alter, transform or build up on it. For any reuse or redistribution, researchers must make clear to others the licence terms of this work.

In memory of my grandmother,

Valerija

ABSTRACT

iTFM: Improved Travelling Fires Methodology for Structural Design and the Effects on Steel Framed Buildings

by

Egle Rackauskaite

Doctor of Philosophy in Mechanical Engineering

Imperial College London, 2017

Supervised by Dr Guillermo Rein

Accidental fire can be disastrous, especially in buildings. Most fire deaths occur due to the toxic effects of smoke before any structural collapse. However, the effect of fire on structural stability is critical in regard to safe evacuation and safe access for fire-fighters, financial losses, and lost business. This is particularly the case in tall buildings where extended evacuation times are required due to phased evacuation practises.

The understanding of fundamental mechanisms of whole building behaviour in fire has significantly increased over the last decades, in particular after the full-scale tests of various multi-storey buildings carried out in Cardington between 1994 and 1999. However, most of the current understanding and consequently the design codes are based on the assumption of uniform fire conditions in a compartment. While this assumption may be suitable for small enclosures, fires in large open-plan compartments have been observed to travel. Examples of such fires include the World Trade Centre Towers 1, 2 & 7 (2001), Windsor Tower fire in Madrid (2006) and the recent fire at the Plasco building in Tehran (Jan 2017). All of these buildings ultimately either partly of fully collapsed.

Current design standards do not account for travelling fires. The standard and parametric time-temperature curves are based on small scale tests, and assume uniform burning of fire and homogeneous temperature distributions in a compartment. In the recent years a new design concept of the Travelling Fires Methodology (TFM) has been developed by G. Rein to account for the travelling nature of fires in large compartments.

This design methodology considers non-uniform temperature distribution in the compartment and a wide range of burning floor areas. In this thesis the Travelling Fires Methodology is improved to account for more realistic fire dynamics and then applied to investigate the structural response of a multi-storey steel frame using finite element software LS-DYNA. This thesis is presented in a manuscript style: each chapter takes the form of an independent paper, which has been published or submitted to a journal for publication. A final chapter summarizes the conclusions, and suggests potential areas of future research.

Firstly, an improved Travelling Fires Methodology (iTFM) that accounts for better fire dynamics is presented in Chapter 2. Equations are introduced to reduce the range of possible fire sizes taking into account fire spread rates from real fires. The analytical equations used to represent the far-field temperatures are presented in continuous form. The concept of flame flapping is introduced to account for variation of temperatures in the near-field region due to natural fire oscillations. iTFM is then used to analyse the effect of non-uniform heating associated with travelling fires on the thermal response of structural members and identification of the location of peak temperature along the fire path. It is found to be mainly dependent on the fire spread rate and the heat release rate. Location of the peak temperature in the compartment is found to mostly occur towards the end of the fire path.

Full-scale testing of real structures is complex, expensive and time consuming. This is especially the case for structures with large compartments. There has only been a limited number of full-scale tests on real buildings carried out worldwide (e.g. Cardington tests). As a result, computational tools are commonly used to assess the structural response of complex buildings under fire conditions. However, they have to be validated first. Therefore, in Chapter 3, prior to the study of the effects of iTFM on the structural response, explicit solver of finite element software LS-DYNA used for the analyses in Chapters 4-7 is benchmarked for structural fire analyses against other static numerical codes and experiments. Four canonical problems that encompass a range of thermal and mechanical behaviours in fire are simulated. The parameter sensitivity study is carried out to study the effects of various numerical parameters on the convergence to quasi-static solutions. The results confirm that when numerical parameters are carefully considered not to induce excessive inertia forces in the system, explicit dynamic analysis using LS-DYNA provide good predictions of the key variables of structural response during fire.

Finally, the structural response of a two-dimensional multi-storey steel frame subjected to uniform design fires and iTFM (presented in Chapter 2) occurring on a single floor

and multiple floors is investigated in Chapters 4, 5, & 7, and Chapters 6 & 7, respectively. Fire type and the location of the fire floor in the frame are varied. The analyses and comparison of structural response mechanisms is presented in Chapter 4. Uniform fires are found to result in higher compressive axial forces in beams compared to small travelling fires. However, results show irregular oscillations in member utilization levels in the range of 2 - 38% for the smallest travelling fire sizes, which are not observed for the uniform fires. Beam mid-span deflections are similar for both travelling fires and uniform fires and depend mainly on the fire duration, but the locations in the frame where these displacements occur are found to be different. Chapter 5 extends the study presented in Chapter 4 and compares the results in the terms of the limiting temperature criteria and various structural limit states. Critical fire scenarios are found to occur on the upper floors of the frame where column sections reduce in size. Also, results show that depending on the fire scenario higher level of fire protection for different members within the frame may lead to either enhanced or worse structural response and/or resistance.

During previous fire events, e.g. the World Trade Centre Towers (WTC) 1, 2 & 7 in New York (2001), flames were observed to not only travel horizontally across the floor plate but also vertically to different floors. In this thesis, the effect of vertically travelling and multiple floor fires on the structural response of a two-dimensional multi-storey steel frame is investigated in Chapter 6. The number of fire floors, and horizontal and vertical fire spread are varied. Results show that the largest stresses develop in the fire floors adjacent to cool floors, and their behaviour is independent of the number of fire floors. All, the fire type, the number of fire floors, and the location of the fire floor, are found to have a significant effect on the failure time (i.e. exceeded element load carrying capacity) and the type of collapse mechanism (Chapter 7). In the cases with a low number of fire floors (1 to 3) failure is dominated by the loss of material strength, while in the cases with larger number of fire floors (5 to 10) failure is dominated by thermal expansion. Collapse is observed to be mainly initiated by the pull-in of external columns or swaying of the frame to the side of fire origin.

Analyses presented in Chapters 4 to 7 highlight that in the structural design for fires it is important to consider more realistic fire scenarios associated with travelling fires as they might trigger previously unnoticed structural mechanisms. Results on the multi-storey steel frame indicate that, depending on the structural metric examined, both travelling fires and uniform fires can be more severe than the other. A single worst case fire scenario under which a structure could be designed and deemed to be safe cannot be established. For different fire exposures failure is found to occur on different range

of floors subjected to fire. Therefore, in order to ensure a safe fire resistance design of buildings with large enclosures, a range of different fires including both travelling fires and uniform fires need to be considered.

ACKNOWLEDGEMENTS

TABLE OF CONTENTS

NOMENCLATURE

A	area (m^2)
c	specific heat (J/kg.K)
d	section depth or thickness (m)
E	Young's modulus (Pa)
f	flapping length (m) or frequency (Hz)
H	height of the compartment (m)
H_p	heated perimeter (m)
k	thermal conductivity (W/m.K) or beam integration refinement factor (-)
L	length of the compartment (m)
L^*	design fire size (-)
L_f	design length of the area involved in fire (m)
q_f	fuel load density (kJ/m^2)
$\dot{Q}$	total heat release rate (kW)
$\dot{Q}''$	heat release rate per unit area (kW/m^2)
r	radial distance away from the fire (m)
s	fire spread rate (m/s)
t	time (s)
t_b	local burning time (s)
t_{total}	total fire duration (s)
T	temperature (°K or °C)
W	width of the compartment (m)
x	location of interest in the compartment (m)
$\dot{x}$	location of the leading edge of the fire (m)

Greeks symbols

α	coefficient of thermal expansion (°C^{-1})
ε	emissivity (-) or strain (-)
θ	flapping angle (°)
ρ	density (kg/m^3)
σ	Stefan-Boltzmann constant (5.67×10^{-8} W/m^2.K^4)
σ_y	yield stress (Pa)
υ	Poisson's ratio (-)
Δt	time step (s)
ΔT	change in temperature (K or °C)

Superscripts

*	normalized

Subscripts

∞	ambient
c	cooling
f	fire or reduced near-field
ff	far-field
g	gas
h	heating
i	insulation
lim	limiting
max	maximum or gas
min	minimum
nf	near-field
pre	preload
s	steel
ss	steady-state
t	time dependent
u	ultimate

Abbreviations

1/2/3D	one/two/three-dimensional
B	beam
BM	benchmark
C	column
CDF	cumulative density function
EC	eurocode
ISO	standard fire
iTFM	improved travelling fires methodology
LC	long-cool
MRF	moment resistant frame
SH	short-hot
TFM	travelling fires methodology or travelling fire

Preface

In this thesis, Travelling Fires Methodology has been improved to account for better fire dynamics (Chapter 2), LS-DYNA has been validated for structural fire analysis (Chapter 3), and the thermal and structural response of the multi-storey steel frame subjected to a range of uniform and travelling fire scenarios has been studied (Chapters 4-7). Single storey (Chapters 4, 5, and 7), multiple storey and vertically travelling (Chapters 6 and 7) fire scenarios have been considered.

This thesis is written in manuscript format. As such each chapter is a standalone document suitable for journal publication. The material is presented as follows:

Chapter 2 presents an improved Travelling Fires Methodology (iTFM) that accounts for more realistic fire dynamics and range of fire sizes. iTFM is then used to analyse thermal gradients in simple steel and concrete structures. The chapter is based on:

> E. Rackauskaite, C. Hamel, A. Law, G. Rein (2015) *Improved Formulation of Travelling Fires and Application to Concrete and Steel Structures*, **Structures** 3:250-260.

Chapter 3 presents a benchmarking study of the explicit solver of LS-DYNA for structural fire analyses. The chapter is based on:

> E. Rackauskaite, P. Kotsovinos, G. Rein (2017) *Model Parameter Sensitivity and Benchmarking of the Explicit Dynamic Solver of LS-DYNA for Structural Analysis in Case of Fire*, **Fire Safety Journal** 90:123-138.

Chapter 4 analyses and compares the structural response of a multi-storey steel frame subjected to travelling fires and uniform fires. The chapter is based on:

> E. Rackauskaite, P. Kotsovinos, A. Jeffers, G. Rein (2017) *Structural Analysis of Multi-Storey Steel Frames Exposed to Travelling Fires and Traditional Design Fires*, **Engineering Structures**, (in press).

Chapter 5 assesses the limiting temperature criterion and investigates the effect of different fire exposures on various structural limit states. The chapter is based on:

> E. Rackauskaite, P. Kotsovinos, A. Jeffers, G. Rein (2017) *Computational Analysis of Thermal and Structural Failure Criteria of a Multi-Storey Steel Frame Exposed to Fires*, **Engineering Structures**, (submitted).

Chapter 6 investigates the structural response of a multi-storey steel frame subjected to horizontally and vertically travelling fires in multiple floors. The chapter is based on:

E. Rackauskaite, P. Kotsovinos, G. Rein (2017) *Structural Response of a Steel-Frame Building to Horizontal and Vertical Travelling Fires in Multiple Floors*, **Fire Safety Journal** (in press).

Chapter 7 extends the work presented in Chapters 4-6 and investigates the initiation of collapse mechanisms of a multi-storey steel frame subjected to a standard fire and horizontally and vertically travelling fires in multiple floors.

Other Publications

The following scholarly output has also been produced as a result of this research:

Conference and magazine papers

○ E. Rackauskaite, P. Kotsovinos, G. Rein, *Structural Response of a Steel-Frame Building to Horizontal and Vertical Travelling Fires in Multiple Floors*, **12th International Symposium on Fire Safety Science (IAFSS'17)**, Lund, Sweden, 12-16 June, 2017.

○ E. Rackauskaite, G. Rein (2016) *Structural fire design: travelling fires versus traditional design fires*, **SFPE Europe**, Issue 4.

○ E. Rackauskaite, P. Kotsovinos, A. Jeffers, G. Rein, *Structural Response of a Generic Steel Frame Exposed to Travelling Fires*, **9th International Conference on Structures in Fire (SiF'16)**, Princeton, USA, 8-10 June, 2016.

○ E. Rackauskaite, P. Kotsovinos, A. Jeffers, G. Rein, *Influence of the Design Fire Scenario on the Response of a 10-Storey Steel Frame: Travelling Fires and Eurocodes*, **11th Conference on Performance-Based Codes and Fire Safety Design Methods, SFPE**, Warsaw, Poland, 23-25 May, 2016.

○ E. Rackauskaite, C. Hamel, G. Rein, *Improved travelling fires methodology - iTFM*, **4th International Conference on Applications of Structural Fire Engineering (ASFE'15)**, Dubrovnik, Croatia, 15-16 October, 2015.

○ E. Rackauskaite, C. Hamel, A. Law, G. Rein, *Travelling fires in large enclosures for structural design: Improved methodology and fire sizes*, **The First International conference on Structural Safety under Fire & Blast**, Glasgow, Scotland, UK, 2-4 September, 2015.

Professional presentations

○ <u>E. Rackauskaite</u>, P. Kotsovinos, A. Jeffers,G. Rein, *Computational analysis of failure criteria of multi-storey steel frame exposed to fires: thermal vs. structural*, **Structures in Fire Forum**, London, England, UK, 11 April, 2017.

○ <u>E. Rackauskaite</u>, P. Kotsovinos, A. Jeffers, G. Rein, *Influence of the Design Fire Scenario on the Response of a 10-Storey Steel Frame: Travelling Fires and Eurocodes*, **SFPE UK CPD Seminar**, London, UK, 19 May 2016.

○ <u>E. Rackauskaite</u>, A. Law, G. Rein, *Closed-form formulation of travelling fires in large enclosures and comparison of the peak temperature location along concrete and steel beam*, **Concrete in Fire Forum**, Edinburgh, Scotland, UK, 18 September, 2014.

Posters

○ <u>E. Rackauskaite</u>, G. Rein, *iTFM: Improved Travelling Fires for the Structural Design of Modern Buildings*, **SET for BRITAIN**, London, UK, 7 March 2016.

Chapter 1

Introduction

1.1 Background

Accidental fire can be disastrous, especially in buildings. Most fire deaths occur due to the toxic effects of smoke before any structural collapse. However, the effect of fire on structural stability is critical in regard to safe evacuation and safe access for firefighters, financial losses, and lost business. This is particularly the case in tall buildings where extended evacuation times are required due to phased evacuation practises.

Understanding of the fundamental mechanisms of whole building behaviour in fire has significantly increased over the last decades, in particular after the full-scale tests of various multi-storey buildings carried out in Cardington between 1994 and 1999. However, current design codes invoke gas time-temperature curves which are based on small enclosure fires and assume uniform fire conditions in the compartments. While uniform fire assumption may be suitable for small enclosures, fires in real buildings with large open-plan compartments have been observed to travel across the floor plate and between different floors. Examples of such fires include the World Trade Centre Towers 1, 2 & 7 (2001), Windsor Tower fire in Madrid (2006) and the recent fire at the Plasco building in Tehran (Jan 2017). All of these buildings ultimately either partly of fully collapsed. Travelling fires result in highly non-uniform temperatures in the compartment and can last up to 20 h (One Meridian Plaza fire in Philadelphia (1991)).

Current design standards do not account for travelling fires. The standard and parametric time-temperature curves are based on small scale tests, and assume uniform burning of fire and homogeneous temperature distributions in a compartment. In the recent years, a new design concept of the Travelling Fires Methodology (TFM) has been developed by G. Rein to account for the travelling nature of fires in large compartments. This design methodology considers non-uniform temperature distribution in the compartment and a wide range of burning floor areas. However, for some compartments very small or large (i.e. a whole floor area) burning floor areas may be unlikely. In addition, the near-field temperatures considered in the methodology are independent of the burning floor area and relative fire size. Therefore, further improvements are needed to

account for more realistic fire dynamics and reduce the family of fires passed to structural analyses.

In the recent years, following the WTC fires in New York in 2001, thermal and structural response of various structures subjected to horizontally and vertically travelling fires has been investigated by many researchers. These studies concluded that consideration of more realistic fire exposure such as travelling fires is important for the structural response, and that a uniform fire assumption is not always the most conservative. However, for steel framed structures, the behaviour of the same structure under uniform and travelling fire exposures has not been considered yet and studies on vertically travelling fires have been limited to tall buildings with long span composite truss systems. Therefore, more research on steel frames is still needed to investigate the differences between the effects of uniform fires and more realistic horizontally and vertically travelling fire exposures and whether the same differences in structural responses are observed as in previous studies on different structures, and further research is needed.

Currently, there is no widely accepted single structural failure criterion to evaluate the performance of structures in fire. Traditionally, structural response and failure have been assessed in the terms of critical member temperature, maximum displacement or rate of deflection and exceeded member load-bearing capacity (i.e. collapse). The latter two criteria require a structural fire analysis using advanced computational methods (i.e. FEM) which can be computationally expensive. It is commonly believed that for regular steel framed buildings without any unusual characteristics structural fire design based on the critical temperature failure criterion is conservative. However, it is unclear of how representative such criterion is of the actual structural response, particularly in the case of non-uniform fires (e.g. travelling fires).

1.2   Aim and objectives

In this thesis, the Travelling Fires Methodology (TFM) is improved and applied to a generic multi-storey steel frame to investigate computationally the differences in the structural response of a frame subjected to travelling and uniform fires using finite element software LS-DYNA. More specifically, the objectives of the present thesis are to:

- Improve the travelling fires methodology (TFM) to account for better fire dynamics (Chapter 2).

- Benchmark the explicit dynamic solver of LS-DYNA for the structural fire analysis (Chapter 3).

- Compare computationally the structural response of a generic multi-storey steel frame subjected to uniform design fires and travelling fires (Chapters 4-7).

○ Investigate how the structural response of a multi-storey steel frame changes with fire occurring on different levels of the same building (Chapters 4, 5, and 7).

○ Investigate the response of a generic multi-storey steel frame subjected to horizontally and vertically travelling fires in a varying number of multiple fire floors (Chapters 6-7).

○ Assess the appropriateness of critical temperature as a failure criterion in comparison to various structural limit states for a multi-storey steel frame subjected to travelling fires (Chapter 5).

1.3 Outline of thesis chapters

Chapter 1 presents a brief discussion of the background to the research, and definition of its aims and objectives.

Chapter 2 presents an improved Travelling Fires Methodology (iTFM) that accounts for more realistic fire dynamics and range of fire sizes. The analytical equations used to represent the far-field temperatures are presented in continuous form. iTFM is then used to analyse thermal gradients in simple steel and concrete structures.

Chapter 3 presents a benchmarking study of the explicit solver of LS-DYNA for structural fire analyses against other static numerical codes and experiments. A parameter sensitivity study is carried out to study the effects of various numerical parameters on the convergence to quasi-static solutions. Four canonical problems that encompass a range of thermal and mechanical behaviours in fire are simulated.

Chapter 4 analyses and compares the structural response of a multi-storey steel frame subjected to travelling fires and uniform fires. The effect of fire occurring on different levels of the same building on the structural response is investigated.

Chapter 5 assesses the limiting temperature criterion and investigates the effect of different fire exposures on various structural limit states. Ultimate strain, member utilization, beam mid-span deflection, and critical member temperature failure criteria are considered.

Chapter 6 investigates the structural response of a multi-storey steel frame subjected to horizontally and vertically travelling fires in varying number of simultaneously heated fire floors. Additionally, this chapter investigates how the structural response of the frame changes with inter-floor time delay, upward and downward fire spread, and opposing fire spread on different floors.

Chapter 7 extends the work presented in Chapters 4-6 and investigates the initiation of collapse mechanisms of a multi-storey steel frame subjected to a standard fire and horizontally and vertically travelling fires in multiple floors.

Chapter 8 summarises the main conclusions from the work and outlines possible areas for further work.

Chapter 2

Improved Formulation of Travelling Fires and Application to Concrete and Steel Structures

Summary [1]

Current design codes and consequently most of the understanding of behaviour of structures in fire are based on the often unrealistic assumption of uniform fire within the enclosure. This assumption is especially wrong in the case of large open-plan compartments, where non-uniform travelling fires have been observed instead. An innovative concept called the Travelling Fires Methodology (TFM) has been developed to take into account this non-uniform fire behaviour. In this chapter, TFM has been improved to account for better fire dynamics. Equations are introduced to reduce the range of possible fire sizes taking into account fire spread rates from real fires. The analytical equations used to represent the far-field temperatures are presented in continuous form. The concept of flame flapping is introduced to account for variation of temperatures in the near-field region due to natural fire oscillations. These updated near-field temperatures cover a range of temperatures between 800 and 1200°C, depending on fire size and compartment characteristics. These incorporated changes are based on a fire model which can be used flexibly and adjusted to fit experimental data when it becomes available in the near future. Improved TFM is applied to generic concrete and steel compartments to study the effect of non-uniform heating associated with the travelling fires by investigating the location of the peak structural member temperature along the fire path. It is found to be mainly dependant on the fire spread rate and the heat release rate. Location of the peak member temperature in the compartment mostly occurs towards the end of the fire path.

2.1 Introduction

Accidental fire can be disastrous, especially in buildings. Most fire deaths occur due to the toxic effects of smoke before any structural collapse [1]. However, the effect of fire on structural stability is critical in regard to safe evacuation and safe access for fire fighters, financial losses, and lost business. This is particularly the case in tall buildings where extended evacuation times are required due to phased evacuation practises [2].

Innovative architectural designs of modern buildings already provide a challenge to structural engineers. This is above all the case in structural fire engineering [3, 4]. The understanding of fundamental mechanisms of whole building behaviour in fire has significantly increased in the last decades, especially after full-scale tests of various multi-storey buildings were carried out in Cardington between 1994 and 1999 [5, 6]. However, most of this understanding and current design codes are based on the assumption of uniform fires in a compartment. An extensive recent work [7, 8] has shown that while the uniform fire assumption may be suitable for small enclosures, fires in large, open-plan compartments, typical of modern architecture, do not cover the full area of compartment but rather travel from one part of it to another with non-uniform temperature distribution. These fires are referred to as travelling fires.

Current design standards (e.g. Eurocodes) do not account for such fires. The standard fire and parametric time-temperature curves are based on small scale tests (< 100 m^2 [9]), and assume uniform burning of fire and homogeneous temperature distributions in the compartment. In large accidental events, fires have been observed to travel across floor plates and between stories. Accidental events where fires were observed to travel include World Trade Centre Towers 1, 2 & 7 (2001); Windsor Tower fire in Madrid (2006); Faculty of Architecture building fire at TU Delft (2008); Interstate Bank fire in Los Angeles (1988); and One Meridian Plaza fire in Philadelphia (1991). In all of these accidents, the fires lasted for up to 7 or even 20 h (i.e. Windsor Tower and Meridian Plaza fires). Such long fire durations are not considered nor can be understood by current design codes. It has been shown in the WTC towers study by NIST [10, 11] that such prolonged periods of heating may result in even protected structural elements reaching temperatures in excess of 600°C. They also concluded that using average uniform gas temperatures rather than travelling fires would have led to significant errors in subsequent thermal and structural analysis of collapse of WTC Towers.

The need and urge of new design methods to incorporate realistic behaviour of fires in large open-plan offices has been recently highlighted [12]. Clifton [13] was the first person to introduce the approach for development of temperature-time relationships which would consider travelling fires. It was published as a part of HERA programme reports in New Zealand in 1996. Clifton defined each fire compartment as a firecell and produced a fire model for generation of gas temperature curves of ventilation controlled fires. Clifton's approach splits the compartment (firecell) into four distinct regions at any one time:

preheat, fire, burned out and smoke logged. Each of these regions has clearly defined characteristics for development of temperature-time curves at any location referred to as design area within a firecell. Ventilation depends on the glass breakage which is assumed to occur once adjacent gas temperatures reach 350°C. Due to the lack of available data from large scale experiments with such fires, a high number of crude assumptions developing this method had to be made [7, 13]. Therefore, it was stated by Clifton [13] that it should not be used for complicated designs as a lot of further improvements and scientific validations are still necessary. However, the model has not been developed or used further.

Recently, an extensive work has been done by Stern-Gottfried, Law and Rein [7, 8, 14, 15] who have developed a new design concept of travelling fires methodology (TFM). It considers non-uniform temperature distributions along the compartment and a wide range of fire sizes (burning floor area). The concept has already been applied by engineering consultant, Arup. In the published work [16, 17] on Arup's approach, the limitations of only using prescriptive codes for the design have been identified. Travelling fires were accounted in probabilistic analysis to identify the most severe fire scenario in regard to fire resistance periods. New Ludgate, a 10 storey office development in the City of London, was described as a case study in [16]. In order to determine the optimum structural fire protection specification in accordance with Part B of the UK Building Regulations, the structural fire performance was expressed in the terms of reliability according to Kirby et al. [18]. Thus, a probabilistic Monte Carlo analysis was carried out by varying the types of fires that are likely to occur (i.e. uniform and travelling fires) and the corresponding key parameters. These parameters include fuel load, heat release rate and fire size, etc. The resultant structural reliability was combined with sprinkler reliability to find the corresponding required fire resistance period based on steel temperature. Use of travelling fires in addition to uniform fires in a building design as in the above approach allows a better understanding of the overall building performance subject to a range of conditions.

The focus of this chapter is the improvement of the TFM to account for better fire dynamics, smaller range of fire sizes, and the analysis of the effect of non-uniform heating associated with travelling fires on the temperatures of structural members. The proposed changes represent a simple yet powerful fire model which can be used flexibly and adjusted to fit experimental data when it becomes available in the near future.

2.2   Travelling Fires Methodology

The Travelling Fires Methodology (TFM) was developed by Stern-Gottfried, Law, and Rein [7, 8, 14]. This framework incorporates the effect of non-uniform fires in large open-plan spaces. It does not supersede traditional design methods, but can be used in addition to them, and investigates a range of possible fire dynamics instead of just one or two design fires.

TFM provides an approach for generation of gas (i.e. hot smoke and flames) temperature-time curves at the ceiling of a medium height compartment at any location in the compartment. Ceiling is the target because this is where maximum temperatures are expected. TFM considers design fires to be composed of two moving regions: the near-field (flames) and the far-field (smoke). Illustration of the two fields is shown in Fig. 2.1 The near-field represents the flames directly impinging on the ceiling and assumes the peak flame temperatures. The far-field model represents smoke temperatures which decrease with distance away from the fire due to mixing with air. Any structural element will experience cooler far-field temperatures which correspond to pre-heating and/or cooling for much longer duration than the short hotter near-field. Test data from the St. Lawrence Burns large compartment tests conducted in 1958 support travelling fire behaviour as in TFM framework [19, 20].

Figure 2.1: Illustration of a travelling fire and distribution of gas temperatures.

Early work by Rein et al. [15] employed computational fluid dynamics to generate temperature fields. Later it was simplified for a single floor in order to pass less information to consequent structural analysis but still provide realistic results. It used ceiling jet correlation to describe the temperature field. The methodology was then extended and various parameter sensitivity analyses carried out by investigating the structural behaviour of a general concrete frame [8]. In this chapter the thermal descriptions of near-field and far-field temperatures used in TFM and the possible range of valid fire sizes are reduced. Also, the thermal response to travelling fires of two structurally equivalent steel and concrete beams is studied. For clarity, previous version [8] of travelling fires methodology is referred to as TFM and the travelling fires methodology with improved formulations presented in this chapter is referred to as iTFM.

2.3 Improved Travelling Fires Methodology - iTFM

2.3.1 Valid range of fire sizes

TFM is flexible in a way that it is not limited to one fire type. It covers a wide range of fire sizes - a family of possible fires depending on the fire coverage of the total floor area from 1% to 100%. The latter represents the whole compartment under uniform fire. In Eurocode 1 Part 1-2 consideration is given to only two different fire sizes: a whole compartment fire (100%), and a static localised fire up to 10 m in diameter. TFM assumes uniform fuel load distribution along the fire path and constant fire spread rate. Therefore, the total fire duration depends on the fire size. For example, for a floor area of 960 m^2, the fire size can range from 38 min for 100% fire size, to 1919 min for 1% (or even longer depending on compartment and fuel load characteristics). Thus, unlike traditional design methods, TFM can explain and takes into account the long fire durations observed in accidental fires.

However, it is unlikely that a very thin line fire (e.g. 1%) across the whole width of the compartment would spread, or that a whole floor (e.g. 2500 m^2) would be involved at once in fire in large compartments. This is due to limitations such as available fuel load, fire spread rate, and burning rate. The aim in this chapter is to provide a better representation of physically possible fire sizes which were not limited in the previous versions of TFM.

In TFM a fire is assumed to be fuel controlled. It was identified in the previous work [7, 8] that ventilation controlled fires are unlikely in large enclosures. Therefore, fuel load density, q_f (kJ/m^2), and heat release rate per unit area, $\dot{Q}''$ (kW/m^2), are used as main design variables. A range of possible values for these parameters for different building occupancies can be found in the Eurocode [21]. Based on these values a local burning time, t_b (s), is calculated (e.g. 1140 s or 19 min) using Eq. (2.1). This variable quantifies the time needed for an area involved in fire to burn out completely.

$$t_b = q_f/\dot{Q}'' \tag{2.1}$$

The front of a travelling fire is referred to as the leading edge (see Fig. 2.1). It depends on a fire spread rate. If the range of the realistic fire spread rates is known it can be used to compute the limiting sizes of possible fires. This can be done by finding the distance that the leading edge of the fire would travel before burning out at the ignition point as in Eq. (2.2) below:

$$L_{f,min/max} = s_{min/max} \cdot t_b \tag{2.2}$$

where $L_{f,min/max}$ is the minimum or maximum possible fire size in terms of length along the fire path (m); and $s_{min/max}$ is the minimum or maximum realistic fire spread rate in building fires (m/s). Available data on typical compartment fire spread rates is very limited. Thus, estimates were made based on the details provided in a number of fire

tests and real building fire investigation reports where the fires have been observed to travel [11, 19, 20, 22–26]. A summary of the reported fire spread rates and estimated values is shown in Table 2.1.

Table 2.1: Realistic fire spread rates, s, based on data from experiments and real fires.

Reference	Details	Spread rates (mm/s)
[23]	Wood cribs in the open	0.1 - 2
[24]	Lateral or downward spread on thick solids	1
[25]	Tests on natural fires in large scale compartments	1.5 - 19.3
[11]	Reconstruction of WTC fires (2001)	2.5 - 16.7
[19, 20]	St. Lawrence Burns tests (1958)	7.5 - 13
[22, 26]	First Interstate Bank Fire (1988)	14.5

From the limited data it can be seen that fire spread rates in the open for wood cribs (a typical fuel source used for fire tests) and in compartments typically vary between 0.1 and 19.3 mm/s. These values are suggested as minimum and maximum fire spread rates for determination of a valid range of fire sizes. Clifton [13] assumed the values of 8.3 and 16.6 mm/s for slow and fast fire spread respectively based on the results from the tests on natural fires in large scale compartments [25] and a rate of fire spread between different workstations of 200 s given by [27]. These values agree well with the suggested range for the iTFM. Based on the limitations from realistic fire spread rates, valid range of fire sizes can be described as below:

$$from \ \frac{L_{f,min}}{L} \ to \ \frac{L_{f,max}}{L}$$

As experimental evidence becomes available (presently not available), the range of possible fire spread rates in compartments can be updated as appropriate. The valid range of fire sizes is necessary to reduce the family of fires passed to structural analysis, reduce computational time, and neglect unrealistic results.

2.3.2 Far-field - the analytical solution

In TFM the far-field model represents cooler smoke temperatures which decrease with distance away from the fire. TFM is flexible in stating that any available temperature-distance correlation could be used to describe the far-field temperature depending on the accuracy required. Alpert's ceiling jet correlation [28], which is based on a set of experiments created for sprinkler design, is used in TFM to represent the far-field temperatures. It is shown in Eq. (2.3).

$$T_{max} - T_\infty = 5.38 \frac{(\dot{Q}/r)^{2/3}}{H} \tag{2.3}$$

where T_{max} is the hot gas temperature near the ceiling (°C); T_∞ is the ambient temperature (°C); $\dot{Q}$ is the total heat release rate (kW); r is the radial distance away from the fire (m); and H is the ceiling height (m).

The first version of TFM used a single far-field temperature [15] and then to incorporate radiative heat transfer the 4th power average was used [14]. In the last version [8], TFM assumes the compartment to be divided into discrete nodes and uses gas temperatures that vary with distance from fire. The use of compartment floor discretization adds unnecessary complexity to the problem. Moreover, in a parameter sensitivity study [8], errors of up to 12.7% and 20% were found for peak rebar bay temperatures and total burning durations respectively, depending on the grid size chosen.

Recently, a few new methods for calculation of ceiling-jet temperatures have been proposed based on computational simulations [29, 30]. Suzuki [29] created a new model by expanding Alpert's theory [31] to include terms that account for time considerations and the heat transfer to the ceiling. The resultant temperatures showed no significant differences from Alpert's correlation [28] and were slightly lower than the values predicted by Heskestad [32]. In [29] comparisons were also made to a full-scale experiment in an office building and calculated values were found to be lower by 10-25% in some cases. Suzuki [29] concluded that this may be due to the presence of a side wall which was not included in the model. In the recent work by Johansson et al. [30], 90 computational simulations were performed to study ceiling-jet temperatures. The resultant average ceiling jet temperatures compared well with Alpert's ceiling jet correlation [28]. However, this was not the case for recorded maximum temperatures and a new correlation was developed.

Both of the models identified previously require additional variables in comparison to simpler Alpert's correlation for the calculation of ceiling jet temperatures. However, taking into account the additional complexity, computational time required and uncertainty in the parameters associated with these two methods, the differences in resultant temperatures are negligible. Thus, for the reasons of simplicity, the far-field model in iTFM continuous to be based on Alpert's correlation [28]. iTFM has been improved by developing the analytical expression for the far-field temperatures, thus removing the errors that were imposed using the discrete method. The proposed equations can be used to rapidly calculate temperature variations at any time and location along the structural member in the compartment.

TFM assumes a uniform fuel load across the fire path (q_f) and constant heat release rate ($\dot{Q}''$). Also, the fire is defined by a specified surface area of burning fuel, A_f (m²), at any fixed time. Considering this, the total heat release rate can be calculated by the following equation:

$$\dot{Q} = A_f \cdot \dot{Q}'' \tag{2.4}$$

To consider fire growth and decay and to represent varying fire size at the beginning and

end of the fire, respectively, the following equation can be used:

$$A_f = L \cdot L_t^* \cdot W \tag{2.5}$$

where L_t^* is the varying dimensionless fire size which depends on the location of the leading edge of the fire $\dot{x}$; L is the length of the compartment (m); and W is the width of the compartment (m). Dimensionless design fire size L^*, fire spread rate s (m/s), total fire duration t_{total} (s), and location of the leading edge of the fire relative to the end of the compartment where the fire started $\dot{x}$ (m) can be calculated as follows:

$$L^* = L_f/L \tag{2.6}$$

$$s = L_f/t_b \tag{2.7}$$

$$t_{total} = t_b(1/L^* + 1) \tag{2.8}$$

$$\dot{x} = s \cdot t \tag{2.9}$$

where L_f (m) is the design length of the area involved in fire and t (s) is time.

Combining Eqs. (2.3-2.9) results in a correlation for near-field and far-field gas temperatures near the ceiling, T_{max}, at any location x (m) along the fire path and time t (s) of interest:

$$T_{max}(x, t) = T_\infty + \frac{5.38}{H}\left(\frac{LL_t^* W \dot{Q}^*}{|x + 0.5LL_t^* - \dot{x}_t|}\right)^{2/3} \tag{2.10}$$

$$T_{max}(x, t) = T_{nf}, \ \ if \begin{cases} T_{max}(x, t) > T_{nf}; \\ |x + 0.5LL_t^* - \dot{x}_t| \le 0.5LL_t^*. \end{cases} \tag{2.11}$$

$$for \ \dot{x} \le L \ \rightarrow \ \dot{x}_t = s \cdot t; \ \ L_t^* = min[L^*, (s \cdot t)/L] \tag{2.12}$$

$$\dot{x} > L \ \rightarrow \ \dot{x}_t = L \ ; \ \ L_t^* = 1 + (L_f - s \cdot t)/L \tag{2.13}$$

where $\dot{x}_t$ is the time dependent location of the leading edge of the fire relative to the end of the compartment where the fire started (m); and T_{nf} is the near-field temperature (°C).

Conditions described by Eq. (2.11) represent the near-field temperature. It implies that gas temperatures (i.e. far-field) described by Eq. (2.10) cannot exceed the near-field flame temperature. It also sets the near-field temperature value for the whole length of the area involved in fire (LL_t^*). Eqs. (2.12) and (2.13) are used to define varying fire size

and location of the leading edge based on whether fire is still increasing in size or is at its maximum size (Eq. (2.12)) or has reached the far end of the compartment and is decaying (Eq. (2.13)). Illustrative examples of resulting gas temperature surroundings experienced by structural members at two different locations within a typical compartment are shown in Fig. 2.2. It should be noted that further improvements to the methodology are needed to account for more realistic conditions during the growth and decay of the fire, i.e. eliminate instantaneous heating to very high temperatures at the fire origin and instantaneous cooling to ambient temperature at the end of fire exposure, respectively.
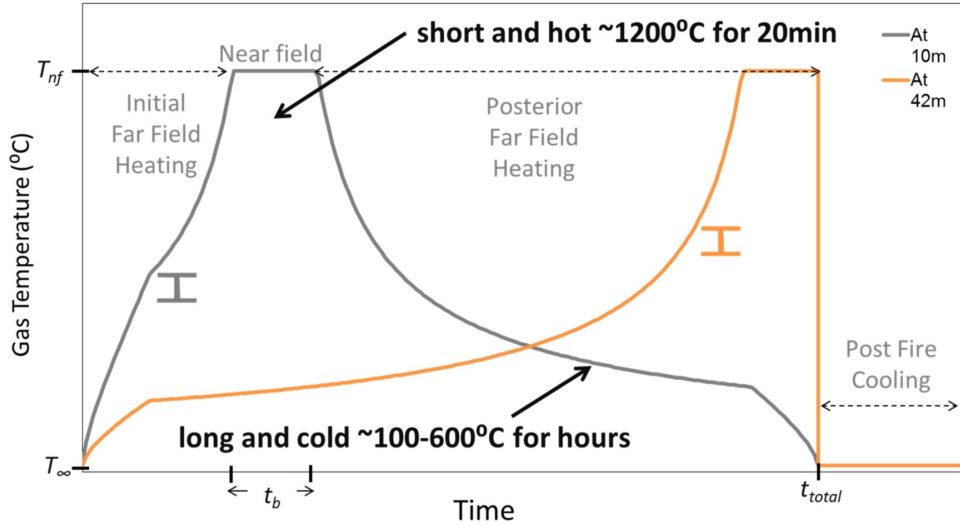
Figure 2.2: Near-field and far-field exposure duration at an arbitrary location and at the far end of the compartment [8].

2.3.3 Near-field - flame flapping

In TFM the near-field represents the flames directly impinging on the ceiling and assumes the peak flame temperatures. Such temperatures in various building fires and experiments have been measured in the range of 800-1200°C [33–36]. To stay on the conservative side TFM described in [8, 14, 15] assumed the near-field temperature to be 1200°C.

In reality, due to natural lateral fluctuations of the flames on the ceiling, gas temperatures are typically continuously varying between the observed temperatures of 800 and 1200°C [24, 37, 38]. In iTFM this is included and referred to as flame flapping. For this reason, structural members will actually experience lower average gas temperatures rather than the peak flame temperatures observed in fires. There is no experimental evidence from large compartment fires or correlations based on which this reduced near-field temperature could be related to either fire size or oscillations. In previous work of TFM [8, 14] this was indirectly taken into account by calculating the average bay temperatures for structural members. However, this assumption and its implications were

not studied. In order to apply reduced near-field temperatures due to flapping for iTFM, the concept of the flapping angle is introduced. The angle from the main axis of the flame (θ), as shown in Fig. 2.3, is chosen to represent the length on the ceiling over which fluctuations of the impinging flame occur.
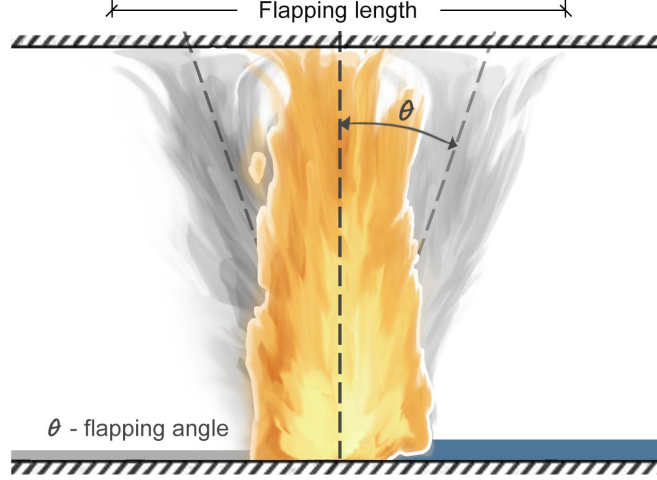
Figure 2.3: Representation of the flapping length (f) on the ceiling and angle (θ).

The review of available data on flapping angles is discussed in Appendix 2.A. For iTFM the flapping angle of $\pm 6.5°$ was chosen based on results from Quintiere et. al [39] experiments (see Appendix 2.A). The flapping angle is used to calculate the ceiling length over which the impinging fire fluctuations occur. The average temperature over this length (f) is calculated accounting for both far-field and peak near-field temperatures (set at 1200°C). This represents the mixing of cooler smoke with the fluctuating flame, resulting in a lower near-field temperature. This reduced near-field temperature is used to generate travelling fire time-temperature curves instead of a fixed peak value of 1200°C. The equation used to calculate the reduced near-field temperature due to flapping, T_f (°C), is shown below and is derived from Alpert's ceiling jet correlation. For derivation see Appendix B.

$$T_f = T_\infty + \frac{T_{nf}(2r_{x1} + L_f) - 2T_\infty \cdot r_{x2}}{f} + \frac{32.28\dot{Q}^{2/3}}{H \cdot f}\left(r_2^{1/3} - r_{x2}^{1/3}\right) \tag{2.14}$$

where,

$$r_2 = f/2 \tag{2.15}$$

$$r_{x1} = max[0, r_0 - L_f/2] \tag{2.16}$$

$$r_{x2} = max[L_f/2, r_0] \tag{2.17}$$

$$T_{nf} = 1200°C \tag{2.18}$$

$$r_0 = \dot{Q}\left(\frac{5.38}{H(T_{nf} - T_\infty)}\right)^{3/2} \tag{2.19}$$

Variation of reduced near-field temperatures with flapping angle for different fire sizes is shown in Fig. 2.4. It can be seen that with increasing flapping angle the resulting temperature for each fire size decreases. This could be expected as a larger flapping length incorporates a greater amount of smoke in comparison to direct flame impingement. Thus, due to the mixing of these two fields, the resulting gas temperatures are lower. Fig. 2.4 also shows that the effect of flapping angle is only important for smaller fire sizes ($< 12\%$) as these are more susceptible to the flapping disturbances. Also, flapping leads to reduced near-field temperatures in the range of 800-1200°C [33–36], in agreement with observed temperatures in real fires. All of this considered, this is still a crude approximation and more research on peak flame temperatures in relation to fire size in large enclosures is necessary.
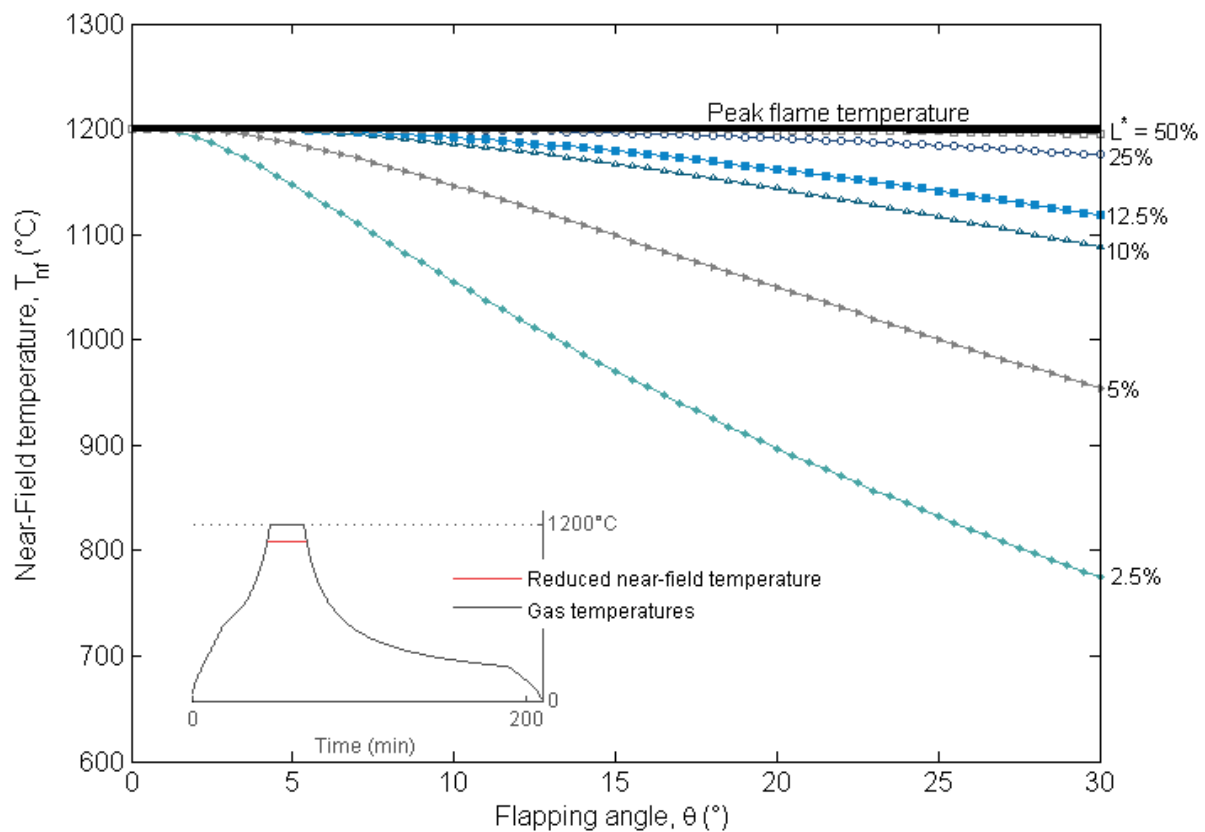
Figure 2.4: Variation of reduced near-field temperature with flapping angle and fire size.

2.4 Case Study

To investigate the impact of iTFM on resulting temperatures within structural members, it was applied to the steel and concrete frames. A given floor was assumed to be

24 m wide, 40 m long and 3.6 m high as for a typical office building. It was divided into 5 spans along the compartment length, each 8 m long. Simply supported steel and concrete beams were designed in accordance with Eurocode 3 [40] and Eurocode 2 [41], respectively, for the same factored uniformly distributed load of 56.4 kN/m. Thus, the two sections can be considered as structurally equivalent. Each of the sections was also designed for 60 min and 120 min of standard fire resistance (typical resistance requirements for office buildings). Steel insulation properties were taken as for high density perlite (thermal conductivity $k_i = 0.12$ W/m.K, density $\rho_i = 550$ kg/m^3 and specific heat $c_i = 1200$ J/kg.K) [3]. These properties were assumed to stay constant with temperature for the reasons of simplicity and lack of experimental data for fire exposures similar to travelling fires with long pre-heating durations. The details of the designed sections are shown in Table 2.2 and Fig. 2.5.

Table 2.2: Details of the steel and concrete sections used for the case study.

	Steel beam	**Concrete beam**
Fire resistance	457×191 UB133	500×300
	Steel protection thickness (m)	Rebar cover (m)
60 min	0.007	0.038
120 min	0.018	0.042
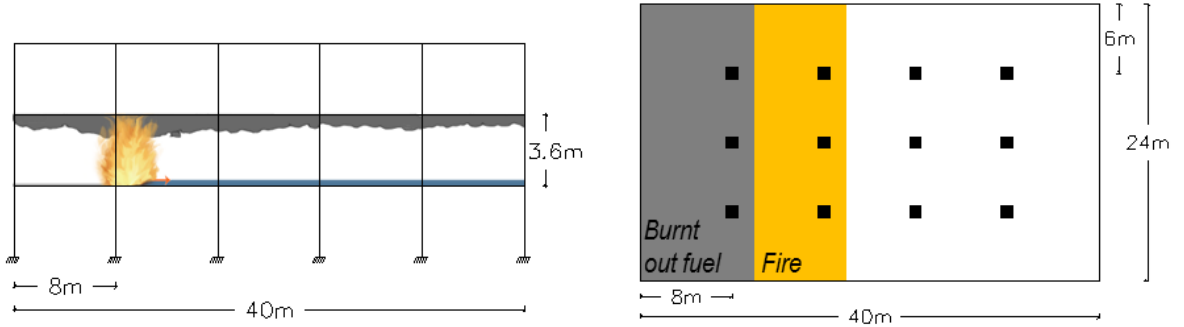
Figure 2.5: Elevation and floor plan building use for the case study.

Heat release rate per unit area and fuel load density were assumed to be 500 kW/m^2 and 570 MJ/m^2, respectively [8]. A base case flapping angle of 6.5° was chosen. Time-temperature gas curves obtained from iTFM were used as an input for a heat transfer analysis to heated beams. All heat transfer calculations were carried out as in [8] (See Appendix 2.C). Lumped mass heat transfer method [3] was used to calculate resulting steel beam temperatures. The convective heat transfer coefficient, density of steel and radiative emissivity were assumed to be 35 W/m^2.K (as for natural fire models [21]), 7850 kg/m^3 [42] and 0.7 [8], respectively. Temperature dependent specific heat of steel was taken from [3]. In-depth concrete temperatures were calculated using explicit

one-dimensional finite difference model for heat conduction. Radiation and convection were taken into account for the boundary conditions. The density of concrete of 2300 kg/m^3 [3, 43], the specific heat of concrete of 1000 J/kg.K [3], convective heat transfer coefficient for the exposed surface of 35 W/m^2.K (as for natural fire models [21]), convective heat transfer coefficient for the backside surface of 4 W/m.K [21], thermal conductivity of concrete of 1.3 W/m.K [3] and a radiative emissivity of 0.7 [8] were assumed. Steel has a much higher thermal conductivity coefficient than concrete. Thus, steel rebar was assumed to have the same temperature as adjacent concrete. Concrete material properties are conservatively assumed to be temperature independent. In the parameter sensitivity study on concrete temperatures exposed to TFM Stern-Gottfried et al. [8] have found that final concrete temperatures are most sensitive to building and fire scenario related parameters (e.g. rebar depth, fuel load, fire size, etc.) than to physical parameters (convective heat transfer coefficient, radiative emissivity, etc.). For investigated parameter ranges concrete temperature sensitivity was in the ranges of -30% to +45% and -10% to +5%, respectively. Time steps used for heat transfer calculations satisfying the stability criteria were 10 s [3, 8] and 1.9 s [8, 44] for steel and concrete, respectively. An in-depth concrete grid size of 0.002 m, which meets stability criteria [8, 44], was chosen.

2.4.1 Valid range of fire sizes

As identified in Section 2.3.1, limiting fire sizes for the case study have been calculated based on the fire spread rates. The resultant values are shown in Table 2.3.

Table 2.3: Valid range of fire sizes for the case study.

Limitation	Minimum fire length $L_{f,min}$ (m)	Maximum fire length $L_{f,max}$ (m)
Spread rates (0.1 - 19.3 mm/s)	0.11 (0.3%)	22.00 (55%)

Valid fire sizes are in the range between 0.3% and 55%. This leads to elimination of half of the fire sizes ranges used in previous TFM, thus reducing required analysis times. This also indicates, as mentioned previously, that very small fire sizes (i.e. thin fires) and well-ventilated fires covering a whole floor area are unlikely to occur in large compartments unless a lower heat release rate is assumed. From Fig. 2.6, it can be clearly seen that lower heat release rates result in larger fire sizes as a result of longer local burning durations. Minimum fire sizes are unrealistically low and almost constant for all fuel load densities as it is based on very small spread rates from wood crib fires. This also indicates that much research on flame spread rates is still needed in order to gain a better understanding of fire dynamics and optimise fire curves for structural design further.
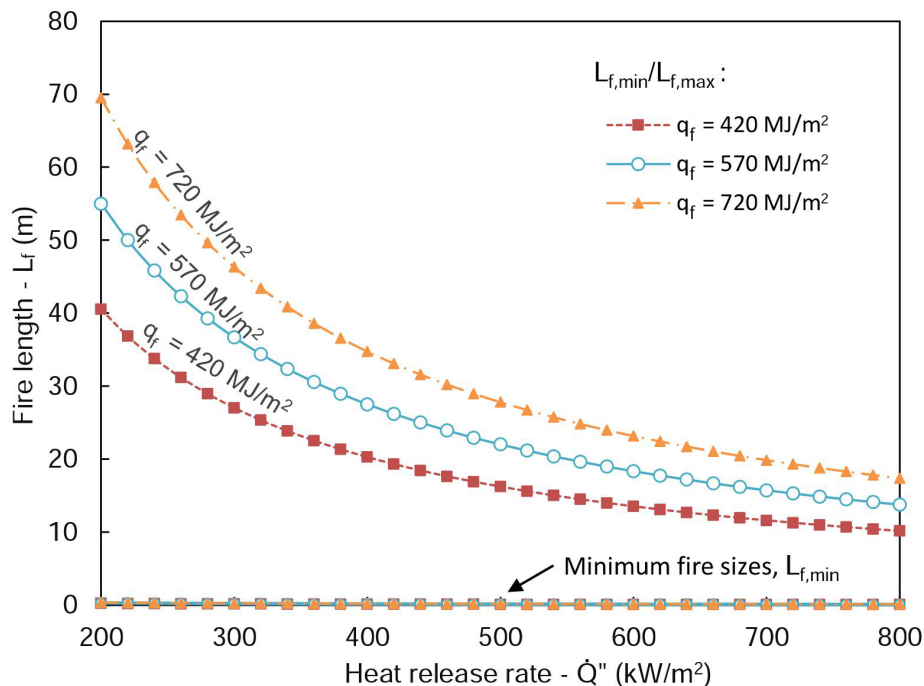
Figure 2.6: Valid range of fire sizes for varying heat release rates and fuel load densities.

2.4.2 Flapping angle

In previous TFM studies [8, 14] it was identified that the fire sizes between 5 and 20% result in the highest peak member temperatures. The influence of the varying flapping angles defined in Section 2.3.3 on the peak steel and concrete temperatures with increasing fire size can be seen in Fig. 2.7. Clearly, the highest peak temperatures at the smallest fire sizes dissipate with increasing flapping angle (i.e. decreasing near-field temperature). It indicates that the effect of fire spread rate is less dominant at lower near-field temperatures due to a smaller heat flux. Also, flapping influence diminishes with fire sizes larger than 20%, 25% and 30% for 120 min protected steel beam, 60 min protected steel beam, and concrete and unprotected steel beams, respectively. The thermal protection of structural members results in the delayed heating. Thus, the thicker the protection, the narrower the range of fire sizes which result in highest peak member temperatures.

Due to lower thermal conductivity, the resultant peak temperatures in concrete rebar are approximately 600°C lower than in unprotected steel beam. In this case concrete rebar peak temperatures are between the limits of peak temperatures in 60 min protected and 120 min protected steel beam. For the same reason the thickness of concrete cover has little influence. For 60 min and 120 min fire protection, the difference in concrete rebar temperatures is approximately 40°C while for steel beams it is up to 250°C. On the other hand, variations in flapping angle have a similar influence on both steel and concrete temperatures, which can cause variations up to 200°C. However, structural analysis has
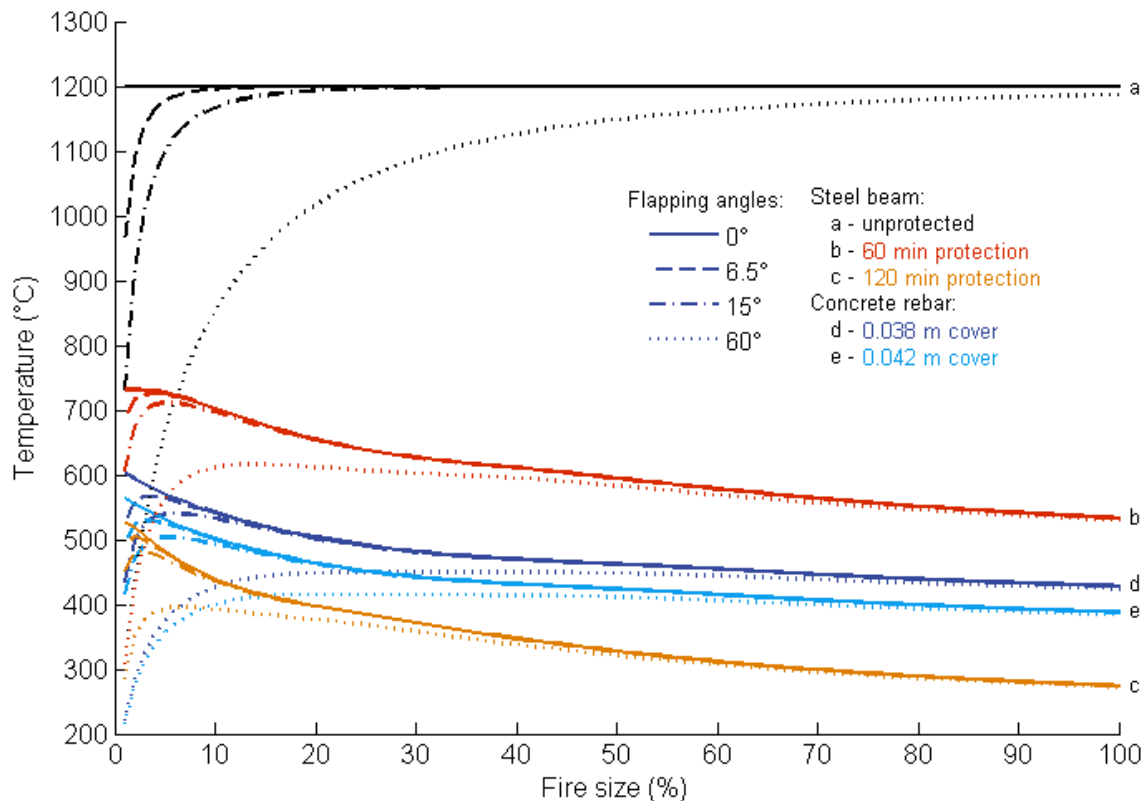
Figure 2.7: Influence of flapping angle on variation of peak steel and concrete temperatures with fire size.

to be carried out in order to make a valid comparison of steel and concrete beam structural resistance in fire.

2.4.3 Location of peak member temperature in the compartment

Overall structure performance in a real fire depends on a number of factors. They include temperature rise, loading, restraint, composite action effects, and continuity within the structure [45]. In this section the location of the peak temperature of structural members in the compartment as a result of iTFM is studied. This is to give an insight of how non-uniform heating associated with a spreading fire would affect the resultant structural member temperatures. The general conclusions drawn herein may be important for the identification of critical structural members within the structure.

Location of the peak temperature within steel beam in the compartment was investigated by varying various iTFM parameters. They include the length of the compartment L, thickness of fire protection, heat release rate per unit area $\dot{Q}''$, fuel load density q_f, and flapping angle θ. Variation of peak temperatures along the fire path in the compartment is shown in Fig. 2.8. These temperatures represent the highest temperatures reached in different locations during the fire. They do not represent temperature distribution occurring at the same time during the fire in the compartment. Variation of peak tem-

perature in the compartment and its location with fire size for steel and concrete beams is shown in Fig. 2.9. The location of peak temperature x^* is represented as the ratio of the distance along the fire path from the origin of the fire to the total length of the fire path as in Eq. (2.20).

$$x^* = x/L \tag{2.20}$$
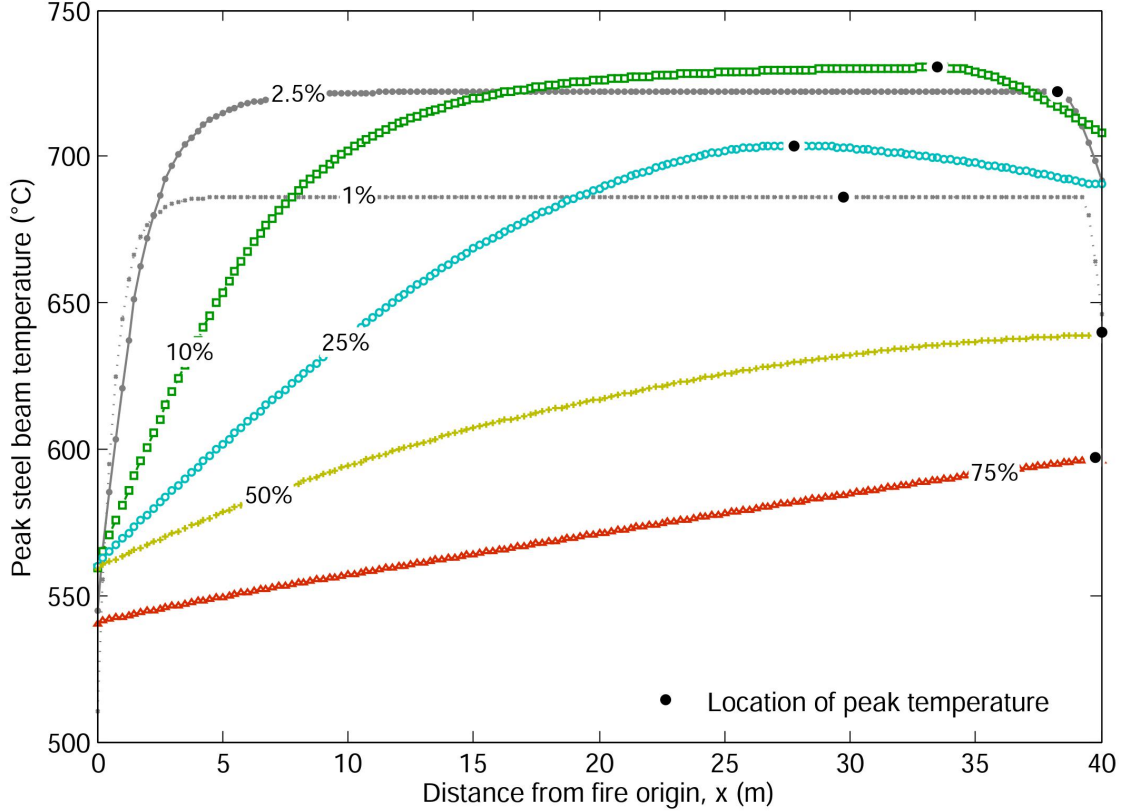
Figure 2.8: Peak 60 min protected steel beam temperatures along the fire path for different fire sizes. Highlighted points on the curves indicate the location of the peak temperature.

The highest peak temperature differences along the fire path are found for fire sizes larger than 10%. Figure 2.8 shows that for smaller fire sizes, temperature variations across the length are minimal, except for the compartment ends where fire growth and extinction are assumed to occur. The reasons for low variability in peak temperatures along the compartment for small fires are slow fire spread rate and resultant long pre-heating periods. The exposure to high gas temperatures for small fires is long enough for steel to reach similar high peak temperatures everywhere. On the other hand, in the case of larger fires ($> 10\%$) fire spread rate is much faster. Therefore, structural elements close to fire origin experience pre-heating only for a very short duration. This duration is not long enough for structural elements to heat up to peak temperatures as at the far
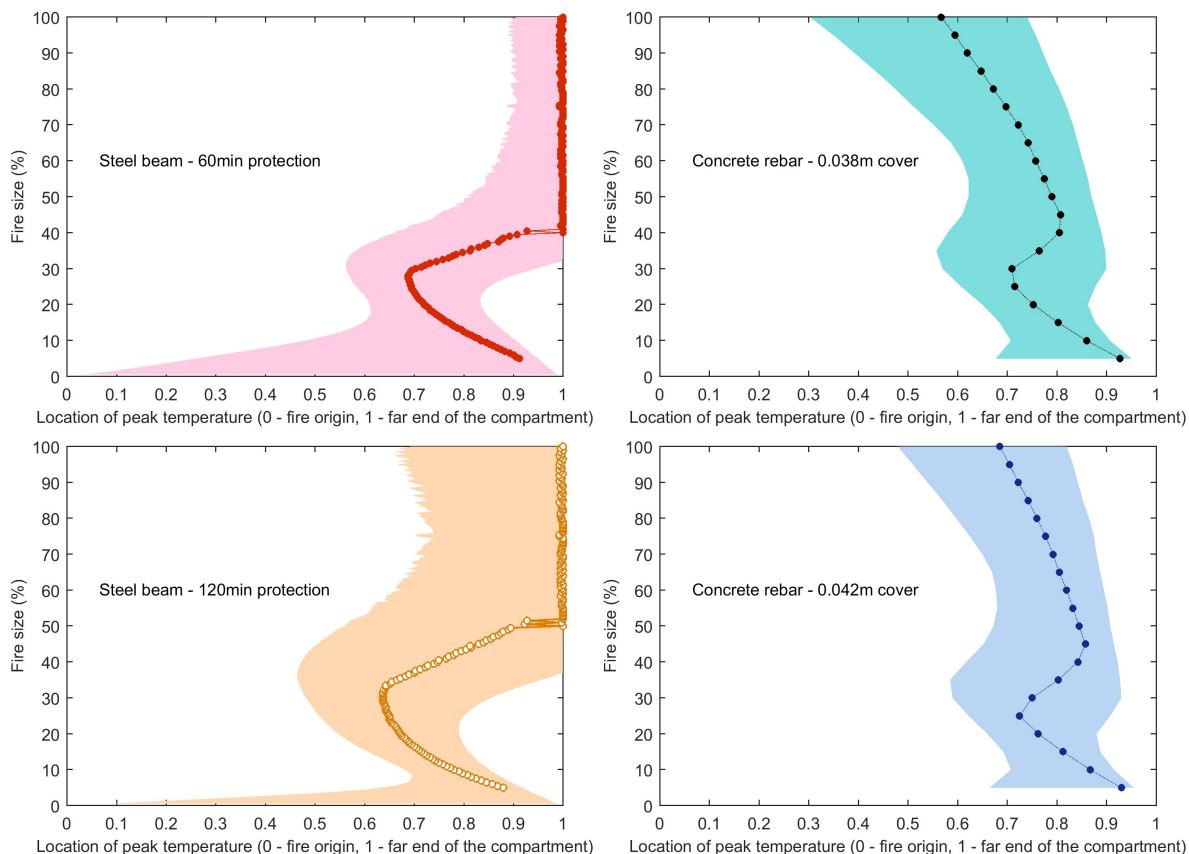
Figure 2.9: The peak steel and concrete rebar temperatures and their location in the compartment from the fire origin (a ratio to the full fire length) for various fire sizes; Shaded region displays locations of maximum temperature within 5°C difference from the peak temperature.

end. Thus, variation of peak steel temperatures along the compartment is in the range of 60-170°C.

It can be seen from both Figs. 2.8 and 2.9 that for all fire sizes the peak steel and concrete temperatures occur at the locations further than x^* - 0.6 from the fire origin. For very small fire sizes ($< 2\%$) a sudden increase of distance from fire origin with fire size can be seen. As identified previously, for such small fires the peak temperatures vary little. This can be seen from the 5°C variation from the peak temperature shaded region. Thus, high variation in location of peak temperatures can be neglected.

For larger fires, with increasing fire sizes the distance of location of peak temperatures from the fire origin in both steel and concrete members is decreasing up to fire sizes of 25-33%. It represents the location slightly further than where the fire size starts to decrease. The reason for that is that members up to that location are exposed to the same far-field temperatures for increasing durations. However, as the fire starts to decay the members at the far end of the compartment are exposed to peak near-field temperatures for shorter durations as well as lower far-field temperatures during cooling. Thus, the

resulting temperatures are lower at the end and peak temperature occurs at the location close to where fire decay begins.

On the other hand, fires larger than approximately 25% are large enough to produce high smoke temperatures above the temperatures of the beams. Thus, the temperatures at the far end of the compartment keep on significantly increasing even during the decay phase. In addition to that, steel temperatures for larger fires are lower than for smaller fire sizes due to faster fire spread rates (see Fig. 2.8) and are exposed to shorter cooling durations. Therefore, as seen in Figs. 2.8 and 2.9, the distance from the fire origin of the peak temperature starts to increase for large fire sizes. Though, for concrete rebar the location of the peak temperature in the compartment for fires larger than 40% of floor area decreases.

It can be concluded that the location of the peak temperature in the compartment is a function of both the fire size (i.e. heat release rate and resulting smoke temperatures) and spread rate (i.e. time, for which structural members are exposed to pre-heating). For fire sizes smaller than 25% the effects of fire spread rate are more dominant while for larger fires the size of the fire becomes more dominant.

Fig. 2.10 shows variation of the location of the peak member temperature in the compartment for different heat release rates. For both steel and concrete rebar, the higher the heat release rate or the thickness of fire protection (see Fig. 2.9) the closer the
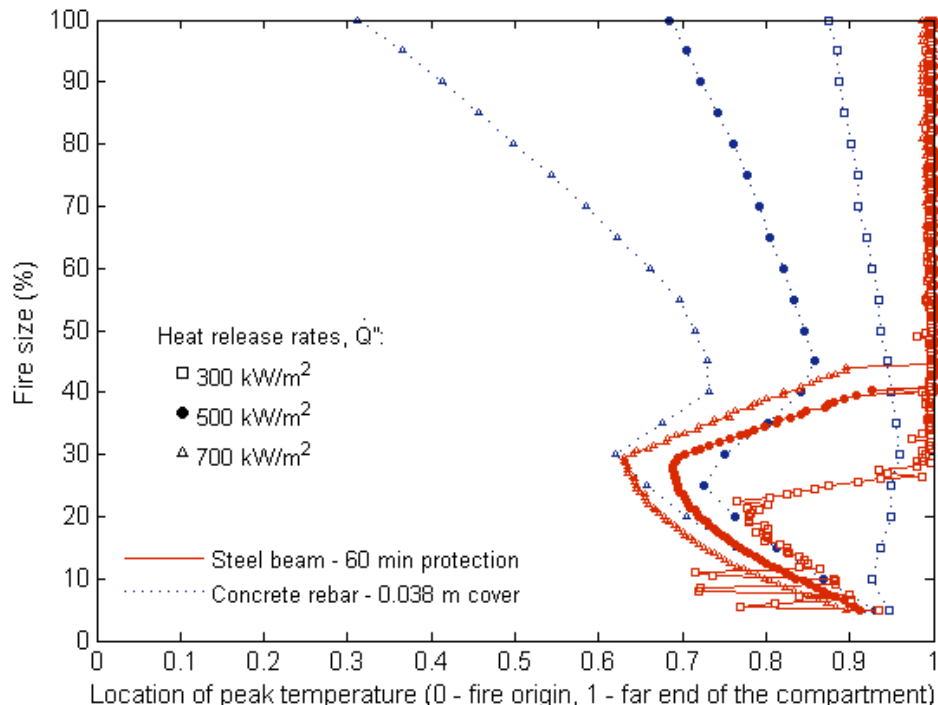
Figure 2.10: Variation of location of peak steel and concrete rebar temperatures in the compartment for heat release rates per unit area $\dot{Q}''$ of 300 kW/m², 500 kW/m², and 700 kW/m².

location to the fire origin. The thicker is the fire protection the slower the response to the changes in gas temperatures. Other parameters such as length of the fire compartment, fuel load density and flapping angle were varied as well. However, no influence on the location of peak member temperature from the fire origin have been observed as these parameters varied.

2.5   Conclusions

Current design codes invoke gas time-temperature curves which are based on small enclosure fires. Uniform temperature distributions in the compartments are proposed while in real buildings fires have been observed to travel. The World Trade Center Tower fires in 2001 have highlighted the need of more realistic design tools to represent fires in large compartments. Travelling Fires Methodology has been developed to account for the travelling nature of fires. In this chapter, the TFM has been refined based on a better fire model and used to analyse temperature distributions in structural members along the fire path in a simple structure.

The introduced limitation on the range of possible fire sizes reduces the computational time required by eliminating unrealistic fire coverage areas based on fire spread rates observed in experiments and real fires. Analytical correlation presented for generation of gas time-temperature curves is independent of grid size and can be easily calculated with any mathematical tool. Also, introduction of flapping term leads to reduced near-field temperatures for smaller fire sizes which cover a range between 800-1200°C observed in real building fires. The occurrence of peak member temperatures for fire sizes in the range of 5 to 20% diminishes with increasing flapping angle.

Finally, the location of the peak temperature of structural members in the compartment is found to occur at the end of the fire path (i.e. $> 0.6L$).It is dominated by fire spread rate for small fire sizes (up to 30%) although it depends on the thickness of fire protection and heat release rate. Total heat release rate becomes more dominant for large fires.

The proposed changes represent a crude fire model which can be used flexibly and updated as the new data becomes available. More experimental evidence in large compartments is necessary for further development and improvements.

Acknowledgements

Heidari and Panos Kotsovinos. Data supporting this chapter can be obtained from http://dx.doi.org/10.5281/zenodo.18873 under a Creative Commons Attribution license.

References

[1] J. R. N. Hall, "Burns, Toxic Gases, and other Fire-Like Hazards in Non-Fire Situations," no. February, 2004.

[2] D. T. Butry, R. E. Chapman, A. L. Huang, and D. S. Thomas, "A Life-Cycle Cost Comparison of Exit Stairs and Occupant Evacuation Elevators in Tall Buildings," *Fire Technology*, vol. 48, pp. 155–172, apr 2012.

[3] A. H. Buchanan, *Structural Design for Fire Safety.* John Wiley & Sons, Ltd, 2001.

[4] G. Flint, S. Lamont, B. Lane, H. Sarrazin, L. Lim, D. Rini, and C. Röben, "Recent Lessons Learned in Structural Fire Engineering for Composite Steel Structures," *Fire Technology*, vol. 49, pp. 767–792, jul 2013.

[5] B. R. Kirby, "The Behaviour of a Multi-storey Steel Framed Building Subjected to Fire Attack Experimental Data," tech. rep., Rotherham, 1998.

[6] G. M. Newman, J. T. Robinson, and C. G. Bailey, "Fire Safe Design: A New Approach to Multi-Storey Steel-Framed Buildings (Second Edition)," tech. rep., Ascot, 2006.

[7] J. Stern-Gottfried and G. Rein, "Travelling fires for structural designPart I: Literature review," *Fire Safety Journal*, vol. 54, pp. 74–85, nov 2012.

[8] J. Stern-Gottfried and G. Rein, "Travelling fires for structural design-Part II: Design methodology," *Fire Safety Journal*, vol. 54, pp. 96–112, nov 2012.

[9] J.-M. Franssen, "Improvement Of The Parametric Fire Of Eurocode 1 Based On Experimental Test Results," *Fire Safety Science*, vol. 6, pp. 927–938, 2000.

[10] T. P. McAllister, F. Sadek, J. L. Gross, S. Kirkpatrick, R. A. MacNeill, R. T. Bocchieri, M. Zarghamee, O. O. Erbay, and A. T. Sarawit, "Structural Analysis of Impact Damage to World Trade Center Buildings 1, 2, and 7," *Fire Technology*, vol. 49, pp. 615–642, jul 2013.

[11] R. G. Gann, A. Hamins, K. McGrattan, H. E. Nelson, T. J. Ohlemiller, K. R. Prasad, and W. M. Pitts, "Reconstruction of the Fires and Thermal Environment in World Trade Center Buildings 1, 2, and 7," *Fire Technology*, vol. 49, pp. 679–707, jul 2013.

[12] N. M. Post, "9/11 Blazes Debunk Code Assumptions About Fire Behavior in Open-Plan Offices," *Engineering News Record*, jul 2013.

[13] C. G. Clifton, "Fire Models for Large Firecells, HERA Report R4-83," tech. rep., 1996.

[14] A. Law, J. Stern-Gottfried, M. Gillie, and G. Rein, "The influence of travelling fires on a concrete frame," *Engineering Structures*, vol. 33, pp. 1635–1642, may 2011.

[15] G. Rein, X. Zhang, P. Williams, B. Hume, A. Heise, A. Jowsey, B. Lane, and J. L. Torero, "Multi-Storey fire analysis for high-rise buildings," in *The 11th International Interflam Conference*, no. September, (London), 2007.

[16] A. Law, N. Butterworth, J. Stern-gottfried, and Y. Wong, "Structural fire design: many components, one approach," in *The 1st international conference on performance based and life cycle structural engineering*, no. December, (Hong Kong), 2012.

[17] A. Law, J. Stern-Gottfried, and N. Butterworth, "A Risk Based Framework for Time Equivalence and Fire Resistance," *Fire Technology*, vol. 51, pp. 771–784, jul 2015.

[18] B. R. Kirby, G. M. Newman, N. Butterworth, J. Pagan, and C. English, "A new approach to specifying fire resistance periods," *The Structural Engineer*, pp. 34–37, oct 2004.

[19] J. Gales, "Travelling Fires and the St. Lawrence Burns Project," *Fire Technology*, vol. 50, pp. 1535–1543, nov 2014.

[20] G. Williams-Leir, "St. Lawrence Burns Temperature Measurements," Tech. Rep. 152, National Research Council. Canada. Division of Building Research, Ottawa, 1959.

[21] CEN, "EN 1991-1-2:2002 - Eurocode 1. Actions on structures. General actions. Actions on structures exposed to fire," 2002.

[22] H. E. Nelson, "An Engineering view of the fire of may 4, 1988 in the First Interstate Bank building Los Angeles, California," tech. rep., 1989.

[23] P. H. Thomas, "Some Aspects of the Growth and Spread of Fire in the Open," *Forestry*, vol. 40, no. 2, pp. 139–164, 1967.

[24] J. G. Quintiere, *Principles of Fire Behaviour*. Cengage Learning, 1998.

[25] B. R. Kirby, D. E. Wainman, L. N. Tomlinson, T. R. Kay, and B. N. Peackok, "Natural fires in large scale compartments - A British Steel technical, Fire Research Station collaborative project," 1994.

[26] J. G. Routley, "Interstate Bank Building Fire - USFA-TR-022," Tech. Rep. May, Homeland Security, 1988.

[27] Warren Centre, "Passive systems and building fire safety design - Task group six report; Fire Safety and Engineering, Technical Papers, Book Two," tech. rep., The Warren Centre for Advanced Engineering, University of Sydney, Sydney, Australia, 1989.

[28] R. L. Alpert, "Calculation of response time of ceiling-mounted fire detectors," *Fire Technology*, vol. 8, pp. 181–195, aug 1972.

[29] K. Suzuki, "Unsteady ceiling jet model for large building spaces," *Fire Safety Journal*, vol. 61, pp. 83–91, oct 2013.

[30] N. Johansson, J. Wahlqvist, and P. van Hees, "Numerical experiments in fire science: a study of ceiling jets," *Fire and Materials*, vol. 39, pp. 533–544, aug 2015.

[31] R. L. Alpert, "Turbulent Ceiling-Jet Induced by Large-Scale Fires," *Combustion Science and Technology*, vol. 11, pp. 197–213, nov 1975.

[32] G. Heskestad, "Physical modeling of fire," *Journal of Fire and Flammability*, vol. 6, pp. 253–273, 1975.

[33] P. H. Thomas, "Fires in Enclosures," in *Heat transfer in fires: thermophysics, social aspects, economic impact* (P. L. Blackshear, ed.), ch. II.2, p. 13, Washington: Building Research Establishment, 1974.

[34] D. Drysdale, *An introduction to fire dynamics*. Wiley, 3rd editio ed., 2011.

[35] B. R. Kirby, D. E. Wainman, L. N. Tomlinson, T. R. Kay, and B. N. Peacock, "Natural fires in large scale compartments," *International Journal on Engineering Performance-Based Fire Codes*, vol. 1, no. 2, pp. 43–58, 1999.

[36] T. Lennon and D. Moore, "The natural fire safety conceptfull-scale tests at Cardington," *Fire Safety Journal*, vol. 38, pp. 623–643, nov 2003.

[37] P.-A. Santoni, T. Marcelli, and E. Leoni, "Measurement of fluctuating temperatures in a continuous flame spreading across a fuel bed using a double thermocouple probe," *Combustion and Flame*, vol. 131, pp. 47–58, oct 2002.

[38] N. L. Crauford, *The structure of an unconfined buoyant turbulent diffusion flame.* PhD thesis, University of Southampton, 1984.

[39] J. G. Quintiere, W. J. Rinkinen, and W. W. Jones, "The Effect of Room Openings on Fire Plume Entrainment," *Combustion Science and Technology*, vol. 26, pp. 193–201, oct 1981.

[40] CEN, "EN 1993-1-1:2005 - Eurocode 3. Design of steel structures. General rules and rules for buildings," 2005.

[41] CEN, "EN 1992-1-1:2004 - Eurocode 2. Design of concrete structures. General rules and rules for buildings," 2004.

[42] CEN, "EN 1993-1-2:2005 - Eurocode 3. Design of steel structures. General rules. Structural fire design," 2005.

[43] CEN, "EN 1992-1-2:2004 - Eurocode 2. Design of concrete structures. General rules. Structural fire design," 2004.

[44] F. Incropera, D. DeWitt, T. Bergman, and A. Lavine, *Fundamentals of Heat and Mass Transfer.* John Wiley & Sons, Ltd, 2007.

[45] J. C. M. Forrest, "The whole structure," in *The International Conference on Design of Structures Against Fire* (R. D. Anchor, H. L. Malhotra, and J. A. Purkiss, eds.), (Birmingham), pp. 111–125, Elsevier Applied Science Ltd., 1986.

[46] A. S. Langman and G. J. Nathan, "Influence of a combustion-driven oscillation on global mixing in the flame from a refinery flare," *Experimental Thermal and Fluid Science*, vol. 35, pp. 199–210, jan 2011.

[47] B. J. McCaffrey, "Purely buoyant diffusion flames: Some experimental results. National Bureau of Standards Report NBSIR 79-1910.," tech. rep., Centre for Fire Research, National Engineering Laboratory, Washington, 1979.

[48] B. M. Cetegen and T. A. Ahmed, "Experiments on the periodic instability of buoyant plumes and pool fires," *Combustion and Flame*, vol. 93, pp. 157–184, apr 1993.

[49] J. Chen and Q. Bao, "Digital image processing based fire flame color and oscillation frequency analysis," *Procedia Engineering*, vol. 45, pp. 595–601, jan 2012.

Appendices

2.A Flapping angle

Quintiere et al. [39] carried out experiments to study the effects of openings in the room on fire plume entrainment. One of the measurements taken was flame angle. It can be seen from their results that the measured angle was not constant but rather was fluctuating with time. For all experiments, variation of flame angle was between $\pm 4°$

and $\pm 15°$ with an average value of $\pm 6.5°$ independent of fire size. For this study an effort was made to measure the angles (i.e. the length over which the flame fluctuates in relation to fuel base) from the published photographs of oscillating flame plumes in various experiments [38, 46–49]. The maximum angle amplitude was in a range of $\pm 3°$ to $\pm 15°$ (see Table 2.A1). In most of these experiments the maximum effort was taken to avoid any disturbances. The measured average angles were also plotted against the dimensionless heat release rate, which is shown in Fig. 2.A1. However, no significant dependency between the two was observed. It can be seen that the measured angle only minimally increases with higher heat release rates. Thus, for the updated version of TFM the flapping angle of 6.5 was chosen based on results from Quintiere et al. [39] experiments. It also falls within the range of other measured values.

Table 2.A1: Flapping angles based on data published in literature.

Ref.	Year	Angle (°)	$-\Delta\theta_{max}(°)$	$\Delta\theta_{max}(°)$	Fr	$\dot{Q}$ (kW)	D (m)		Q^*	Fuel
[39]	1981	6.5	2.5	8.5	-	62.9	0.30	○	1.16	methane
		5.6	1.6	4.4	-	158	0.30	○	2.91	methane
[46]	2011	7.6	1.1	2.2	0.695	-	1.32	○	162.5	propane
		6.7	1.0	1.1	0.742	-	1.32	○	167.9	propane
[49]	2012	4.7	3.7	2.3	-	-	0.30	□	-	n-heptane
[38]	1984	2.3	0.3	0.7	0.000117	28	0.25	○	0.81	methane
		5.7	1.7	1.3	8.66E-05	54	0.34	□	0.74	methane
[47]	1979	4.3	3.3	4.7	-	33	0.34	□	0.45	methane
[48]	1993	3.4	2.4	4.6	-	60	0.30	○	1.11	propane
		5.8	0.8	1.2	-	3	0.30	○	0.06	propane

Fr - Froude number; D - Fire source diameter; Q^* Dimensionless heat release rate.

Figure 2.A1: Relationship of flapping angles measures based on the data published in the literature with dimensionless heat release rate.
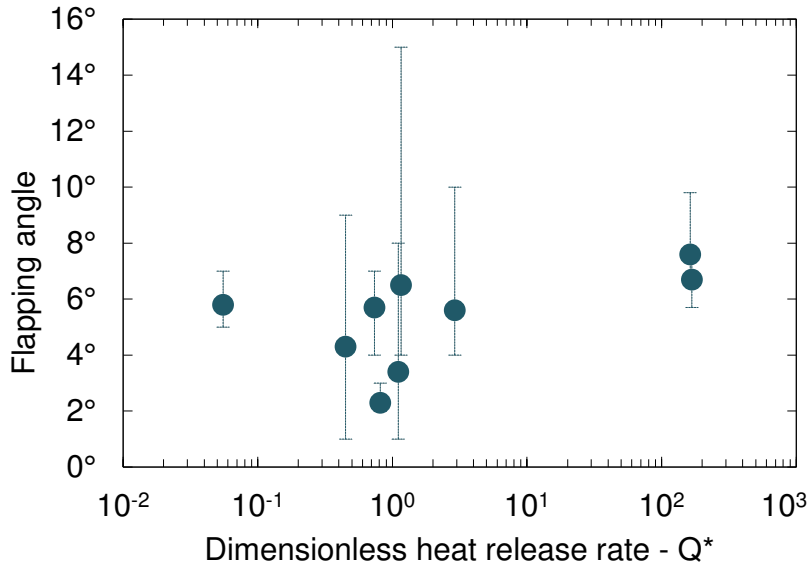
2.B   Calculation of reduced near-field temperature

Reduced near-field temperature due to flapping is calculated by taking an average gas temperature over the flapping length as shown in Fig. 2.B1. The far-field temperature function is integrated from the near-field edge to the flapping length edge, near-field temperatures over fire length are added, and an average reduced near-field temperature is calculated, see Eq. (2.21).

$$T_f = (A_{ff} + 1200L_f)/f \tag{2.21}$$

where T_f is the reduced near-field temperature (°C) and A_{ff} is a sum of far-field temperatures in the region of flapping length. The latter is calculated by integrating the Alpert's correlation [29] from the end of the flapping length ($r_2 = f/2$) to the end of the fire length ($r_1 = L_f/2$). The far-field limits r_1 and r_2 are represented in Fig. 2.B1.
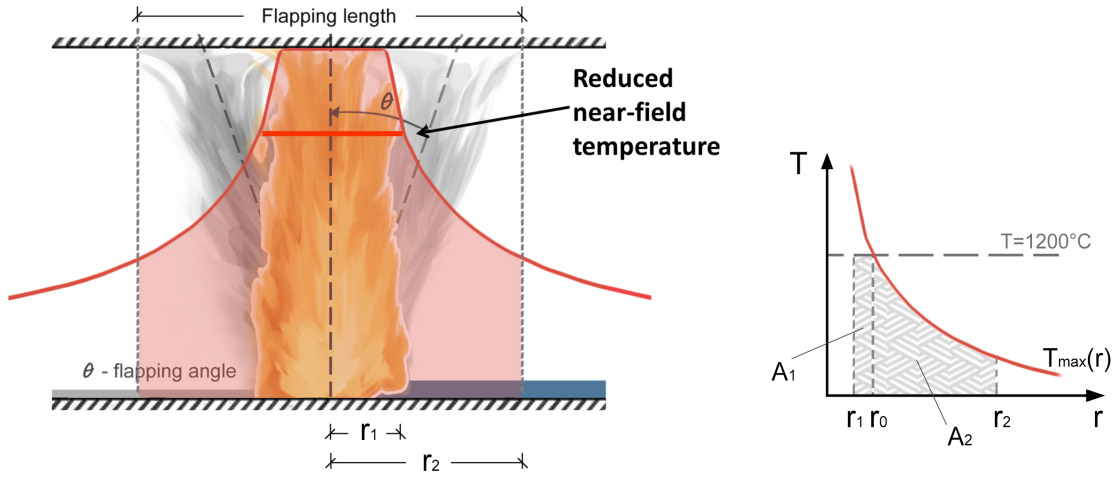
Figure 2.B1: Region over which gas temperatures are averaged to find a reduced near-field temperature (left); and limits of integration for calculating the average of far-field temperatures over the flapping length (right).

Using Alpert's correlation function [28] the far-field temperatures over a certain distance might be higher than a set maximum near-field temperature of 1200°C. These higher temperatures in TFM are reduced to maximum near-field temperature. This introduces another variable r_0, which is required for integration of far-field temperature function and does not allow far-field temperatures to be higher than a near-field temperature. r_0 is the crossing point between gas temperatures obtained using Alpert's correlation function [28] and near-field temperature of 1200°C.

$$T_{nf} = T_\infty + 5.38\frac{(\dot{Q}/r_0)^{2/3}}{H} \tag{2.22}$$

$$r_0 = \dot{Q}\left(\frac{5.38}{H(T_{nf} - T_\infty)}\right)^{3/2} \tag{2.23}$$

There are three possible crossing point r_0 locations in relation to near-field edge r_1 and flapping length edge r_2. They are shown in Fig. 2.B2.
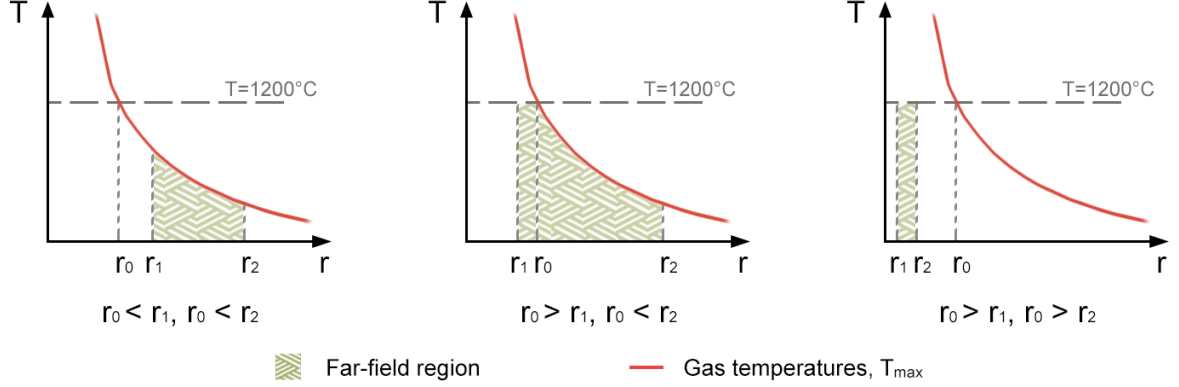
Figure 2.B2: Different possible scenarios of relation of far-field temperatures calculated using Alpert's correlation T_{max} [28], near-field temperature T_{nf}, near-field edge r_1 and flapping edge r_2.

Thus, the sum of far-field temperatures over the flapping length can be calculated as follows:

$$A_{ff} = 2(A_1 + A_2) \tag{2.24}$$

$$A_1 = T_{nf} \cdot r_{x1} \tag{2.25}$$

$$A_2 = \int_{r_{x2}}^{r_2} T_{max}(r)dr = \int_{r_{x2}}^{r_2} \left(T_\infty + 5.38 \frac{(\dot{Q}/r)^{2/3}}{H} \right) dr$$
$$= T_\infty(r_2 - r_{x2}) + \frac{16.14\dot{Q}^{2/3}}{H}\left(r_2^{1/3} - r_{x2}^{1/3} \right) \tag{2.26}$$

$$r_{x1} = max[0, r_0 - L_f/2] \tag{2.27}$$

$$r_{x2} = max[L_f/2, r_0] \tag{2.28}$$

where A_1 is the sum of temperatures, when those in the far-field calculated using Alpert's equation [28] are above the near-field temperature and the length over which this occurs is defined by r_{x1}. A_2 is the sum of temperatures, when those in the far-field calculated using Alpert's equation [28] are below the near-field temperature. This is done by integrating over the limits of flapping length edge r_2 and r_{x2}. r_{x2} defines the lower limit based on where the crossing point r_0 is located (see Fig. 2.B2). Therefore, combining Eqs. (2.21-2.26) the reduced near-field temperature due to flapping, T_f (°C), can be calculated as in Eq. (2.29).

$$T_f = T_\infty + \frac{T_{nf}(2r_{x1} + L_f) - 2T_\infty \cdot r_{x2}}{f} + \frac{32.28\dot{Q}^{2/3}}{H \cdot f}\left(r_2^{1/3} - r_{x2}^{1/3} \right) \tag{2.29}$$

2.C   Heat transfer

In this Appendix heat transfer calculations for steel and concrete used in Section 2.4 are presented. All calculations were carried out as in [8] using a numerical computing program MATLAB.

Steel

Heat transfer to unprotected and protected steel beams was carried out assuming lumped capacitance according to [3] as shown in Eqs. (2.30) and (2.31), respectively.

$$\Delta T_s = \frac{H_p}{A} \frac{1}{\rho_s c_s} [h_c(T_g - T_s) + \sigma \varepsilon (T_g^4 - T_s^4)] \Delta t \tag{2.30}$$

$$\Delta T_s = \frac{H_p}{A} \frac{k_i}{d_i \rho_s c_s} \frac{\rho_s c_s}{[\rho_s c_s + (H_p/A)d_i \rho_i c_i/2]} (T_g - T_s) \Delta t \tag{2.31}$$

where T_s is the steel temperature (K); T_g is the gas temperature (K); H_p is the heated perimeter of the beam (m); A is the cross-section area of the beam (m²); ρ_s is the density of steel (kg/m³); c_s is the specific heat of steel (J/kg.K); d_i is the thickness of fire protection (m); ρ_s is the density of the protection (kg/m³); c_i is the specific heat of the protection (J/kg.K); h_c is the convective heat transfer coefficient (W/m².K); σ is the Stefan-Boltzmann constant (5.67×10^{-8} W/m².K⁴); ε is the radiative and reradiative emissivity of the material and gas combined; and Δt is the time step (s).

Concrete

In-depth concrete temperatures were calculated using explicit one-dimensional finite difference model for heat conduction according to [44] as shown in Eqs. (2.32)-(2.34). Radiation and convection were taken into account for the boundary conditions.

Exposed surface, *0*:

$$T_0^{t+1} = \frac{2\Delta t}{\rho_c c_c \Delta z} \left[h_0(T_g - T_0^t) + \sigma \varepsilon (T_g^4 - T_0^4) + \frac{k_c}{\Delta z}(T_1^t - T_0^t) \right] + T_0^t \tag{2.32}$$

Internal nodes, *i*:

$$T_i^{t+1} = Fo(T_{i+1}^t - T_{i-1}^t) + (1 - 2Fo)T_i^t \tag{2.33}$$

Backside surface, *n*:

$$T_n^{t+1} = \frac{2\Delta t}{\rho_c c_c \Delta z} \left[h_n(T_\infty - T_n^t) + \sigma \varepsilon (T_\infty^4 - T_n^4) + \frac{k_c}{\Delta z}(T_{n-1}^t - T_n^t) \right] + T_n^t \tag{2.34}$$

where T_i^t is the concrete temperature at time t, and location, i (K); T_g is the gas temperature (K); T_∞ is the ambient temperature (K); ρ_s is the density of concrete (kg/m³); c_s is the

specific heat of concrete (J/kg.K); k_c is the thermal conductivity of concrete (W/m.K); h is the convective heat transfer coefficient (W/m^2.K); σ is the Stefan-Boltzmann constant (5.67×10^{-8} W/m^2.K^4); ε is the radiative and reradiative emissivity of the material and gas combined; Δt is the time step (s); Δz is the element length (m); and Fo is the Fourier number ($(k_c \Delta t)/(\rho_c c_c \Delta z^2)$).

Chapter 3

Model Parameter Sensitivity and Benchmarking of the Explicit Dynamic Solver of LS-DYNA for Structural Analysis in Case of Fire

Summary [1]

Due to the complex nature of structural response in fire, computational tools are often necessary for the safe design of structures under fire conditions. In recent years, the finite element code LS-DYNA has grown considerably in research and industry uses for structural fire analysis, but there is no benchmarking of the code available in the fire science literature for such applications. Moreover, due to the quasi-static nature of structural response in fire, the majority of the computational structural fire studies in the literature are based on the use of static solvers. Thus, this chapter aims at benchmarking the explicit dynamic solver of LS-DYNA for structural fire analysis against other static numerical codes and experiments. A parameter sensitivity study is carried out to study the effects of various numerical parameters on the convergence to quasi-static solutions. Four canonical problems that encompass a range of thermal and mechanical behaviours in fire are simulated. In addition, two different modelling approaches of composite action between the concrete slab and the steel beams are investigated. In general, the results confirm that when numerical parameters are carefully considered such as to not induce excessive inertia forces in the system, explicit dynamic analyses using LS-DYNA provide good predictions of the key variables of structural response during fire.

---

1. This chapter is based on "E. Rackauskaite, P. Kotsovinos, G. Rein (2017) *Model Parameter Sensitivity and Benchmarking of the Explicit Dynamic Solver of LS-DYNA for Structural Analysis in Case of Fire*, **Fire Safety Journal** 90:123-138."

3.1 Introduction

Modern building designs and innovative architectural solutions pose a challenge to structural engineers. This is particularly the case for structural fire engineers due to the complex interactions of modern structural systems in fire. The performance of even generic structures exposed to fire is not straightforward and cannot be easily predicted. As a result, there is often the engineering need to be able to assess structural behaviour under fire conditions from first principles and not rely on blanket prescriptive guidance.

The behaviour of isolated structural elements under standard fire conditions through furnace testing has been extensively studied over the past decade, and can now be predicted with some degree of accuracy using analytical and computational means [1]. However, it has been shown in the past [1–3] that structural fire performance of isolated elements does not resemble the performance of a whole structure. The whole structure performance in a real fire depends on a number of factors. They include restraint, stress redistribution, composite action, and continuity within the structure [4]. The involvement of the many variables makes the analysis and prediction of the fire performance of realistic structures a difficult process. Standard fire tests provide unrealistic results [5]. They do not represent real fire conditions in the compartment and base fire resistance on the performance of the individual elements ignoring the effects of the surrounding structure. Conversely, full-scale testing of real structures is complex, expensive and time consuming. In addition, the limited number of full-scale experiments carried out worldwide (e.g. Cardington tests [5]) has been on buildings of generic rectangular geometry. Thus, they cannot be generalised to predict the performance of all structures, especially where more innovative irregular structural arrangements are used. As a result, designers use computational tools to predict and assess the performance of complex structures under fire conditions.

With increasing computational capabilities, the fire resistance assessment of various structural arrangements under different fire scenarios is becoming more and more used in practice. However, these models have to be benchmarked against experimental data or known solutions to make sure that they produce accurate and physically correct results. Most commonly used numerical models for structural fire analysis include commercial general finite element analysis packages (Ansys, Abaqus) and purpose-based finite element models developed or extended specifically for structural fire analysis (Vulcan, SAFIR and OpenSees). All of these models have been widely used for structural fire analysis in the recent years and have been validated against various small-scale and full-scale tests (e.g. Cardington) [6–17].

More recently, researchers and designers [18–20] have adopted LS-DYNA for structural fire analysis. Kilic and Selamet [19], and Selamet [18] used LS-DYNA to investigate the effect of fire location on the collapse of a 49 storey high-rise steel structure. The whole 3D building model was used for the analysis. Law et al. [20] studied the structural re-

sponse of structural arrangements with bi-linear columns to fire. A slice of the 3D model of a generic substructure was used that included a 4-storey high bi-linear column with adjacent composite beams and concrete slabs. In all of these studies [18–20] the authors used beam and shell elements to represent steel beams and concrete slab respectively. However, neither of them included the benchmarking of the adopted LS-DYNA model. Both et al. [21] published a benchmark for predicting the structural fire response of a centrally loaded steel-concrete column. The column was modelled using solid elements. The results of the coupled thermal-mechanical analysis were presented for ANSYS, LS-DYNA, and ABAQUS. Temperature and displacement development in column showed a good agreement between those software packages. The maximum differences between the peak values in relation to LS-DYNA results were approximately 23°C (5%) and 0.23 mm (23%), respectively. Kwasniewski et al. [22] carried out a coupled thermal-mechanical analysis of a restrained steel column subjected to fire using LS-DYNA and validated against experimental results. The detailed 3D model (as in the benchmark by Both et al. [21]) adopted solid elements.

LS-DYNA is a commercial general purpose finite element software originally developed for highly nonlinear and transient dynamic analysis [23]. It is robust in the analysis of problems involving transient effects, contact and large deformations and has high computational efficiency. As a result, LS-DYNA is one of the most commonly used numerical explicit integration simulation programs. Common applications of LS-DYNA include automotive, aerospace, metalforming, and multi-physics problems. In structural engineering, common applications include earthquake, blast impact, and progressive collapse analysis. LS-DYNA has been used for the aircraft impact and progressive collapse analysis of the World Trade Centre (WTC) towers by NIST [24, 25]. However, most likely due to the lack of available scientific work using LS-DYNA, for structural fire response analysis in the same WTC study a different numerical program was used. LS-DYNA as a software has been fully validated and verified by its developers (Livermore) for its generic applications. Even though, in recent years, the explicit dynamic solver of LS-DYNA has grown considerably in research and industry uses for the analysis of structures in fire [18–22], to the best of the author's knowledge, there is still no benchmarking of the code available in the literature specifically with regards to the structural fire performance. Available research is limited to the internal benchmarking work carried out in Arup [26] and detailed 3D solid element based individual structural member models [22]. Solid elements are not frequently used for global models or for design purposes. In addition, due to the quasi-static nature of the structural response in fire, the majority of the structural fire analyses available in literature are carried out using static solvers.

Thus, this chapter aims at benchmarking the explicit dynamic solver of LS-DYNA for the structural fire analysis of 3D composite structures and 2D steel frames against experiments and other numerical codes. An extensive parameter sensitivity study is carried out to study the effects of various modelling parameters on the kinetic energy and

convergence to quasi-static solution. Four canonical problems that encompass a range of thermal and mechanical behaviours in fire are simulated. The term benchmarking is used in this chapter to refer to verification and validation of computational models, based on the definitions adopted by the ASTM [27]. That is, evaluating the software for correct application to known benchmark problems and for physical correctness of the results [15, 16]. The LS-DYNA model is benchmarked against fire tests on loaded steel framework results [28–30], two benchmarks published by Gillie [31] and results published by Rackauskaite and El-Rimawi [32] on the numerical study of 2D steel frames subject to localised fires.

3.2   LS-DYNA benchmarking models

For the benchmarking of LS-DYNA for structural fire analysis, the double precision LS-DYNA (Release 7.1.1) version is used. Each benchmarking case chosen for this study encompasses different mechanisms of structural response in fire, which are required to get a realistic response. In total four benchmark cases are considered. The first benchmark is based on the natural fire test of the 2D steel frame carried out in 1987 [28–30]. It allows the benchmarking of LS-DYNA against experimental results and assessing whether the model correctly captures the effects of non-uniform heating, material non-linearity, restraint, and stress redistribution.

The remaining 3 benchmarks are based on and allow benchmarking of LS-DYNA against the results of numerical analysis published in the literature [31, 32]. Gillie [31] has published results for 2 problems which provide benchmark solutions for structural fire analysis. They allow users to check whether their models capture the required phenomena, which occur when structures are heated. The first benchmark [31] is on a uniformly heated steel beam with 75% support stiffness. This benchmark allows to confirm whether the model captures the effects of material non-linearity, geometric non-linearity and restraint conditions [31]. The second benchmark [31] is on a heated composite concrete floor. This benchmark assesses whether phenomena such as stress redistribution, localised heating and composite action effects can be captured. These two benchmarks provide a computational challenge against most of the fundamental mechanisms that occur when structures are heated and, thus, were chosen for the benchmarking of LS-DYNA. In addition to the above, a third benchmark has been chosen based on the study by Rackauskaite and El-Rimawi [32] on the heating effects on a 2D steel frame. In the latter study non-uniform heating of the beams was assumed. Therefore, the adoption of this study as a benchmark allows to assess whether thermal bowing, restraint from the surrounding structure and stress redistribution are appropriately captured in the analysis. In the following sections these benchmarks are described and the results from the LS-DYNA analyses are presented.

3.2.1 Benchmark #1 (BM1): fire test on a loaded steel framework

Benchmark #1 (BM1) represents a natural fire test on a 2D steel frame carried out in 1987 [28]. The test frame comprised of a 4.55 m long steel beam and two 2.53 m high columns. It was connected to secondary framework to prevent lateral instability. Details of the frame and loading are shown in Fig. 3.1. This test has already been successfully modelled in CEFICOSS [29], Abaqus and SAFIR [30]. Therefore, a similar modelling approach was used in LS-DYNA for comparative purposes.

Beam web temperature measurement from the test is only available at one instant during the whole fire exposure. Thus, member temperatures, which show a good agreement with the measured test data for beam flanges and column (see Fig. 3.1), were taken from [29]. The beam was subjected to non-uniform gas temperatures along its length. To account for this, a temperature reduction function following a sinusoidal shape was applied along the beam as in [29, 30] with the temperature at the connection being 0.9 of the beam temperature at mid-span. Column temperatures along the height were assumed to be constant.

In LS-DYNA, the steel frame was modelled using Hughes-Liu beam elements with user defined cross-section integration. This element has a single integration point along its length in the middle of the element, where sectional plasticity is monitored. Hughes-Liu beam elements allow for the treatment of finite strains and are simple, computationally efficient and robust. It is the first beam element implemented in LS-DYNA and thus it
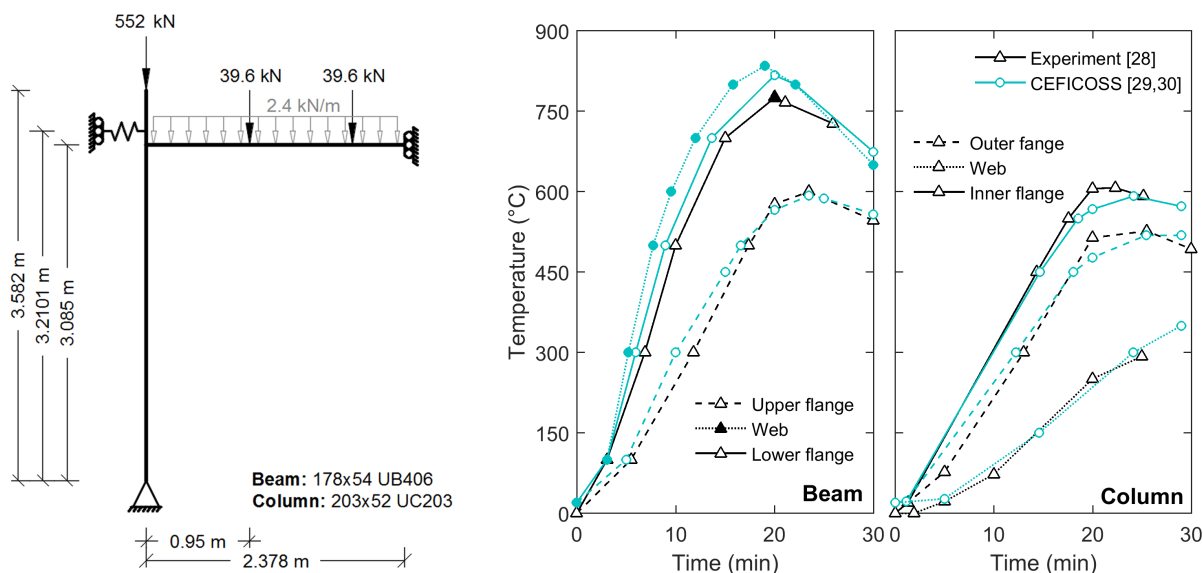
Figure 3.1: Details of Benchmark #1 used for benchmarking of LS-DYNA for fire analysis: illustration of the tested frame (left), and comparison of beam temperatures at mid-span and column temperatures at mid-height measured during the test [28] with CEFICOSS numerical simulation results [29, 30] that were used as an input in LS-DYNA analysis (right).

is used as the default element type in the program [33]. The same beam formulation was used in [18–20]. A thermally-sensitive steel material type MAT 202 formulation based on Eurocode 3 (EN 1993-1-2:2005) [23] was used for the analysis. Thermal loading to the beam and columns was applied using the formulation (i.e. load thermal variable beam) that allows the definition of variable through-thickness temperature distribution. Using this formulation, a known temperature-time history at different cross-section coordinates of beam elements can be defined. Along the length of the beam element only a single uniform temperature can be defined, due to the Hughes-Liu beam element formulation. Therefore, for this benchmark a uniform average temperature value over the beam element length was calculated and applied.

Due to symmetry, only half of the frame was modelled with the support conditions set as shown in Fig. 3.1. To represent the support from the secondary framework a discrete beam element was used at the column height of 3.2101 m with nonlinear elastic material (MAT 67) formulation. This material model allows defining 6 springs acting about the local degrees of freedom and nonlinear spring stiffness [23]. Spring behaviour was taken from [29, 30]. LS-DYNA has a 3D model space and as a result, out of plane translational restraint to the nodes was added to simplify the benchmark into a two dimensional space.

3.2.2 Benchmark #2 (BM2): uniformly heated beam

Benchmark #2 (BM2) [31] represents a 1 m long restrained rectangular steel beam with cross-section dimensions of 35 mm × 35 mm. A uniform load of 4250 N/m is applied to the beam (see Fig. 3.2). The beam is linearly heated up to a temperature of 800°C and then cooled down to room temperature. The temperature distribution within the beam is assumed to be uniform. Different levels of restraint are considered and include 0% (i.e. simply supported), 5%, 10%, 25%, 50%, 75%, and 100% (i.e. pinned) of beam axial stiffness.

In LS-DYNA, the steel beam was modelled using Hughes-Liu beam elements as for BM1. The elastic-plastic material (MAT 4) formulation was used to represent the steel. This material model allows the user to define temperature dependent material properties as provided in the original benchmark [31]. One end of the beam was set as pinned and
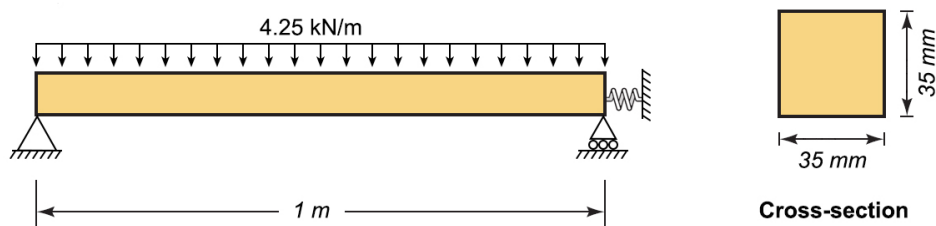
Figure 3.2: Details of Benchmark #2 [31] used for the benchmarking of LS-DYNA for fire analysis.

on the other end a discrete beam element was used with a linear elastic material (MAT 66) formulation. This material model allows defining 6 springs acting about the local degrees of freedom [23]. The discrete beam element was used to represent varying support restraint conditions of the beam. To model the 75% support restraint, the translational stiffness in the discrete beam material model was set to 1.902×10^8 N/m (75% of the beam axial stiffness, EA/L) as suggested in [31]. Out of plane translational restraint was added to all nodes to ensure a two dimensional behaviour. Illustration of this benchmark (BM2) is shown in Fig. 3.2.

3.2.3 Benchmark #3 (BM3): composite steel-concrete floor

Between 1994 and 1996 a series of full-scale fire tests were conducted on an 8-storey composite steel and concrete within the UK Building Research Establishment at Cardington to gain a better understanding of global structural performance in fire [5]. In total four major tests were conducted. They include the restrained beam, the plane frame, the corner, and office fire tests. Restrained beams test was the first test carried out on the 7th floor of the structure. The aim of this test was to investigate the structural behaviour of the composite structure when a single beam is heated restrained by the concrete slab [5]. During the test the beam and concrete slab were heated by the gas fired furnace (8 m × 3 m) built under the composite floor and along the beam. The total beam length was 9 m. Ends of the beam and the rest of the structure remained at ambient temperature.

Benchmark #3 (BM3) represents a simplified idealisation of the first Cardington test according to [31]. Some of the idealisations include simplified boundary conditions and thermal loading. In this benchmark part of the 4.5 m × 4.5 m × 0.13 m composite steel-concrete floor is exposed to linearly increasing heating and cooling. The heated area and the geometry of the benchmark are shown in Fig. 3.3. The concrete floor slab is connected to primary and secondary steel beams. The heated part of the secondary beams has a uniform temperature distribution and reaches a peak temperature of 800°C. The heated part of the floor slab is assumed to have a linear through thickness thermal gradient with the absolute peak temperature values of 600°C at the bottom of the slab and 0°C at the top. The uniform gravity loading applied on the slab is 5.48 kN/m².

For this benchmark two LS-DYNA models were developed to compare two different approaches used to represent the composite action between steel beams and the concrete slab. In Model A (BM3-A), the beam elements representing the steel beams and the shell elements representing the concrete slab were defined using separate nodes. To represent composite action, a tied contact between beam and shell elements was used. Tied contact uses a penalty based formulation and force and moment resultants are transferred by beam like springs [23]. In Model B (BM3-B), the beam and shell elements share the same nodes in order to account for composite action effects between steel beams and concrete slab. Beam and shell element formulations with offset option were used to offset the central axis of the elements to geometrically represent the position of the elements in relation
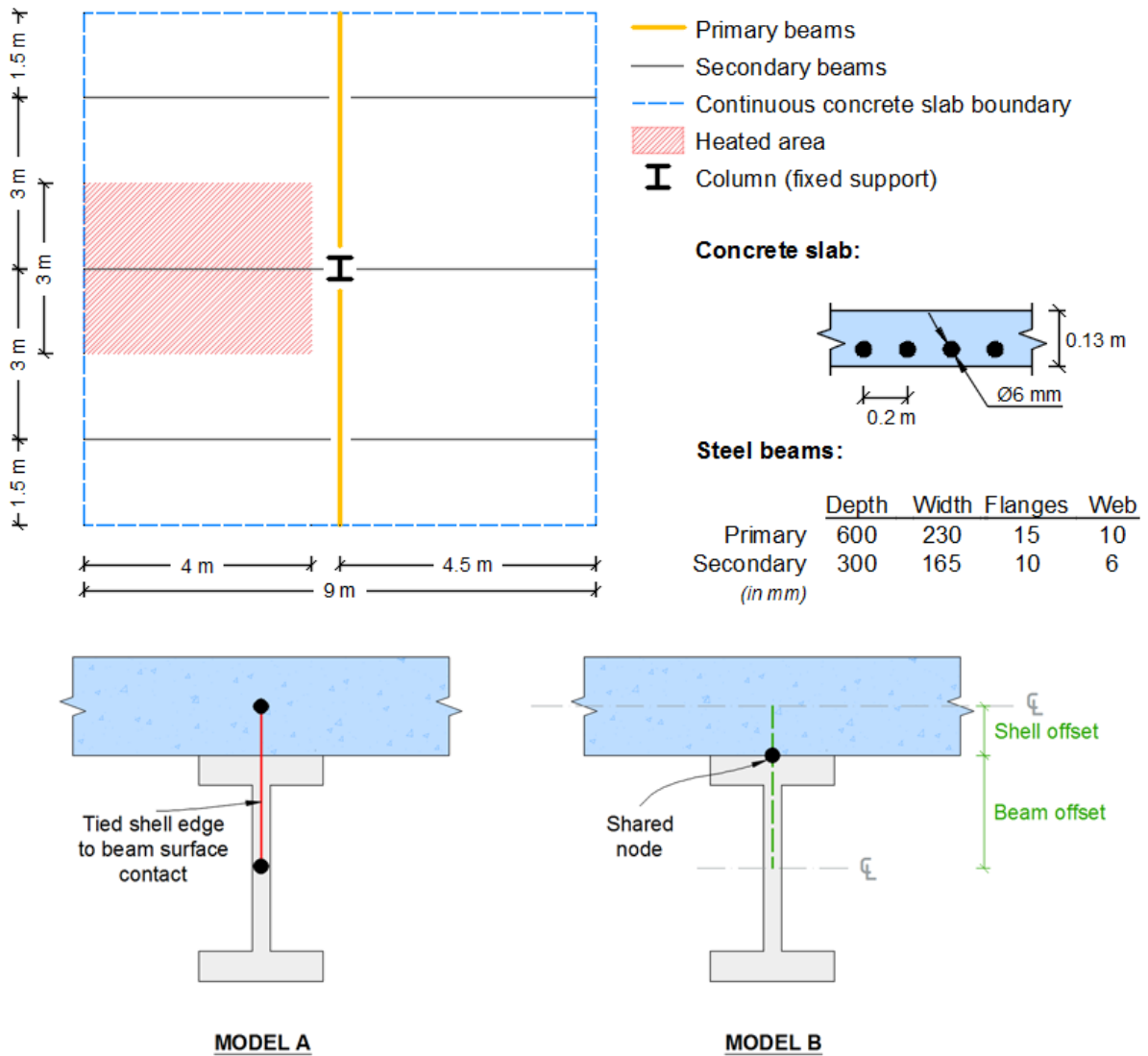
Figure 3.3: Illustration of Benchmark #3 from [31] used for benchmarking of LS-DYNA for fire analysis (top); Visualisation of Model A and Model B of Benchmark #3 where different formulations were used to simulate composite action between steel beams and the concrete slab (bottom).

to one another. The illustration of the geometry and the two models are shown in Fig. 3.3. Both modelling approaches assume that there is a perfect contact between the steel beams and the concrete slabs, and that shear stud failure does not occur during the fire.

The remaining parameters and configuration (e.g. mesh size, material properties, loading) were the same in both Model A and Model B. For primary and secondary steel beams, the Hughes-Liu beam element formulation was used. The concrete slab was modelled using the Belytschko-Tsay shell element formulation, which is computationally efficient. It is based on a combined co-rotational and velocity-strain formulation [33]. Material type MAT 172 and MAT 202 formulations were used for concrete and steel respectively. The steel material model is based on Eurocode 3 (EN 1993-1-2:2005) and

the concrete model is based on Eurocode 2 (EN 1992-1-2:2004). Both material models are thermally-sensitive and allow the users to define temperature dependant properties by overriding the values from the Eurocodes. MAT 172 can be used to represent plain concrete, plain steel or a smeared combination of concrete and steel [23]. In this bench-marking study two materials were created using this formulation for plain concrete and plain reinforcement. These were then used to represent different through-thickness layers of the concrete slab section. The slab was divided into a chosen number of layers, each representing either plain concrete or plain reinforcement, with the middle layer charac-terising steel reinforcement. The equivalent thickness of the reinforcement layer (0.283 mm) was calculated based on the total volume of steel rebars in the concrete slab.

The thermal load to the beams and shell elements was applied using the formulations that allow the definition of varying through-thickness temperatures. It was identified by Gillie [31] that gravity loading was included in the uniformly distributed load on the concrete slab and thus it was not explicitly applied in the current model. The concrete slab was modelled as continuous with appropriate lateral and rotational constraints around the boundary.

3.2.4 Benchmark #4 (BM4): 2D steel frame

The fourth LS-DYNA benchmark model used for benchmarking, Benchmark #4 (BM4), is based on the numerical study by Rackauskaite and El-Rimawi [32] on the structural response of 2D frames subject to localised fires. The latter study [32] was conducted using an in-house specialist finite element software based on the secant stiffness approach that was developed specifically for structural fire modelling purposes [32, 34–36]. A three-storey three-bay steel frame was subject to six different fire scenarios. Details of the frame are shown in Fig. 3.4. The heated columns were assumed to have uniform temperature distribution. The steel beams were subjected to a temperature gradient
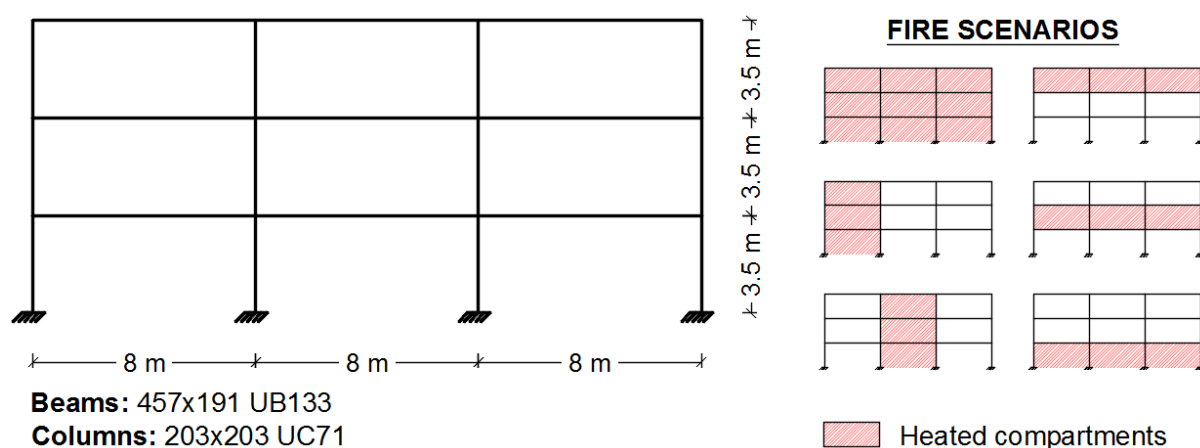
Figure 3.4: Details of the 2D steel frame [32] used for Benchmark #4 for benchmarking of LS-DYNA for fire analysis.

through the section. For the top flange, web and bottom flange of the heated beams temperature scaling ratios of 0.85, 1, and 0.86 were used, respectively. This is to account for the increased temperatures of the web compared to the bottom flange due to its thickness and the heat sink effect of the slab. The structural members were linearly heated until the failure of the frame occurred.

As for the previous benchmarks, the steel beams were modelled using the Hughes-Liu beam element formulation. The element lengths for beams and columns were 1 m and 0.875 m respectively. This mesh density was used in [32] and thus the same mesh density was adopted in the current study as well for comparative purposes. Steel material type MAT 202 formulation was used for steel beams and columns with the default Eurocode temperature dependent material properties. Thermal loading to the beams was applied using the formulation that allows the definition of variable through-thickness temperature distribution. The uniformly distributed load on beams of 41.1 kN/m was converted to equivalent nodal loads in accordance to the original study [32]. Gravity loads (i.e. self-weight of the beam) are included in the latter load and, therefore, were not considered separately. Column base boundary condition was set as fixed. Out of plane translational restraint was added to all nodes to ensure a two dimensional behaviour.

3.3 Parameter sensitivity

Prior to benchmarking of LS-DYNA for structural fire analysis, a model parameter sensitivity study was carried out in order to determine the optimum balance between accuracy and computational efficiency. The effect of parameters such as load time scaling, mesh density, number of beam and shell element integration points on the convergence of the solution was investigated. The initial model parameters are identified in Table 3.1 and are described in the following sections. During the parameter sensitivity study only one parameter was varied at a time. The other model parameters were kept constant as

Table 3.1: Initial model parameters used for parameter sensitivity study.

Model	Preload duration, t_{pre}	Thermal load application duration, t_h & t_c	Element length	Beam integration refinement factor, k	Number of shell through thickness integration points
BM1	1 s	100 (time scale factor)	~0.25 m [a]	5	n/a
BM2	0.026 s (damping)	16 s	0.10 m	0	n/a
BM3-A	1 s	4 s	0.25 m	5	5
BM3-B	1 s	4 s	0.25 m	5	5
BM4	1 s	4 s	1 m [a]	0	n/a

a. Refers to beam element length. Column element length for BM1 and BM4 is ~0.39 m and 0.875 m, respectively.

shown in Table 3.1. Based on this parameter sensitivity study, the final model parameters were then chosen for benchmarking and the comparison of the LS-DYNA analyses results with the test or model outputs as provided in [30–32].

3.3.1 Time scaling

The response of structures to fire is frequently idealised as a quasi-static problem [37]. This is due to the relatively slow increase in temperatures and therefore the rate of change of displacements (until a failure occurs) of structural components during a fire. Dynamic instabilities generated during fire are relatively small compared to the natural frequency of a structure [37]. In addition, commonly used material models for structures in fire are temperature dependent only, e.g. Eurocode [38]. Therefore, the heating or cooling rate does not influence the modelled material response. LS-DYNA is a non-linear transient dynamic finite element code. Thus, it uses real-time to solve the equation of motion, Eq. (3.1) [33].

$$m\ddot{u} + c\dot{u} + f_{int}(u) = p(t) \tag{3.1}$$

where m is the mass, $\ddot{u}$ is the acceleration, c is the damping coefficient, $\dot{u}$ is the velocity, $f_{int}(u)$ are the internal forces, and $p(t)$ are the external forces.

The modelling of structural response in fire using the real time fire duration would require a significant computational time. Due to the mainly quasi-static nature of the structural response to fire problem, when a dynamic analysis is carried out, the most common approach is to scale-down the "real" time in the model and therefore apply static and thermal loads over a shorter period. However, scaling the load application time implies that the scaled down "load" will be applied faster. Thus, for the LS-DYNA explicit dynamic solver (or any other dynamic solver), it could lead to the introduction of significant inertia forces to the system, which could impact the structural response. During the thermal load application inertia effects could be initiated by thermal expansion and large deflections due to high temperatures developing over a short period of time.

A general approach to avoid inertia effects and, thus, high dynamic oscillations is to ramp the load linearly over a period of time to minimise any numerical instabilities and to reach a near to steady-state solution (due to static loads) or quasi-static solution (due to thermal loads). This approach can be combined with the application of damping, which dissipates the kinetic energy in the system and allows the use of shorter preload and thermal load durations and thus computational time. Other approaches could also involve mass scaling, however, this approach is not assessed in this work. In this chapter, the effect of preload and thermal load application duration (see Fig. 3.5) and damping on the kinetic energy and force development in LS-DYNA is investigated for the four benchmark cases identified in the previous section. Kinetic energy gives an indication on the amount of inertia force present in the system. A general rule of thumb is that a solution is considered to be steady state and quasi-static when the kinetic energy to

internal energy ratio in the system for most of the time is less than 0.1% and 5% [39–42], respectively. In this study the same criterion is used based on the kinetic to internal energy ratio for 95% of the fire exposure time (see Appendix 3.A).
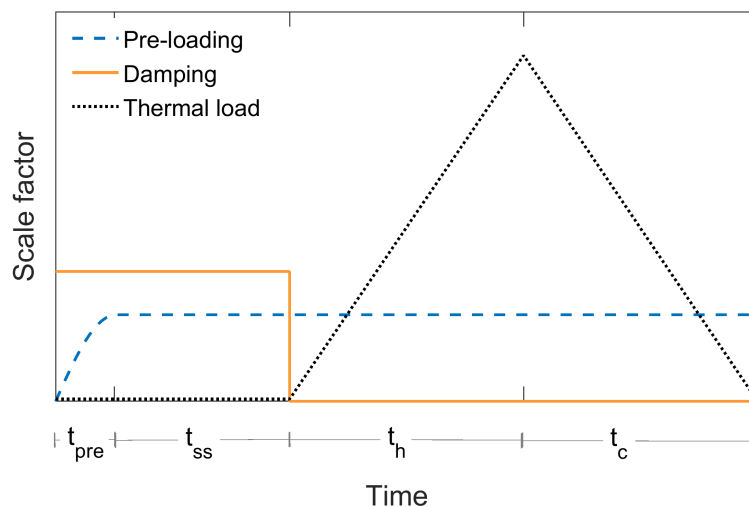
Figure 3.5: The sequence of load application used in the LS-DYNA modelling approach for structural response to fire analysis. t_{pre} is the preload duration, t_{ss} is the steady-state, t_h is the heating duration, and t_c is the cooling duration.

Preload durations, t_{pre}, are varied between 1 and 64 s for BM1, BM2, and BM4, and between 1 and 256 s for BM3. The thermal load application duration, t_h, up to a maximum temperature is varied from 0.5 to 512 s for all benchmarks. The upper boundaries used are based on the convergence of the output and kinetic to internal energy ratios for different models. The preload is applied first and then kept constant for 1 s. Following that once the steady-state solution has been reached, the thermal load is applied. In the cases where cooling is considering, cooling duration to ambient temperature, t_c, is the same as the heating duration, i.e. $t_c = t_h$. During the thermal load application period, the static load is unchanged and considered to be constant. In the cases where damping is applied during preload only, the critical damping factor is reduced to 0 before the application of the thermal load. The order of load application is shown schematically in Fig. 3.5.

In addition to varying the preload and thermal load duration, the application of global damping was considered. For each benchmark, an LS-DYNA implicit eigenvalue analysis was run to determine the lowest fundamental frequency of the structural system. Material type MAT 202 formulation is not currently available on the implicit solver of LS-DYNA R7.1. Thus, to carry out the eigenvalue analysis for BM1, BM3 and BM4 an elastic material (MAT 1) formulation for steel parts was used. The resulting frequencies, f, were 62.4, 77.06, 7.70, 7.71, and 4.28 Hz for BM1, BM2, BM3-A, BM3-B, and BM4, respectively. These frequencies were used to determine the critical damping factor, d_{cr},

for the structural system using Eq. (3.2) as suggested in [23]:

$$d_{cr} = 4\pi f \tag{3.2}$$

The static load was applied using a half sine function shape over the duration 2 times the normal period $(1/f)$ of the system in the damped cases. After preload, the load was kept constant for 1 s. It should be noted that there may be cases where a dynamic analysis would be best suited for structural fire analyses such as in the case of fire induced progressive collapse [37, 43] and therefore selecting the appropriate analysis parameters that would minimise the introduction of pseudo-inertia effects is crucial.

3.3.2 Mesh density

One of the key model parameters that can influence the accuracy of the numerical solution is mesh density. Thus, for all the benchmark cases, a mesh convergence study is carried out. For cases BM1, BM2, BM3, and BM4, the beam element length is varied between 0.03 and 0.476 m, 0.00625 and 0.5 m, 0.0625 and 0.5 m, and 0.0625 and 4 m, respectively. Column element length for cases BM1 and BM4 is varied between 0.048 and 0.386 m and between 0.0625 and 0.875 m, respectively. The beam and shell element lengths for case BM3 are the same. For the mesh density study of BM1, a uniform temperature along the beam length is assumed for simplicity.

3.3.3 Beam element integration

As noted earlier, in LS-DYNA, the Hughes-Liu beam element formulation has a single integration point in the middle of the element and user defined cross-section integration [33]. Integration points for a rectangular cross-section (BM2) and an I-section (BM1, BM3, and BM4) are defined as shown in Fig. 3.6. The number of integration points can vary depending on the desired accuracy required on the through-depth plasticity. Each fibre has a prescribed uniaxial stress-strain relationship. A greater number of integration points can also more accurately represent the thermal gradients within a structural member. In this study the beam cross-section integration refinement factor, k (see Fig. 3.6), for all cases was varied between 0 and 11. That is, the number of cross-sectional integration points was varied for the beam elements between 9 and 169 for the rectangular cross-section (BM2), and between 6 and 50 for the I-section (BM1, BM2, and BM3).

3.3.4 Shell element integration

In LS-DYNA, based on the modelling approach presented for BM3 in this chapter (see Section 3.2.3), the concrete slab is modelled as a composite section. Different shell through-thickness integration points are defined for steel rebars and slab with appropriate material models. A smeared cracking approach is adopted and therefore rebar rupture is
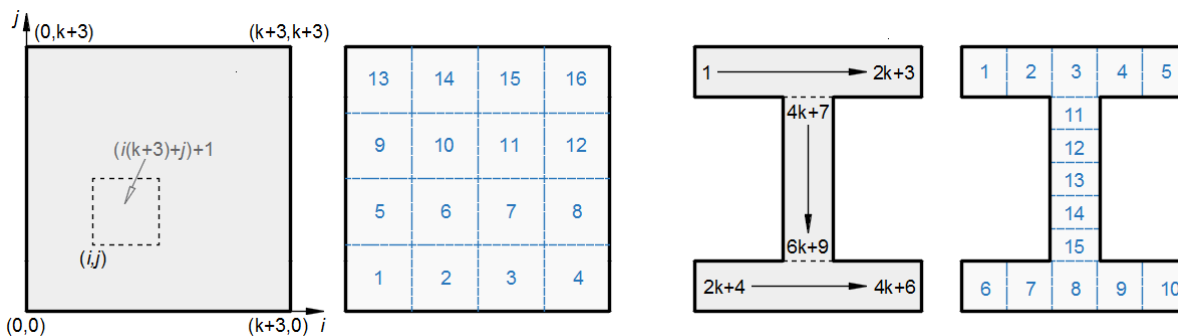
Figure 3.6: Rectangular and I-section beam element cross-section refinement used in LS-DYNA. Number of integration points for integration refinement factor $k = 1$ [23].
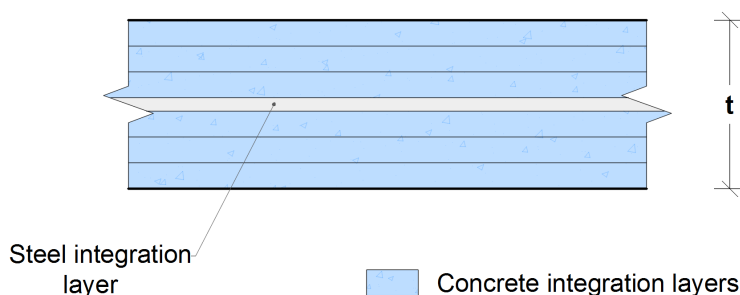
Figure 3.7: Representation of shell through thickness integration layers as modelled in LS-DYNA BM3. t is the total thickness of the concrete slab. The image represents a shell element with 7 integration layers.

not explicitly considered and would need to be assessed by the modeller independently. The rebar layer is modelled at the centre of the shell element with an equivalent number of concrete layers at the top and bottom of the shell (see Fig. 3.7). The total number of layers defines the number of integration points. In this study, the number of shell integration layers was varied between 3 and 11. The upper boundary used was based on the convergence of the output. In all cases only one layer at half thickness of the shell element was used to represent the steel rebars. In the original benchmark, [31] the exact location of the rebar in the concrete slab is not defined. The rebar position used in this chapter was chosen based on the previous work by Gillie [44] on Cardington tests that this benchmark originated from and a study where the geometry of BM3 has been used as one of the investigated cases [45]. In the latter work, the depth of rebar in a concrete slab with trapezoidal decking was indicated as 55 mm, which is approximately at the centre of the concrete slab.

3.4 Results and discussion

3.4.1 Parameter sensitivity

Effect of preload due to gravity and static load

The variation of the kinetic to internal energy ratio, displacement and axial force with preload duration during the steady-state (t_{ss}) are shown in Fig. 3.8 for all benchmark cases. It can be seen that with an increased preload duration the amount of kinetic energy reduces. The same load is applied over a longer period and thus the pseudo-inertia effects which are associated with the time scaling decrease. For BM1, BM2 and BM4, the kinetic energy present in the system is very low, in the range of $1 \times 10^{-4}\%$ and $2 \times 10^{-3}\%$ of total energy in the system even for the shortest preload duration of 1 s. That is less than 0.1% and indicates a steady-state solution. Some oscillations can be seen in the heated beam mid-span displacement and axial force results for preload application durations up to 32 s in BM1, BM2 and BM4. However, their amplitudes are very low - up to 0.01 mm (BM1), 0.007 mm (BM2) and 0.06 mm (BM4) for displacements, and up to 115 N (BM1), 10 N (BM2) and 150 N (BM4) for axial forces for a preload time of 1 s. Thus, the impact of the preload duration (t_{pre}) can be considered to be negligible for these benchmarks.

On the other hand, for BM3-A and BM3-B, the results show a much higher sensitivity of the heated beam mid-span displacements and axial forces with varying preload application duration. The kinetic energy is below 5% of the internal energy for the two cases and is decreasing as expected with increasing preload duration. A steady-state solution (kinetic / internal energy < 0.1%) is only reached for preload times of 64 s (BM3-A) and 128 s (BM3-B). The resultant beam mid-span displacements and axial forces show oscillations and average values changing with time even after preload. Unlike in BM1, BM2 and BM4, for BM3 the displacements and axial forces do not oscillate around a similar steady-state solution for varying preload durations. This may be due to the less confined boundary conditions in the model as vertical restraint is only provided at the centre of the concrete slab with continuity restraint conditions around the edges and due to the larger mass. Large slab mass and displacement rate contribute to higher inertia effects. In addition, the steady-state displacement solution for the highest preload time of 64 s is similar for both cases BM3-A and BM3-B and is around 3.1 mm. However, the difference in the axial forces is quite high, approx. 10 kN, considering that both cases represent the same benchmark problem.

When damping is applied, the kinetic energy in all cases is close to 0%. Results do not indicate any oscillations and show a nearly perfect steady-state solution. This solution in cases BM1, BM2 and BM4 is almost identical to results where damping was not applied. Nevertheless, this is not the case for BM3. The damping solution differs by up to 5 kN and 2 kN when compared to the solution with no damping for cases BM3-A and BM3-B, respectively.
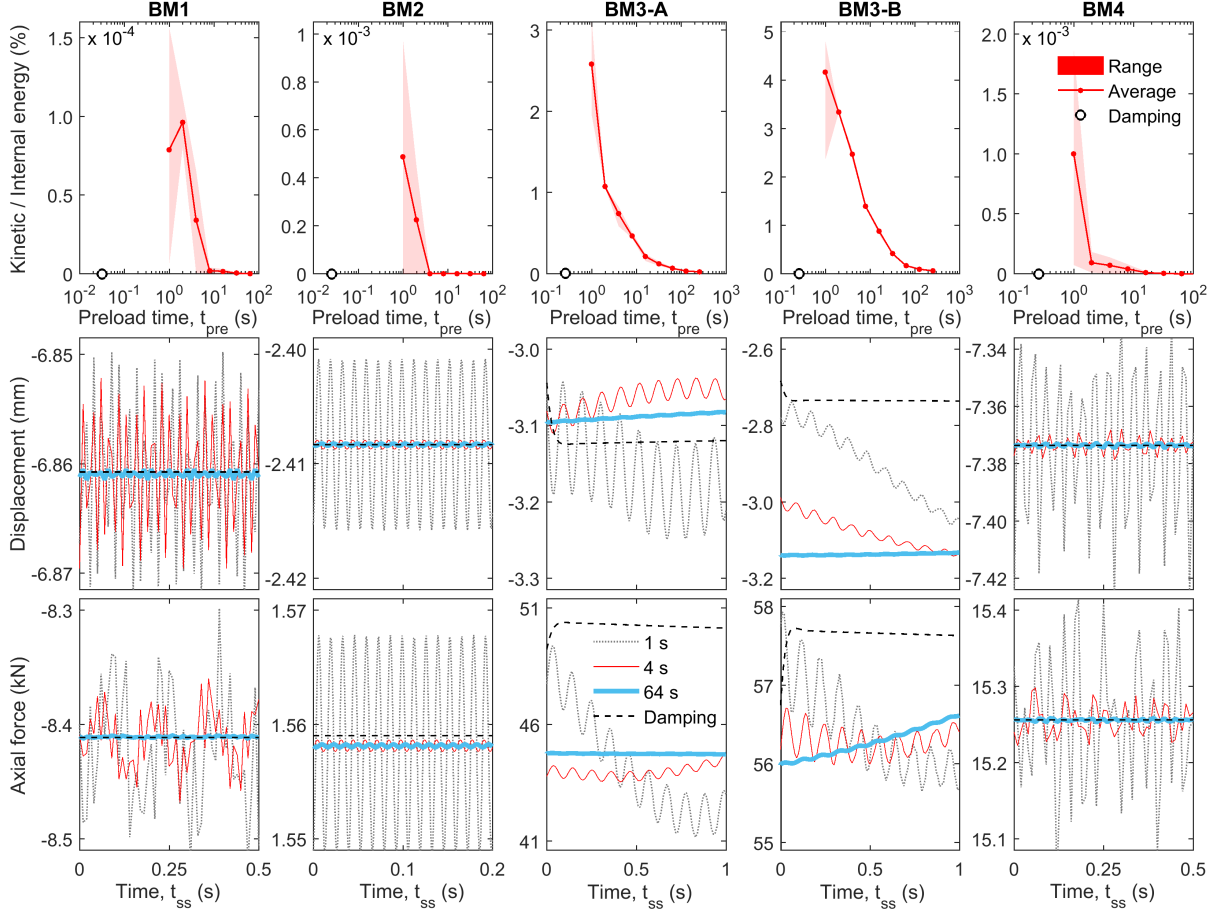
Figure 3.8: Variation of the kinetic to internal energy ratio with preload application time (top), and the effect of preload application time on displacement (middle), and axial force (bottom) for all benchmark cases. Displacements and axial forces shown are during 1 s (t_{ss}) after the preload was applied and kept constant. Plotted data is of the following structural members: BM2 - beam mid-span displacement and axial force; BM3 - heated beam mid-span displacement and axial force; and BM4 - mid-span displacement and axial force of the ground floor edge beam.

Effect of thermal load

The variation of the relative error, the kinetic energy ratio for 95% of the time, displacement and axial force with preload and thermal load application duration are shown in Fig. 3.9. The relative error is based on the results of the case with longest preload (i.e. 32 s) and longest thermal load (i.e. 512 s) application duration for each benchmark. This is because for this case the inertia effects are the smallest and the solution is expected to be the one that is closest to quasi-static. It can be seen from Fig. 3.9 that thermal load duration induces larger inertia forces in the system compared to preload duration (see Fig. 3.8). For the same application duration of static and thermal load of 1 s kinetic energy excited in the system for the latter is between 0.3 and 450% for all cases, while for static load it is only between 1×10^{-5}% and 5% of the internal energy.

The quasi-static solution based on the kinetic to internal energy ratio criteria ($< 5\%$) is reached for the time scale factor of 100 (BM1) and heating durations of 0.5 s (BM2), and 1 s (BM4) (see Table 3.2). However, axial forces for cases BM1, BM2 and BM4 indicate dynamic oscillations even though kinetic to internal energy ratio is below 5% for a time scale factor of 1000 (BM1) and a thermal load duration of 1 s (BM2 and BM4). Based on the relative error and convergence of the results a quasi-static solution is only reached for a time scale factor of 100 (BM1) and heating duration of 16 s (BM2 and BM4). At these values kinetic energy ratio is less than 0.01%. This indicates that the generally applied ad-hoc rule that the kinetic to internal energy ratio needs to generally be less than 5% to achieve a quasi-static solution might be too high for structural analysis in case of fire although further research would be required to make generalised conclusions.

Table 3.2: Quasi-static solution details based on the kinetic to internal energy ratio criteria ($< 5\%$).

Model	BM1	BM2	BM3-A	BM3-B	BM4
Thermal load application duration, t_h & t_c	100 [a]	0.5 s	128 s	128 s	1 s
Kinetic / Internal energy	0.5%	0.9%	4.5%	3.3%	2.2%
Relative error	2.3%	2.8%	7.2%	5.2%	19.2%

a. Time scale factor.

For BM3-A and BM3-B, the peak mid-span displacement and axial force do not show a clear convergence. Also, some influence of the preload duration can be seen, unlike in BM2 and BM4. Yet, this influence seems to be smaller in comparison to the effect of the thermal duration. An interesting observation is that for case BM3-A the kinetic to internal energy ratio does not decrease with higher heating duration (between 2 and 32 s) as in other cases. For BM3-A, the peak beam mid-span displacement is converging to approximately 0.06 m higher value in comparison to the results of BM3-B. This indicates a stiffer response for BM3-B due to using shared nodes for beam and shell elements. For the cases of BM3-A and BM3-B the quasi-static solution based on the kinetic energy criteria is only reached for a thermal load application duration of 128 s.

Mesh density convergence

The results for all cases assessed are shown in Fig. 3.10. Relative errors were calculated based on the difference to the finest mesh. It can be seen from Fig. 3.10 that for cases BM1, BM2 and BM4, the results converge with decreasing element size as it would be expected for a correct solution. Result convergence is reached for beam element sizes of 0.24 m, 0.05 m, and 0.5 m for cases BM1, BM2, and BM4, respectively, with relative error less than 2%. However, for case BM3 as for the time scaling study, results do not show clear convergence. In addition, for the finest mesh size, oscillations
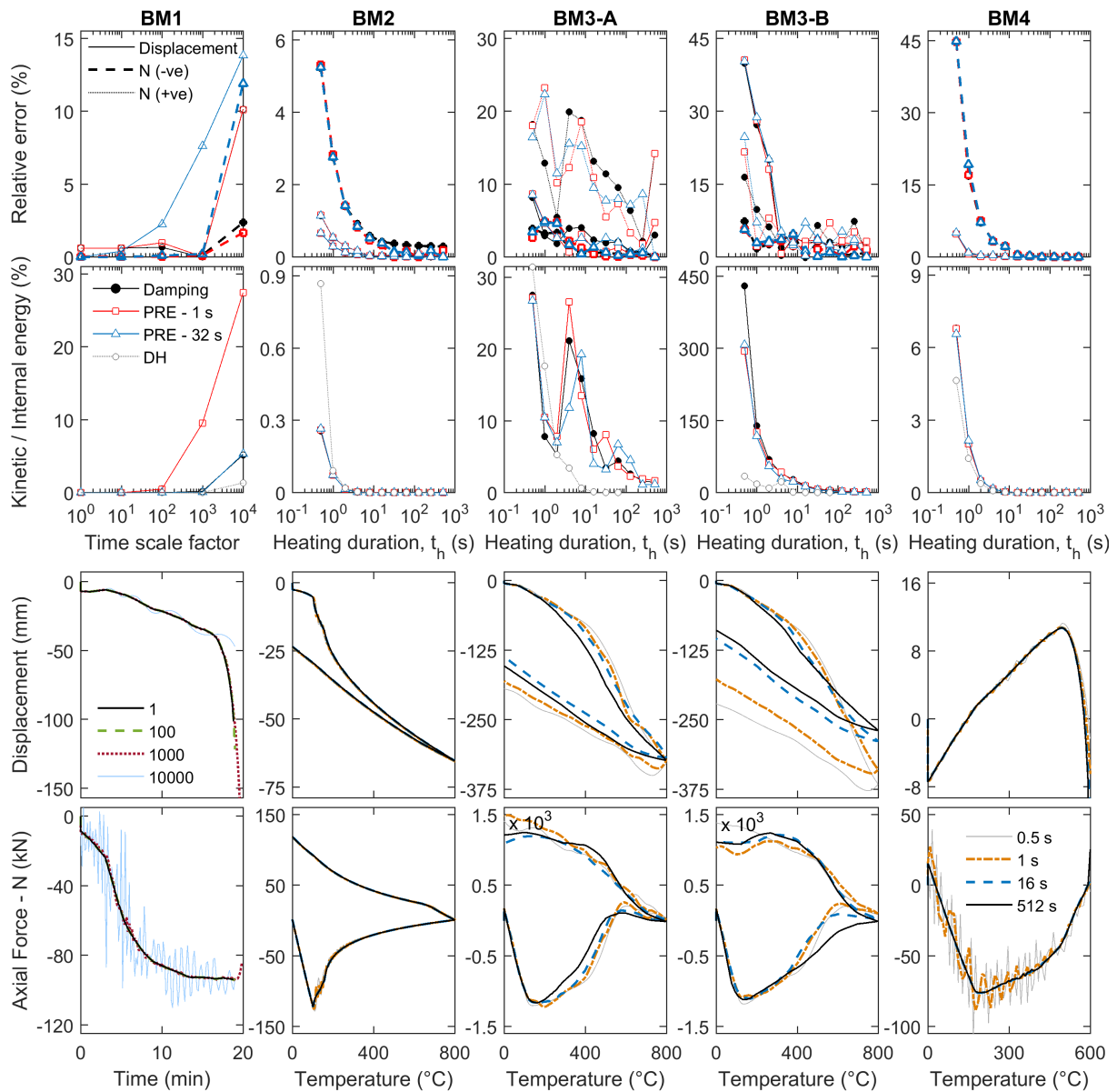
Figure 3.9: Variation of relative error of peak displacement and axial force, kinetic to internal energy ratio for 95% of the fire exposure time, displacement (preload 32 s), and axial force (preload 32 s) with preload and thermal load application duration for all benchmark cases. Plotted data is of the following structural members: BM2 mid-span displacement and axial force; BM3 heated beam mid-span displacement and axial force; and BM4 mid-span displacement and axial force of the ground floor edge beam. DH refers to the cases where damping was continued during the heating.

and instabilities (BM3 - 0.0625 m) and an early failure (BM1 0.06 m) in the axial force development can be observed. This is likely due to the development of high localised stresses because Hughes-Liu beam elements have only one integration point along the length. Therefore, with a decreasing element size the constant stress along the length would increase. There is no clear relationship between the kinetic energy in the system

and the change in element length comparing the different cases. Due to the instabilities present in the solutions for the finest mesh densities, the mesh with the beam element length of 0.25 m is selected as the "converged" solution for BM3. It should be noted that these analyses are based on capturing the global structural fire behaviour. The selected mesh densities for these problems would likely need to be different if localised responses such as concrete cracking are desired to be captured.

Effect of the number of beam element integration points

The variation of the relative errors of the beam peak mid-span displacement and axial force, kinetic energy and heated beam mid-span displacement development with the change of the integration refinement factor is shown in Fig. 3.11. The errors were calculated based on the numerical results for an integration refinement factor of 11,
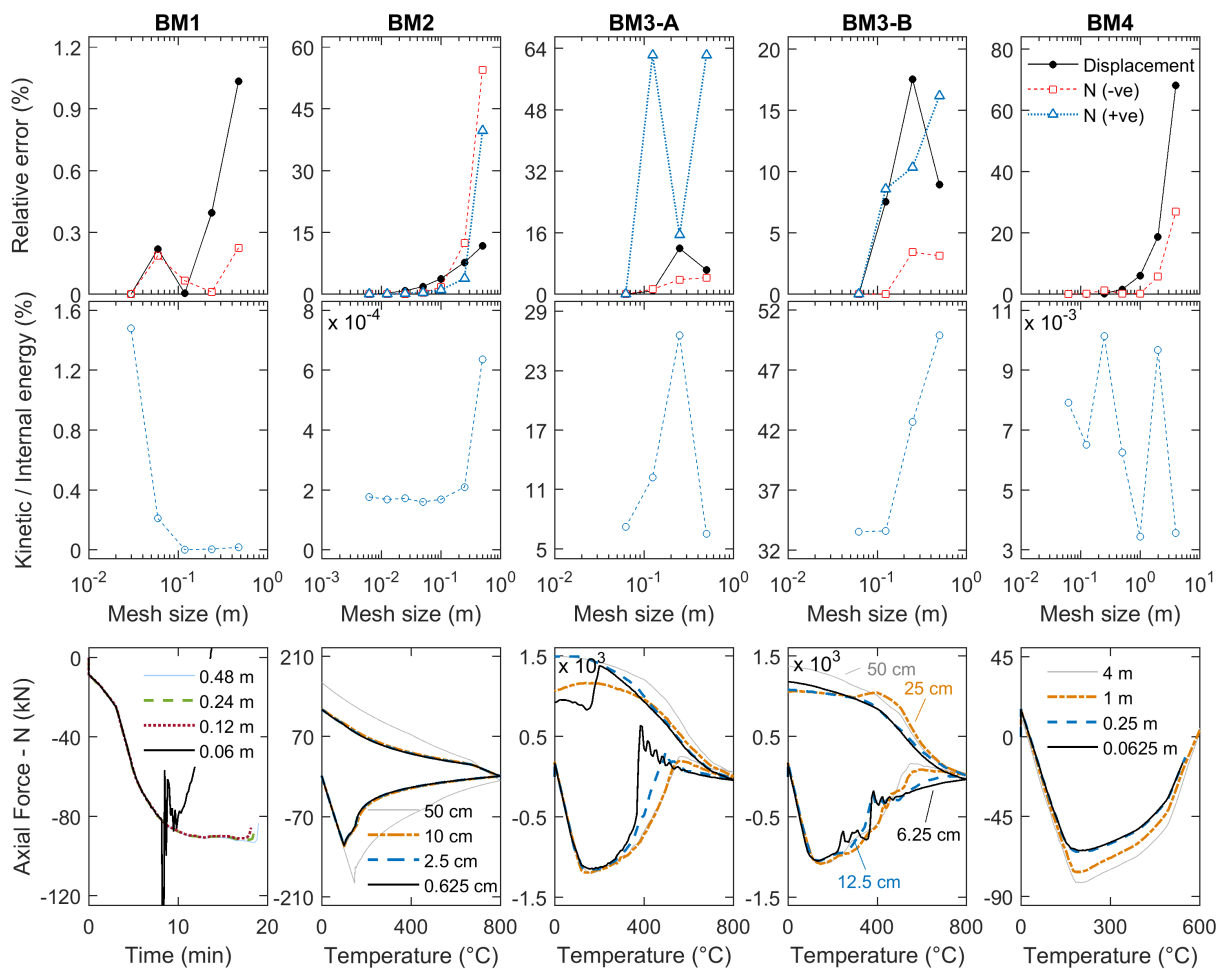

Figure 3.10: Variation of relative error of peak displacement and axial force; kinetic to internal energy ratio for 95% of the fire exposure time; and axial force with mesh size for all benchmark cases. Plotted data is of the following structural members: BM2 mid-span displacement and axial force; BM3 heated beam mid-span displacement and axial force; and BM4 mid-span displacement and axial force of the ground floor edge beam.

which includes the maximum number of fibres. For all cases except for case BM3-A, a convergence of the resultant values with an increasing integration factor can be observed. Yet, the relative errors for BM1, BM3-A, BM3-B and BM4 are small ($< 3.5\%$) as it can be seen from the development of beam mid-span displacement (Fig. 3.11). This indicates that increasing the number of beam integration points for these models (BM1, BM3, and BM4) does not improve the solution significantly. However, this is not the case for BM2. The development of beam mid-span displacement and the resultant values are affected by beam integration refinement. Convergence is only reached for a refinement factor, k, of 5 which gives a more refined solution in comparison to the case when k is 0. In the cases with $k = 1$ and $k = 3$ relative error reaches up to 20%. Thus, in some cases integration factor has to be carefully chosen in order to obtain conservative results.

The kinetic energy in all cases shows negligible variation with the change in the
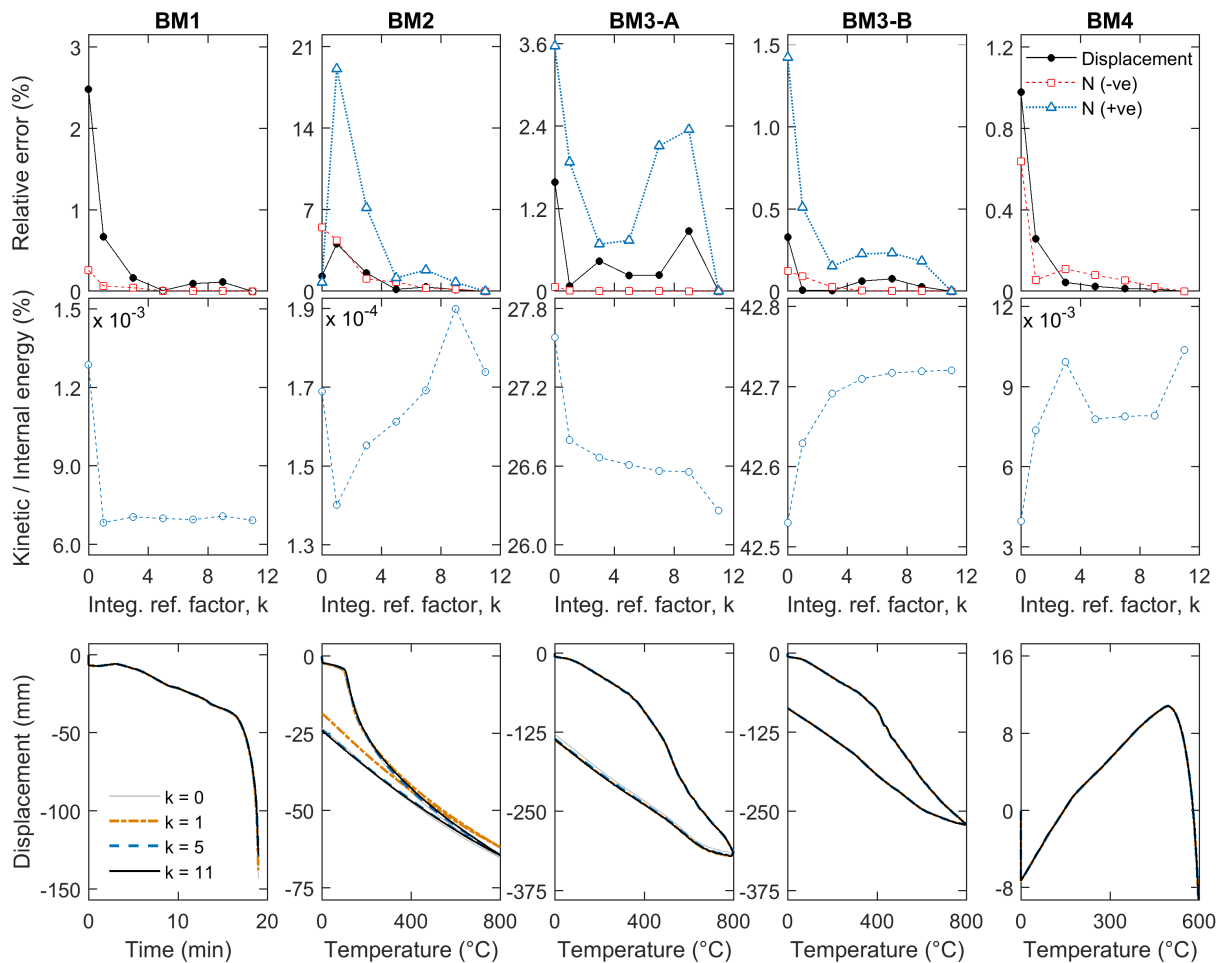
Figure 3.11: Variation of relative error of peak displacement and axial force (N), kinetic to internal energy ratio for 95% of the fire exposure time, and displacement development with beam integration refinement factor, k, for all benchmark cases. Plotted data is of the following structural members: BM2 mid-span displacement; BM3 heated beam mid-span displacement; and BM4 mid-span displacement of the ground floor edge beam.

number of beam integration points. The maximum difference is less than 1.5%. This indicates that the number of beam cross-section integration points is unlikely to affect the inertia of the model. It should be noted that if there is a scenario such that the response is significantly underestimated with a chosen number of integration points, this assumption may need to be reassessed.

Effect of the number of shell element integration layers

The variation of the key structural variables with the number of shell element integration layers is shown in Fig. 3.12. The relative errors, as in the previous sections, have been calculated based on the outcome for the model with the largest number of shell element through-thickness integration layers (i.e. 11). The results show a convergence with an increasing number of slab layers. The difference in the peak axial forces between the models with lowest and highest number of slab layers is up to 75% and 39% for BM3-A and BM3-B, respectively. However, these high values of error may be misleading. The cases with the number of shell element through-thickness integration layers between 5 and 11 have significantly higher values of kinetic energy present in the system compared to the models with only 3 integration layers. The differences in kinetic energy are between 12.5 to 16% (BM3-A) and 6 to 12% (BM3-B) of the internal energy. This indicates sufficiently larger inertia that could influence the results. On the other hand, the axial force development for the 3 integration layers indicates some instabilities between

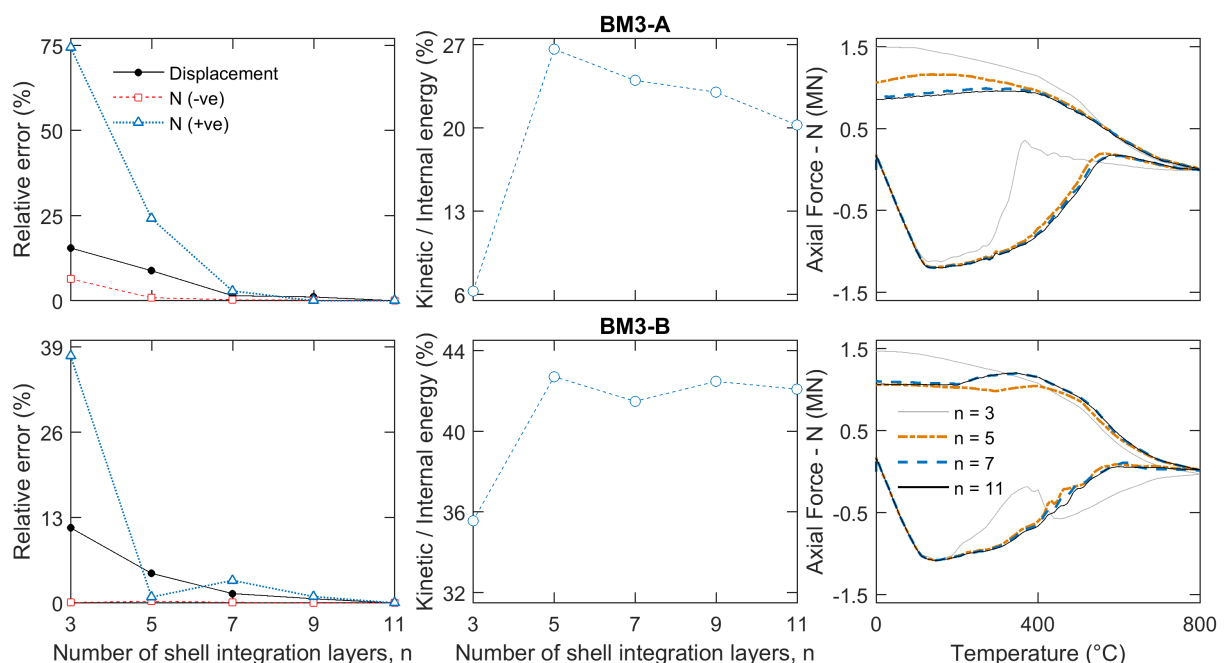**Figure 3.12**: Variation of relative error of peak displacement and axial force, kinetic to internal energy ratio for 95% of the fire exposure time, and heated beam axial force development with number of shell element integration layers for BM3-A (top) and BM3-B (bottom).

temperatures of 300 and 400°C. Thus, for the purposes of this study the convergence is assumed to be reached for 7 shell element integration layers. Though, for the final model 5 layers have been chosen for the reasons of computational efficiency.

3.4.2 Benchmarking of LS-DYNA

In this section, the final results for each benchmark case obtained with LS-DYNA are presented and compared with the results published by Cooke and Latham [28], Santiago et al [30], Gillie [31], and Rackauskaite and El-Rimawi [32]. Based on the time scaling and parameter sensitivity studies, the final model parameters were chosen and are shown in Table 3.3. The parameters were determined based on the convergence of results and computational time efficiency. The results for BM1, BM2, BM3, and BM4 are shown in Fig. 3.13, Fig. 3.14, Fig. 3.17, and Fig. 3.18, respectively. The LS-DYNA final solution errors in respect to other software packages and/or experimental results are summarised in Table 3.4.

Table 3.3: Final model parameters used for the LS-DYNA simulations.

Model	Preload duration, t_{pre}	Thermal load application duration, t_h & t_c	Element length	Beam integration refinement factor, k	Number of shell through thickness integration points
BM1	1 s	100 (time scale factor)	∼0.25 m	5	n/a
BM2	0.026 s (damping)	16 s	0.01 m	5	n/a
BM3-A	32 s	512 s	0.25 m	5	5
BM3-B	32 s	512 s	0.25 m	5	5
BM4	1 s	32 s	1 m [a]	0	n/a

a. Element length used in [32].

Benchmark BM1 represents the experiment on the 2D steel frame heated until failure. The results shown in Fig. 3.13 show a good agreement between the LS-DYNA solution and the experimental results [28] for the beam mid-span deflection and deflected shape of the frame at 16 min. Predictions from LS-DYNA on the deflections also compare well with other software packages (CEFICOSS [29], SAFIR and Abaqus [30]) and indicate a conservative solution. However, in comparison to the latter software packages, LS-DYNA underestimates peak axial forces by approximately 30 kN (25%). The sensitivity study presented in the previous sections indicates that there is very little or no influence from the investigated parameters on the development of axial forces. Therefore, LS-DYNA errors in comparison with other software packages could be associated with the inherent assumptions in the programs and the element types used to represent the support from the secondary framework. In the case without the lateral support (i.e. that discrete elements are not used), LS-DYNA underestimates peak axial forces by only approximately 2.9 to
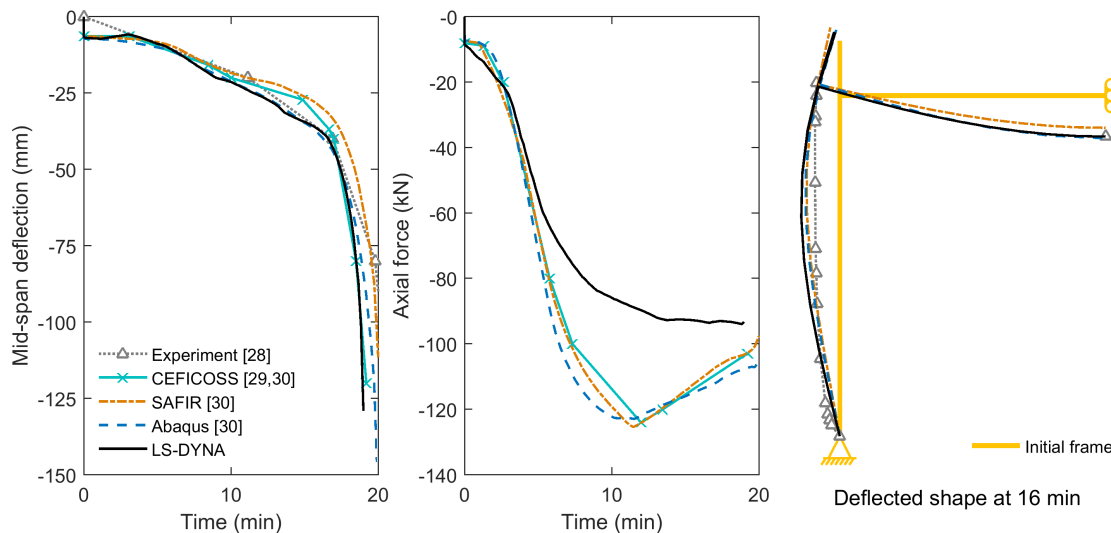
Figure 3.13: Comparison of the experimental BM1 results [28] and finite element analysis results from CEFICOSS, SAFIR and Abaqus [29, 30] with results obtained using LS-DYNA. Variation of heated beam mid-span deflection (left) and axial forces (middle) with temperature and the deflected shape of the frame at 16 min. Deflected shape scale factor is 10.

4.3 kN (6.7 to 11.7%) in comparison with CEFICOSS, SAFIR and Abaqus [30].

In benchmark BM2 a single rectangular steel beam with 75% restraint was heated and then cooled. For the BM2 model as seen in Fig. 3.14 LS-DYNA predicts well the development of heated beam mid-span displacements and axial forces with temperature in comparison to other software packages (Abaqus, Vulcan, and Ansys [31]). Unlike in BM1, in BM2 the peak axial force predicted with LS-DYNA is within the same range as predicted by other software packages with the LS-DYNA solution being closest to the Abaqus explicit-dynamic solution. A comparison of the results from LS-DYNA and Abaqus for varying support stiffness is shown in Fig. 3.15. The results indicate that with the final chosen model parameters, LS-DYNA is able to predict well the development of deflections and axial forces for all restraint levels except for the 0 to 10%. For the latter cases high dynamic oscillations occur indicating large inertia effects for very low restraint levels. An interesting observation is that for these cases inertia effects could only be dissipated to achieve a quasi-static solution as in Abaqus by applying damping during the heating duration (see Fig. 3.15). The comparison of the kinetic to internal energy ratios (see Fig. 3.16) shows a significant reduction (a factor up to 30,000) in kinetic energy in the system when damping (see Section 3.3.1) is applied for cases with low restraint levels (0 to 10%). Results shown in Fig. 3.16 also indicate that the application of damping during the heating duration may not always be the most effective or efficient solution. For restraint levels higher than 10% solutions with damping have very similar level of kinetic energy in the system as solutions without damping. The maximum difference in kinetic to internal energy ratio is up to 6×10^{-5}%.
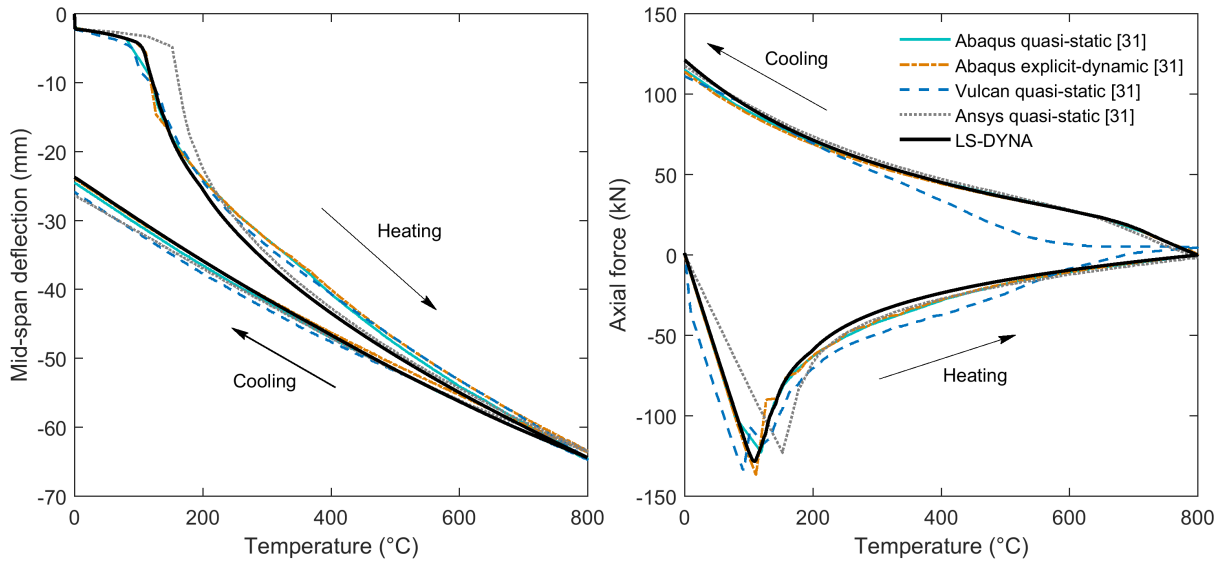
Figure 3.14: Comparison of BM2 results published by Gillie [31] with results obtained using LS-DYNA. Variation of heated beam mid-span displacement (left) and axial forces (right) with temperature. Support restraint stiffness - 75% of the axial stiffness of the beam.
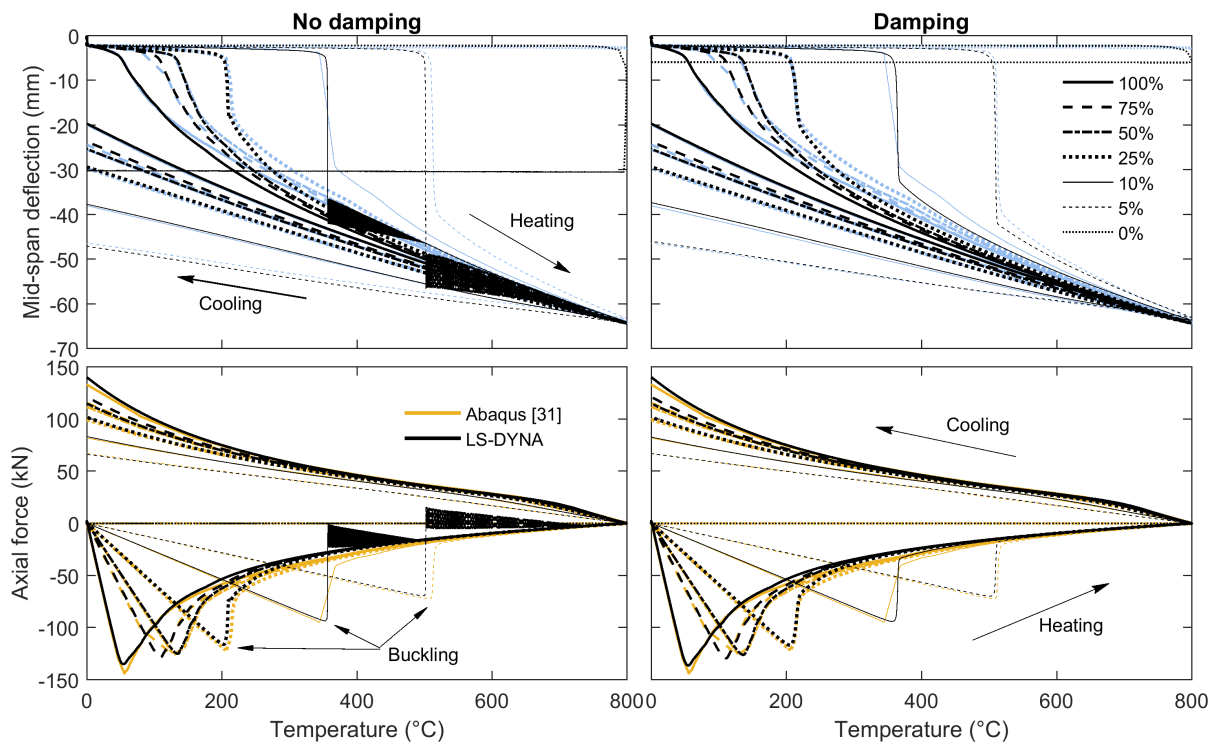
Figure 3.15: Comparison of BM2 results published by Gillie [31] with results obtained using LS-DYNA for varying levels of support restraint stiffness. Variation of heated beam mid-span displacement and axial forces with temperature for the models without (left) and with (right) damping (see Section 3.3.1) included during heating.
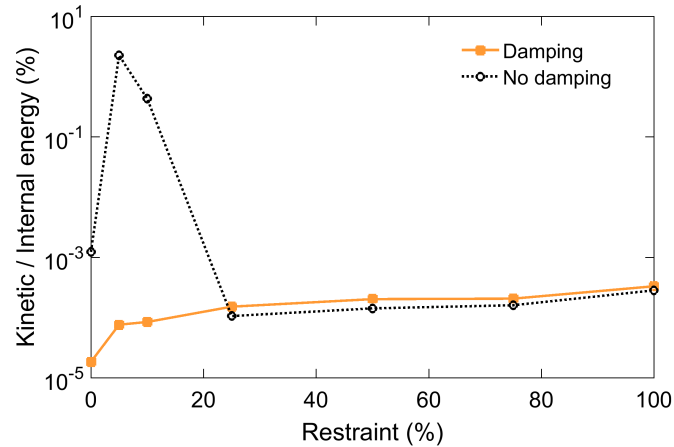
Figure 3.16: Variation of the kinetic to internal energy ratio for 95% of the fire exposure time with varying levels of support restraint stiffness for the models with and without damping included during heating.
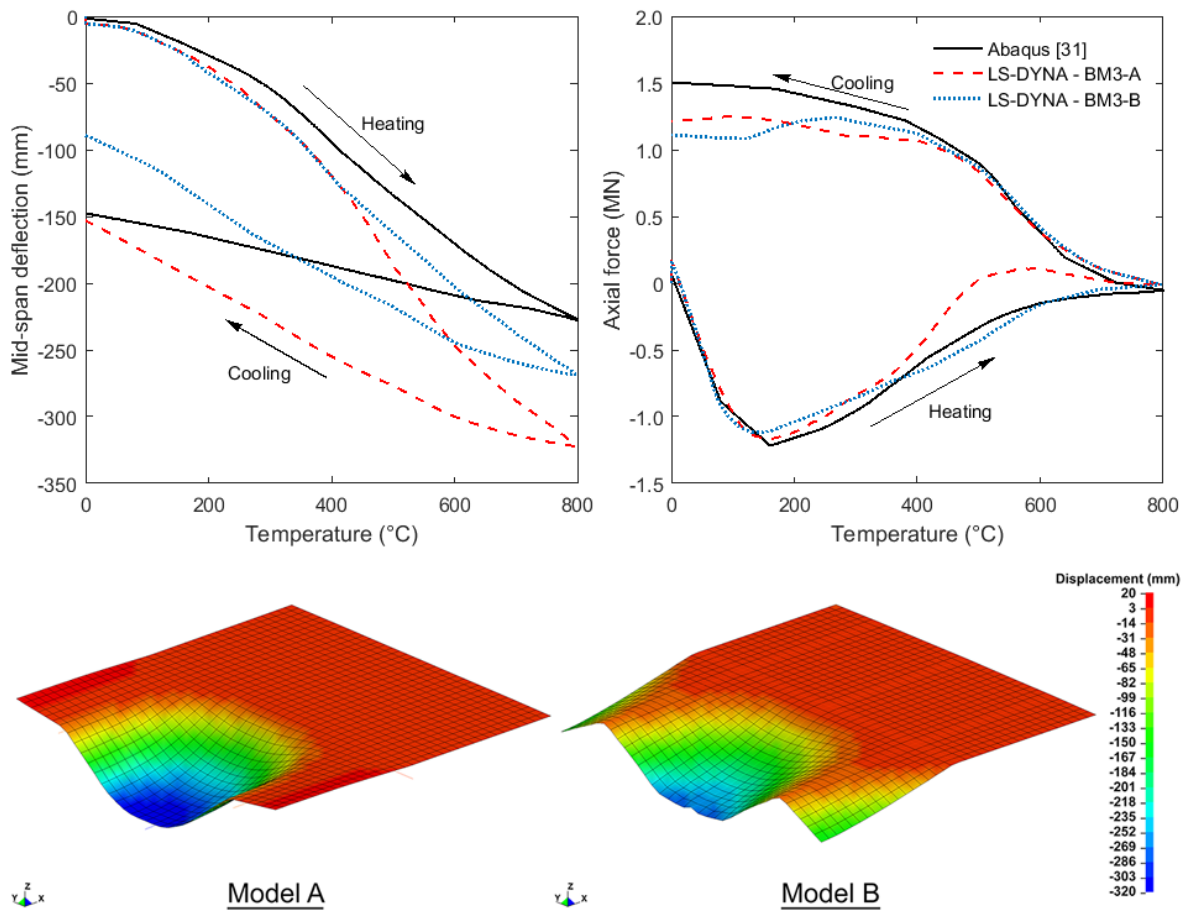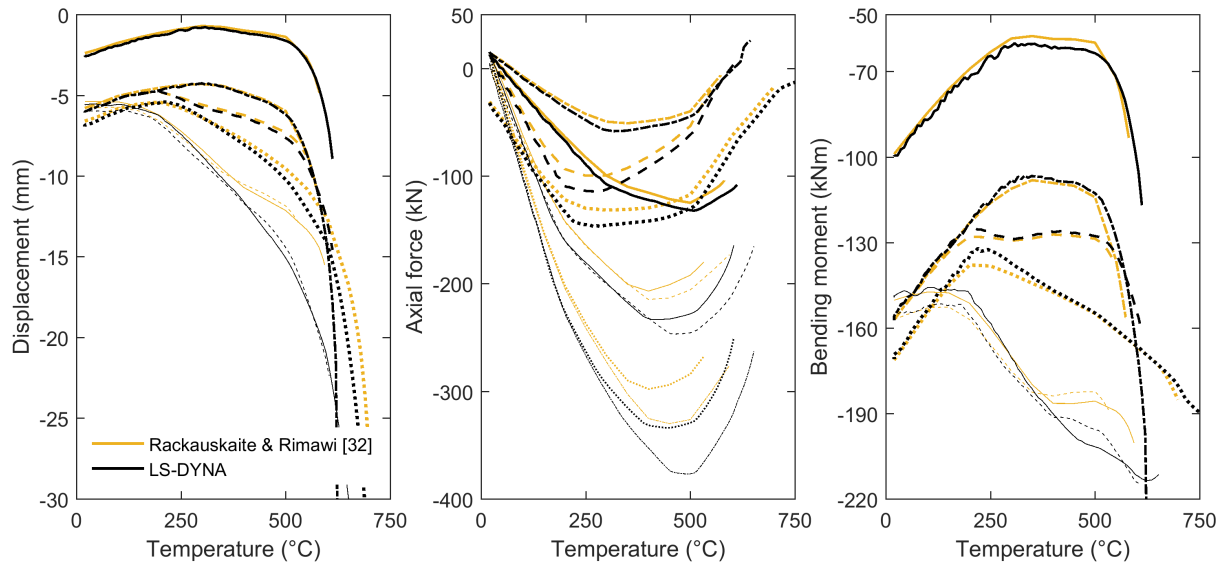

Figure 3.17: Comparison of BM3 results published by Gillie [31] with results obtained using LS-DYNA models BM3-A and BM3-B. Variation of the heated beam mid-span displacement and axial forces with temperature (top), deflected shape at the end of heating from LS-DYNA model (bottom). Displacement scale factor is 5.

In benchmark BM3, part of the composite concrete floor slab and the supporting beams was heated and then cooled. For BM3, the LS-DYNA prediction in comparison to the prediction by Abaqus [31] is worse than for BM1 and BM2 (see Fig. 3.17). While LS-DYNA is able to predict the development of axial forces during the heating for BM3, it underestimates the values during cooling below the temperature of 400°C. LS-DYNA is unable to capture the peak axial force of approximately 1.5 MN at the end of cooling. The predicted values are 293 kN (19%) and 394 kN (26%) lower for BM3-A and BM3-B, respectively. Interestingly, this value has been captured by the model with the lower value of shell through-thickness integration points (i.e. 3) (see Fig. 3.12). Comparing models BM3-A and BM3-B, the latter one gives a closer prediction of axial force development in the beam during heating in comparison to Abaqus. In BM3-B a shared node between beam and shell elements was used to represent the composite action. Both BM3 models (A and B) show significantly higher beam mid-span deflection development values than Abaqus. Displacement results using BM3-A and BM3-B models are by up to approximately 1.4 and 1.2 times higher, respectively, compared to Gillies [31] results. Thus, in the terms of deflections LS-DYNA solution can be considered as conservative.

The differences in LS-DYNA and Abaqus solutions could be due to different inherent assumptions in the analysis programs or input parameters used. No details of the input file for Abaqus [31] for BM3 have been published. Moreover, some details on the benchmark were not clearly defined in [31], for example, the location of steel rebar in the concrete slab and whether the self-weight of the members is to be included. Considering the uncertainty in the benchmark itself, Abaqus parameters used for the analysis, and significant sensitivity of the LS-DYNA solution to various parameters investigated in this chapter, it is difficult to identify more specific reasons for the differences in LS-DYNA and Abaqus solutions. In addition, LS-DYNA models BM3-A and BM3-B at the end of heating give considerably different deflected shapes, especially in the bays adjacent to the heated slab. Deflections in these unheated bays in BM3-B are almost as high as in the heated part of the slab and thus they do not seem to be realistic. Gillie [31] has not published the deflected shape of the whole model for benchmarking.

In benchmark BM4 various bays of the 3 storey × 3 bay 2D steel frame [32] were subjected to heating. The comparison of the results from [32] and the LS-DYNA solution for the different cases is shown in Fig. 3.18. For most localised fire cases the results show a good agreement. The development of the beam mid-span displacements and bending moments is almost identical in LS-DYNA and [32]. For axial forces LS-DYNA produces slightly higher axial forces (up to approximately 15 kN or 15% for cases A to D), but they can be considered to be conservative. Also, the trend of axial force development is the same in the results produced by LS-DYNA and [32]. Nevertheless, for the BM4 cases where the top floor and middle floors were heated, even though LS-DYNA predicts similar general trends as in [32], the values predicted after a temperature of approximately 350°C are considerably higher than in [32]. At the temperature of 500°C the difference in

the displacement, axial force, and bending moment values is up to 2.94 mm (24%), 47.3 kN (16%), and 16.1 kNm (9%), respectively. It is difficult to judge which model gives a better prediction but the results from LS-DYNA seem to be more conservative.

Figure 3.18: Comparison of BM4 results published by Rackauskaite and El-Rimawi [32] with results obtained using LS-DYNA. Variation of heated beam mid-span displacement (left), axial forces (middle) and bending moments (right) with temperature. For the references of beams in the frame refer to [32].

Considering all four cases, LS-DYNA is shown to be capable of predicting the general behaviour of structures subjected to fire and to capture key phenomena such as the effects of material and geometric non-linearity, restraint conditions and stress redistribution. The maximum differences between LS-DYNA and other numerical analysis programs are up to 28% (42% for BM3-A) and 25%, for the prediction of deflections and axial forces, respectively (see Table 3.4). The highest differences are observed for the cases where symmetry or continuity boundary conditions were used (i.e. BM1 and BM3). In general, any discrepancies are likely of numeric nature due to the differences in finite element packages and their algorithms and are within acceptable limits. During cooling predictions are slightly worse and thus, LS-DYNA should be used cautiously when cooling is considered until further research is carried out. In some of the cases in order to achieve stable results and eliminate the effects of inertia long scaled heating durations had to be used. This led to very long computational times, which might be unpractical sometimes. This could be overcome by using mass scaling. However, mass scaling should be used carefully. If it is too large additional inertia might be excited, which might have a significant influence on the final result.

Table 3.4: Comparison of the final LS-DYNA solution with other software packages and/or experimental results for all benchmark cases.

Model	BM1 - LS-DYNA	Experiment	CEFICOSS	SAFIR	Abaqus	BM2 - LS-DYNA	Abaqus quasi-static	Abaqus explicit dynamic	Vulcan quasi-static	Ansys quasi-static	BM3-A - LS-DYNA	Abaqus	BM3-B - LS-DYNA	Abaqus	BM4 (Case B) - LS-DYNA	FEM	BM4 (Case C) - LS-DYNA	FEM
Axial force (kN) [a]	94	n/a	124	125	123	128	123	137	134	123	1164	1216	1118	1216	58	51	132	125
Axial force error [a]		-	24%	25%	24%		4%	6%	4%	4%		4%		9%		15%		6%
Average relative error		-	21%	20%	25%		8%	8%	98%	22%		207%		190%		24%		11%
50% of the time		-	21%	21%	24%		4%	5%	31%	11%		16%		12%		14%		7%
75% of the time		-	24%	26%	30%		13%	12%	99%	26%		91%		27%		17%		9%
95% of the time		-	28%	29%	53%		18%	16%	329%	56%		170%		160%		53%		19%
Displacement (mm) [b]	42.9	40.0	39.2	33.4	44.1	64.4	64.6	63.6	64.7	63.5	322.1	227.6	268.8	227.6	6.2	6.0	1.6	1.4
Displacement error [b]		7%	9%	28%	3%		0.1%	0.1%	0.1%	0.1%		42%		18%		4%		18%
Average relative error		21%	11%	22%	7%		3%	3%	5%	11%		39%		27%		2%		11%
50% of the time		9%	10%	19%	3%		2%	2%	4%	1%		38%		19%		2%		11%
75% of the time		20%	14%	30%	10%		4%	4%	7%	4%		43%		32%		3%		16%
95% of the time		96%	25%	43%	26%		10%	10%	14%	35%		84%		90%		4%		18%

a. Maximum compressive axial force for BM1, BM2, BM3, and BM4.

b. BM1 – displacement at 16.92 min, BM2 and BM3 – maximum displacement, and BM4 – displacement at 500°C.

Average relative error and 50%, 75%, and 95% of the time represent relative errors over the whole or specified percentage (calculated as in Appendix 3.A) of heating and cooling duration.

3.5 Conclusions

In recent years, LS-DYNA has grown considerably in research and industry uses for the analysis of whole structures in fire. However, a benchmarking of the explicit dynamic solver of LS-DYNA for structural fire analysis has not been published in literature. Thus, in this chapter, a benchmarking study of the explicit dynamic solver of LS-DYNA for the analysis of the structural response in fire and a model parameter sensitivity and convergence to quasi-static solution studies have been carried out. Four different canonical problems have been modelled in LS-DYNA based on various experimental and numerical studies published in the literature.

The results of this study indicate that the explicit dynamic solver of LS-DYNA is able to capture the key phenomena of heated structures. For all the benchmarks, it is able to predict the development trends of displacements, axial forces, and bending moments with increasing temperature within acceptable level of accuracy. However, during cooling in the composite concrete slab model, the LS-DYNA solution differs from the published results below the temperature of 400°C and is less conservative in predicting tensile axial forces. It is unknown whether this is because of the inherent assumptions in LS-DYNA or whether it is related to different input used. The predictions for the rectangular steel beam (BM1) during cooling compare well with other software packages which implies that LS-DYNA correctly captures the unloading behaviour of the steel material during cooling.

The time scaling sensitivity study indicated that inertia effects generated during the application of the thermal load to the system have a more significant influence on the final result of the LS-DYNA explicit solution than preloading due to static loads. The high variation in the results and kinetic energy with different parameters, especially for the composite concrete floor slab case, highlights that an extensive parameter sensitivity study has to be carried out for every model to ensure that the LS-DYNA solution converges and is quasi-static. In addition, the time scaling study shows that the generally applied ad-hoc rule in explicit dynamic analysis that the kinetic to internal energy ratio for the most of the time has to be less than 5% to achieve a quasi-static solution might be too high for structural analysis in case of fire for LS-DYNA.

In this study LS-DYNA (Release 7.1.1) version was used. It should be noted that results obtained using a different LS-DYNA version might be to some extent different. Thus, it should be used cautiously and the model should be benchmarked before carrying out the analysis of interest. Additionally, further research is required to assess other element types such as solid elements or formulations of beams or shell elements different to those examined in this chapter.

Acknowledgements

References

[1] V. K. R. Kodur, M. Garlock, and N. Iwankiw, "Structures in Fire: State-of-the-Art, Research and Training Needs," *Fire Technology*, vol. 48, pp. 825–839, oct 2012.

[2] A. Haksever, "Fire response of total systems in a local fire," *Fire Safety Journal*, vol. 4, pp. 141–146, jan 1981.

[3] J. A. Purkiss, "Developments in the fire safety design of structural steelwork," *Journal of Constructional Steel Research*, vol. 11, pp. 149–173, jan 1988.

[4] J. C. M. Forrest, "The whole structure," in *The International Conference on Design of Structures Against Fire* (R. D. Anchor, H. L. Malhotra, and J. A. Purkiss, eds.), (Birmingham), pp. 111–125, Elsevier Applied Science Ltd., 1986.

[5] British Steel, "The Behaviour of Multi-Storey Steel Framed Buildings in Fire," tech. rep., British Steel, Rotherham, 1999.

[6] Vulcan-Solutions, "Comparisons against experimental and clasical results."

[7] J.-M. Franssen, "SAFIR: A thermal-structural program for modelling structures under fire," *Engineering Journal*, vol. Q3, pp. 143–158, 2005.

[8] R. Sun, Z. Huang, and I. W. Burgess, "The collapse behaviour of braced steel frames exposed to fire," *Journal of Constructional Steel Research*, vol. 72, pp. 130–142, may 2012.

[9] J. Jiang, L. Jiang, P. Kotsovinos, J. Zhang, and A. Usmani, "OpenSees Software Architecture for the Analysis of Structures in Fire," *Journal of Computing in Civil Engineering*, vol. 29, no. 1, pp. 1–13, 2015.

[10] J. Jiang and A. Usmani, "Modeling of steel frame structures in fire using OpenSees," *Computers & Structures*, vol. 118, pp. 90–99, mar 2013.

[11] V. K. R. Kodur and M. Z. Naser, "Effect of shear on fire response of steel beams," *Journal of Constructional Steel Research*, vol. 97, pp. 48–58, jun 2014.

[12] W.-Y. Wang and G.-Q. Li, "Fire-resistance study of restrained steel columns with partial damage to fire protection," *Fire Safety Journal*, vol. 44, pp. 1088–1094, nov 2009.

[13] M. Gillie, A. S. Usmani, and J. M. Rotter, "A structural analysis of the first Cardington test," *Journal of Constructional Steel Research*, vol. 57, pp. 581–601, jun 2001.

[14] H. Yang, F. Liu, S. Zhang, and X. Lv, "Experimental investigation of concrete-filled square hollow section columns subjected to non-uniform exposure," *Engineering Structures*, vol. 48, pp. 292–312, 2013.

[15] F. Wald, I. W. Burgess, L. Kwasniewski, K. Horová, and E. Caldova, eds., *Benchmark studies. Experimental validation of numerical models in fire engineering.* Prague: CTU Publishing House, Czech Technical University, 2014.

[16] F. Wald, I. W. Burgess, L. Kwasniewski, K. Horová, and E. Caldova, eds., *Benchmark studies. Verification of numerical models in fire engineering.* Prague: CTU Publishing House, Czech Technical University, 2014.

[17] G. Flint, *Fire Induced Collapse of Tall Buildings.* Doctor of philosophy, University of Edinburgh, 2005.

[18] S. Selamet, "The impact of fire scenario to the collapse of a tall structure," in *SEMC Fifth International Conference on Structural Engineering, Mechanics and Computation. 2 - 4 September, 2013*, (Cape Town, South Africa), pp. 711–716, 2013.

[19] S. A. Kilic and S. Selamet, "Symmetric and Asymmetric Collapse Mechanisms of a Multi-Story Steel Structure subjected to Gravity and Fire," in *Structures Congress 2013*, (Reston, VA), pp. 2545–2554, American Society of Civil Engineers, apr 2013.

[20] A. Law, P. Kotsovinos, and N. Butterworth, "Engineering geometrically bi-linear columns to deliver fire resistance: Standard heating," *Engineering Structures*, vol. 100, pp. 590–598, oct 2015.

[21] I. Both, K. Ostapska, L. Kwasniewski, R. Zaharia, and D. Dubina, "Composite column subjected to compression and fire.," in *Benchmark studies: Verification of numerical models in fire engineering* (F. Wald, I. Burgess, L. Kwasniewski, K. Horová, and E. Caldova, eds.), pp. 196–201, Prague: CTU Publishing House, Czech Technical University, 2014.

[22] L. Kwaśniewski, F. Ali, and M. Balcerzak, "Coupled Structural-thermal Calculations for Restrained Steel Columns in Fire," *Journal of Structural Fire Engineering*, vol. 4, pp. 59–70, mar 2013.

[23] LSTC, *LS-DYNA Keyword User's Manual, Volumes I to III (Version R7.1).* Livermore: Livermore Software Technology Corporation (LSTC), 2014.

[24] A. Irfanoglu, "Using Numerical Simulations and Engineering Reasoning under Uncertainty: Studying the Collapse of WTC-1," *Computer-Aided Civil and Infrastructure Engineering*, vol. 27, pp. 65–76, jan 2012.

[25] T. P. McAllister, F. Sadek, J. L. Gross, S. Kirkpatrick, R. A. MacNeill, R. T. Bocchieri, M. Zarghamee, O. O. Erbay, and A. T. Sarawit, "Structural Analysis of Impact Damage to World Trade Center Buildings 1, 2, and 7," *Fire Technology*, vol. 49, pp. 615–642, jul 2013.

[26] Arup, "Benchmarking and validation for LS-DYNA. Internal report.," tech. rep., 2013.

[27] ASTM, "ASTM E176-15ae1 Standard Terminology of Fire Standards," tech. rep., ASTM International, West Conshohocken, PA, 2015.

[28] G. M. E. Cooke and D. J. Latham, "The inherent fire resistance of a loaded steel framework," *Steel Construction Today*, vol. 1, pp. 49–58, 1987.

[29] J.-M. Franssen, G. M. E. Cooke, and D. J. Latham, "Numerical simulation of a full scale fire test on a loaded steel framework," *Journal of Constructional Steel Research*, vol. 35, pp. 377–408, jan 1995.

[30] A. Santiago, C. Haremza, F. Lopes, and J.-M. Franssen, "Numerical behaviour of steel columns under localized fire loading.," in *Benchmark studies: Experimental validation of numerical models in fire engineering* (F. Wald, I. Burgess, L. Kwasniewski, K. Horová, and E. Caldova, eds.), pp. 60–72, Prague: CTU Publishing House, Czech Technical University, 2014.

[31] M. Gillie, "Analysis of heated structures: Nature and modelling benchmarks," *Fire Safety Journal*, vol. 44, pp. 673–680, jul 2009.

[32] E. Rackauskaite and J. A. El-Rimawi, "A Study on the Effect of Compartment Fires on the Behaviour of Multi-Storey Steel Framed Structures," *Fire Technology*, vol. 51, pp. 867–886, sep 2015.

[33] J. O. Hallquist, *LS-DYNA theory manual.* Livermore Software Technology Corporation, 2006.

[34] I. W. Burgess, J. A. El-Rimawi, and R. J. Plank, "A secant stiffness approach to the fire analysis of steel beams," *Journal of Constructional Steel Research*, vol. 11, pp. 105–120, jan 1988.

[35] J. A. El-Rimawi, I. W. Burgess, and R. J. Plank, "The analysis of semi-rigid frames in firea secant approach," *Journal of Constructional Steel Research*, vol. 33, pp. 125–146, jan 1995.

[36] J. A. El-Rimawi, I. W. Burgess, and R. J. Plank, "Studies of the Behaviour of Steel Subframes with Semi-rigid Connections in Fire," *Journal of Constructional Steel Research*, vol. 49, pp. 83–98, jan 1999.

[37] R. Sun, I. W. Burgess, Z. Huang, and G. Dong, "Progressive failure modelling and ductility demand of steel beam-to-column connections in fire," *Engineering Structures*, vol. 89, pp. 66–78, 2015.

[38] CEN, "EN 1993-1-2:2005 - Eurocode 3. Design of steel structures. General rules. Structural fire design," 2005.

[39] Abaqus, "ABAQUS Analysis User's Manual. Version 6.5," tech. rep., ABAQUS, Inc, 2004.

[40] J. T. Wang, T. Chen, D. W. Sleight, and A. Tessler, "Simulating Nonlinear Deformations of Solar Sail Membranes Using Explicit Time Integration," in *45th AIAA/ASME/ASCE/AHS/ASC Structures, Structural Dynamics, and Materials Conference*, (PalmSprings, CA, USA), pp. 1–15, 2004.

[41] F. Pan, J. Zhu, A. O. Helminen, and R. Vatanparast, "Three point bending analysis of a mobile phone using LS-DYNA explicit integration method," in *9th International LS-DYNA Users Conference* (W. L. Mindle, ed.), (Dearbron, Michigan USA), pp. 13–31, LSTC, 2006.

[42] H. Yu, I. W. Burgess, J. B. Davison, and R. J. Plank, "Numerical simulation of bolted steel connections in fire using explicit dynamic analysis," *Journal of Constructional Steel Research*, vol. 64, no. 5, pp. 515–525, 2008.

[43] P. Kotsovinos and A. Usmani, "The World Trade Center 9/11 Disaster and Progressive Collapse of Tall Buildings," *Fire Technology*, vol. 49, no. 3, pp. 741–765, 2013.

[44] M. Gillie, *The Behaviour of Steel-Framed Composite Structures in Fire Conditions.* Phd, University of Edinburgh, 2000.

[45] C. Röben, *The effect of cooling and non-uniform fires on structural behaviour.* Phd, The University of Edinburgh, 2009.

Appendices

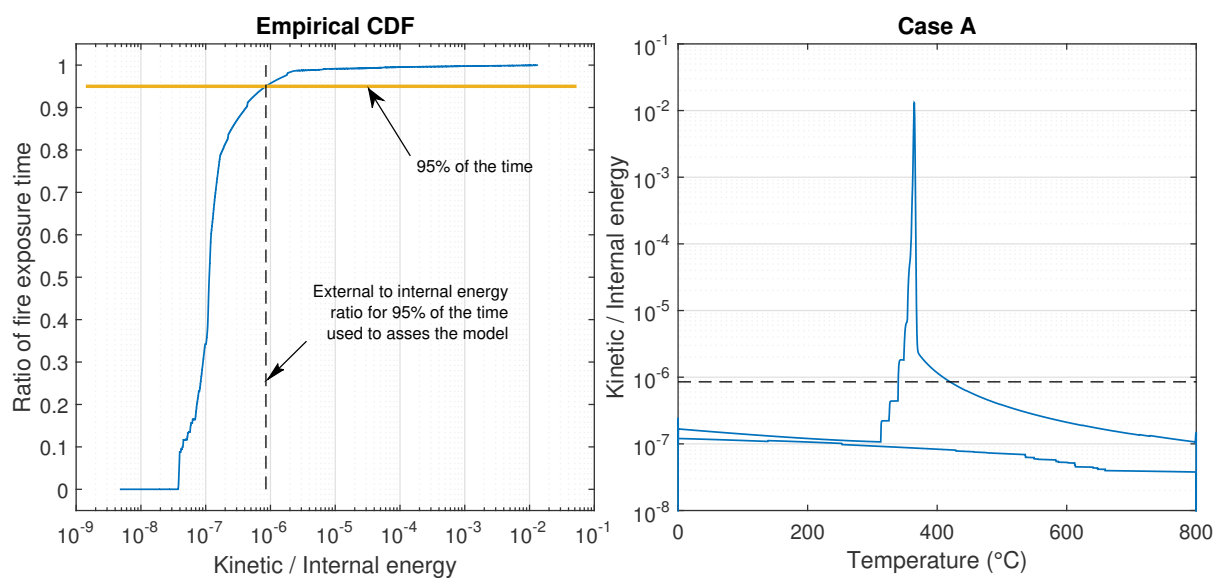## 3.A   Kinetic to internal energy ratio

When quasi-static (e.g. structural response to fire) or steady state problems are solved using explicit dynamic solvers, there are no well defined rules or parameters to indicate that such solution has been reached. Whether the amount of inertia force present in the system is not too high is based on the judgement of the modeller. Though, as already identified in Section 3.3.1, a general rule of thumb used by some researchers is that a solution is considered to be steady state and quasi-static when the kinetic energy to internal energy ratio in the system for most of the time is less than 0.1% and 5% [39–42], respectively. In this chapter a similar criterion has been assumed. Kinetic to internal energy ratio for 95% of the fire exposure time has been used to assess and compare between different cases the amount of inertia force present in the system.

95% of the time have been considered to eliminate single instantaneous high peaks in kinetic energy which are not representative of the kinetic energy in the system during the most of fire exposure (see Fig. 3.A1), which is the interest in this study. High instantaneous peaks in kinetic energy may occur, for example, when the section suddenly buckles resulting in high deflections over a short period of time and thus higher kinetic energy (Fig. 3.A1, Case A) or just before the failure of the element when the quasi-static problem becomes dynamic (Fig. 3.A1, Case B). Kinetic to internal energy ratio for 95% of the time for each case has been calculated based on the empirical cumulative density function (CDF) as illustrated in Fig. 3.A2. That is the kinetic to internal energy ratio at every time step has been arranged in the ascending order and the value at 0.95 of the ratio of fire exposure time has been taken as the indicator of the inertia force present in the system. Therefore, it indicates what value kinetic to internal energy ratio is equal to or lower than for 95% of fire exposure time eliminating high instantaneous levels of kinetic energy. The result time step sampling rate used in the analyses has a negligible effect with an error of approx. 0.001% in comparison to the simulation time step.
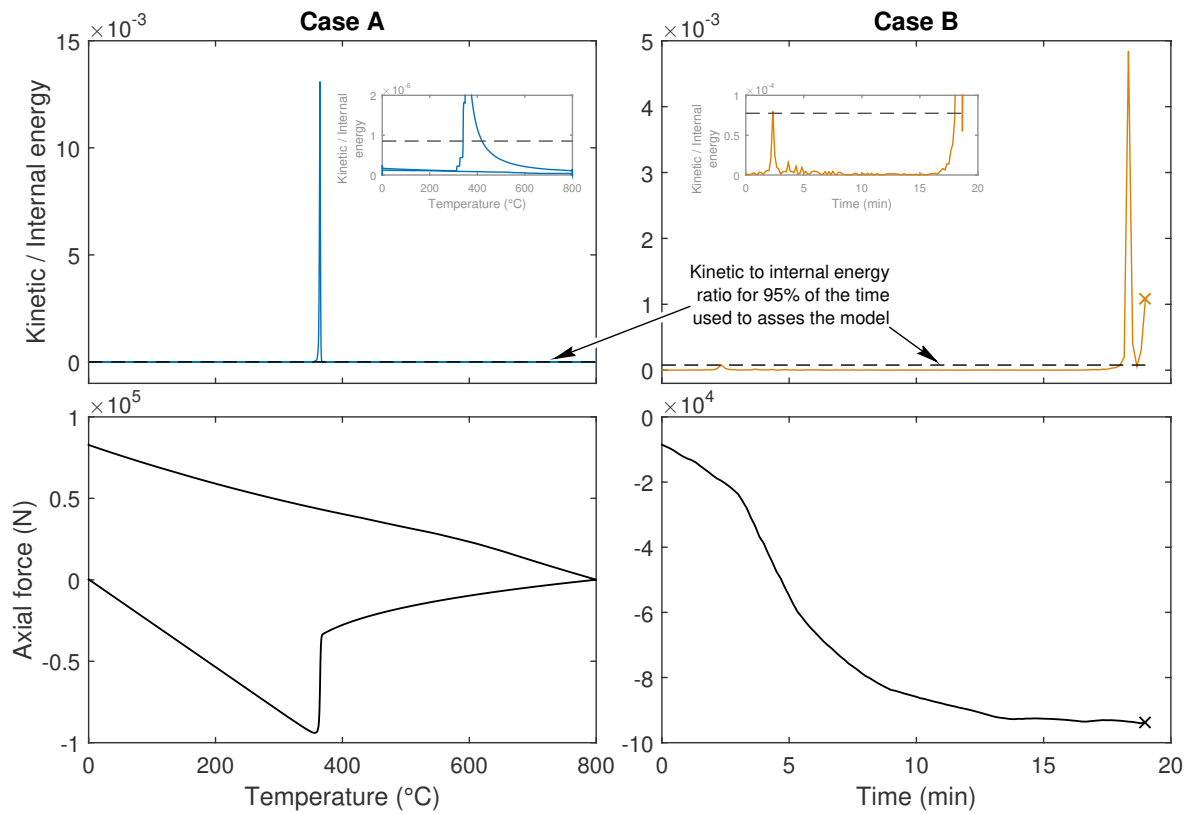
Figure 3.A1: Illustration of kinetic to internal energy ratio during the fire exposure (top) and axial force development in the heated members (bottom) for two different cases. '×' indicates failure.

.

Figure 3.A2: Illustration of the empirical cumulative density function (CDF) used to select the kinetic to internal energy ratio for 95% of the time for Case A illustrated in Fig. 3.A1.

.

Chapter 4

Structural Analysis of Multi-Storey Steel Frames Exposed to Travelling Fires and Traditional Design Fires

Summary [1]

Most of the current understanding of building behaviour in fire is based on the adoption of the standard and parametric temperature-time fire curves. However, these design fires are based on small scale tests and idealize the thermal environment as uniform. Thus, they have important limitations on their applicability to large enclosures. Instead, in large open-plan compartments, travelling fires have been observed. To account for such fires, a design tool called Travelling Fires Methodology (TFM) has been developed and used for design. The aim of this chapter is to compare computationally the structural response of a multi-storey steel frame subjected to both uniform design fires (available in current standards) and travelling fires. A two-dimensional 10-storey 5-bay steel frame designed according to ASCE 7-02 is modelled in the general finite element program LS-DYNA. Different fire exposures are investigated. They include travelling fires, Eurocode parametric curves, ISO-834 standard fire and the constant compartment temperature curve from the SFPE standard. These fires are applied to different floors, one at a time, to explore the influence on the structural response, resulting in a total of 80 different fire scenarios. The development of deflections, axial forces and bending moments is analysed. Uniform fires are found to result in approx. 15 to 55 kN (3 - 13%) higher compressive axial forces in beams compared to small travelling fires. However, the results show irregular oscillations in member utilization levels in the range of 2 - 38% for the smallest travelling fire sizes, which are not observed for any of the uniform fires. Peak beam mid-span deflections are similar for both travelling fires and uniform fires and depend mainly on the fire duration, but the locations in the frame and times when these peak displacements

---

1. This chapter is based on "E. Rackauskaite, P. Kotsovinos, A. Jeffers, G. Rein (2017) *Structural Analysis of Multi-Storey Steel Frames Exposed to Travelling Fires and Traditional Design Fires*, **Engineering Structures**, (in press)."

occur are different. The results indicate that travelling fires and uniform fires trigger substantially different structural responses which may be important in the structural design and selection of the critical members.

4.1 Introduction

Most of the current understanding of building behaviour in fire is based on the adoption of the standard and parametric temperature-time fire curves. However, these design fires are based on small scale tests, assume flashover and therefore an idealized uniform thermal environment in a compartment. Thus they are only applicable to small enclosures (<100 m^2 [1]). In large open-plan compartments, fires have been observed to travel, resulting in a highly non-uniform temperature distribution within the enclosure [2]. These fires are referred to as travelling fires. Examples of such accidental events include the World Trade Centre Buildings 1, 2 & 7 (2001), the Windsor Tower fire in Madrid (2006), and the Plasco building fire in Tehran (2017).

The use of post-flashover design fires that assume uniform temperature conditions within a compartment that are used in codes are justified by the assumption that they result in the most severe condition for structural members and therefore represent the worst case scenario irrespective of the structure details and the structural metric examined. However, following the aforementioned travelling fire incidents, the structural fire engineering community expressed concerns about the validity of traditional post-flashover fires for large compartments. More specifically questions were raised about the effect of longer fire durations and the effect of non-uniform temperatures on structural performance. As a result, Stern-Gottfried and Rein developed a novel design methodology called Travelling Fires Methodology (TFM) to represent the travelling nature of fires in large compartments [3]. In Chapter 2, TFM has been improved to account for more realistic fire dynamics and range of fire sizes and is referred to as Improved Travelling Fires Methodology (iTFM). In this methodology, the traveling fire size is varied to simulate cases where different percentages of the floor area are engulfed in flames at a given point in time. Temperatures in the compartment are described by two regions referred to as near-field and far-field. Near-field represents hot temperatures in the vicinity where fire directly impinges on the ceiling, and far-field represents the cooler smoke temperatures further away from the fire.

In recent studies [3–5] on the thermal response it has been found that structural members are likely to reach higher temperatures when subjected to travelling fires in comparison to uniform fires (i.e. Eurocode parametric temperature-time curves [6]). Higher temperatures lead to a higher loss of material strength. This is especially important for steel as it exhibits a rapid reduction in yield strength for temperatures higher than 400°C and can drop by 25% of its room temperature strength at 500°C [7]. The peak bay rebar temperature in the study by Stern-Gottfried and Rein [3] was found to

be 556°C under travelling fires, while for the same fuel load density considering Eurocode parametric curves, the rebar only reached temperatures from 252°C to 363°C. Law et al. [4] investigated the structural response of a concrete frame to travelling fires using an earlier version of TFM. The authors observed that the parametric curves lead to less severe conditions than travelling fires in terms of peak rebar temperature as well.

In terms of the structural response, in the studies [8, 9] where a localized fire was considered, it was concluded that the assumption of uniform temperature distribution within steel beams may lead to unconservative results. The exposure of a structure to a travelling fire, which is a localized fire that moves, can have an even more adverse effect. In a study on a steel space frame exposed to a localized travelling fire [10] authors identified that travelling fire can result in more extensive fire damage than a stationary localised fire. This is not only due to the likely higher peak temperatures within members, as identified previously, but also due to the simultaneous heating and cooling at different locations within the structure.

The first study to consider structural response under travelling fires and to highlight the need for more realistic thermal field correlations was carried out by Bailey et al. [11]. In the computational study of a two-dimensional steel frame they observed that a travelling fire caused larger residual displacements in the source bays than a uniform fire by up to 92 mm (29%). Similar study has been undertaken by [12] assuming reduced loading on the structure and the same observations were made. Additionally, the work by [11, 12] and recent work on the influence of travelling fires on composite construction [13] and post-tensioned concrete floors [14] indicated a cyclic behaviour of stresses and deflection development with time patterns in structural elements which have not been previously noted. However, to represent a travelling fire in these studies parametric temperature curves were used and shifted from one bay to another after a prescribed period. As noted by Stern-Gottfried and Rein [2], such representation ignores the pre-heating and post-heating of structural elements by hot smoke. They state that the latter might be the reason for the observation of a cyclic behaviour in structures subjected to travelling fires. Röben et al. [13] investigated the response of composite steel-concrete structures to vertically travelling fires. In this case, as identified by [2], observations of cyclic stresses seem to be more realistic because significant preheating of the upper floor (non-fire floor) prior to fire occupying it is unlikely.

Behaviour of structures subjected to travelling fires that assume non-uniform temperature distributions have been investigated by a number of researchers [4, 10, 15–18]. Röben [15] and Law et al. [4, 16] applied an early version of TFM [19] to study the response of a composite structure and a generic multi-storey concrete frame, respectively, subject to travelling fires. Results in [15] showed larger displacements (by approx. 80-500 mm, 12-56%) and compressive axial forces (by up to approx. 1.7 MN) for uniform fires. However, for travelling fires, irregular (i.e. not symmetrical) displacement patterns that are not experienced in case of uniform fires, and larger residual tensile forces (by up to

approx. 0.7 MN, 18%) and bending moments (by up to approx. 82.5 kNm, 5 times) have been observed. On the other hand, in the work by Kotsovinos [18], on the behaviour of tall composite buildings with a concrete core and perimeter long-span steel beams, travelling fires (using TFM [3]) were found to result in larger floor displacements (by approx. 380-1220 mm, 25-122%) and plastic deformations (by 30-90 mm, 2 to 7 times) compared to parametric fires but lower compressive (by approx. 155-270 kN, 24-38%) and tensile (by approx. 125-545 kN, 44-83%) axial forces in the steel beams. Work by [4, 16] showed that travelling fire scenarios resulted in more onerous stresses within the concrete frame than parametric temperature-time curves. It was also identified in the latter studies [4, 16] that fire sizes between 10% and 25% of the floor area resulted in the most severe conditions in the terms of critical deflection, rebar temperature and strain. Utilization analysis of columns in [16] identified the fires of 5%-10% of the floor area to be the critical scenarios. Rezvani and Ronagh [17] investigated the structural response of a 2D moment resisting frame subject to travelling fire represented by TFM [3]. Results indicated that fire size can have a significant effect on the failure time and temperature as well (by up to 62% and 11%, respectively).

In the previously identified studies the differences between the effects of travelling fires and uniform fires on the structural response have been evaluated for a post-tensioned concrete floor [14], a concrete frame [4, 16], a tall structure with a concrete core and perimeter long-span composite beam truss system [18], a composite construction [15], and a steel frame [11, 12]. The differences between the effects of the travelling and uniform fires on the structural response appear to be mainly affected by the extended total duration of travelling fires, changing location of higher localised near-field or bay temperatures with time (i.e. travelling nature of fire), and structural system examined. These studies concluded that consideration of more realistic fire exposure such as travelling fires is important for the structural response, because such fires may induce higher stresses and deflections than uniform fires, and that a uniform fire assumption is not always the most conservative.

However, some of these studies [4, 15, 16] used earlier TFM versions where far-field temperatures were represented by a single temperature. The studies on a more generic steel frame [11, 12] assumed uniform parametric fire temperatures for smaller bays and shifted them at arbitrary spread rates from one to another ignoring the effects of pre-heating as discussed previously. Parametric fires are based on different fire dynamics and therefore their use for non-uniform fires is not representative. In other studies on steel frames analysis was limited to the consideration of only one travelling fire scenario [10] and the behaviour of the same structure under uniform fire exposure was not considered [10, 17]. Therefore, more research on steel frames is still needed to investigate the differences between the effects of uniform fires and more realistic travelling fire exposures and whether the same differences in structural responses are observed as in [11, 12].

This chapter has two aims. The first aim of this chapter is to extend the work on

the structural response of a generic multi-story steel frame subjected to a more realistic travelling fire exposure (Chapter 2), which unlike previous studies on steel frames [11, 12] accounts for spatially varying temperatures in the compartment, physically possible fire spread rates, and temperatures. The second aim of this work is to investigate how the structural response of the frame changes with fire occurring on different levels of the same building, which to the best knowledge of the author has previously only been considered on a 3-storey steel frame [20]. The building examined in this study is a very generic steel frame based on the case study presented by NIST on typical US construction. As a result, although the conclusions of this chapter are specific to this steel structure, they are likely to have a much wider applicability compared to previous studies on concrete buildings or other more unique structural forms.

4.2   Finite element model

4.2.1   Multi-storey frame

The multi-storey steel frame considered in this analysis is based on the moment resistant frame published by NIST [21]. It is a 10-storey 5-bay frame, representative of a generic office building, with a floor layout of 45.5 m × 30.5 m. It is designed according to the American Society of Civil Engineers (ASCE 7-02) standard. The plan layout and elevation of the building are shown in Fig. 4.1. In this study the structural fire response of a 2D internal frame with the longest beam span of 9.1 m is investigated. This frame is chosen because it is likely to be more susceptible to instabilities compared to the shorter beams (6.1 m) spanning in the perpendicular direction. All columns in the frame are 4.2 m in height except for the ground floor columns which are 5.3 m high.
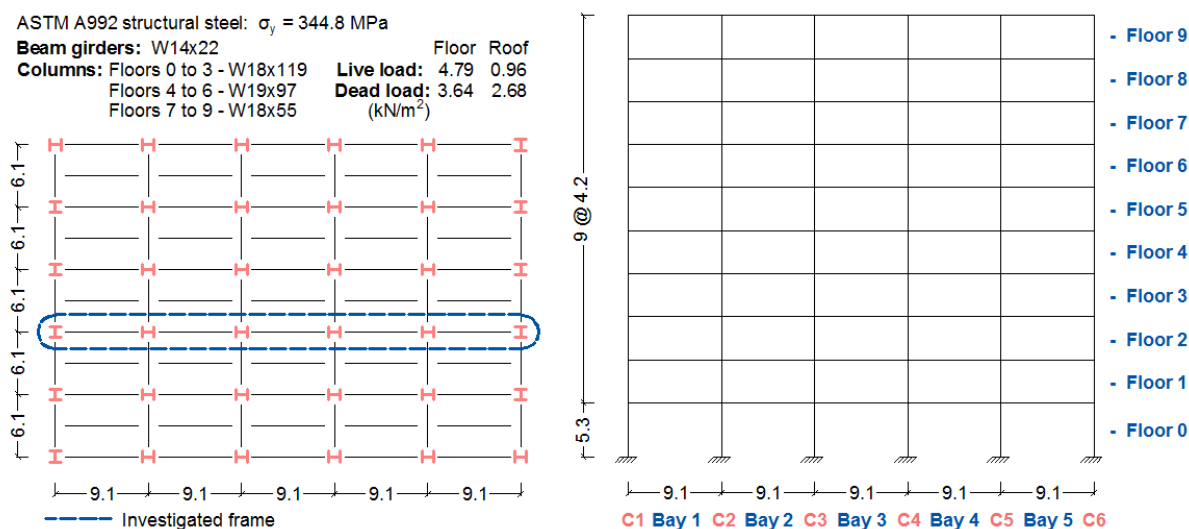
Figure 4.1: Plan layout (left), elevation (right) and structural member details of the investigated multi-storey steel frame from [21]. Frame dimensions are given in meters.

The steel beams are designed to support a lightweight concrete floor slab, and composite action is achieved through shear studs. This study utilizes the design dead and live loads and no attempt was made to apply reduction factors to the loads. Design loads on the floor beams are 3.64 kN/m^2 (dead) and 4.79 kN/m^2 (live). For the roof, design loads are 2.68 kN/m^2 (dead) and 0.96 kN/m^2 (live) [21]. In this chapter, the unfactored design loads where used as the combination for the fire limit state. The beam sections are W14×22 on all floors. The column sections on Floors 0 to 3, Floors 4 to 6, and Floors 7 to 8 are W18×119, W19×97, and W18×55, respectively. ASTM A992 structural steel with the yield strength (σ_y) of 344.8 MPa is considered for all beams and columns. In this chapter, different bays and columns are referred to as Bay 1 to Bay 5, corresponding to different beam spans, and column 1 (C1) to column 6 (C6), respectively, from the left side to the right side of the frame. Different floors of the building are referred to as Floor 0 to Floor 9, going up from the ground floor to the top floor of the frame (see Fig. 4.1).

Due to the 2D representation of the building, the composite action between the beams and concrete floor slab is not taken into account, which has been shown to have a beneficial effect on the structural response during fire as a result of tensile membrane action [22]. However, the effect of cooling due to the presence of the concrete slab on the steel beams is considered in the heat transfer analysis as discussed in Section 4.2.3. In previous numerical studies on the composite structures [15], a high-rise moment-resisting steel frame [23], and tall composite buildings with a concrete core and perimeter long-span steel beams and trusses, [18, 24] it was found that a 2D model using beam elements, in general, gives a good representation of the structural response to fire when compared to the 3D model using beam and shell elements. In a previous study on composite structures [15], the effects of the concrete slab on the structural response were determined to be more significant during cooling than heating, leading to reduced axial forces and higher residual moments as the slab cools down more slowly than steel beams. Also, in the same study, the 2D model was observed to underestimate deflections, but the load due to the concrete slab was not taken into account, which could have resulted in lower values compared to the 3D model. However, the results showed a close agreement in the trends in global structural behaviour. In a study on tall composite buildings with a concrete core and perimeter long-span steel beams and trusses, [24] it was also observed that the 2D model is less redundant and, therefore, results in a more onerous response. This is because, unlike the 3D model, in the 2D model redistribution of forces is to a lesser extent of the structure. For the cases investigated in this study, if composite action between the steel beam and the concrete slab was considered in the model, it would likely result in lower beam deflections horizontal displacements due to a stiffer response of the concrete slab. It could also lead to lower tensile axial forces during cooling and thus affect the observations of this study in particular for the smaller travelling fires, where structural members in different areas of the floorplate experience heating and cooling simultaneously for long durations during the fire exposure.

In general, the 2D models in previously identified studies [15, 18, 23, 24] were found to be conservative and show a good agreement qualitatively with 3D models. Therefore, the 2D representation is considered to be acceptable for this study as the primary objectives are to analyse the general trends and to compare the outcomes of the model for the different fire scenarios considered. In addition, a 2D analysis has been chosen for the reasons of simplicity, computational time to allow comparison of many different fire exposures (i.e. 80) and due to the fact that iTFM defines fires spreading along a linear path. A uniform thermal profile in the side perpendicular to the direction of fire travel is assumed. Moreover, a consistent level of crudeness in the assumptions regarding the fire definition and the structural modelling is important. The travelling fire model adopted in this chapter is a simplified fire model developed for design purposes and based on simple algebraic relationship (in a similar fashion to the parametric fires). As a result, the level of complexity of the fire models used in this study and the relatively simplified structural model are consistent and in line with standard design practice where simplifications are necessary.

4.2.2 Fire scenarios

The structural response of the frame subjected to travelling fires (TFM) (Chapter 2) and standard design fires such as Eurocode (EC) parametric temperature-time curves [6], the standard fire (ISO) [6, 25], and the SFPE constant compartment temperature design fire [26] is investigated.

To represent a travelling fire exposure, iTFM presented in Chapter 2 is used. It is the most recent version of the Travelling Fires Methodology (TFM), which was developed by [2–4]. Key difference with any other scenario for structural design is that TFM considers the non-uniform temperature distribution in the compartment and the long fire durations observed in many large fires. It should be noted that the methodology, although it represents the state of the art of the field, has not been extensively validated yet due to the lack of experiments in large scale compartments. However, the standard fire and Eurocode parametric curves are not validated for large compartments either [2, 3]. The travelling fire model presents an idealised exposure for studying the structure under non-uniform fires with the aim of removing complexities and simplifying its use but equally capturing the key phenomena experienced by non-uniform fires. This is similar to other loadings such as earthquakes, blast, or wind that are simplified in terms of representing their key responses to the structure for design purposes, rather than representing the event in a more complex form. Despite its relatively recent inception, the methodology has already been used by several consultancies as a complementary design tool for the design of 39 iconic buildings in UK (primarily open-plan offices, e.g. [27, 28]) and in previous studies has been found to be more onerous than other scenarios [3, 4, 11, 12, 15, 16, 18]. More experimental research in large compartments is still needed to advance the methodology further and represent more realistic fire dynamics by fitting experimental data when

it becomes available in the near future. Although, travelling fires have already been observed in a number of experiments [2].

An illustration of a travelling fire is shown in Fig. 4.2. This methodology considers a family of fires represented by the percentage of floor area engulfed in flames at any time. It is assumed that the floor area has uniform fuel and, once alight, burns at a constant rate [2, 3]. Thus, fire size is governed by the fire spread rate. TFM considers design fires to be composed of two moving regions: the near-field (flames) and the far-field (smoke) (see Fig. 4.2). The near-field represents the flames directly impinging on the ceiling and assumes the peak flame temperatures measured in real fires [2]. The far-field model represents smoke temperatures, which decrease with distance away from the fire due to mixing with air. Each floor of the frame in this study is subjected to four TFM scenarios: fire sizes of 2.5%, 10%, 25%, and 48% of the floor area. TFM sizes of 2.5% and 48% correspond approximately to the limits of likely realistic fire spread rates in compartments, as identified in Chapter 2, i.e. spread rates of 1 mm/s and 19.2 mm/s, respectively. TFM sizes of 10% and 25% have been found to be the worst case scenarios in previous studies on a concrete frame [3, 16]. In this frame, travelling fires are assumed to travel from Bay 1 to Bay 5 (see Fig. 4.1). The fuel load density and heat release rates are assumed to be 570 MJ/m² (80th percentile design value for offices) and 500 kW/m² (typical value for densely furnished places) [3], respectively.
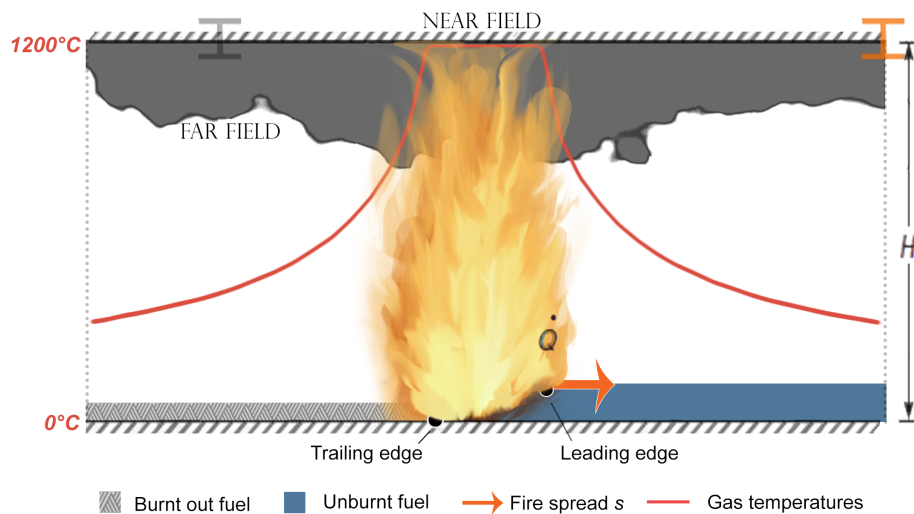
Figure 4.2: Illustration of a travelling fire and distribution of gas temperatures in the near-field and far-field.

Two Eurocode [6] parametric temperature-time curves are considered, representing short-hot and long-cool fire exposures based on the study by Lamont et al. [29]. The short-hot fire is characterized by high temperatures and short duration while long-cool fire is characterized by lower temperatures and longer duration. In [29] it was found that these two parametric fires resulted in different structural behaviour and for this reason they are included in this study. For the structure examined in the latter study [29] the

short-hot EC fire resulted in large initial deflections within a short period of time, while the long-cool EC fire resulted in larger deflections but much later in time as a result of different heating rates and durations. The EC parametric curves were generated assuming the same fuel load density as for travelling fires (570 MJ/m^2) and opening factors of 0.176 m$^{0.5}$ (short-hot) and 0.044 m$^{0.5}$ (long-cool). These opening factors correspond to 100% and 25% glass breakage (assuming a weighted average window height of 2.5 m), respectively.

The correlation to represent the standard fire (referred to as the ISO standard fire in this chapter) is taken from the Eurocode [6]. Only 60 min of standard fire exposure are considered because of the 60 min fire resistance given to the steel beams (see Section 4.2.3). In addition, the design fire scenario by the SFPE standard [26] is included in this work. In the SFPE standard, a constant and uniform compartment temperature of 1200°C is defined until the calculated burnout time. For different opening factors the burnout time can vary from approx. 15 min to 5 h or longer depending on the assumed glass breakage. For this study, the temperature of 1200°C is kept constant for 60 min, which corresponds to 100% glass breakage (as in the EC long-cool fire scenario). This fire scenario is referred to as SFPE. SFPE standard fire scenario was chosen to represent the worst case uniform fire in terms of heating exposure, i.e. even more severe than ISO. It should be noted that the method is not explicitly based on physical parameters.

Each fire scenario is considered on every floor of the frame, one at a time. Therefore, in total 80 fire scenarios are investigated. Illustration of the gas temperatures for all fire scenarios at the mid-span of Bay 2 and at the right end of Bay 5 is shown in Fig. 4.3. By the definition for the parametric fires (EC), the standard fire (ISO) and the SFPE fire, the temperatures are assumed to be uniform across the whole compartment. Thus, for these scenarios, the temperatures shown in Fig. 4.3 at the two locations are identical. However, the travelling fire gas temperatures for Floor 0 are lower in comparison to the other floors because of the higher column height (floor 0 - 5.3 m, floors 1 to 9 - 4.2 m). Alpert's correlation [30] used to define gas temperatures in the iTFM is a function of ceiling height.

It should be noted that this study does not suggest that such a wide range of fire scenarios needs to be selected by designers when undertaking commercial projects. Designers could follow local or other guidance, exercise qualitative judgement or use probabilistic methods to derive an appropriate selection of fires relative to their building. The aim of selecting a high number of fire scenarios in this work was for comparative purposes and in order to reach to qualitative conclusions that could be useful for designers when carrying out structural fire assessments of similar buildings.
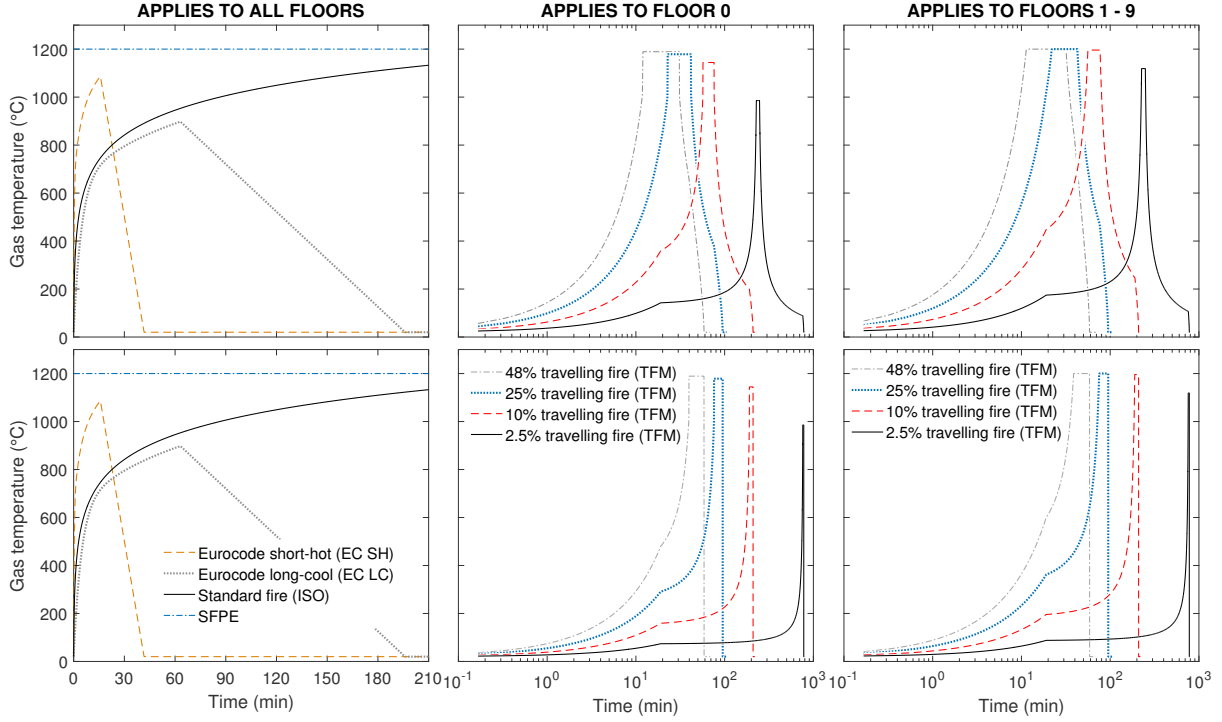
Figure 4.3: Gas temperature histories at mid-span of Bay 2 (top) and right end of Bay 5 (bottom) for the eight fire scenarios on each floor of the frame: EC, ISO, and SFPE fires for all floors (left) and TFM fires for Floor 1 (middle) and Floors 1 to 9 (right).

4.2.3 Heat transfer

Beams and columns are designed for 60 min and 120 min standard fire resistance, respectively, using Eq. (4.1) [31, 32].

$$t = 40(T_{lim} - 140)\left[\frac{d_i/k_i}{H_p/A}\right]^{0.77} \tag{4.1}$$

where t is the time (min), T_{lim} is the limiting temperature of steel (°C), d_i is the thickness of the insulation (m), k_i is the thermal conductivity of the insulation (W/m.K), H_p is the heated perimeter of the section (m), and A is the cross-sectional area (m²).

A limiting temperature of 550°C is commonly accepted as the critical temperature for steel in traditional design [33] and, therefore, is used as T_{lim} in Eq. (4.1). At 550°C steel maintains only 60% of its ambient temperature strength because of the thermal degradation of its mechanical properties.

The main aim of this work is to analyse and compare the structural behaviour of the frame over a long fire exposure (i.e. travelling fires and uniform fires). Thus, to avoid an early failure of the frame during the fire, a higher fire resistance period is assumed for the columns. In the UK, the typical prescriptively required fire resistance standard for an office building with a height to the last occupied floor of 38.9 m would be 120 min [34].

Steel insulation properties are taken as for high density perlite (thermal conductivity $k_i = 0.12$ W/m.K, density $\rho_i = 550$ kg/m³, and specific heat $c_i = 1200$ J/kg.K) [31].

Heat transfer to the structural members was carried out assuming lumped capacitance for separate parts of the cross-section (i.e. web and flanges) according to [3, 31], as shown in Eq. (4.2).

$$\Delta T_s = \frac{H_p}{A} \frac{k_i}{d_i \rho_s c_s} \frac{\rho_s c_s}{[\rho_s c_s + (H_p/A)d_i \rho_i c_i/2]} (T_g - T_s)\Delta t \tag{4.2}$$

where T_s is the steel temperature (K), T_g is the gas temperature (K), ρ_s is the density of steel (kg/m³), c_s is the temperature dependent specific heat of steel taken from the Eurocode [7] (J/kg.K), and Δt is the time step (s).

For beams, the effect of the concrete slab was considered by excluding the top surface of the upper flange, which is in contact with the slab, in the calculation of the heated perimeter. Thus, adiabatic boundary condition was assumed, though, in reality there would be some heat losses into concrete resulting in an even lower temperatures at the top flange. The convective heat transfer coefficient at the free surface, density of steel and radiative emissivity at the free surface are assumed to be 35 W/m².K, 7850 kg/m³ and 0.7, respectively [31]. The time step that satisfies the stability criteria for the heat transfer calculations is 10 s. Vertical temperature distributions in the compartment are not currently taken into account in iTFM. As a result, columns are assumed to be exposed to the same fire conditions as those at the same location in the ceiling, and temperatures along the column height are assumed to be uniform to represent the worst case scenario. An illustration of temperature development and distribution in the beam and column sections is shown in Fig. 4.4.
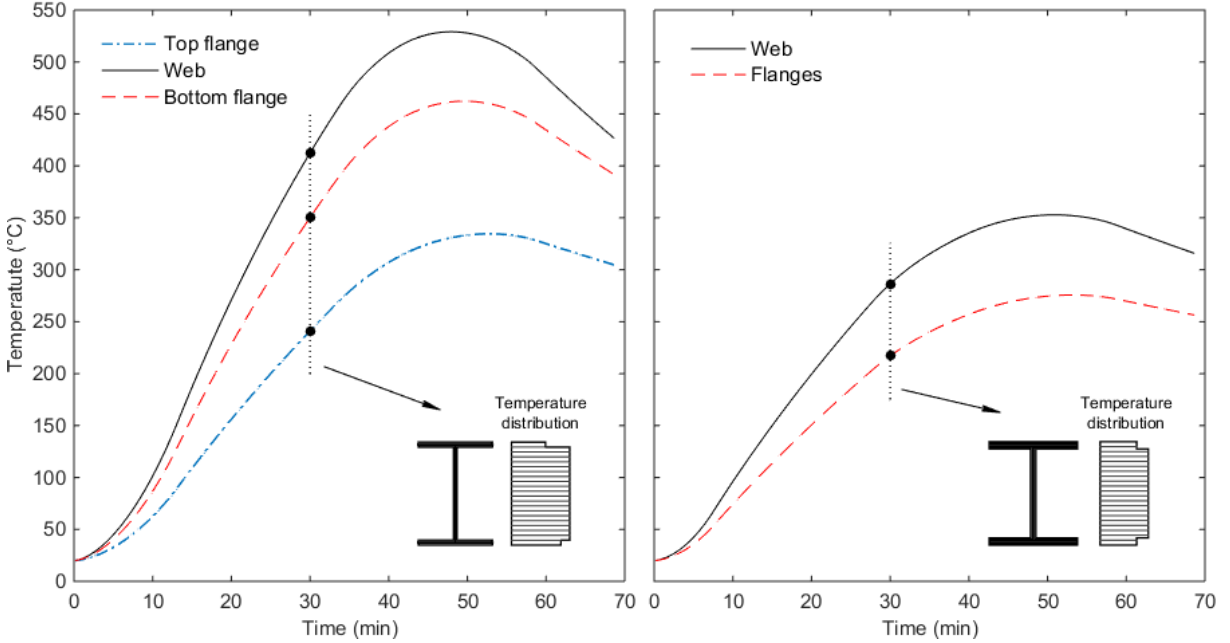
Figure 4.4: Temperature development and distribution in beam section at mid-span of Bay 2 (left) and column 2 (right) for Floor 2 exposed to the 48% travelling fire.

4.2.4 LS-DYNA model

The multi-storey steel frame is modelled using the general purpose finite element program LS-DYNA (Release 7.1.1) explicit solver. The program was originally developed specifically for highly nonlinear and transient dynamic analysis. LS-DYNA is capable of simulating the thermal and thermal-structural coupling analysis and has an extensive element and material library, including the temperature dependent material models from the Eurocode for steel and concrete. Benchmarking of the program against the available benchmarking and fire test data for structural fire analysis has been presented in Chapter 3. In previous research, LS-DYNA has been used in structural fire applications for the analysis of tall structures [35] and structural arrangements with bi-linear columns [36]. All of the parameters for the model presented in this section were chosen based on mesh density and parameter sensitivity convergence studies (Appendix C).

The steel beams and columns are modelled using the Hughes-Liu [37] beam element formulation, with a cross-section integration refinement factor of 5. Hughes-Liu beam elements allow for the treatment of finite strains and are simple, computationally efficient, and robust. Beams, Floor 0 columns, and Floor 1 to 9 columns are divided into 36, 22, and 16 beam elements, respectively. The corresponding beam element length is approximately 0.25 m for all structural members. The supports for the ground floor columns are assumed to be fixed, and the beams and columns are assumed to be rigidly connected. The aim of this study is the investigation of the global structural response, and, thus, no attempt was made to capture localized failures in the beams, columns, or in the beam-to-column connections. It should be noted that 3D global effects are not considered in this study.

A thermally-sensitive steel material type MAT 202 formulation based on Eurocode 3 (EN 1993-1-2:2005 [7]) is used for both steel beams and columns with the default temperature-dependent material properties. In this material model strain-hardening is not taken into account. Steel with initial yield stress of 345 MPa, Young's modulus of 210 GPa [38], and Poisson's ratio of 0.3 [38] is assigned to all members. Both mechanical and gravity loads are considered. Simulations are carried out using the explicit solver of LS-DYNA that uses real-time units to solve the equation of motion. Thus, in order to avoid artificial, high dynamic oscillations, the mechanical and gravity loads are applied in a linear increment over 1 s and then kept constant for the remainder of the analysis. After 2 s, that is once the steady-state solution is attained, thermal loads are applied. Thermal loading to the beams and columns was applied using the formulation which allows the definition of a variable through-thickness temperature distribution as calculated in the previous section. The remainder of the frame is assumed to be at room temperature. In order to reduce the computational time, the temperature development within heated members is scaled by a factor of 100, which was determined to be an appropriate scaling factor in order to control the inertia effects based on the sensitivity analysis. This means that parametric curve which would last 120 min in physical time would be applied in 1.2 min in the simulation time. Once the simulations were completed, data on the develop-

ment of axial forces, bending moments and displacements in frame were extracted and are analysed in the following section.

4.3   Results and discussion

4.3.1   Thermal response

A comparison of the beam and column web temperatures for all fire scenarios is illustrated in Fig. 4.5 and Fig. 4.6, respectively. They show that temperature distributions for a frame subjected to travelling fire scenarios are highly non-uniform in comparison to traditional design fires, as could be expected. As the fire travels along the compartment the magnitude of temperature variation decreases for larger fire sizes from 322°C (25% TFM) and 257°C (48% TFM) to 218°C (25% TFM) and 123°C (48% TFM). For the smallest fire sizes temperature differences in the frame are in the order of 550°C (2.5% TFM) and 400°C (10% TFM) at different times. Peak temperatures develop close to the end of fire and towards the end of the fire path as observed in Chapter 2. Peak temperatures reached in the beam web for different fire scenarios are 692°C for 10% TFM, 682°C for 2.5% TFM, 635°C for 25% TFM, 620°C for EC long-cool fire, 559°C for 48% TFM, and 367°C for EC short-hot fire. The highest peak temperatures and the variation in temperatures for the various TFM scenarios occurs for the smallest travelling fire size of 2.5%. Column temperatures on different floors do not reach similar values because of different column section sizes. For travelling fire scenarios, columns on Floors 1 to 3 experience up to 90°C higher temperatures than columns in Floors 0 and 7 to 9. Temperatures in Floor 0 are low due to high column height as identified in Section 4.2.2. For uniform fire scenarios (EC, ISO and SFPE), temperatures for all columns on the same floor are equal and the highest temperatures are reached in Floors 0 to 3.

4.3.2   Effect of location of fire floor

The development of the beam mid-span displacements, axial forces and bending moments with time for the frame subjected to the 48% travelling fire is shown in Fig. 4.7. For the illustration of the results for other fire scenarios the reader is referred to the Appendix 4.A. Shaded areas represent the range of the displacements and axial forces which develop within the specific beam in relation to the fire location (i.e. floor immediately above or below the fire floor) for different fire floors. 'Floor 0', 'Floor 8' and 'Floor 9' indicate the floors the fire is located on. The development of mid-span displacements, axial forces and moments on these floors is different compared to fire occurring on the intermediate floors due to the reduced number of floors above or below the fire floor and different column sizes, i.e. different level of lateral axial restraint from the surrounding structure. For example, beams on Floor 9 are only connected to the columns on the same floor leading to a low level of axial restraint to thermal expansion,
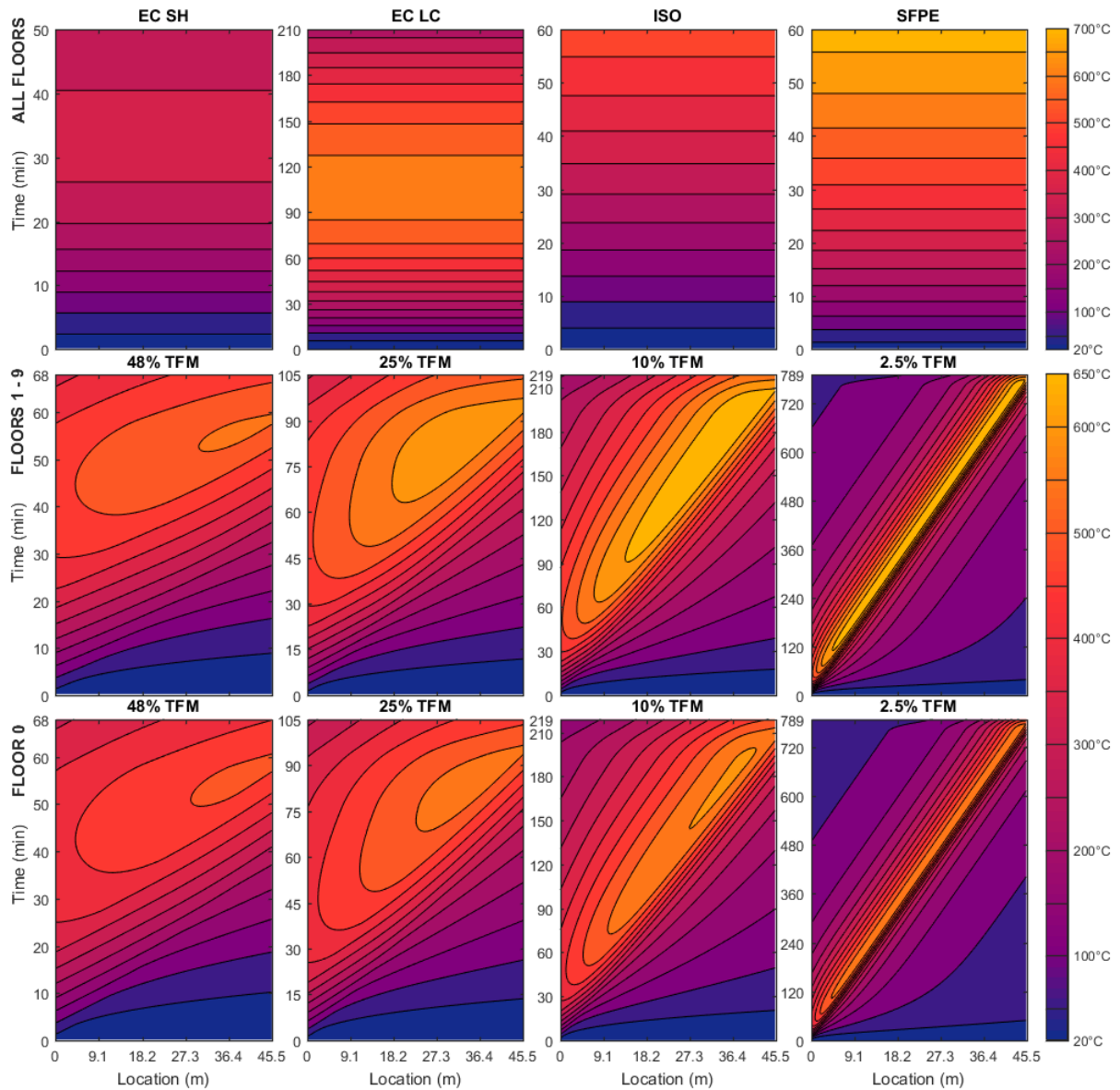
Figure 4.5: Beam web temperature variation with time and location along the fire path in the heated floor for the eight fire scenarios: EC, ISO, and SFPE fires in all floors (top) and TFM fires in Floor 1 (middle) and Floors 1 to 9 (bottom).

while beams on intermediate floors are connected to and restrained by the columns on the floor above as well. This results in higher axial restraint and consequently higher axial forces by up to 240 kN (13% of the heated section capacity at the temperature at that time) in intermediate floors as can be seen in Fig. 4.7. For the 48% TFM at 20 min the difference is up to 300 kN, which is approx. 21% of the maximum axial force capacity of the section at that time.

The results indicate that in general the development of stresses and displacements follows a similar behaviour pattern for all members, even though the fire occurs on different floors. The lowest limiting axial force values correspond to fire occurring on Floor 8. In the bottom floors, the axial force in the heated beams increases by approx. 65
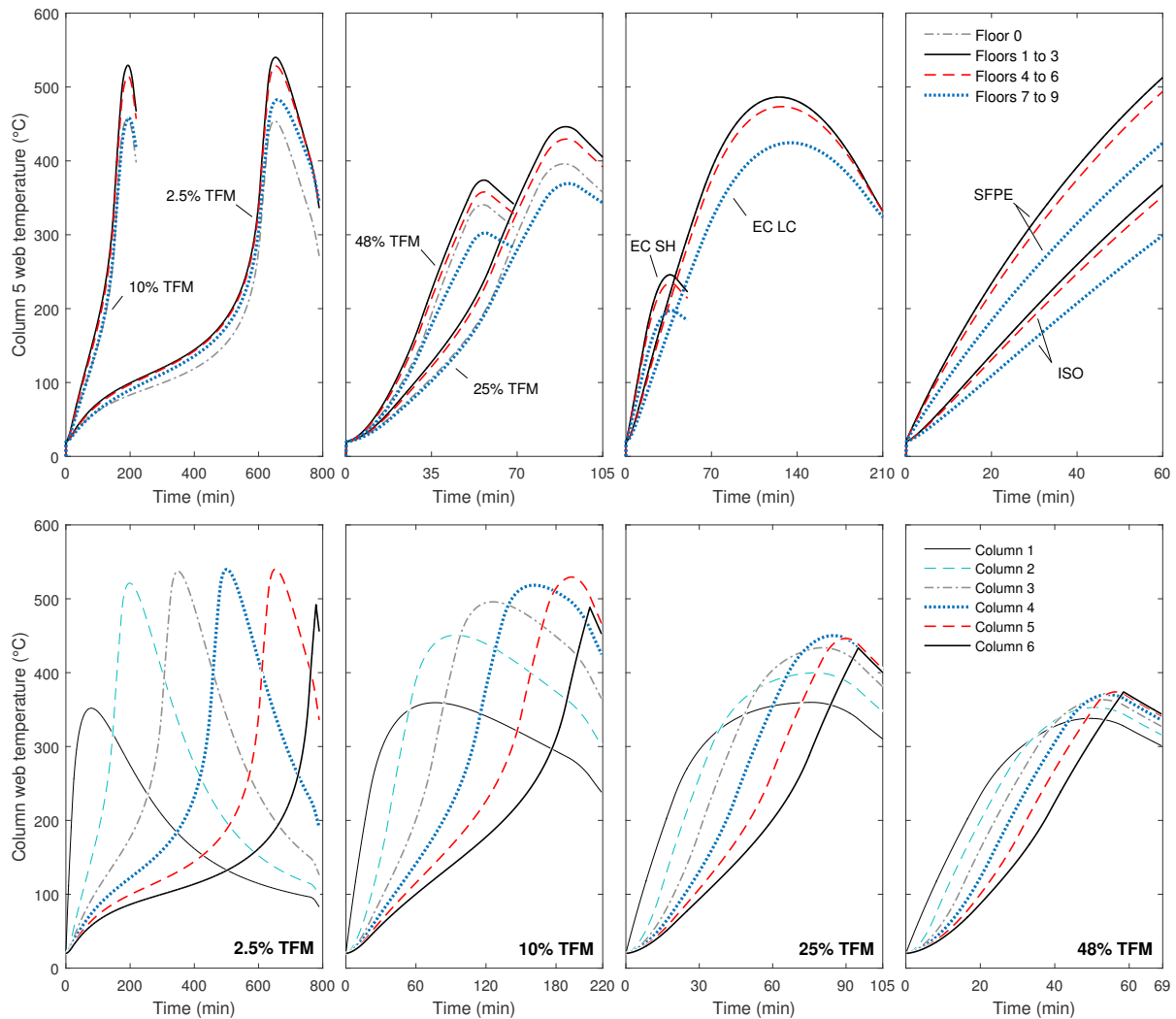
Figure 4.6: Column 5 web temperature development in the heated floor for the eight fire scenarios (top); and comparison of temperature development in all heated columns on Floor 2 exposed to travelling fire scenarios (bottom). For EC, ISO and SFPE fire scenarios temperatures of all columns on the heated floor are equal.

kN (17%) for the 25% TFM, 48% TFM, and ISO fire. This difference goes up to 90 kN (29%) and 124 to 196 kN (50% to 180%) for the 10% TFM and 2.5% TFM, respectively. These values correspond to 5% (25% TFM, 48% TFM, and ISO), 6% (10% TFM), and 9 - 14% (2.5% TFM) of the yield axial force section capacity. This is because heated beams on the top floors of the frame are supported by weaker column sections with a lower cross-section capacity than the beams on the bottom floors. Thus, even though these columns reach lower temperatures (see Fig. 4.6) the axial restraint to thermal expansion is smaller in the upper floors. The variation in peak axial forces with different fire floors for the smallest travelling fire sizes (2.5% and 10%) is the highest. This is probably due to the higher variation of temperatures in the frame. Some of the members on the fire floor in the far-field region are relatively cool, thus, providing more axial restraint. Also, the peak axial forces during 2.5% and 10% travelling fires develop much later (at 50 to
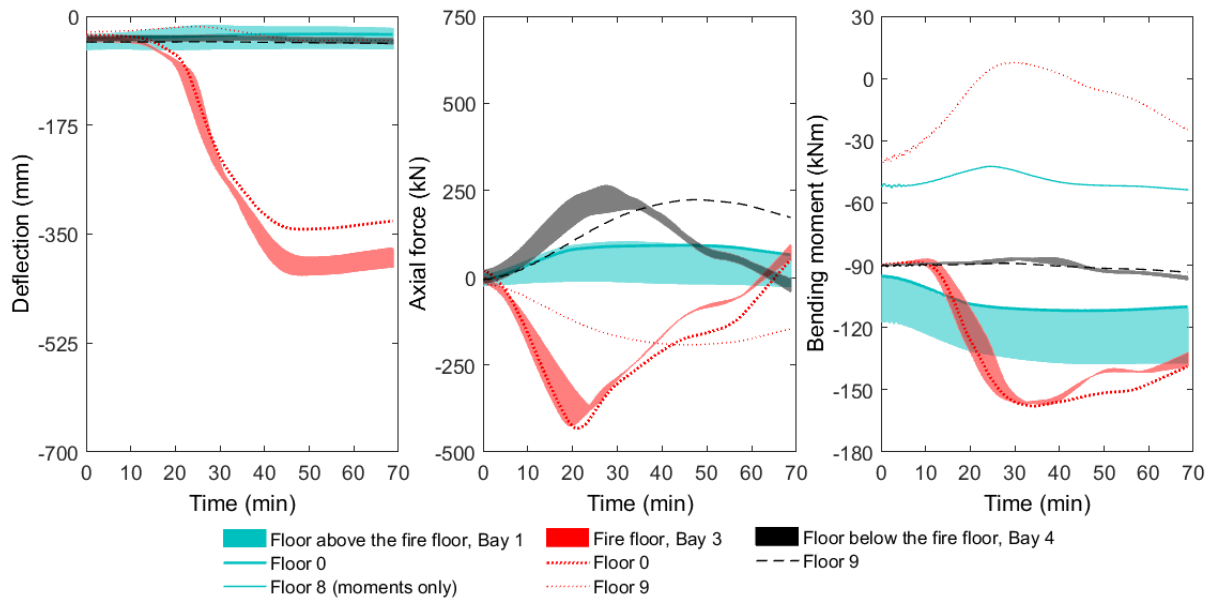
Figure 4.7: Variation of displacement, axial force and bending moment development in beams exposed to a 48% travelling fire scenario. Shaded areas represent a range of results when fire occurs on Floors 1 to 8. Individual lines indicate results when fire occurs on ground floor (0), Floor 8 (moments only), and top floor (9).

160 min) in comparison to larger travelling fires and uniform fires (20 to 30 min).

In the cases when the fire occurs in the upper floors, the initiation of yielding within the heated beams occurs up to 15 min later than in the cases when fire occurs on the lower floors. Typically, yielding takes place when the compressive axial force begins to decrease, followed by elasto-plastic response and a sudden increase in deflection [39]. After yielding, the influence of the fire floor location becomes less significant. Higher displacements (by approx. 30 to 55 mm, or 6.8% to 9.4%) develop within the beams when the fire occurs on the top floors of the building rather than the bottom. These observations agree well with the findings from other researchers who investigated the effects of axial restraint stiffness on heated beams [40–42]. They found that, in the cases where beam behaviour is dominated by restrained thermal expansion, higher axial restraint results in the development of higher compressive forces and lower deflections.

The level of axial restraint on the ground floor beams is affected by more factors than in the intermediate floors, which makes it more difficult to judge and make comparisons. On one hand, ground floor columns have fixed supports, which should lead to higher axial restraint but, on the other hand, these columns are more slender (5.3 m high) (i.e. have a lower bending stiffness) than the columns in the upper floors (4.2 m). In addition to that, for travelling fire scenarios, members on the ground floor are exposed to lower temperatures in comparison to the upper floors. Thus, slightly higher axial forces and lower deflections occur for TFM scenarios because of the combination of previously identified factors. Results for the ISO fire, which are not affected by different thermal

conditions on different floors, indicate that the ground floor beams (i.e. structural beams located at Floor 0) have the highest axial restraint in comparison to intermediate floors. This is because of the higher peak compressive axial forces and lower deflections after yielding of the beam occurs. Analogous results for displacement, axial force, and bending moment in different fire floors were observed for all other scenarios (i.e. EC parametric and SFPE fires).

4.3.3 Axial force redistribution

Fig. 4.8 shows the development of axial forces within different beams in the frame for a 25% travelling fire on Floor 2. In each bay the development of axial forces in the heated floor and in the floors above and below the fire follows the same trend. Compressive axial forces develop within the heated beams while tensile axial forces develop in beams in the adjacent floors. This is because the beams in the adjacent floors have to resist the lateral movement of the columns as the beams on the fire floor try to expand. Therefore, they provide the axial restraint to thermal expansion. The highest axial forces develop in the beams in the floors immediately above and below the fire floor. The axial force within these beams is approximately increasing from 60 to 80% (Floors 0 and 2) of the axial force in the heated beams with time. This drops to from 5 to 30% on the floors further away from the fire by one floor. For a fire occurring on the top floor, axial force development in the floors below is even higher as there is no available axial restraint from any floors above the fire (see Appendix 4.A). In this case the axial force in beams one floor below the fire (Floor 8) is from 90 to 110% for end bays and 140 to 180% in internal bays of the
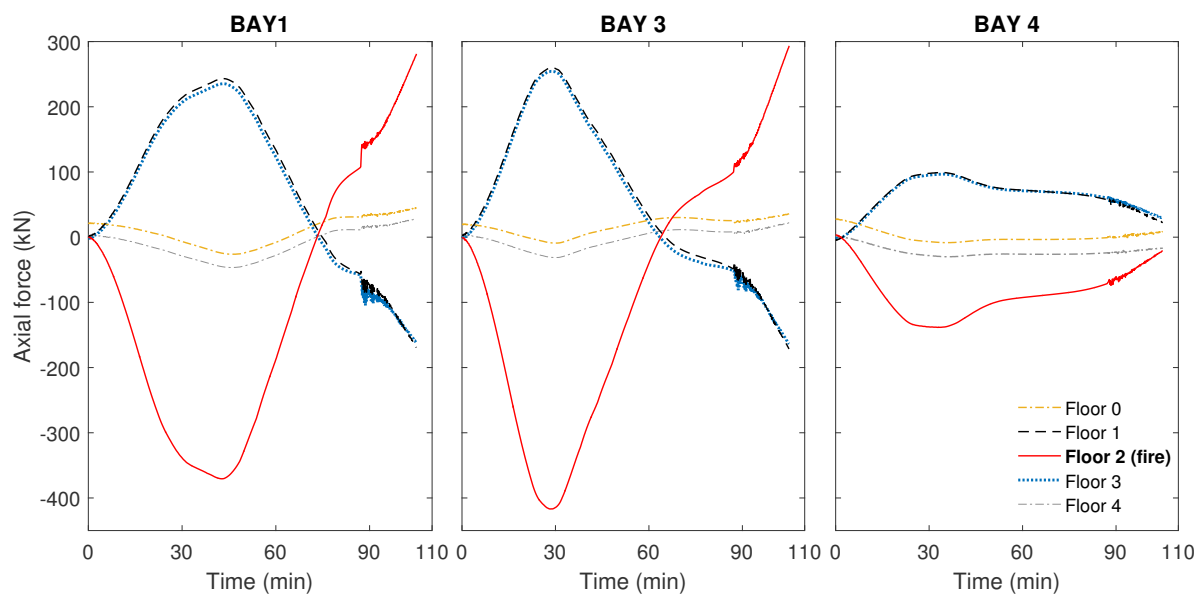
Figure 4.8: Variation of axial forces within different bays for a frame subjected to a 25% travelling fire on Floor 2. Bays 1 is the end bay and Bays 3 and 4 are the internal bays of the frame.

axial force in the heated beams. It drops to 0 to 15% (end bays) and 45 to 80% (internal bays) in Floor 7. It should be noted that conventional guidance does not consider the effect of load redistribution and the increased utilisation at other levels during a fire.

No significant axial forces were observed in any other floors. This indicates that the stress distribution is negligible in the frame floors more than 2 floors away from the fire. Later, in Section 4.3.4, it will be shown that the same observation is made for the bending moment distribution in columns. Therefore, modelling only these floors of the frame is likely to be sufficient to capture the correct restraint conditions and stress development. However, more studies on different geometries should be carried out to confirm this, and the column boundary conditions need to be carefully chosen by designers. In agreement, Law [43] in his study on perimeter column boundary conditions noted that representing 3 floors and 4 column heights resulted in the most significant improvement in accuracy of column bending moment prediction. Similar results as presented in Fig. 4.7 and discussed in this section were observed for all other fire scenarios occurring in the intermediate floors.

### 4.3.4 Effect of fire scenario - travelling fires and uniform fires

Deflections

The comparison of axial force, bending moment, mid-span deflection and lateral displacement development in the heated beams on Floor 2 is shown in Fig. 4.9. The typical deflected shape of the frame for different fire exposures on Floor 2 is shown in Fig. 4.10. For all travelling fire (TFM) scenarios beam displacements in Bay 1 (end bay) are relatively low in comparison to other bays. Once the cooling begins, the displacements remain constant while in the other bays there is a small recovery. This is because the beams in Bay 1 reach lower temperatures than the beams in other bays, thus resulting in lower thermal expansion and lower compressive axial forces in Bay 1. For the same reason, the peak displacement reached in Bay 1 keeps on increasing with decreasing fire size as the beam is exposed to the near-field for a longer duration. Due to a low axial restraint available, the majority of thermal stresses go into the development of displacements. A similar beam response occurs in Bay 5, but in this case peak displacements are the highest in the frame because beams reach higher temperatures. It can also be observed that for TFM sizes of 10%, 25%, and 48%, the highest axial forces develop in Bay 2 followed by Bay 3 and Bay 4. This is because as the fire progresses more of the structure is heated leading to lower stiffness and thus available restraint.

Higher displacements initially develop in Bay 3 for the standard ISO, SFPE and EC fires and in Bays 1 or 2 for the travelling fires. For the standard fire, SFPE fire, short-hot EC fire, and 48% TFM, displacements develop more rapidly at the early stages of the fire. However, the peak mid-span deflections reached during the latter scenarios (40 cm for the 48% TFM and 24 cm for the EC short-hot fire) are at least 20 cm lower than
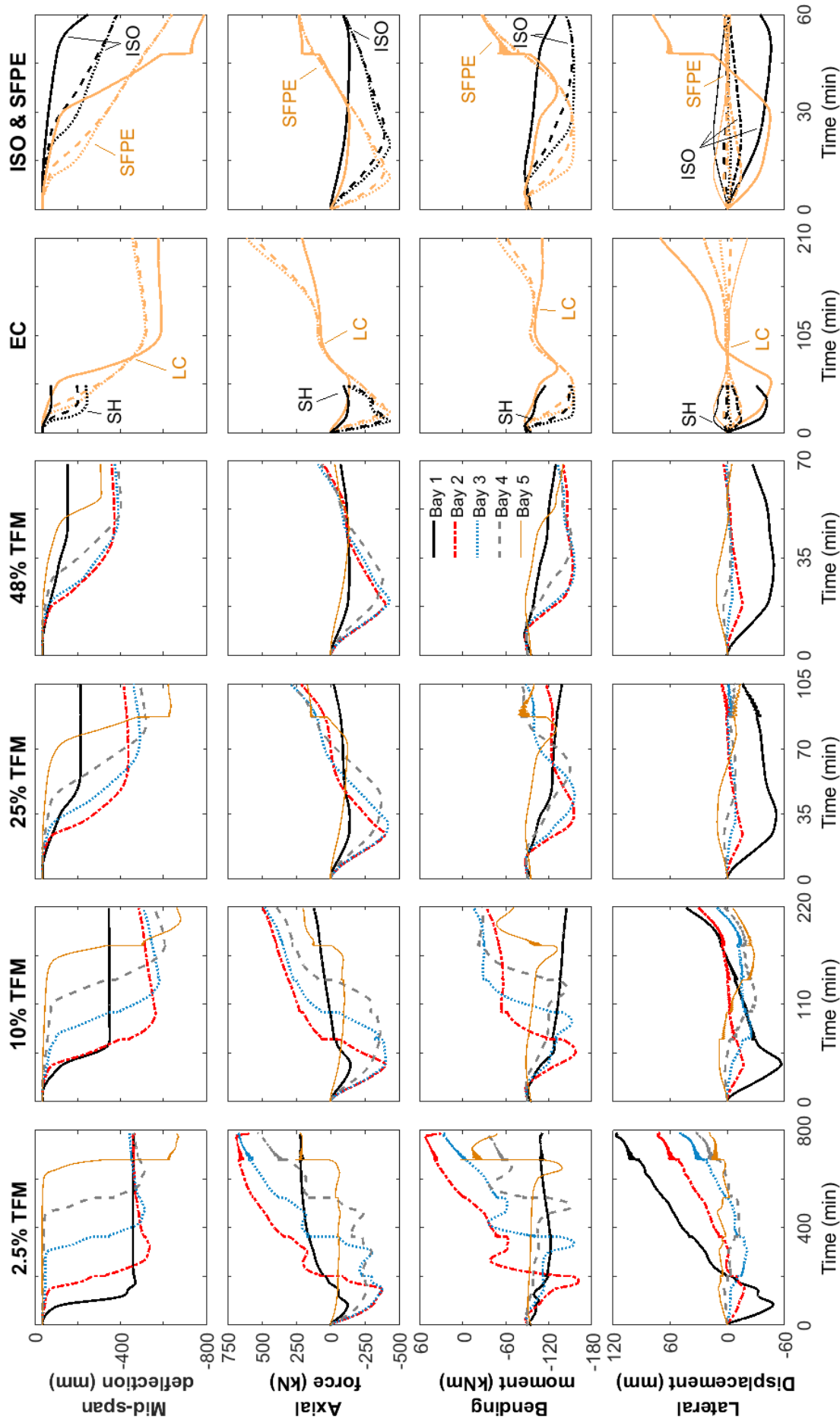
Figure 4.9: Development in time of mid-span deflections, axial forces, and bending moments at each of the beams in Floor 2; and development of lateral displacements at the beam to column nodes on the left hand side of the beam. Fire occurs on Floor 2.
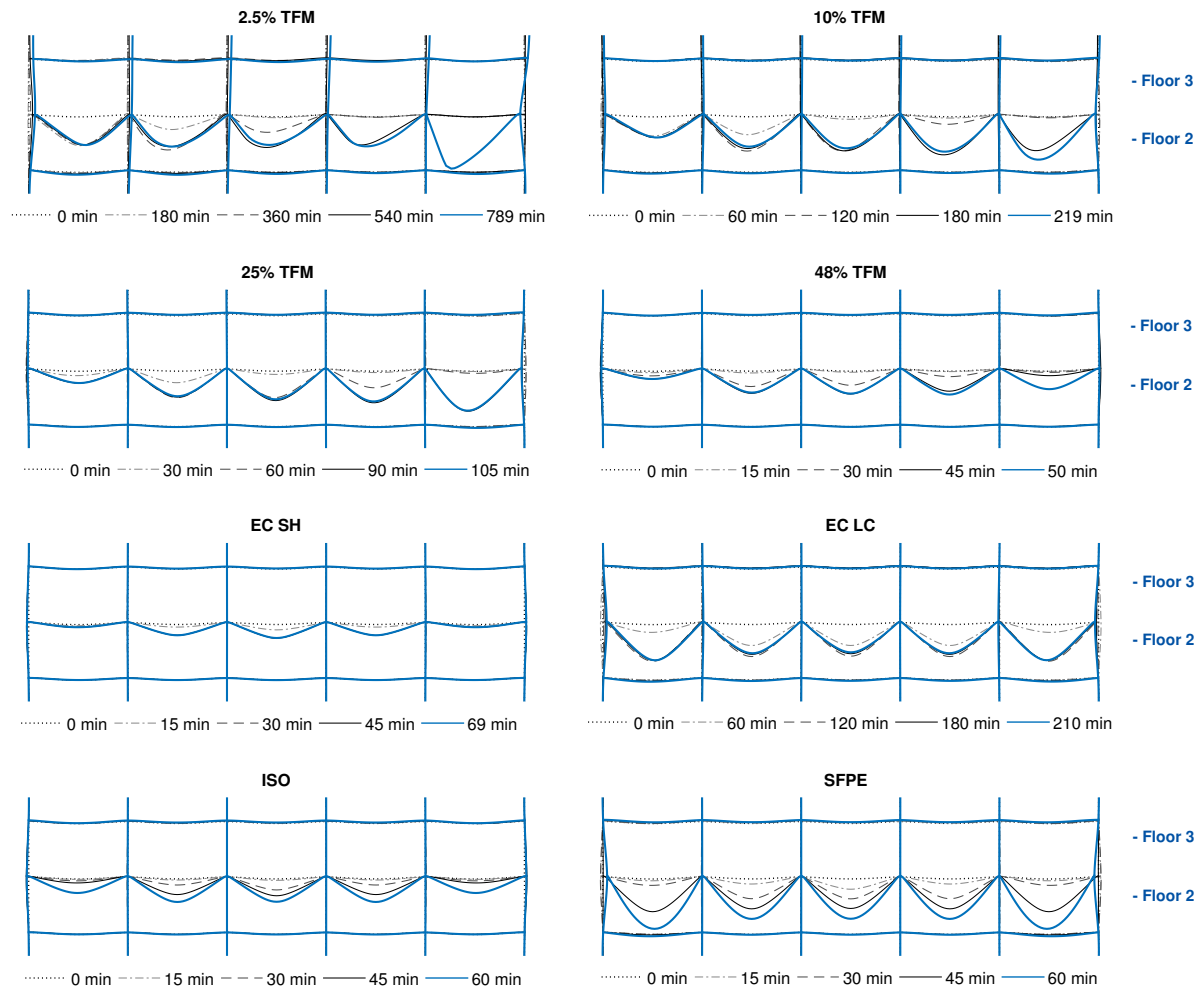
Figure 4.10: Deflected shape of the frame at different times of fire exposure for the eight fire scenarios investigated. Fire occurs on Floor 2. Displacement scale factor is 5.

for other fire cases. No cooling phase for ISO and SFPE fires is considered; therefore, deflections are the highest and would continue increasing until the failure of the frame (i.e. when the load-bearing capacity is reached).

In the work by Bailey et al. [11], Liew et al. [12] and Kotsovinos [18] it was found that travelling fires produced higher displacements than parametric fires for the range of fire sizes and type of structures that the authors examined. However, in the work by Röben [15] the opposite conclusions were made. Ellobody and Bailey [14] reported that maximum displacements can develop either during the travelling fire or uniform fire for the case study examined in the paper, a fully protected MRF. The results shown in Fig. 4.9 agree with the latter and indicate that it is not the fire type which governs the displacements but the fire duration. In general, in the work presented in this chapter, maximum deflections reached are higher for fire scenarios with longer fire durations (2.5%, 10% and 25% travelling fires and EC long-cool fire) than for shorter and hotter fires (45% TFM and EC short-hot fires). This agrees with the findings by Lamont et al. [29]

for a protected steel-concrete composite structure regarding the short-hot and long-cool parametric fires. Short and hot fires were observed to result in faster initial displacements, while long and cool fires resulted in larger maximum displacements but occurring later during the fire. Thus, travelling fires, depending on their fire spread rates and thus duration, could be grouped into similar categories as well (such as "slow" and "fast" travelling fires).

The main difference between travelling fires and uniform fires appears to be that these fires result in different locations where the maximum deflections develop at different times (see Fig. 4.10). For travelling fires and uniform fires, initially the highest deflections develop in the end bays and central bay, respectively. However, towards the end of the fire, irrespective of fire scenario (TFM or uniform fires), for long-cool fires the peak displacements develop in end bays, while for short-hot fires (EC short-hot fire and 48% TFM) they develop in internal bays. Displacements for travelling fires are also more irregular along the frame as observed in the work by Röben [15].

Axial forces

For all fire scenarios, compressive axial forces in end bays (Bay 1 and Bay 5) are significantly lower than in internal bays. This is because, as identified previously, the axial restraint to thermal expansion is provided by only one column on one of the sides. The highest axial forces develop when the frame is subjected to large fire sizes (e.g. ISO, SFPE, EC, and 48% TFM). Peak axial forces under these fires are 15 kN to 55 kN (2 - 13%) higher in comparison to 25%, 10%, and 2.5% travelling fires. Under uniform fires and 48% TFM, all beams in the floor are either in compression or tension at the same time, while under smaller travelling fire exposures this is not the case. This is because the total thermal expansion, even if the beams reach much lower peak temperatures exposed to uniform parametric fires, is larger than in beams with very high but localised peak temperatures. For example, beams exposed to the EC short-hot and 2.5% TFM reach the peak temperatures of 367°C and 578°C, respectively, but the peak compressive axial force for the EC short-hot fire is 55 kN higher than for the 2.5% TFM.

In addition, yielding of the first beams occurs sooner for more uniform fires, i.e., in the first 10 to 20 min of fire exposure. For the 25% TFM, 10% TFM, and 2.5% TFM, yielding only takes place at approximately 24 min, 42 min, and 148 min, respectively. After yielding, the compressive axial forces reduce and beams go into tension, initiating the catenary action. Stresses are redistributed to the stiffer surrounding structure, and the rate of increase in deflections reduces. Once the ultimate tensile strength is reached for the 25% TFM and the EC LC, the tensile forces begin to dissipate (see Fig. 4.9). However, after the average temperature of the heated beam begins to reduce (i.e. cooling begins), the beam regains some of its stiffness, and contraction leads to the increase in tensile forces again until the end of the fire. For other fires, similar behaviour is observed, but the beams do not reach their ultimate tensile strength before cooling because their

peak temperatures are lower. As the cooling begins, a small recovery in beam mid-span deflections takes place between 4 to 80 mm. The highest tensile axial forces during the fire develop for the smallest travelling fire sizes.
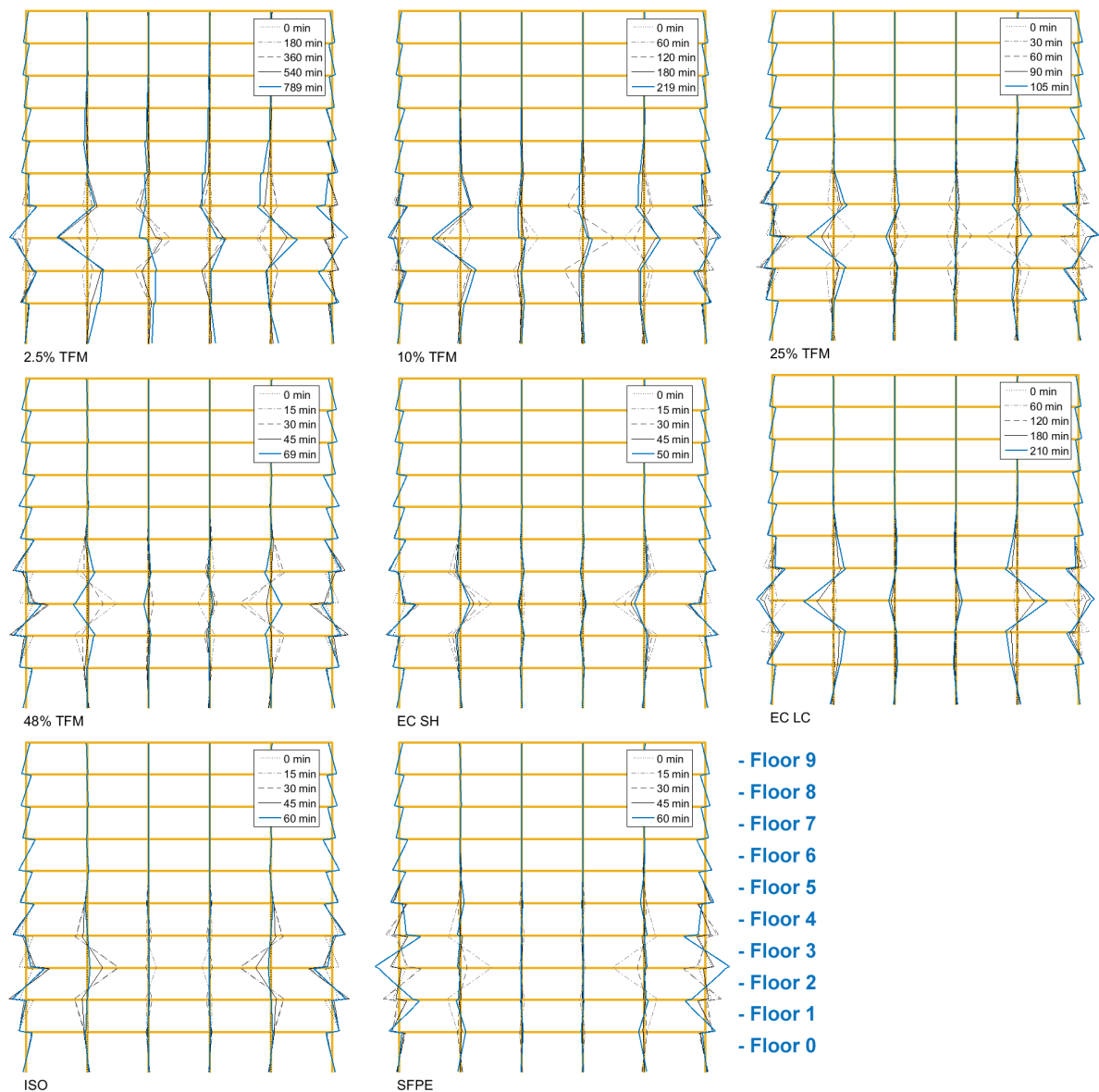
Bending moments

Peak mid-span bending moments for all fire scenarios are in the same range up to 160 kN.m. Larger bending moments tend to develop first in internal Bay 2 for the travelling fire scenarios, and internal Bay 3 for the EC parametric fires. General trends in bending moments follow the behaviour of axial forces. Axial forces increase bending moments and in turn deflections due to the P-Δ effect [41]. The distribution of bending moments in columns at different times of fire exposure is illustrated in Fig. 4.11. It shows that, as identified previously in Section 4.3.2, there is little effect on bending moments in columns during the fire higher than two floors above the fire floor, that is, in Floors 5 and higher for a fire occurring on Floor 2. For travelling fire scenarios, as the fire travels through the compartment, a reversal of column bending moments takes place. This is not the case for the uniform fire scenarios. The highest bending moments for both the uniform and travelling fire scenarios develop in the internal columns.
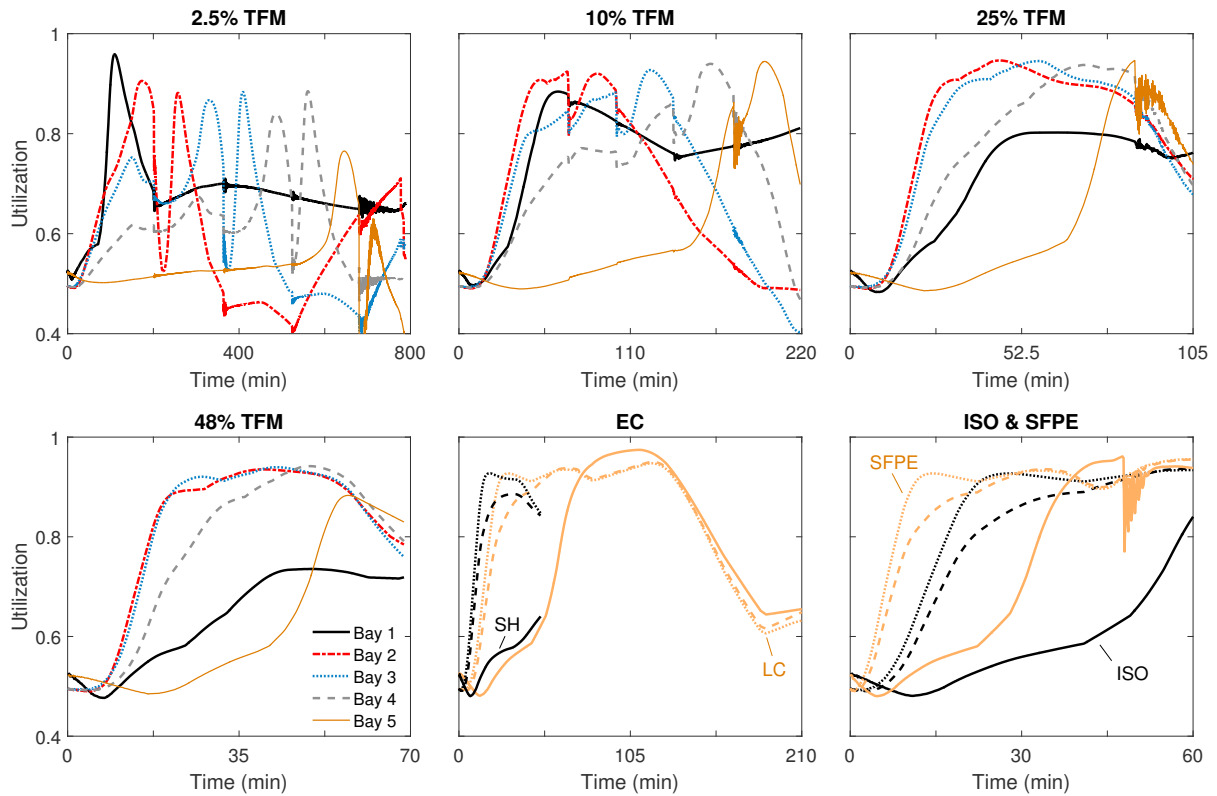
Utilization

The comparison of the evolution in utilization at the mid-point of the heated beams on Floor 2 is shown in Fig. 4.12. Utilization of the beams was calculated based on the plastic axial load and moment (P-M) interaction curves and axial forces and bending moments at every time step. P-M curves were calculated according to Garlock and Quiel [44]. Fig. 4.12 shows that irrespective of the fire scenario maximum utilization reached at the mid-span of the beams is within a similar range between approx. 94 and 97%. However, the members that reach this level of utilization are different. For uniform fire scenarios initially the internal bays are under higher utilization, but towards the end of the fire the end beams (i.e. Bay 1 and Bay 5) have a higher utilization. For travelling fire scenarios the location of the beam with the highest utilization varies with the fire size. For small TFM scenarios (5% and 10%) end beams reach higher utilization while for large travelling fires (25% and 48%) higher utilization develops in internal beams (Bay 2 and Bay 3). In addition, unlike under uniform and large travelling fires, beams in internal bays (Bays 2 to 4) subjected to small travelling fires (2.5% and 10%) experience high oscillations in the level of utilization with time. The oscillation amplitudes are approximately in the ranges of 2 - 38% and 4 - 16% for 2.5% TFM and 5% TFM, respectively.

Small irregular oscillations of bending moments, axial forces, and lateral displacements for 2.5% and 10% travelling fires can also be seen in Fig. 4.9. Their approximate amplitudes are 15 kN.m, 12 - 82 kN, and 4 mm, respectively. This is due to the reduction and then increase in tensile force identified previously and due to the spread of fire

Figure 4.11: Bending moment distribution in the heated columns at different times of fire exposure. Fire occurs on floor 2. Peak bending moments correspond to: 2.5% TFM - 599 kN.m, 10% TFM - 560 kN.m, 25% TFM - 377 kN.m, 48% TFM - 360 kN.m, EC SH - 410 kN.m, EC LC - 535 kN.m, ISO - 348 kN.m, and SFPE - 367 kN.m.

from one bay to another. The fire length for these cases is shorter than the bay length. Therefore, restrained thermal expansion only takes place at one bay at a time. For 2.5% TFM in Bay 3, the axial forces first increase due to the development of compressive forces in Bay 2. Once the beam in Bay 2 yields, the axial force decreases in Bay 3 as well. Then the near-field travels to Bay 3, and the axial forces begin to increase again due to restrained thermal expansion now occurring in this Bay. After the beam in Bay 3 yields, the compressive axial forces dissipate and the beam goes into tension. In the same manner, the beam in Bay 4 responds to changes in axial forces in the other bays, leading to oscillations in axial force and in turn bending moments. This is because, in these fire

Figure 4.12: Evolution in time of utilization at mid-span of the beams in Floor 2; Fire occurs on Floor 2.

scenarios, the beams yield before the fire travels to the other bays. Cyclic axial forces, as already identified in the introduction, can also be observed in the work by Bailey et al. [11]. Such cyclic loading could have an influence on further material degradation. No cyclic forces are present for uniform fires or large fire size TFM exposures.

4.4 Conclusions

Current design standards assume uniform temperature conditions in the compartment, while in reality, fires in large enclosures travel, resulting in highly non-uniform temperature distributions. In this chapter, the structural response of a generic protected steel frame exposed to travelling fires and uniform fires defined in the standards (i.e. the Eurocode and SFPE standards) on different floors of the building has been investigated. Travelling fire scenarios, Eurocode parametric curves, the ISO standard fire and the SFPE constant compartment temperature fire scenarios have been considered.

Results indicate that when different floors of the frame (one at a time) are subjected to the same fire exposure for both travelling and uniform fires, the development trends of displacements and stresses in beams are similar, except for fires occurring on the ground floor and the top floor. Higher displacements and lower axial forces develop within beams in the upper floors, where column section reduces in size, due to the reduced level of axial

restraint. However, beams subjected to fires on the bottom floors yield only up to 15 min later compared to the fires on the top floors of the frame. The development of axial forces and bending moments in the floors more than 2 floors away from the fire floor is found to be negligible. This indicates that modelling of five floors of the structure (with the fire in the middle floor) could be sufficient to capture the correct structural behaviour and stress redistribution. However, further studies on other types of structures need to be carried out to confirm this.

The rate and magnitude of the highest beam mid-span deflections depend mainly on the fire duration and not the fire type (i.e. TFM or uniform fire). Short and hot fires result in faster development of deflections, while long and cool fires result in larger peak deflections. The same observations were made by Lamont et al. [29]. On the other hand, the locations where these peak deflections occur are different for TFM and uniform fire scenarios. For travelling fires and uniform fires, the highest deflections initially develop in the end bays and central bay, respectively. Also, the displacements under travelling fire exposures are more irregular.

In general, uniform fire scenarios are found to result in 15 to 55 kN (2 - 13%) larger compressive axial forces in comparison to travelling fires, while peak bending moments are in the similar range for both travelling fires and uniform fires. When the frame is subjected to travelling fire scenarios, smaller than the width of the bay irregular oscillations of axial forces, bending moments, lateral displacements and thus member utilization (in the range of 2 - 38%) are observed. This is not the case when the frame is exposed to uniform fires or large size travelling fires. The oscillations in forces and moments could affect material strength.

The assessed case study indicates that travelling fires and uniform fires may trigger different structural responses for the same structure which may be important in the structural design and selection of the critical members. While uniform fires might lead to higher axial forces, travelling fires might result in larger displacements at different times and locations.

Acknowledgements

References

[1] J.-M. Franssen, "Improvement Of The Parametric Fire Of Eurocode 1 Based On Experimental Test Results," *Fire Safety Science*, vol. 6, pp. 927–938, 2000.

[2] J. Stern-Gottfried and G. Rein, "Travelling fires for structural designPart I: Literature review," *Fire Safety Journal*, vol. 54, pp. 74–85, nov 2012.

[3] J. Stern-Gottfried and G. Rein, "Travelling fires for structural design-Part II: Design methodology," *Fire Safety Journal*, vol. 54, pp. 96–112, nov 2012.

[4] A. Law, J. Stern-Gottfried, M. Gillie, and G. Rein, "The influence of travelling fires on a concrete frame," *Engineering Structures*, vol. 33, pp. 1635–1642, may 2011.

[5] J. Stern-gottfried, A. Law, G. Rein, M. Gillie, and J. L. Torero, "A Performance Based Methodology Using Travelling Fires for Structural Analysis," in *8th International Conference on Performance-Based Codes and Fire Safety Design Methods*, (Lund, Sweden), Society of Fire Protection Engineers (SFPE), 2010.

[6] CEN, "EN 1991-1-2:2002 - Eurocode 1. Actions on structures. General actions. Actions on structures exposed to fire," 2002.

[7] CEN, "EN 1993-1-2:2005 - Eurocode 3. Design of steel structures. General rules. Structural fire design," 2005.

[8] C. Zhang, G.-Q. Li, and A. Usmani, "Simulating the behavior of restrained steel beams to flame impingement from localized-fires," *Journal of Constructional Steel Research*, vol. 83, pp. 156–165, apr 2013.

[9] C. Zhang, J. L. Gross, and T. P. McAllister, "Lateral torsional buckling of steel W-beams subjected to localized fires," *Journal of Constructional Steel Research*, vol. 88, pp. 330–338, 2013.

[10] H.-X. Yu, X.-Q. Sun, and K. Wong, "Resistance of steel space frames subjected to localized travelling fire," in *Proceedings of the 8th International Conference on Structures in Fire* (G.-Q. Li, V. K. R. Kodur, S.-C. Jiang, J. Jiang, S.-W. Chen, and G.-B. Lou, eds.), (Shanghai, China), pp. 1121–1128, Tongji University Press, 2014.

[11] C. G. Bailey, I. W. Burgess, and R. J. Plank, "Analyses of the effects of cooling and fire spread on steel-framed buildings," *Fire Safety Journal*, vol. 26, pp. 273–293, jun 1996.

[12] J. Y. R. Liew, L. K. Tang, T. Holmaas, and Y. S. Choo, "Advanced analysis for the assessment of steel frames in fire," *Journal of Constructional Steel Research*, vol. 47, pp. 19–45, aug 1998.

[13] C. Röben, M. Gillie, and J. L. Torero, "Structural behaviour during a vertically travelling fire," *Journal of Constructional Steel Research*, vol. 66, pp. 191–197, feb 2010.

[14] E. Ellobody and C. G. Bailey, "Structural performance of a post-tensioned concrete floor during horizontally travelling fires," *Engineering Structures*, vol. 33, pp. 1908–1917, jun 2011.

[15] C. Röben, *The effect of cooling and non-uniform fires on structural behaviour*. Phd, The University of Edinburgh, 2009.

[16] A. Law, *The Assessment and Response of Concrete Structures Subject to Fire*. Doctor of philosophy, The University of Edinburgh, 2010.

[17] F. H. Rezvani and H. R. Ronagh, "Structural response of a MRF exposed to travelling fire," *Proceedings of the Institution of Civil Engineers - Structures and Buildings*, vol. 168, no. 9, pp. 619–635, 2015.

[18] P. Kotsovinos, *Analysis of the structural response of tall buildings under multifloor and travelling fires*. Doctor of philosophy, The University of Edinburgh, 2013.

[19] J. Stern-Gottfried, G. Rein, B. Lane, and J. L. Torero, "An innovative approach to design fires for structural analysis of non-conventional buildings, a case study," in *Applications of Structural Fire Engineering*, no. February, (Prague), pp. 34–40, Czech Technical University in Prague, 2009.

[20] E. Rackauskaite and J. A. El-Rimawi, "A Study on the Effect of Compartment Fires on the Behaviour of Multi-Storey Steel Framed Structures," *Fire Technology*, vol. 51, pp. 867–886, sep 2015.

[21] F. Sadek, J. A. Main, H. S. Lew, S. D. Robert, V. P. Chiarito, and S. El-Tawil, "NIST Technical Note 1669. An Experimental and Computational Study of Steel Moment Connections under a Column Removal Scenario," tech. rep., National Institute of Standards and Technology (NIST), 2010.

[22] G. Flint, S. Lamont, B. Lane, H. Sarrazin, L. Lim, D. Rini, and C. Röben, "Recent Lessons Learned in Structural Fire Engineering for Composite Steel Structures," *Fire Technology*, vol. 49, pp. 767–792, jul 2013.

[23] S. E. Quiel and M. E. M. Garlock, "3-D versus 2-D modeling of a high-rise steel framed building under fire," in *Proceedings of the 5th International Conference on Structures in Fire (SiF'08)* (K. H. Tan, V. K. R. Kodur, and T. H. Tan, eds.), (Singapore), pp. 278–289, 2008.

[24] G. Flint, *Fire Induced Collapse of Tall Buildings*. Doctor of philosophy, University of Edinburgh, 2005.

[25] BSI, "BS ISO 834-10:2014 Fire resistance tests. Elements of building construction. Specific requirements to determine the contribution of applied fire protection materials to structural steel elements," 2014.

[26] SFPE, "SFPE Engineering Standard on Calculating Fire Exposures to Structures . SFPE S.01 2012.," 2011.

[27] A. Law, J. Stern-Gottfried, and N. Butterworth, "A Risk Based Framework for Time Equivalence and Fire Resistance," *Fire Technology*, vol. 51, pp. 771–784, jul 2015.

[28] F. M. Block and T.-S. Kho, "Engineering an Icon or the Probabilistic-based Structural Fire Engineering of the Battersea Power Station," in *Proceedings of the 9th International Conference on Structures in Fire* (M. E. M. Garlock and V. K. R. Kodur, eds.), (Princeton, NJ), pp. 901–908, DEStech Publications, 2016.

[29] S. Lamont, A. S. Usmani, and M. Gillie, "Behaviour of a small composite steel frame structure in a "long-cool" and a "short-hot" fire," *Fire Safety Journal*, vol. 39, pp. 327–357, jul 2004.

[30] R. L. Alpert, "Calculation of response time of ceiling-mounted fire detectors," *Fire Technology*, vol. 8, pp. 181–195, aug 1972.

[31] A. H. Buchanan, *Structural Design for Fire Safety*. John Wiley & Sons, Ltd, 2001.

[32] ECCS, "Design Manual on the European Recommendations for the Fire Safety of Steel Structures," tech. rep., European Convention for Constructional Steelwork - Technical Committee 3 - Fire Safety of Steel Structures, 1985.

[33] B. R. Kirby, "Recent developments and applications in structural fire engineering designA review," *Fire Safety Journal*, vol. 11, pp. 141–179, dec 1986.

[34] HMGovernment, "Fire safety: Approved Document B. Volume 2 - Buildings other than dwelling houses," 2006.

[35] S. A. Kilic and S. Selamet, "Symmetric and Asymmetric Collapse Mechanisms of a Multi-Story Steel Structure subjected to Gravity and Fire," in *Structures Congress 2013*, (Reston, VA), pp. 2545–2554, American Society of Civil Engineers, apr 2013.

[36] A. Law, P. Kotsovinos, and N. Butterworth, "Engineering geometrically bi-linear columns to deliver fire resistance: Standard heating," *Engineering Structures*, vol. 100, pp. 590–598, oct 2015.

[37] J. O. Hallquist, *LS-DYNA theory manual.* Livermore Software Technology Corporation, 2006.

[38] CEN, "EN 1993-1-1:2005 - Eurocode 3. Design of steel structures. General rules and rules for buildings," 2005.

[39] M. M. S. Dwaikat and V. K. R. Kodur, "A performance based methodology for fire design of restrained steel beams," *Journal of Constructional Steel Research*, vol. 67, pp. 510–524, mar 2011.

[40] A. S. Usmani, J. M. Rotter, S. Lamont, A. M. Sanad, and M. Gillie, "Fundamental principles of structural behaviour under thermal effects," 2001.

[41] V. K. R. Kodur and M. M. S. Dwaikat, "Response of steel beamcolumns exposed to fire," *Engineering Structures*, vol. 31, pp. 369–379, feb 2009.

[42] Y. Z. Yin and Y. C. Wang, "A numerical study of large deflection behaviour of restrained steel beams at elevated temperatures," *Journal of Constructional Steel Research*, vol. 60, no. 7, pp. 1029–1047, 2004.

[43] A. Law, "Perimeter Column Boundary Conditions in Structural Fire Modelling," *Fire Technology*, sep 2015.

[44] M. E. Garlock and S. E. Quiel, "Plastic Axial Load and Moment Interaction Curves for Fire-Exposed Steel Sections with Thermal Gradients," *Journal of Structural Engineering*, vol. 134, pp. 874–880, jun 2008.

Appendices

4.A Supporting data

In Sections 4.3.2 and 4.3.3, the effect of location of the fire floor in compartment on the structural response of the frame are illustrated for selected fire sizes (Figs. 4.7 and 4.8). In this appendix, comparison of the results for all fire scenarios investigated in this chapter is presented. Figs. 4.A1 and 4.A2 show variation of displacement, axial force, and bending moment in beams exposed to fire, and variation of axial forces within different bays of the frame, respectively. In Fig 4.A1, the high variation present in the development of axial forces and bending moments towards the end of the 25% TFM (i.e.

when the beam goes into tension) are because of the oscillations from the explicit dynamic simulation in LS-DYNA.

In addition, illustration of the bending moment distribution in the heated beams for all fire scenarios investigated is provided, Fig. 4.A3. Uneven bending moment distributions at later stages of the fire indicate the formation of plastic hinges and the redistribution of stresses. Plastic hinges during the fire form in the EC, LC, and SFPE fires, and in all travelling fire scenarios except for the 48% TFM.
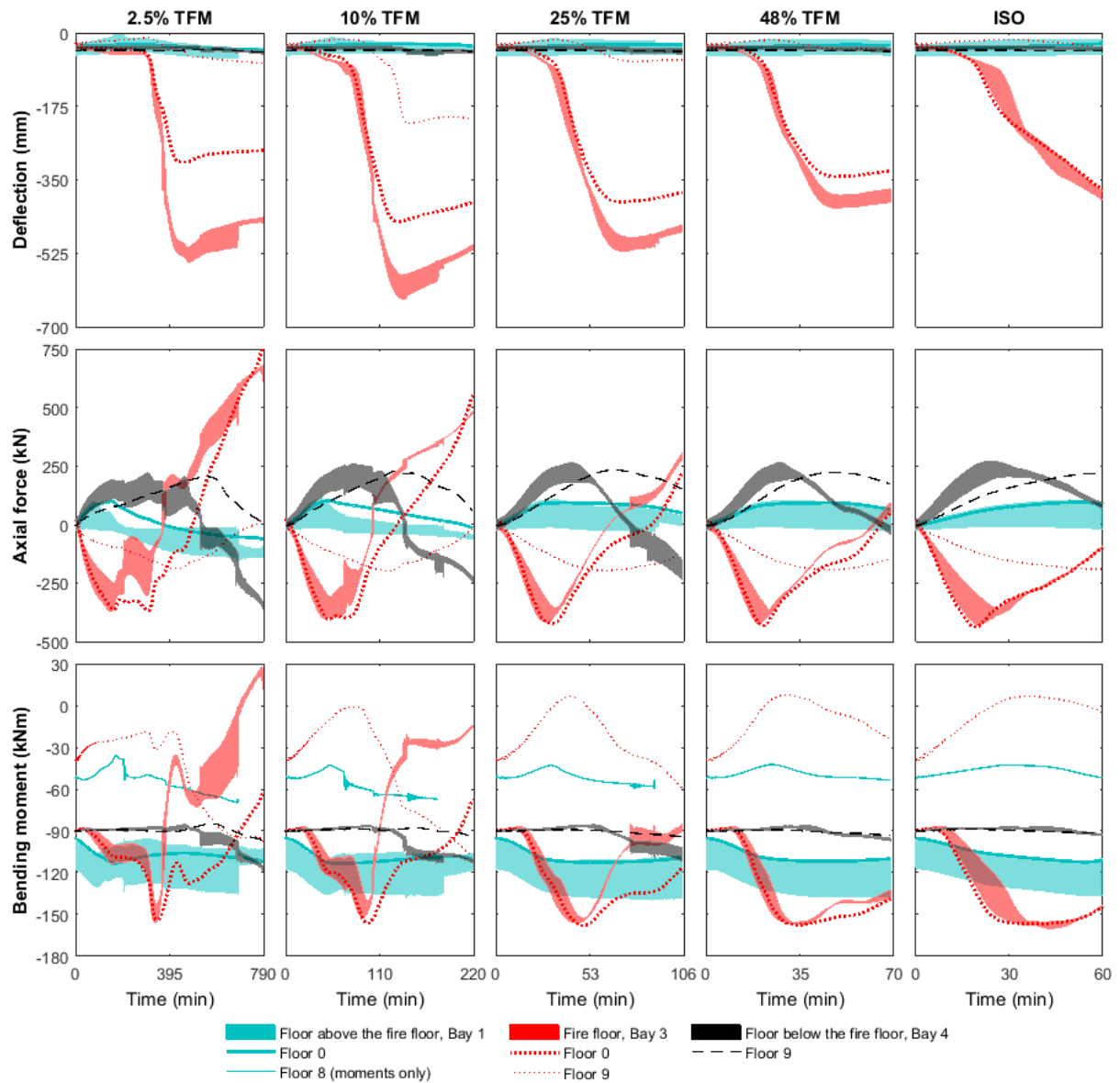
Figure 4.A1: Variation of displacement, axial force and bending moment development in beams exposed to different fire scenarios. Numbers for each of the lines indicate results when fire occurs on ground floor (0), Floor 8 (moments only), and top floor (9).

.
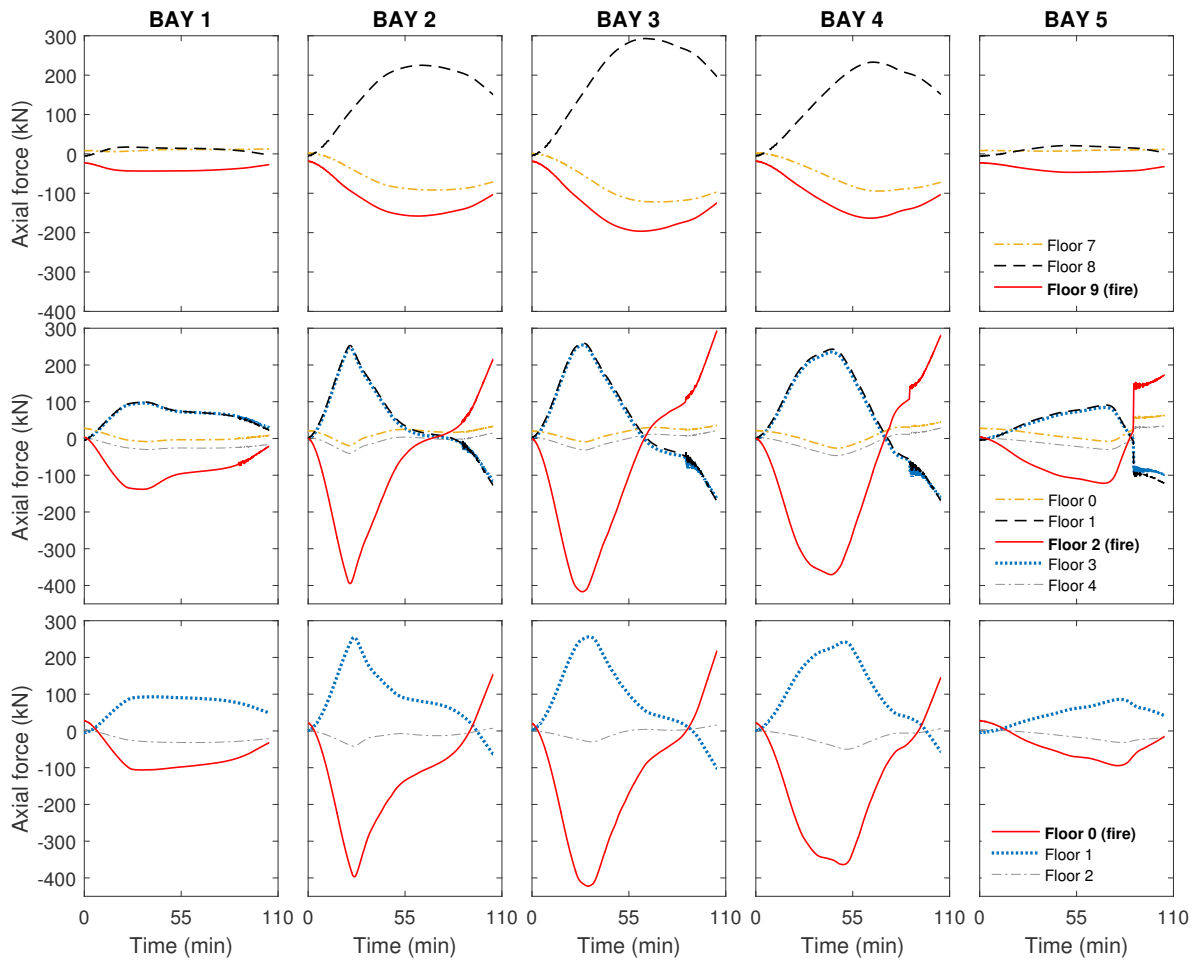
Figure 4.A2: Variation of axial forces within different bays for a frame subjected to a 25% travelling fire on Floor 0 (bottom), Floor 2 (middle), and Floor 9 (top). Bays 1 and 5 are the end bays and Bays 2 to 4 are the internal bays of the frame.

.
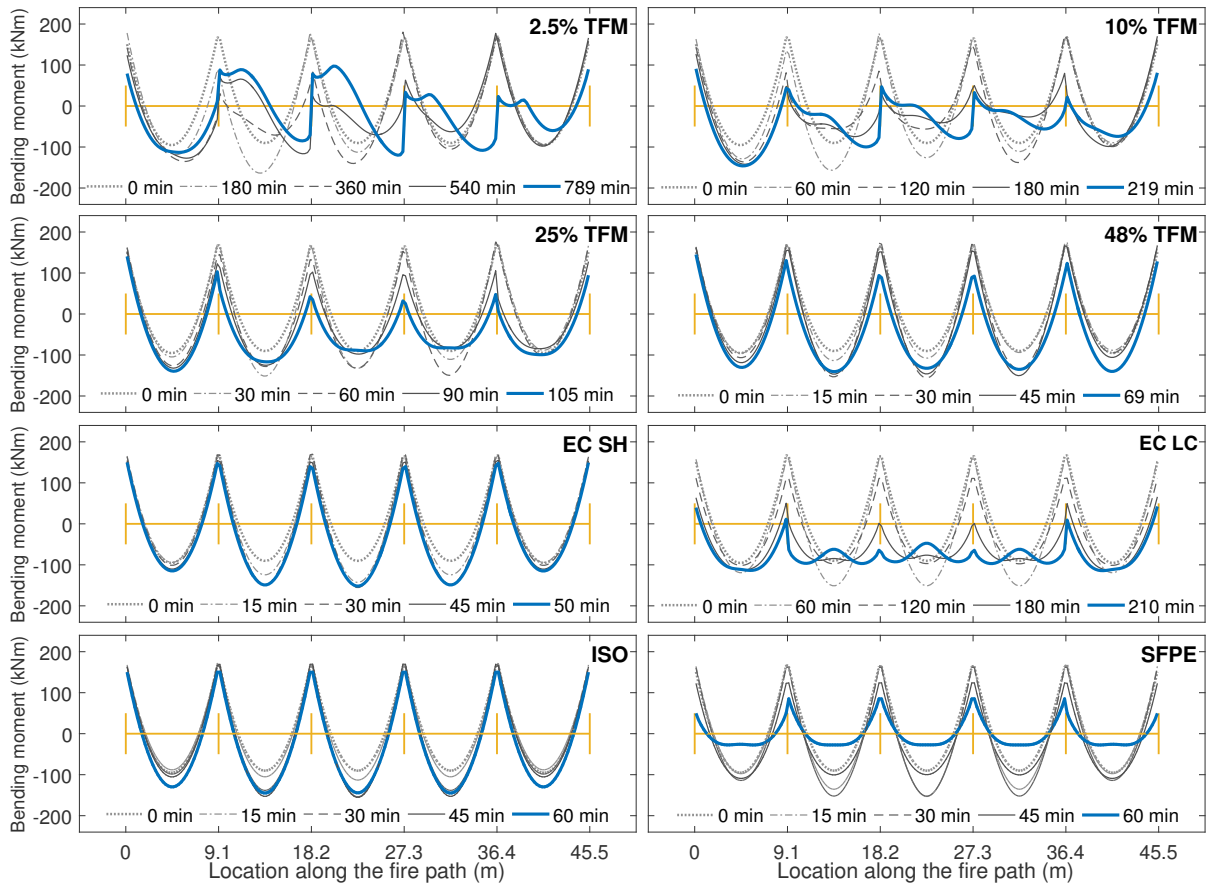
Figure 4.A3: Bending moment distribution in the heated beams at different times of fire exposure for all fire scenarios investigated. Fire occurs on Floor 2.

Chapter 5

Computational Analysis of Thermal and Structural Failure Criteria of a Multi-Storey Steel Frame Exposed to Fires

Summary [1]

The evaluation of the structural performance in fire in the prescriptive design and probabilistic analyses is typically based on the critical structural member temperature criteria. However, it is unclear of how representative such criterion is of the actual structural response, particularly in the case of non-uniform fires. In this chapter, the appropriateness of critical temperature as a failure criterion for structures subjected to non-uniform fires is assessed. Additionally, this chapter investigates the effects of different fire exposures (uniform and travelling fires), location of the fire floor location, level of protection, and beam section size on various structural limit states. A two-dimensional 10-storey 5-bay steel frame designed according to ASCE 7-02 and representative of a generic steel framed building is modelled using the general finite element software LS-DYNA. The fire exposures investigated include travelling fires, Eurocode parametric, ISO-834 standard fire and the SFPE constant compartment temperature curves. These fires are applied one at a time at different floors of the building. In total 117 different scenarios are investigated. Ultimate strain, member utilization, beam mid-span deflection, and critical member temperature failure criteria are considered. The results indicate that there is no single fire scenario which would represent the worst case. For different fire exposures, failure occurs on different floors. Nevertheless, results show that the critical member temperature in the compartment could be safely used as the conservative failure criterion in the assessments of generic steel framed buildings without any particularly unusual characteristics when subjected to both uniform and non-uniform fires.

---

1. This chapter is based on "E. Rackauskaite, P. Kotsovinos, A. Jeffers, G. Rein (2017) *Computational Analysis of Thermal and Structural Failure Criteria of a Multi-Storey Steel Frame Exposed to Fires*, (submitted)."

5.1 Introduction

Structural fire design until recently has been based on the assumption of uniform fires in the compartment (i.e. standard fire, the Eurocode parametric time-temperature curves or another post-flashover fire methodology). While this assumption may be suitable for small enclosures, fires in large open-plan compartments, representative of modern architecture, have been observed to travel resulting in a highly non-uniform transient temperature distributions within the enclosure [1]. Such fires have been observed most recently during the recent fire at the multi-storey composite Plasco building in Tehran (Jan 2017), which ultimately collapsed. In order to account for travelling fires a design concept called Travelling Fires Methodology (TFM) [1, 2] has been developed.

Given that the majority of modern buildings have layouts which fall outside the limitations of current prescriptive standards and are more likely to experience travelling fires, there has been a significant increase in industry in the performance based design of such buildings by employing both travelling fires and uniform fires in a probabilistic approach [3–5]. Due to the stochastic nature of fire, a probabilistic approach allows a better understanding of the overall building performance, e.g. to determine the fire resistance period or the design fires for a building that correspond to its individual target reliability. When carrying out probabilistic assessment, there is often the need to use a simple structural failure criterion which allows multiple simulations of the same analysis. The outcome of the assessment would be therefore sensitive to the assumptions regarding the structural failure criterion. Currently, there is no widely accepted single structural failure criterion. Traditionally, structural response and failure have been assessed in the terms of critical member temperature, maximum displacement or rate of deflection and exceeded member load-bearing capacity (i.e. collapse). The latter two criteria would require a structural fire analysis using advanced computational methods (i.e. FEM) and therefore are not feasible for probabilistic assessment in a design context due to the computational time and the high number of simulations required. In the future, the current improvements in the efficiency of probabilistic methodologies to reduce number of samples needed and increased computing power could make such an approach feasible. Thus, most of probabilistic methods used in design for assessing structural response to fire are currently based on the critical member temperature failure criterion [3–6].

It is commonly believed that for regular steel framed buildings without any unusual characteristics (such as those noted in [7, 8]) structural fire design based on the critical member temperature failure criterion is conservative. However, even in the early stages of the development of the standard fire tests (ASTM E119) there has been a lot of disagreement on the critical temperature for steel members because it is significantly affected by the restraint conditions and load redistribution [9]. Since then Eurocode [10] and other proposals [11, 12] have been introduced in the literature to predict critical member temperatures based on the utilization of the members at ambient temperature.

While these may be able, to some extent, to indicate the temperature at which the structure is near to collapse, they are limited to individual members with longitudinally uniform temperatures. In addition, the link between the critical member temperature based on load-bearing capacity and other failure criteria and which of these criteria is more conservative is unclear. It should be noted that the recently developed ASCE/SEI 7-16 Appendix E does not accept the use of the critical temperature as a performance indicator of structural failure and obligates the designer to analyse the structural response due to the thermal demand without exception.

Skowronski [13] in his work on heated steel beams has found that critical member temperature based on load bearing capacity and deformation limit state can be up to 30% different and that depending on the beam slenderness, load and heating rate either of them can be more critical. This difference could likely be even higher for structures subjected to non-uniform transient fire exposures such as travelling fires due to non-uniform heating and longer fire durations. In the work on the thermal response of structures subjected to travelling fires [2, 14, 15] it has been found that in general travelling fires are likely to result in higher peak member temperatures in comparison to uniform fire scenarios (e.g. Eurocode parametric temperature-time curves [16]). In terms of structural response, the recent work has shown that both travelling fires and uniform fires can represent the worst case scenario depending on the structural metric examined (e.g. deflections, plastic strains, axial forces, etc.) since they introduce a different range of behaviours for the same building [14, 17–21]. However, in only a few of the latter studies [14, 19] the thermal response and critical member temperatures have been analysed and/or compared to other failure criteria.

Law et al. [14] investigated the structural response of a concrete frame subjected to travelling fires and uniform fires. Peak temperatures, rebar strains and deflections were assessed as the failure criteria and were compared for the different fire exposures. The results indicated that the temperature and deflection criteria were more critical, i.e. indicated that the structure was closer to failure [14] compared to the strain criterion. Structural distress trends with varying travelling fire sizes were similar for all the failure criteria. Rezvani and Ronagh [19] investigated the structural response of an unprotected moment resisting steel frame subjected to travelling fires and reported the critical times and the corresponding temperatures for column buckling and beam deflection limit states. Larger travelling fire sizes resulted in shorter times to failure and larger corresponding member temperatures. In general, column buckling was more critical in terms of potential failure than beam mid-span deflection limit state (it should be noted that the structure was unprotected).

The aim of this chapter is to study the structural response of a multi-storey steel frame subjected to travelling fires and uniform fires. The effects of different fire exposures, location of the fire floor in the frame, level of protection, and beam section size on various failure criteria and corresponding failure temperatures are investigated. Load-bearing

capacity, beam mid-span deflection, limiting temperature and member utilization limit states are considered. In Chapter 2 locations of the peak temperature in the compartment for different travelling fire scenarios have been reported. In this Chapter they are compared to the actual failure locations in the compartment for different failure criteria related to the structural response. To the best of the author's knowledge a similar study assessing the failure criteria of steel frames exposed to non-uniform fires has not been reported in literature. This is a continuation of the work presented in Chapter 4.

5.2   Finite element model

Full-scale testing of real structures is complex, expensive and time consuming. This is especially the case for structures with large compartments. There has only been a limited number of full-scale tests on real buildings carried out worldwide (e.g. Cardington tests). As a result, computational tools are commonly used to assess the structural response of complex buildings under fire conditions. For the same reasons analyses presented in this chapter are based on the computational study of a 2D steel frame using a finite element software LS-DYNA. A 2D analysis has been chosen for the reasons of simplicity, computational time to allow comparison of many different scenarios (i.e. 117), and due to the fact that the travelling fire methodology defines fires spreading along a linear path. A uniform thermal profile in the side perpendicular to the direction of fire travel is assumed.
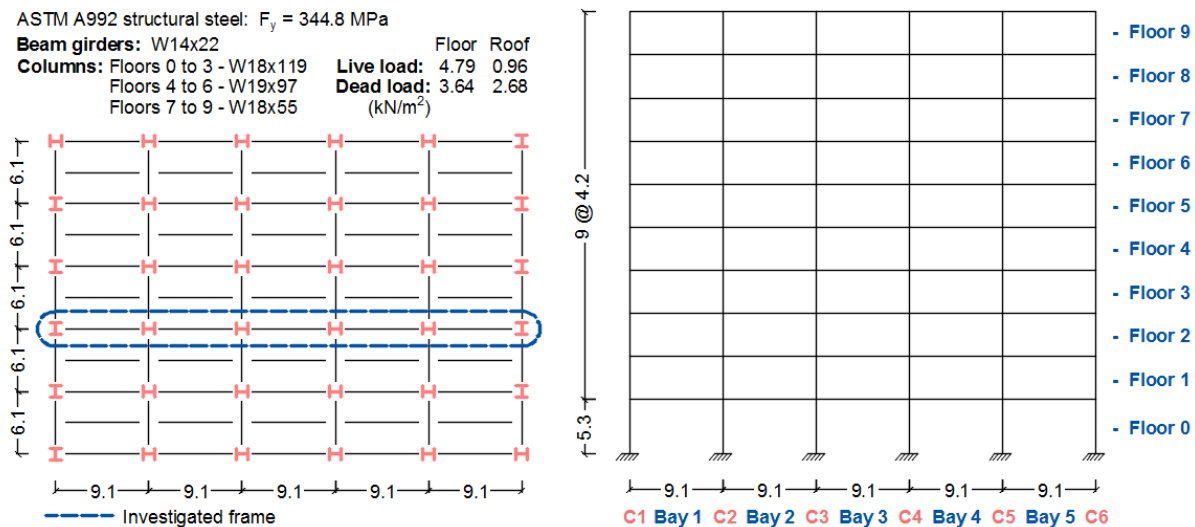
5.2.1   Multi-storey frame

The multi-storey steel frame considered in this analysis is the same as in Chapter 4 and is based on the moment resistant frame published by NIST [22]. It is a 10-storey 5-bay frame representative of a generic office building with a floor layout of 45.5 m × 30.5 m. The frame is quite regular and does not present any unusual structural characteristics which would make it particularly sensitive to thermal expansion. It is designed according to the American Society of Civil Engineers (ASCE 7-02) standard. The plan layout and elevation of the building are shown in Fig. 5.1. In this study the structural fire response of a 2D internal frame with the longest beam span of 9.1 m is investigated. For more details the reader is referred to Chapter 4, Section 4.2.1 of this thesis.

5.2.2   Fire scenarios

The structural response of the frame subjected to travelling fires (TFM) (Chapter 2) and uniform design fires such as Eurocode (EC) parametric temperature-time curves [16], the standard fire (ISO) [16, 25], and the SFPE standard constant compartment temperature design fire [26] is investigated.

To represent the travelling fire exposure, iTFM presented in Chapter 2 and illustrated in 5.2 is used. Each floor of the frame in this study is subjected to five TFM scenarios: fire

Figure 5.1: Plan layout (left), elevation (right) and structural member details of the investigated multi-storey steel frame from [22]. Frame dimensions are given in meters.
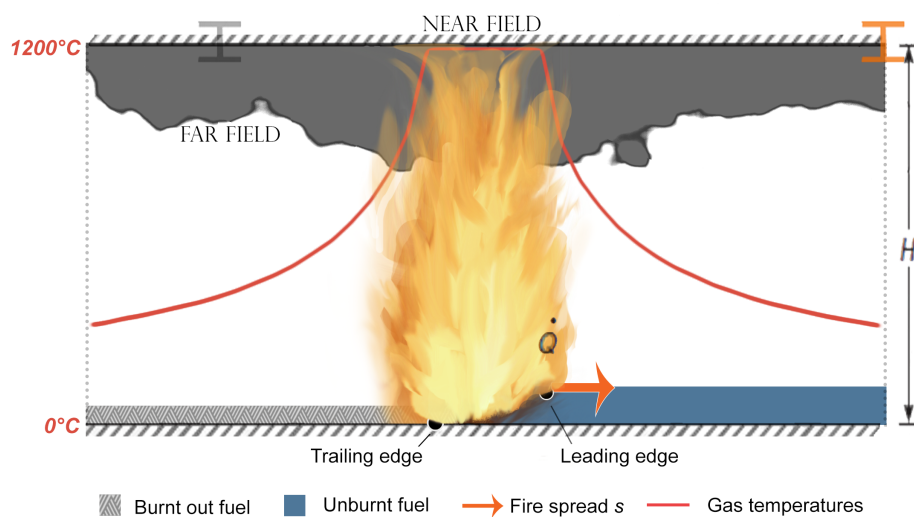
Figure 5.2: Illustration of a travelling fire and distribution of gas temperatures in the near-field and far-field.

sizes of 2.5%, 5%, 10%, 25%, and 48% of the floor area. In addition, two Eurocode [16] parametric temperature-time curves are considered, representing short-hot (EC SH) and long-cool (EC LC) fire exposures based on the study by Lamont et al. [28]. The correlation to represent the standard fire (referred to as the "ISO standard fire" in this chapter) and constant compartment temperature design curve (referred to as "SFPE" in this chapter) are taken from the Eurocode [16] and SFPE standard [26], respectively. The same fire scenarios were considered and more details are given in Chapter 4, Section 4.2.2 of this thesis.

Each fire scenario is applied, one at a time, on every floor of the frame. In addition, for each fire scenario occurring on Floor 7 the level of member protection and beam section

size is varied to assess the effects of the unevenness in fire protection and increase in beam section size in the achieved fire resistance of the frame. These effects are presented and discussed in Appendix 5.A. Therefore, in total 117 scenarios are investigated. All the investigated scenarios of this study are summarised in Table 5.1. B60 and C60 refer to the equivalent standard fire resistance of beams and columns, respectively. Illustration of the gas temperatures for all fire scenarios at the mid-span of Bay 2 and at the right end of Bay 5 is shown in Fig. 5.3.

Table 5.1: Details of the fire scenarios considered in the study.

Reference	Equivalent standard fire resistance [a]		Beam section size	Fire floors	Fire exposures
	Beams	Columns			
B60 C120	60 min	120 min	W14×22	0, 1, 2, 3, 4, 5, 6, 7, 8, & 9	2.5%, 5%, 10%, 25%, & 48% TFM, EC SH, EC LC, ISO, & SFPE
B60 C60	60 min	60 min	W14×22	7	
B120 C120	120 min	120 min	W14×22	7	
B60 C120 LC	60 min	120 min	W16×26	7	

a. Equivalent standard fire resistance refers to the different thicknesses of fire protection based on the limiting steel temperature of 550°C under a standard fire exposure.
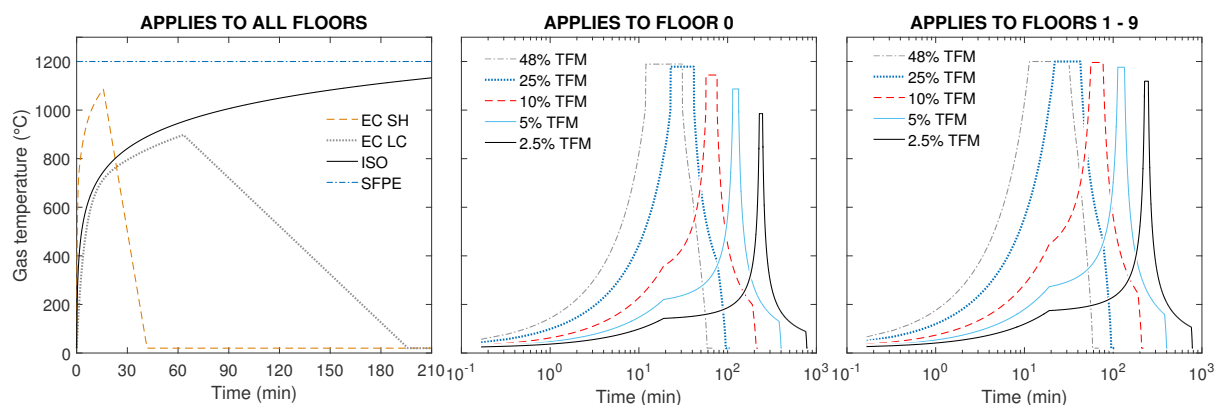
Figure 5.3: Gas temperature histories at mid-span of Bay 2 (top) and right end of Bay 5 (bottom) for the nine fire scenarios on each floor of the frame: EC, ISO, and SFPE fires for all floors (left) and TFM fires for Floor 1 (middle) and Floors 1 to 9 (right).

5.2.3 Heat transfer

Beams and columns are designed for either 60 min or 120 min standard fire resistance depending on the investigated scenario (see Table 5.1). The fire protection thickness required to deliver these fire resistance standards was based on the simplified and conservative empirical equation (see Chapter 4, Section 4.2.3, Eq. (4.1) [30, 31]) assuming a

limiting temperature of steel of 550°C. (see Section 5.2.5). Heat transfer to the structural members was carried out assuming lumped capacitance for separate parts of the cross-section (i.e. web and flanges) according to [2, 30]. For more information, see Chapter 4, Section 4.2.3.

5.2.4   LS-DYNA model

The multi-storey steel frame is modelled using the general purpose finite element software LS-DYNA (Release 7.1.1) explicit solver. The LS-DYNA model used was the same as in Chapter 4 and, therefore, all the details are given and the reader is referred to Chapter 4, Section 4.2.4 for more information.

The aim of this study is the investigation of the global structural response, and, thus, no attempt was made to capture any localized failures, local buckling and/or connection failure. However, it should be noted that the frame is provided with a concrete slab and therefore lateral torsional buckling of the beams is prevented [10]. Additionally, the beams do not have any web openings or asymmetries and, therefore, a localised failure is not likely to govern [37].

Once the simulations were completed, data on the development of axial forces, bending moments and displacements in frame were extracted and are analysed in the following section.

5.2.5   Failure criteria

In Chapter 4 the generic structural response of this steel frame has been analysed in the terms of development of stresses and deflections. Even though these metrics give a useful overview of structural behaviour, they give no indication of how close is the frame to failure for different fire scenarios. Thus, the aim of this Chapter is to extend previous work and assess structural fire performance in terms of different failure criteria and the corresponding critical member temperatures. Critical member temperature, load-bearing capacity, and beam mid-span deflection criteria and overall frame utilization are considered.

It should be noted that the failure criteria examined in this chapter are only concerned with the load bearing fire resistance of a structural frame and not with other criteria such as integrity or insulation that may sometimes govern the fire safety design. Additionally, designer needs to show caution in which criteria they adopt in conjunction with other elements of construction that may not be represented in a structural model but may have their own failure/criteria or limits such as fire protection materials (for example the strain limits of intumescent paint), deflection heads in compartment walls, fire stops in compartment floors, etc.

Critical member temperature criterion

In the standard fire test (ASTM E119 [45])) of individual members the critical temperature criterion is used as a measure of their performance. A structural member would be exposed to a standard fire curve (if a steel member, typically provided with a fire protection material) and the time taken for the member to reach the prescribed failure temperature would be recorded as the rating of the member (e.g. 30 min or 2 h). In ASTM E119 the temperature criterion was first introduced in 1964 [9] for steel beams. Previously, it was required that the member does not collapse, which was judged by the furnace operator. Though, time when the critical member temperature had been reached was considered of known interest [39]. In 1964, the standard required that the average temperature of the steel beam does not exceed 1200°F (649°C) and that the maximum temperature at any location does not exceed 1400°F (760°C) during the classification period. In 1967 the unrestrained and restrained beam classifications were introduced to account for the fact that restrained beams usually showed a better performance in fire (i.e. based on the evidence of structural failure) in comparison to unrestrained beams [9]. It was also based on theories that restrained beams performed better due to, for example, redistribution of stresses, restraint developed compressive stresses, developed negative moments, composite action, etc. [9]. For the restrained beams the temperature criterion was left the same and for unrestrained beams the average and the maximum temperature at any location temperature requirements were 1000°F (538°C) and 1200°F (649°C), respectively. These temperatures were chosen based on the assumption that at 1000°F (538°C) steel retains approximately half of its' original strength [9] and that the tests carried out at the time showed rapid development of deflections at temperatures higher than 1200°F (649°C) [40]. In 1988, the critical member temperatures for restrained beams were decreased by 100°F (38°C) and have not been updated. In the BS 476-8:1972 and BS 476-23:1987 standards similar criterion was introduced for the steel beams protected by suspended ceilings in 1972 and 1978, respectively. Member average and maximum temperature limits were 550°C and 650°C, respectively, for loaded beams and for the unloaded beams the maximum temperature limit was 400°C.

In structural fire design, the critical member temperature has been used as one of the limit states since the first attempts in European standardisation for fire in 1983, and is defined as the temperature at which structure is expected to be at the point of collapse. In the current Eurocode (EN 1993-1-2 [10]) the critical member temperature limit state is based on the value of member utilization at ambient temperature assuming a uniform temperature distribution. For the range of utilization factors from 0.2 and 0.8 the critical member temperatures are typically in the range between 500°C and 700°C. Critical member temperatures used in the ASTM E119 standard fall inside this range as well. Thus, the lower limiting temperature of 550°C is commonly accepted [32] as the critical member temperature in the structural design and is used for assessment of structural performance. At 550°C steel maintains only 60% of its ambient temperature

strength because of the thermal degradation of its mechanical properties. For simplicity, the same critical member temperature of 550°C is assumed in this study. It should be noted that other beams such as beam with holes may have lower critical member temperatures but these beams are not included as part of this study.

Critical deflection criterion

The first nationwide attempts at the standardisation of structural fire tests in the USA and UK were in the early 20th century [41]. However, these early standards had no prescribed failure criterion and the collapse (i.e. failure) relied instead on the judgement of the furnace operator. Ryan and Bender [39] and Ryan and Robertson [42] were the first to attempt to define a general criterion for load failure during the standard fire test. The criterion was defined in terms of the limiting mid-span deflection of the beam of $L^2/800d$ and a rate of deflection of $L^2/9000d$ over 1 min, where L and d are beam length and section depth, respectively [42]. Authors noted that high deflections might not necessarily indicate structural collapse and suggested that both previously identified criteria ($L^2/800d$ and $L^2/9000d$ over 1 min) need to be exceeded to give a crude practical indication of a load failure. The proposed criteria were empirical and based on the equation for the maximum deflection of the beam (Eq. (5.1)).

$$y_{max} = k \left(L^2/d \right) (e_1 - e_2) \tag{5.1}$$

where k is the numerical constant depending on the type of support and loading, and $e_1 - e_2$ is the difference between the strains in the planes of the two surfaces of the specimens separated by the distance d.

Ryan and Robertson criterion is still today widely used in standard fire tests (BS 476-10:2009 [43], ISO 834-1 [44], ASTM E119-16 [45]) and in the assessment of the structural performance. Nevertheless, the critical deflection has been increased to $L^2/400d$ in ISO 834-1 [44] and ASTM E119-16 [45] and replaced by $L/20$ in BS 476-10:2009 [43]. In addition, the limiting rate of deflection of $L^2/9000d$ over 1 min in BS 476-10:2009 [43] is only considered after the mid-span deflection of the beam of $L/30$ has been exceeded. According to Law et al. [14] and Lamont et al. [46], the deflection criterion of $L/20$ is based on the standard test furnace and was chosen to ensure that it is not damaged during testing. In structural fire design of steel structures, the deflection criteria ($L/30$) has only been included in European recommendations for fire safety of steel structures in 1983 [47].

Since the development of these deflection criteria and it is now known that large beam deflections do not necessarily indicate the onset of structural collapse [48]. However, they may be important for the integrity of fire protection and fire compartmentation (e.g. fire walls are breached due to gap as a result of large deflections). In the BS 5950-8 a deflection limit state of $L/100$ existed for beams which have fire resisting walls under

them. In this study the maximum deflection criteria of $L/20$, $L^2/400d$ and the limiting rate of deflection of $L^2/9000d$ over 1 min are chosen as performance indicators.

Ultimate strain

The critical member temperature and maximum deflection criteria are simple measures to assess the structural performance in fire, particularly in the standard fire test. However, they do not give an indication and the relation to the actual load-bearing capacity of the structure and the occurrence of collapse is uncertain. Structural failure occurs once the stresses that develop within the member due to fire exceed its load-bearing capacity. In this study structural failure is based on the calculated failure of structural members, i.e. the ultimate strain, during the computational LS-DYNA analysis. Failure in the LS-DYNA analysis is defined according to the Eurocode EN 1993-1-2 material model and takes place in any member when the ultimate strain of 0.2 for steel is exceeded. Failure of the first element is considered as an indication of collapse (as commonly assumed in prescriptive guidance). Progressive collapse of the frame was not considered and was not taken into account in the computational model.

Utilization

Utilization is considered here as the ratio of the load carried by the member and its load carrying capacity. Unlike critical member temperature and deflection criteria, it gives an indication of how close the member is to structural failure. In EN 1993-1-2 [10], member utilization is used to determine the critical member temperature of a member. However, it is based on uniform temperature distribution and the applied loading at ambient temperature. The thermally induced forces that develop due to restrained thermal expansion and thermal bowing or other effects are not taken into account. The utilization analysis in this study is based on the work by Garlock and Quiel [49] where the yield capacity is represented by plastic axial load and moment (P-M) interaction curves for steel sections with non-uniform through-depth temperature distributions. The P-M curves are determined by moving the neutral axis (i.e. axis of zero strain) through the depth of the section and integrating the stresses at each location to find the axial load P and bending moment M according to Eq.(5.2) and Eq.(5.3), respectively [49].

$$P = \int_A \sigma_y dA \tag{5.2}$$

$$M = \int_A \sigma_y z dA \tag{5.3}$$

where σ_y is the yield stress as a function of the temperature distribution, A is the cross-section area, and z is the distance to the reference axis. LS-DYNA uses geometric centroid as the reference axis for the calculation. Thus, for an easy comparison with computational results the geometric centroid is used as the reference axis to calculate the bending

moment for the P-M curves in this study as well. Temperature dependent steel yield strength reduction factors are taken from the Eurocode [10] as in the LS-DYNA analysis. The same sign convention as in [49] is used. Positive bending moment represents tension in the top flange and positive axial force represents compression.

Illustration of P-M curves at ambient temperature and during the 25% travelling fire occurring on Floor 8 is shown in Fig. 5.4. P-M curves are shown for the beam mid-span in Bay 3 and the element that failed first in the terms of ultimate strain criteria. In this study, based on these curves, and the axial force and bending moment output from the computational analysis using LS-DYNA, the utilization of each element is calculated at every time step.
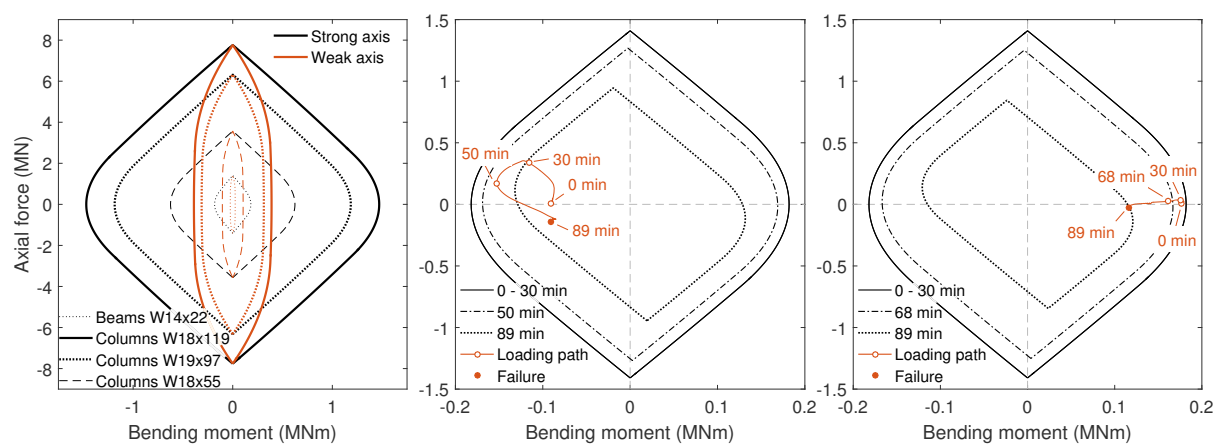
Figure 5.4: Illustration of the P-M interaction curves for frame elements at room temperature (left); during the 25% TFM occurring on Floor 8 for the Bay 3 beam mid-span (middle), and the element that failed (right) and their utilization. Failure indicates a time close to the ultimate strain failure.

5.3 Results and discussion

5.3.1 Peak temperatures

A comparison of the peak temperatures that develop within the heated steel beams for different fire exposures (travelling fires and uniform fires) and the time to reach them are shown in Fig. 5.5. For the ISO and SFPE fires the temperature is shown at the corresponding beam fire resistance time, i.e. at 60 min (B60) and at 120 min (B120). The limiting temperature used in the design of this fire protection was 550°C. However, beams B120 under standard fire exposure after 120 mins only reach the temperature of 400°C. This is because different equations were used for the calculation of fire protection thickness than for the actual heating of the beam. For the former, a very simple empirical equation was used (Eq. (4.1)) that assumed uniform heating of the beam, while in the heat transfer calculations (Eq. (4.2)) for the structural analysis separate temperatures

were calculated for the flanges and web. This is a conservative approach and equally it is not uncommon for fire protection providers to overdesign fire protection materials based on a simplified assessment rather than a detailed thermal response assessment. It should be noted that the use of different equations for fire protection thickness and heat transfer calculations does not affect the results on the structural response as the main aim of this work is to compare the structural response and failure criteria between different cases investigated in this study.

As could be expected at 60 min and 120 min, for both beams B60 and B120, the SFPE fire results in higher temperatures than ISO fire by 190°C and 110°C, respectively. In general, the results indicate that between fires with fire decay period (i.e. TFM and EC) 2.5 - 10% travelling fires lead to the highest peak temperatures of up to 700°C (B60) and 400°C (B120). The same observations were made in other studies on the thermal response of steel [2] and concrete [2, 14] structures. Small TFM sizes lead to higher temperatures mainly because of longer heating durations in comparison to other fires (Chapter 2). The lowest temperatures develop within beams exposed to EC SH fire.
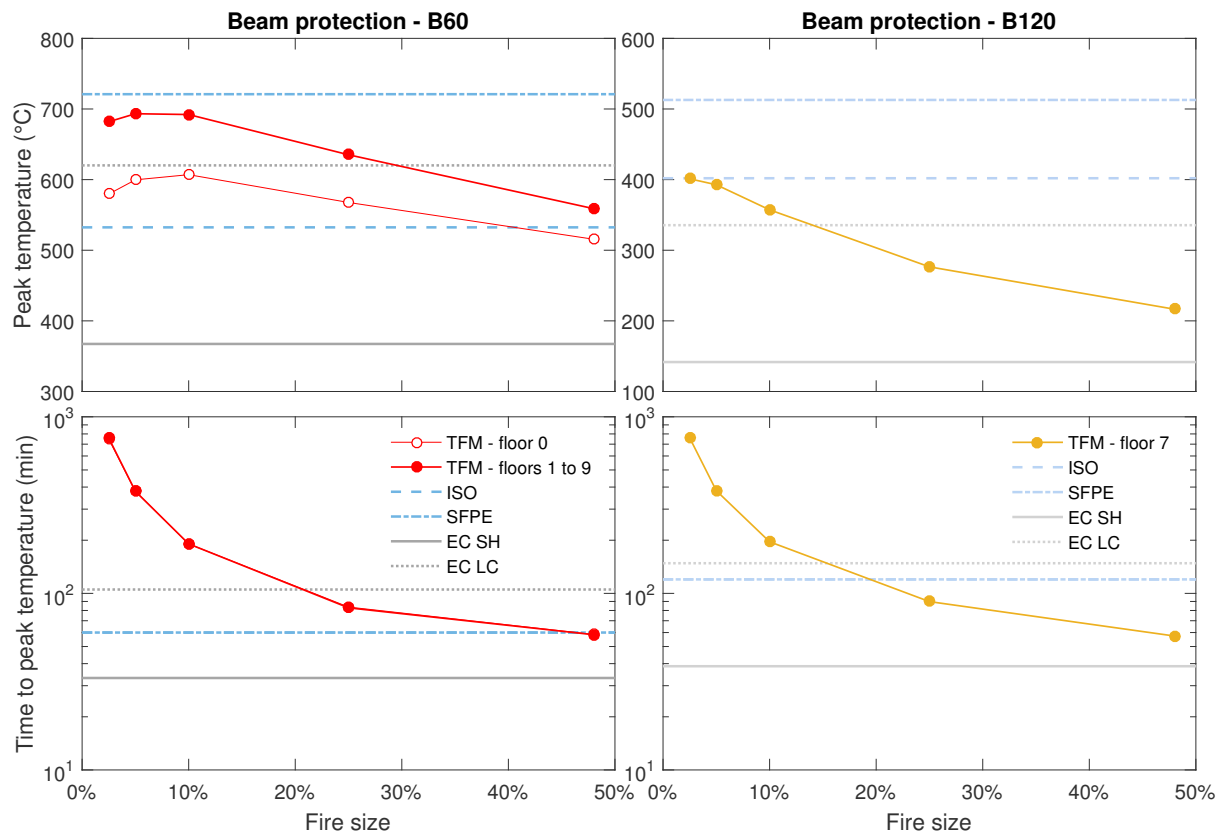
Figure 5.5: Peak temperatures that develop within steel beams with fire protection designed for 60 min (B60) and 120 min (B120) of standard fire resistance for travelling fire (TFM) and uniform fire (EC, ISO and SFPE) scenarios and time to reach these temperatures. For ISO and SFPE fires temperatures are shown at the corresponding beam fire resistance period.

They are 367°C and 142°C for B60 and B120, respectively. On the other hand, the time taken to reach the peak temperatures is shorter for large TFM scenarios and uniform fires (58-105 min) than for small TFM fires (up to 758 min). The time to reach critical member temperature of 550°C is also shorter for larger TFM fires (e.g. 48% TFM) than for the smaller ones (2.5% TFM) [2].

5.3.2 Utilization

Plot of the evolution of utilization of the frame with time for the 10% TFM, EC SH and ISO fires in shown in Fig. 5.6. For the beams on the floor subjected to fire, utilization increases with time. Beam elements in the proximity of the connections to the columns experience the highest utilization because of the development of high bending moments as connections in the analysis are assumed fixed. Results also indicate significant increasing utilization in the beams in the floors directly above and below the fire floor, although they are not heated. In the floors further away from the fire there is no significant change in beam utilization. This is due to the development of high axial forces in the floors adjacent to the fire floor. Similarly, results show significant redistribution of the forces, i.e. utilization, in the columns up to 2 floors away from the fire floor. The increase in utilization of internal columns connected to Bay 3 on the fire floor is smaller than for the end columns for the 10% TFM and ISO fires. For example, for the 10% TFM, the utilization in internal columns increases by 37% (from 17 to 54%) while in the end columns it increases by up to 59% (from 27 to 86%). For the ISO fire the increase in the utilization of internal columns is only 4%. The axial load on the columns during the fire does not increase significantly and their changes in utilization are mainly affected by the development of bending moments.

A comparison of the change in utilization of the beams with time for the different fire scenarios is shown in Fig. 5.7. It shows, as identified in the previous paragraph, that for all fire scenarios, the beam locations that are close to connections are under the highest utilization. However, during cooling, the utilization of the connections decreases and the utilization at the beam mid-span increases. For small TFM scenarios (i.e. 5% and 10% TFM), the numbers of the beams under high utilization are smaller and more localized close to the location of the near-field. For uniform fires, the level of utilization in different bays at the same time is similar. As the travelling fire size increases the patterns of utilization along the fire path approach that of the uniform fires. In general, for all fire scenarios different sections of the beams (e.g. connections and mid-span) or columns are under significantly different levels of utilization as a result of the distribution of bending moments and axial forces. This is illustrated in Fig. 5.6 and Fig. 5.7.

A change in the typical range of utilizations along the beam with time and the 20th, 40th, 60th, and 80th percentiles are shown in Fig. 5.8. At ambient temperature, 80% of the beam is at an utilization of 50% or lower. For the case illustrated, the 80th percentile utilization increases up to 90% in Bay 4 as the fire travels along the frame. In
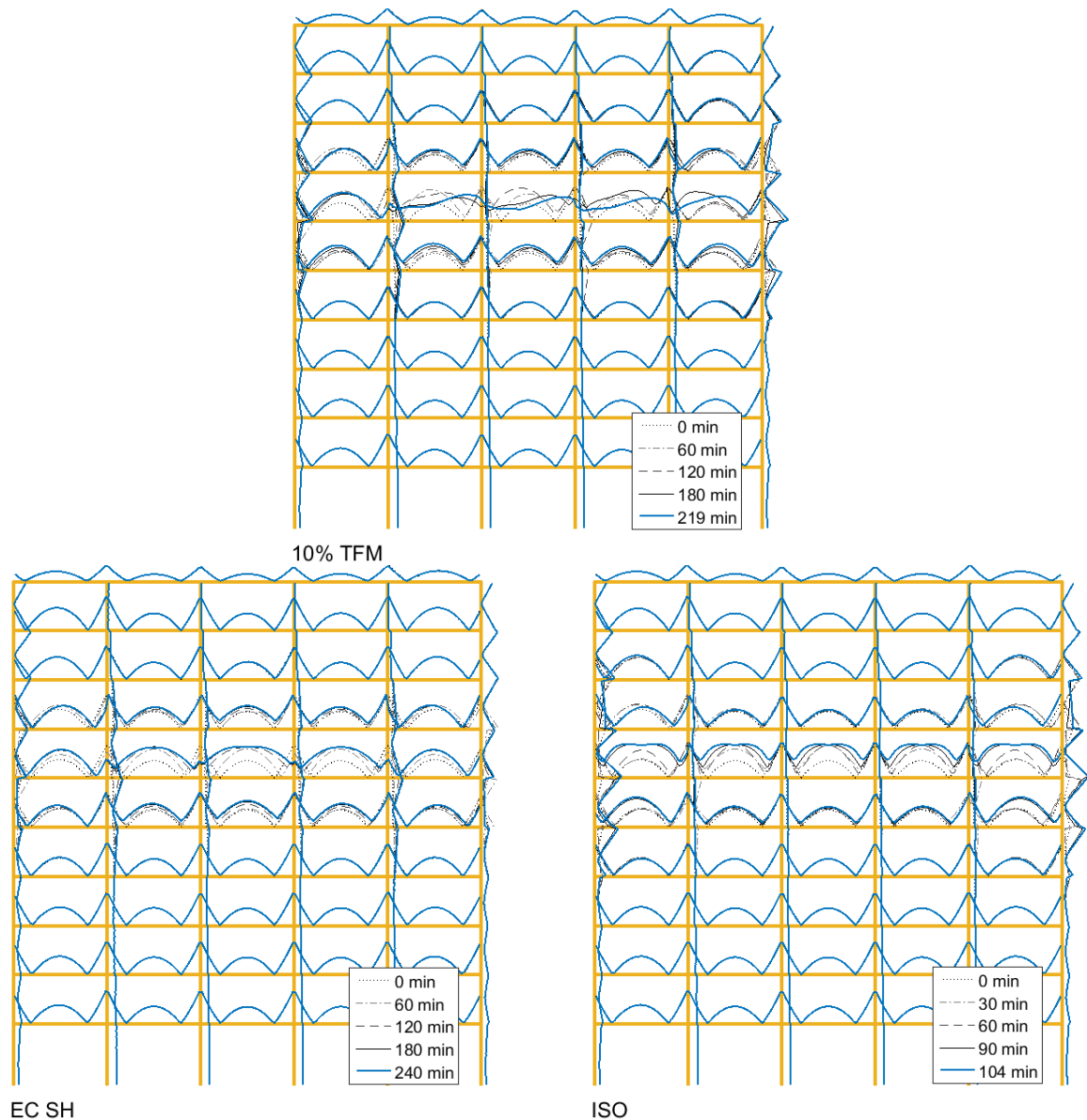
Figure 5.6: Illustration of frame subjected to 10% TFM, EC SH and ISO fires on Floor 5 utilization at different times of fire exposure. 100% utilization is scaled to 3 m (i.e. a third of the beam length).

order to allow an easy comparison of all fire scenarios for each member in the frame (i.e. beams and columns) the mean and the maximum were taken as the representative values of its utilization. The maximum value indicates how close the member is to yielding. Cumulative density functions (CDF) were then plotted to give an indication of the overall frame utilization and performance in fire. CDF illustrate what percentage of the members in the frame is under the utilization equal to or lower than the specified value. Fig. 5.9 provides an illustration of the change of CDF with time for a frame exposed to the 48% TFM on Floor 2. The lower and upper bounds show CDF of the average and peak (i.e. maximum) utilization, respectively, of different members. It should be noted that even at ambient temperature peak utilization of the frame is relatively high. Approximately

30% of the members have a peak utilization of 90%. 10% of the members with a peak utilization between 40 and 50% are the Floor 9 beams. These beams are subjected to
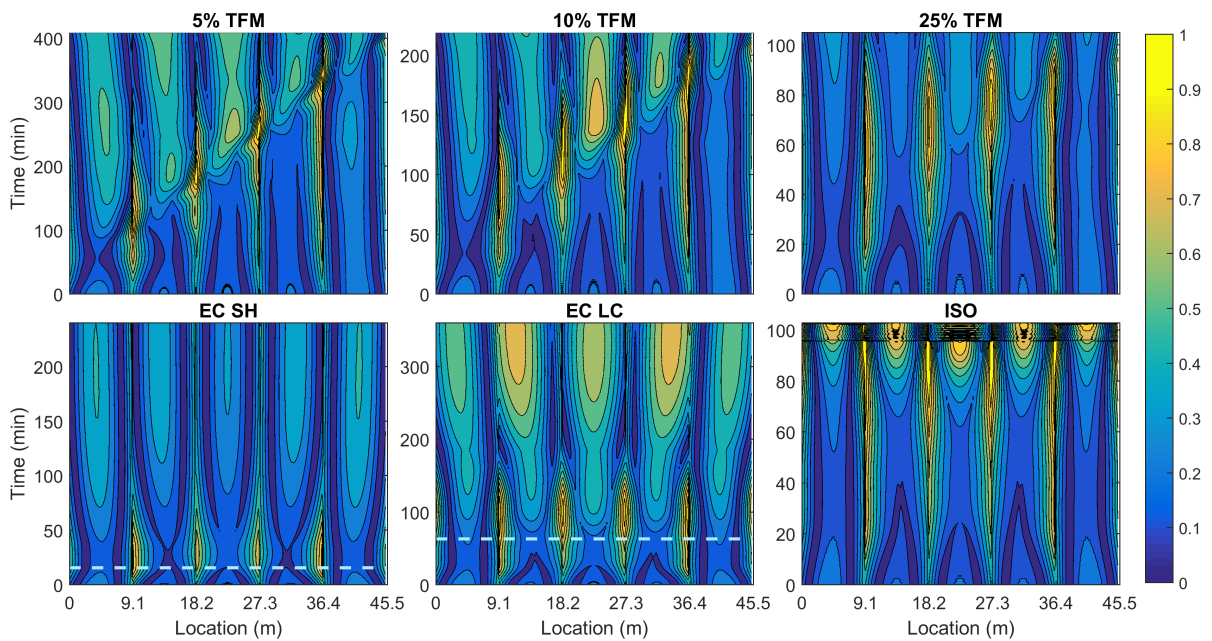

Figure 5.7: Evolution of utilization in beams with time for the Floor 10 of the frame exposed to different fire scenarios. For TFM fires x-axis locations of 0 m and 45.5 m indicate the origin of the fire and end of fire path, respectively. Dashed lines indicate when cooling begins for Eurocode short-hot (EC SH) and long-cool (EC LC) fires.
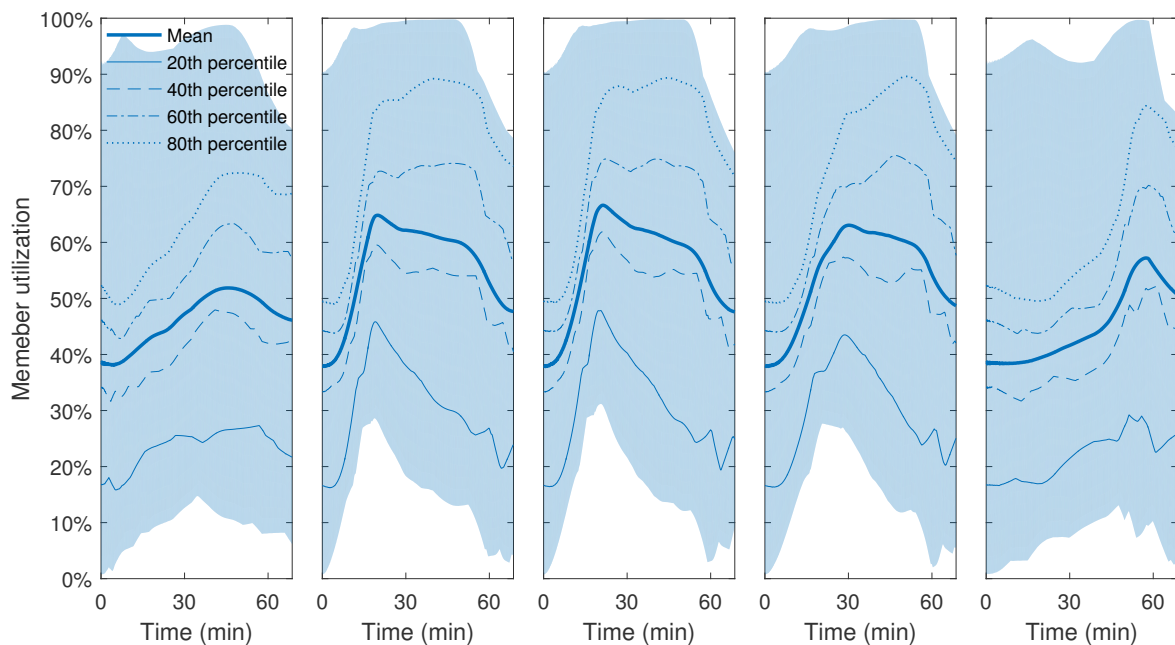
Figure 5.8: Variation of the utilization in different beams along the fire path for Floor 2 exposed to 48% TFM. Shaded area represents minimum and maximum utilizations along the beam with time. Figures from the left to right show results for beams in Bays 1 to 5.

smaller permanent and variable loads than beams on the floors below. Normally, with time and increasing temperature, the utilization of the frame increases as illustrated in Fig. 5.9. The peak utilization factor values that are close to 1 indicate the number of the members in the frame that have yielded or are close to yielding.
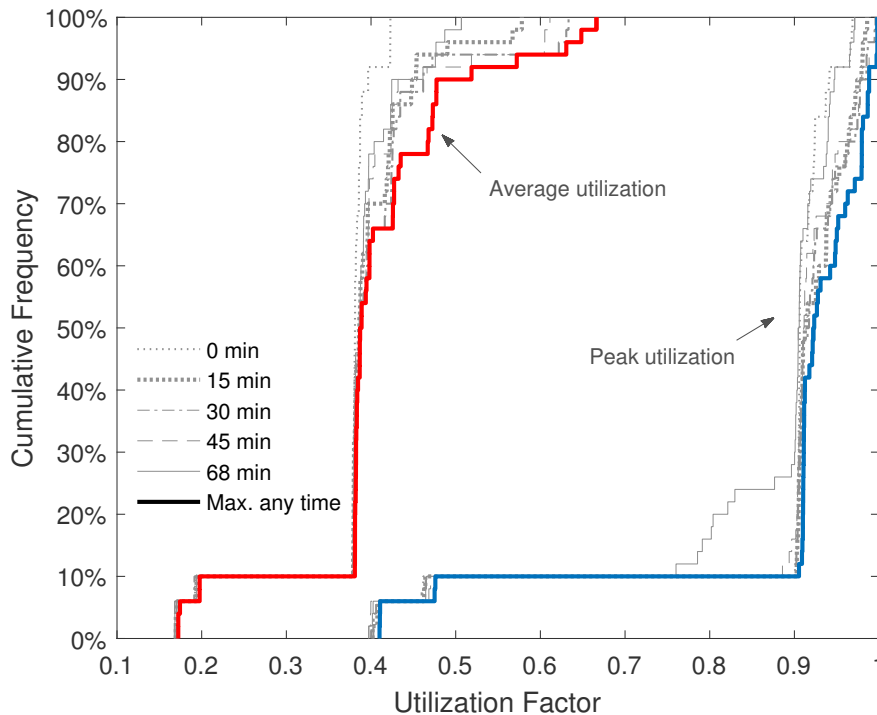
Figure 5.9: CDF of average (lower bound) and peak (upper bound) utilization of members in the frame exposed to 48% TFM on Floor 2 at different times of fire exposure and the maximum at any time.

Comparisons of the CDF of the maximum at any time mean and peak utilization of the members (as shown in Fig. 5.9) in the frame for different fire scenarios and fire floors are shown in Figs. 5.10 and 5.11. Fig. 5.10 shows that the frame subjected to any fire scenario on Floor 9 is under the lowest level of utilization in comparison to fires occurring on other floors. This is because the beams at this location at ambient temperature are under the lowest utilization, as identified previously, and have a lower level of restraint to expansion. Axial forces that develop in fire Floor 9 are up to 240 kN lower than in other fire floors (Chapter 4). Fires on floor 9 mainly affect the minimum utilization factor of the frame. This factor decreases as the number of the fire floor decreases. Similarly, the upper limit of the average frame utilization is highest for fires on Floor 1. Even though the CDF functions appear to be similar for fires occurring in other floors, especially Floors 1 to 8, the highest peak utilizations and the largest number of yielded members occur for the frame subjected to fires on Floors 6 to 8. For ISO and SFPE fires, fire Floor 7 results in the largest utilization. 80% of the members are at the normalised utilization of 0.63 while for the cases with other fire floors it is approximately 0.5. Therefore, these

results indicate that the frame subjected to fires on Floors 6 to 8 is likely to be closer to the onset of collapse. On these floors beams are connected to columns that have the lowest load-bearing capacity, i.e. the smallest sections.
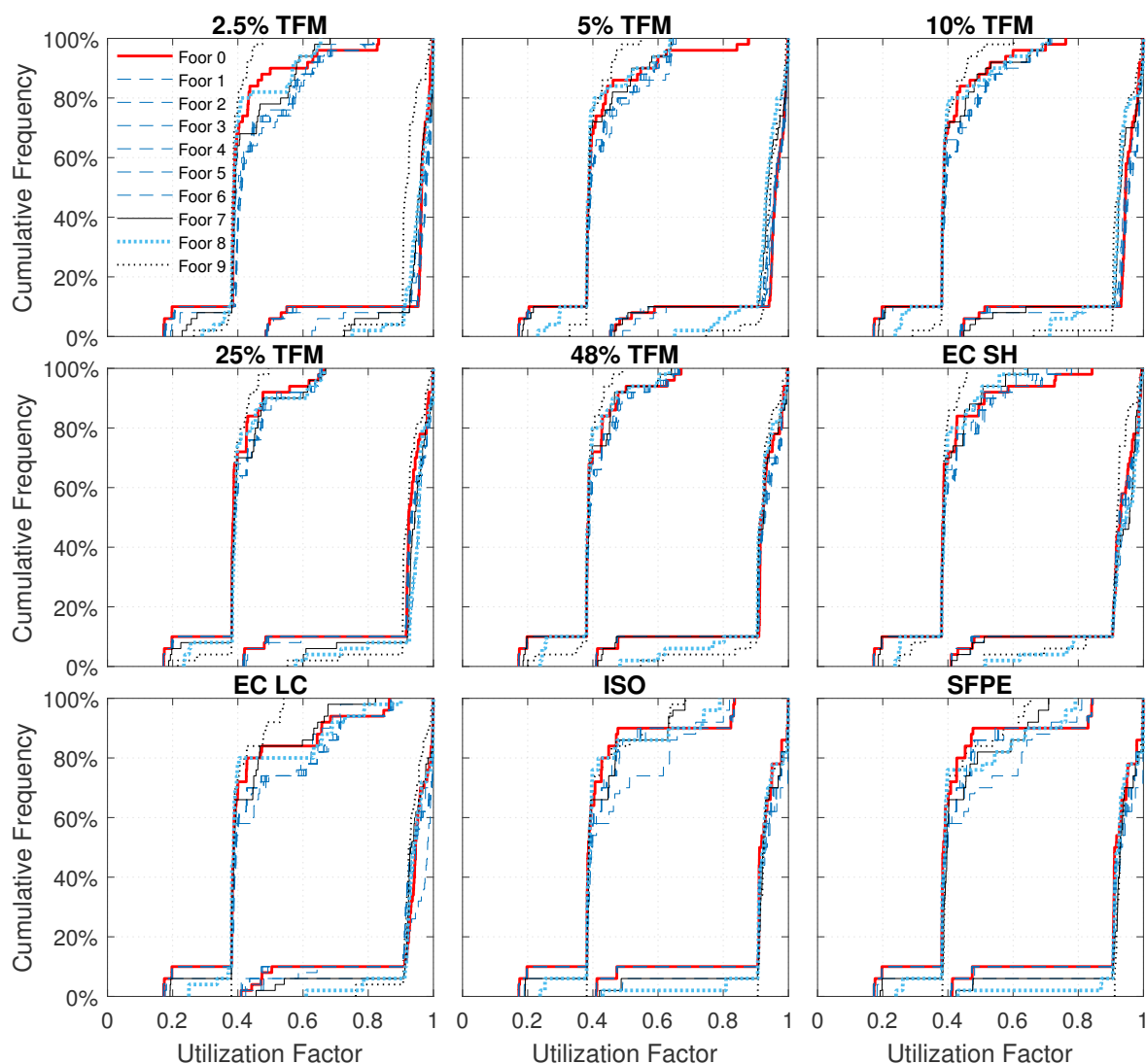
Figure 5.10: The effect of fire floor subjected to fire on the CDF of maximum at any time average (lower bound) and peak (upper bound) utilization of members in the frame for al fire scenarios (TFM, EC, ISO, and SFPE).

Fig. 5.11 shows the same results as Fig. 5.10, but gives a clearer comparison of the effect of fire scenario on the CDF of frame utilization. For all fire floor cases, the uniform fire scenarios (EC LC, ISO, and SFPE) that have a long duration result in the highest average frame utilization. They are followed by the smallest travelling fire scenarios (i.e. 2.5% TFM). With increasing size and, thus, duration of the TFM fires, the highest average frame utilization reduces and is lowest for the 48% TFM and EC SH fires. This is likely because uniform large duration fire scenarios result in higher temperatures and therefore lead to greater overall thermal expansion of the fire floor leading to higher stresses in members compared with shorter fires. For travelling fire scenarios, it is likely
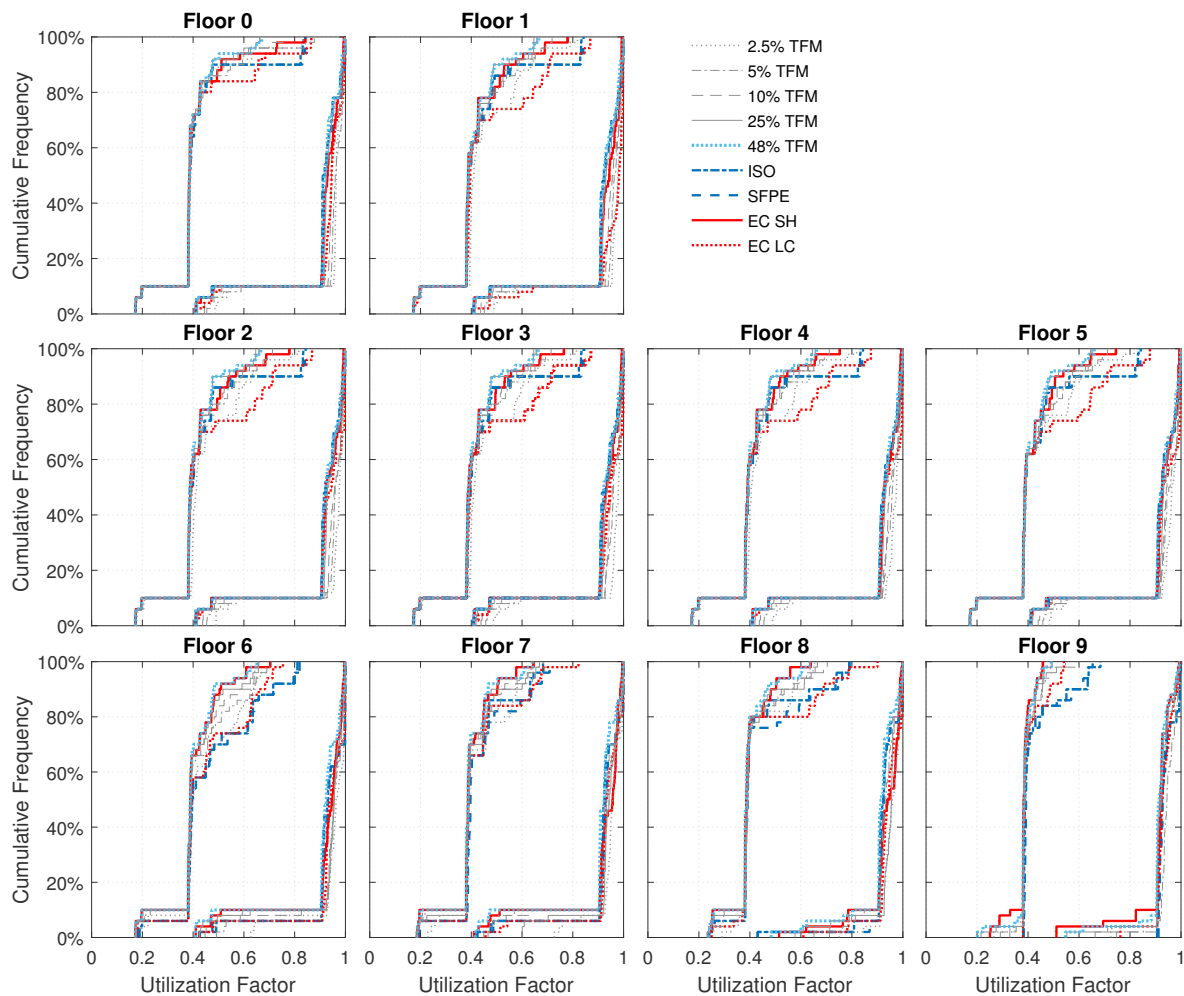
Figure 5.11: The effect of fire scenario on the CDF of maximum at any time average (lower bound) and peak (upper bound) utilization of members in the frame for different fire floors.

a function of the peak and average temperatures that develop within the members and the level of restraint from the adjacent members as the fire travels along the fire path. In addition, the 2.5% - 10% TFM fires result in high tensile axial forces on fire floor even during the fire exposure (Chapter 4). However, the results indicate that for the TFM fires, in comparison with the uniform fires, a higher percentage of members is under higher peak utilization (the CDF curve is shifted towards right which indicates higher utilizations). Similar observations were made by Law [18] on the utilization of concrete structures subjected to travelling fires and uniform fires. He compared the performance of the frame subjected to ISO, SH EC and LC fires and to 2.5%, 5%, 10%, 25%, 50%, and 100% travelling fires separately. Comparing uniform fires and travelling fires, Law [18] determined that the ISO fire and the 5% and 10% TFM to be the most severe exposures, respectively.

5.3.3 Failure

The ultimate strain and three deflection ($L/20$, $L^2/400d$, and $L^2/9000d$ over 1 min) failure criteria are considered in this chapter. High deflections might lead to damage to the fire protection materials, fire suppression systems or compartmentation leading to faster heating or further fire spread, but these effects are not addressed here. Results of different failure times for all fire scenarios are shown in Fig. 5.12. Based on the ultimate strain criterion, failure for the 2.5%, 10%, and 25% TFM and EC LC fires occurs only when Floors 5 to 8 are exposed to fire and the failure times range from 1.5 h to 13 h (2.5% TFM). For these floors, the heated beams are connected to the weakest column sections, which are not able to resist the thermally induced forces. Failure in most cases occurs close to the internal connection in Bay 5 following the pull-in of the end columns. Failure times increase as the fire size decreases and are similar for EC LC and 25% TFM. Even though the CDF of frame utilization indicates that the frame subjected to EC LC fires is under the highest utilization in comparison to other fires, ultimate strain failure only occurs on fire Floors 6 and 7. On the other hand for the ISO, SFPE and 5% TFM, failure occurs for almost all fire floor cases. This failure time decreases on fire floors 6 to 8 by up to 30 min. No failure is observed for EC SH and 48% TFM for all the aforementioned failure criteria. Due to relatively short duration of these fire exposures, members do not reach sufficiently high temperatures that would lead to structural failure as for other fire scenarios. Under the ISO fire the frame fails beyond the 60 min fire resistance of beams at approximately 100 min.

The deflection related failure criteria of $L/20$, $L^2/400d$ and rate of $L^2/9000d$ over 1 min correspond to 0.455 m, 0.593 m, and 0.026 m/min, respectively. Based on the first two criteria (i.e., $L/20$ and $L^2/400d$), failure occurs for all fire scenarios except for the fires on top and bottom floors of the frame. Comparing the natural fires (EC and TFM), the 25% TF appears to be the worst with failure occurring after 60 min of the fire exposure, followed by the 10% TFM (70 min), the EC LC fire (80 min), 5% TFM (1.5 h to 2 h), and the 2.5% TFM (2.5 h to 4 h). The third criterion on deflection rate is also exceeded for most fire cases except for the uniform fire scenarios. For the EC LC the deflection rate limit is only exceeded for fire floors 6 to 8 as for the ultimate strain criteria. For the ISO and SFPE fires on Floors 6 to 9, frame ultimate strain criteria is reached without the development of large rates of beam mid-span deflections. For all the failure criteria, the results indicate that there is no single fire scenario which would represent the worst case. For different fire exposures failure occurs on different range of floors subjected to fire. In terms of the ultimate strain criteria, the natural fires EC LC and 25% TFM lead to the lowest failure times (100 min) but only for Floors 6 to 8. On the other hand, 5% TFM leads to failure for a larger range of fire floors (Floors 1 to 8) but the failure takes place only after a relatively large fire duration of approximately 5.5 h.

A comparison of the corresponding web temperatures of the elements that failed at
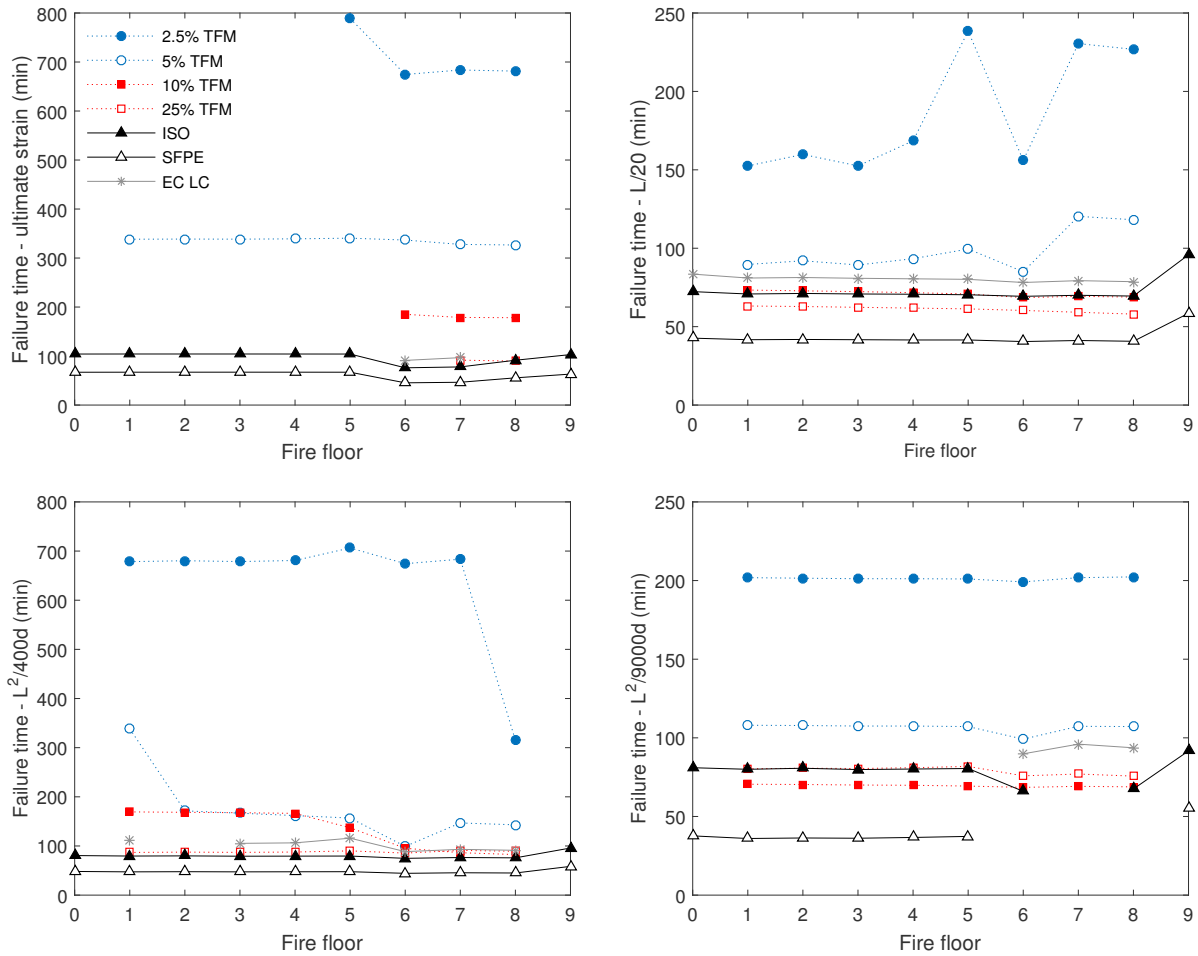
Figure 5.12: Variation of failure time based on ultimate strain and deflection ($L/20$, $L^2/400d$, and $L^2/9000d$ over 1 min) criteria for all cases.

the time of failure according to different failure criteria is shown in Fig. 5.13. The element temperatures at the ultimate strain failure are between 600°C and 740°C, except for the 2.5% TFM occurring on floor 5. For the limiting deflection and the limiting deflection rate failure criteria, failure temperatures are in the ranges of 450-700°C and 320-700°C, respectively. For the uniform fire scenarios, the temperatures of the elements when failure occurs are very similar. The difference for the fires occurring on the same floors ranges between 2 and 33°C only. This difference is even smaller (0.04 to 6.8°C) when the average temperatures of the members where failure occurred are compared (see Appendix 5.B, Fig. 5.B1). Changes in failure temperatures on different fire floors subjected to uniform fires are mainly due to the different levels of restraint and in all cases are above 550°C. Thus, it is likely that for EC SH and 48% TFM fires failure does not occur under any failure criteria because the peak average member (i.e. beam or column) temperatures during the fire are not high enough to reach this critical value. For EC SH and 48% TFM the peak average member temperatures that develop during the fire are 367°C and 480°C (peak localized web temperature is 559°C), respectively. In the previous work it
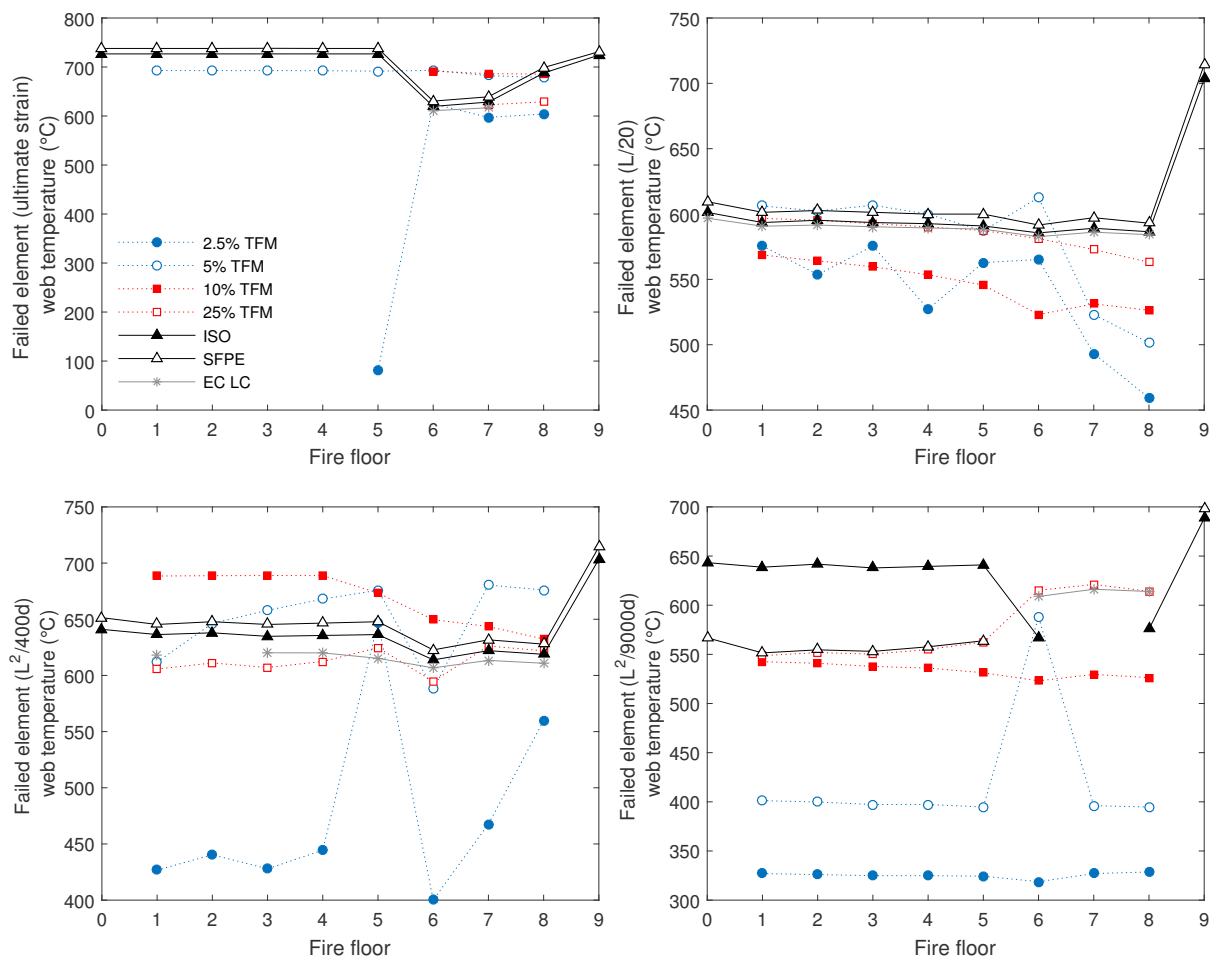
Figure 5.13: Corresponding web temperatures of the failed elements for different failure criteria (ultimate strain, $L/20$, $L^2/400d$, and $L^2/9000d$ over 1 min) for all fire scenarios.

was observed that structural response of the frame subjected to 48% TFM is similar to that under uniform fires due to the relatively large fire size.

For the travelling fire scenarios, the range of element temperatures when failure occurs is larger than for uniform fires with the temperatures being as low as 100°C (ultimate strain failure criteria). In addition, travelling fires, unlike uniform fires, result in highly non-uniform temperature distributions in the compartment at different times of the fire exposure. Therefore, it is difficult to judge the critical member temperature for travelling fires by just looking at the localized temperatures of the elements that failed. These critical member temperatures are analysed further in Section 5.3.4.

It should be noted that deflection criteria are typically evaluated at beam mid-span and therefore this location was selected for the discussion of failure times and the temperatures reported in this study as well. However, the beam mid-span may not always be the location of the maximum deflection of the beam. Comparison of failure times for the different failure criteria considering the whole beam span length with failure times considering beam mid-span only and the locations along the beam where failure first oc-

curs are shown in Fig. 5.14. The results highlight that for the majority of the cases, the failure times are very close for any location in the beam and when mid-span is only considered. Though, in general, failure occurs earlier in locations of the beam other than the mid-span and indicates that the maximum deflections do not necessarily develop at beam mid-span. This is in particular the case for deflection criterion of $L^2/400d$. The failure time difference for the 2.5% TFM occurring on Floor 7 is 6.4 h. Fig. 5.14 illustrates that for the uniform fires, the deflection criteria is first exceeded at beam mid-span or very close to it. However, for travelling fires, the critical deflection locations are further away from beam mid-span by up to 3.3 m (36.5% of the beam length) towards the fire origin.
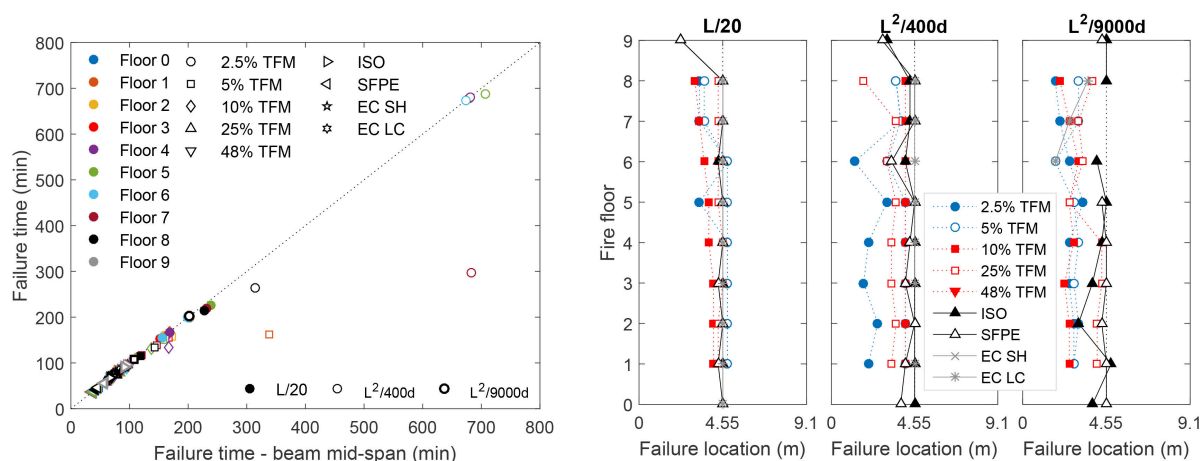

Figure 5.14: Comparison of failure times for deflection criteria considering beam mid-span only and any location along the beam (left) and illustration of the locations where deflection criteria are first exceeded along the beam span (right).

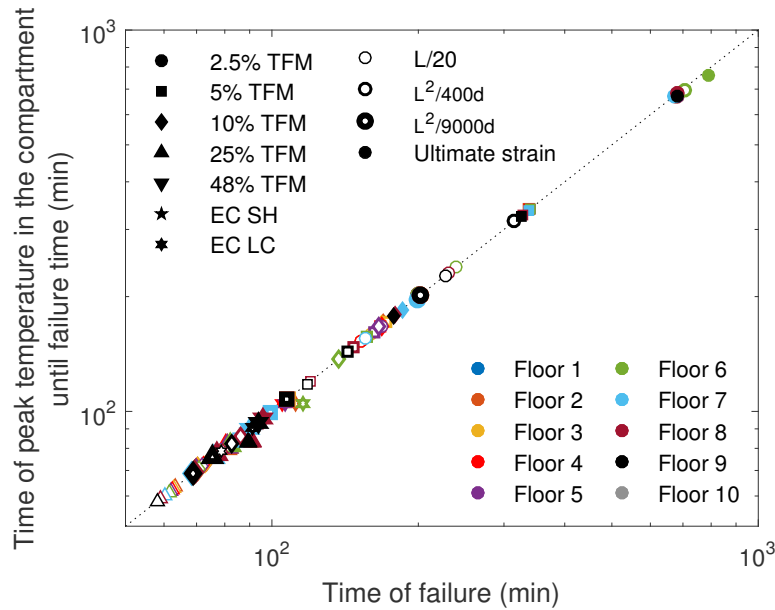### 5.3.4   Critical member temperatures

As already identified previously, travelling fires result in non-uniform and transient temperature distributions in a compartment. Thus, failure cannot simply be related to the temperature of the single element that failed. Other factors such as the peak temperature in the compartment at the time of failure, whether the element failed during the heating or cooling phases and the average member temperatures need to be considered as well. A comparison of the temperature of the failed element with the peak temperature in the element until the failure time and the peak temperature in the compartment when failure occurs are illustrated in Fig. 5.15. Both localised element and average structural member temperatures are investigated. The results indicate that for most of the cases, the elements fail during the heating of the failed element. Element failure during cooling occurs for the small travelling fire scenarios only, i.e. 2.5% and 5% TFM. In most cases, the failed elements are located in the bays that experience heating that is when the near-field of the travelling fire is approaching or is in the same bay. Comparison of the temperature of the failed element and peak temperature in the compartment when failure

occurs demonstrates that in only very few travelling fire scenarios the element that failed is the hottest element at that time. The differences between the temperature of the failed element and peak temperature are up to 460°C (2.5% TFM), 160°C (5% TFM), 90°C (10% TFM), and 80°C (25% TFM). Peak average structural member temperatures in the compartment when failure occurs show a closer link to the failed elements. For approximately half of the fire scenarios irrespective of the fire size, failure occurs in the bay with the highest average temperature in the compartment at the time. Fig. 5.16 shows that for the majority of the cases including the EC fires, failure occurs while the peak temperatures in the frame are still increasing. When the peak temperature in a frame begins to decrease, that is when the near-field has reached the far end of the compartment, failure occurs for a range of fire floors subjected to 25% TFM. In general,
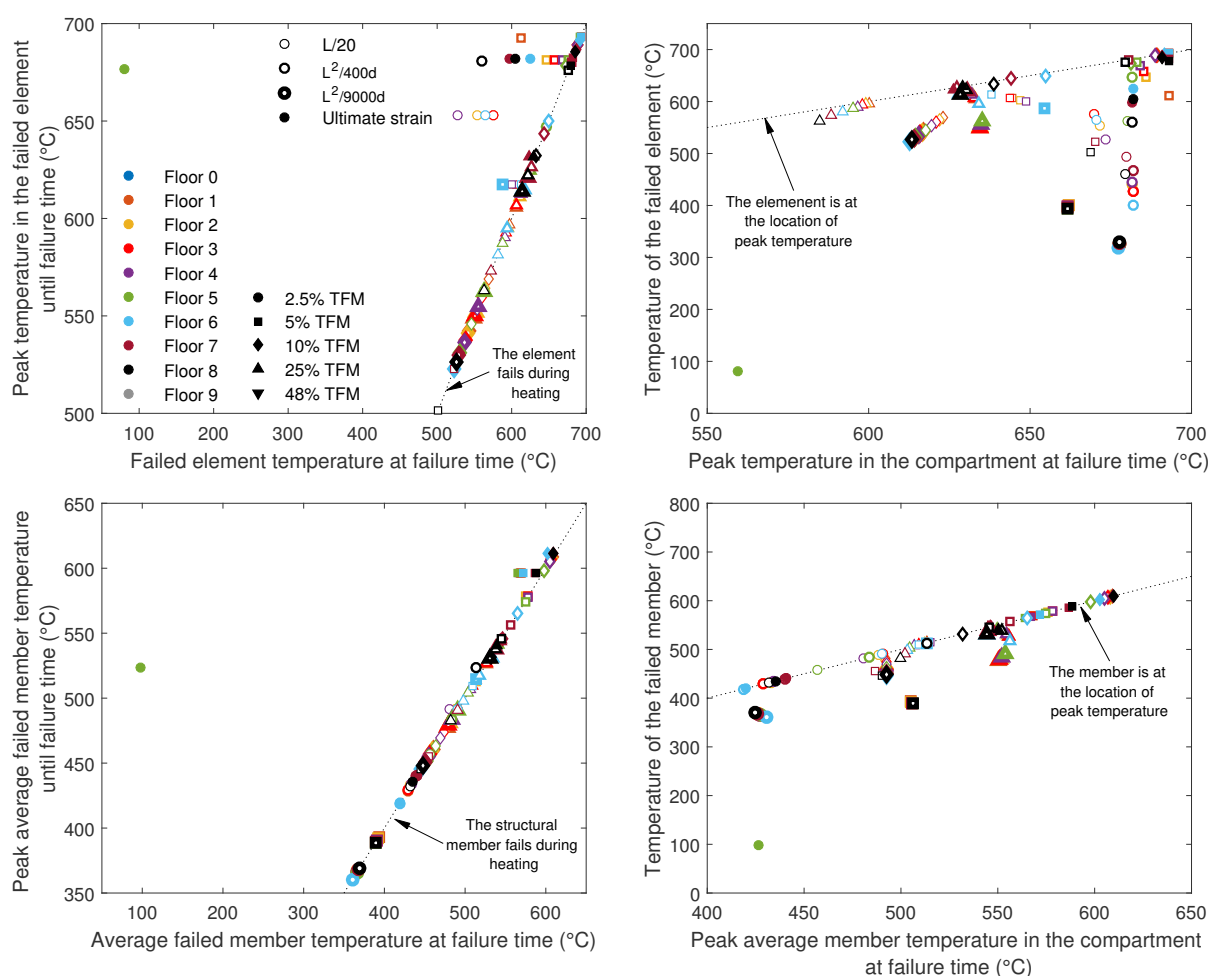
Figure 5.15: Comparison of failed element/average member temperature with peak element/average member temperature until failure and peak compartment temperature at and until failure. Element temperatures (top) and average structural member/bay temperatures (bottom). Results lying on the dashed line indicate that the failed element/member fails during the heating (left) and that the failed element/member is at the location of peak temperature in the compartment (right).
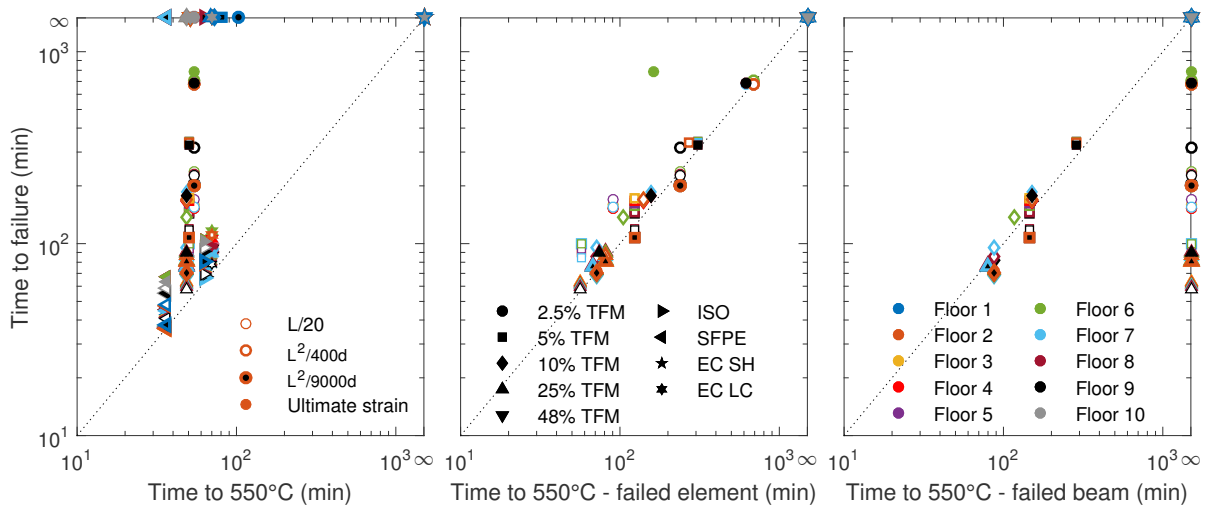
Figure 5.16: Comparison of time of failure and time of peak temperature in the compartment until failure.

the peak element and structural member temperatures in the compartment at failure time are between 550 and 700°C, and 400 and 625°C, respectively.

Fig. 5.17 shows the comparison of the time to failure with the time to reach the critical member temperature of 550°C in the compartment, in the failed element and in the failed beam (average structural member temperature) for all fire scenarios. The results indicate that there is no relationship between the time to reach the critical member temperature in the compartment and the failure time. However, for all the cases, the failure time is reached later than the critical member temperature. This indicates that the critical member temperature is a conservative failure criterion and therefore could be safely used in probabilistic fire severity assessments of generic steel framed buildings without any particularly unusual characteristics when subjected to both uniform and non-uniform fires. Though, a large number of fire scenarios would be considered as critical even though that failure is less likely to occur. The times to reach the critical member temperature in the failed element and times to failure show the best correlation in comparison to the time to critical member temperature in the compartment and failed beam (i.e. average structural member temperature). In the latter case for a large percentage of the fire scenarios average beam temperatures never reach the critical member temperature of 550°C even though the frame fails.
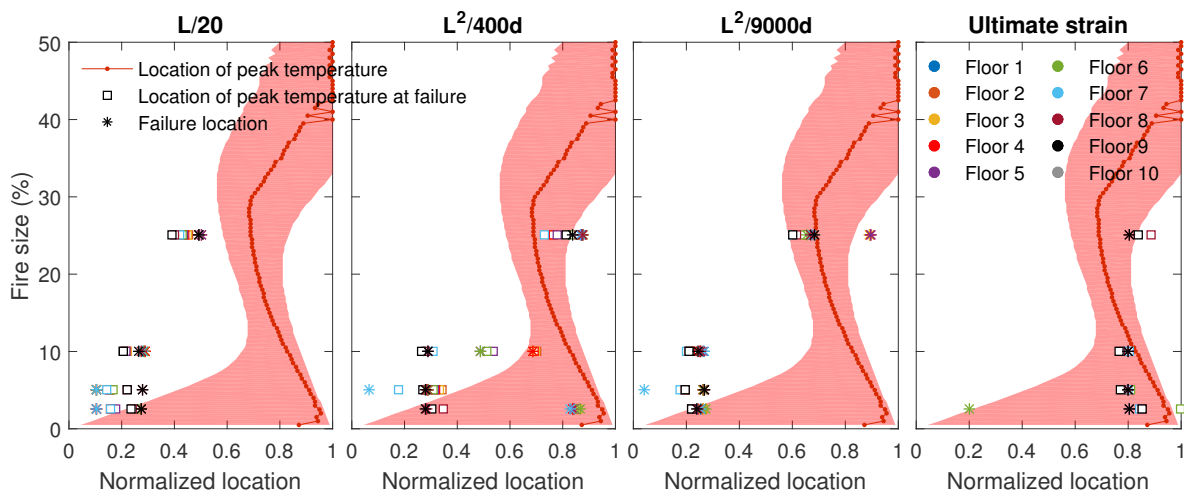
5.3.5   Location of peak temperature

In previous work (Chapter 2) on the thermal response of structures subjected to the iTFM, the location of the peak temperature along the fire path for different fire sizes has been investigated and was found to occur towards the end of the path. In Fig. 5.18

Figure 5.17: Comparison of time of failure with time to reach the critical member temperature in the compartment (left), failed element (middle), and failed beam (average structural member temperature) (right). In two figures on the right only the TFM scenarios are compared. Data points plotted at the time of 1000 min indicate that either failure did not occur or the critical member temperature was not reached depending on the axis.

these locations are compared with the locations of the elements for which failure occurs under the ultimate strain and deflection failure criteria. In addition the locations of peak temperature along the fire path at the time of failure are shown as well. In this figure, the locations of the critical deflections are illustrated considering the whole span of the beam rather than just its mid-point. The results indicate that for the deflection criteria, failure tends to occur in the first few bays of the frame and that there is no correlation with the location of the peak temperature, especially for the 5% and 10% TFM fire scenarios. Though, failure occurs close to the location of the peak temperature in the compartment at the time of failure. This is likely because large deflections start to develop in beams at temperatures as low as 300°C and are not directly linked to the loss of material strength but are a result of the thermally induced strains [48]. On the other hand, failure due to the ultimate strain criterion tends to occur towards the end of the fire path within the region where peak temperatures in the compartment develop. Peak temperatures in the compartment at the time of failure are within the same region as well. In only one case, i.e. 2.5% TFM on fire Floor 5, failure is located in the first bay of the frame, but the location of peak temperature of the compartment is towards the end of the fire path. The element in this case fails due to high tensile axial forces which occur during the cooling of the member.

Fig. 5.19 shows the numbers of cases that failure occurred at different locations along the fire path. The critical deflections for all the uniform fire scenarios tend to occur in the end bays of the frame while for the travelling fires in the internal bays (2.5-10% TFM)

Figure 5.18: Comparison of the location of peak temperature along the fire path (Chapter 2), locations of elements for which failure occurs (∗), and locations of the corresponding peak temperature in the compartment at the time of failure (□). On the x-axis '0' represents the fire origin and '1' the far end of the compartment. Shaded region displays locations of maximum temperature within 5°C difference from the peak temperature.
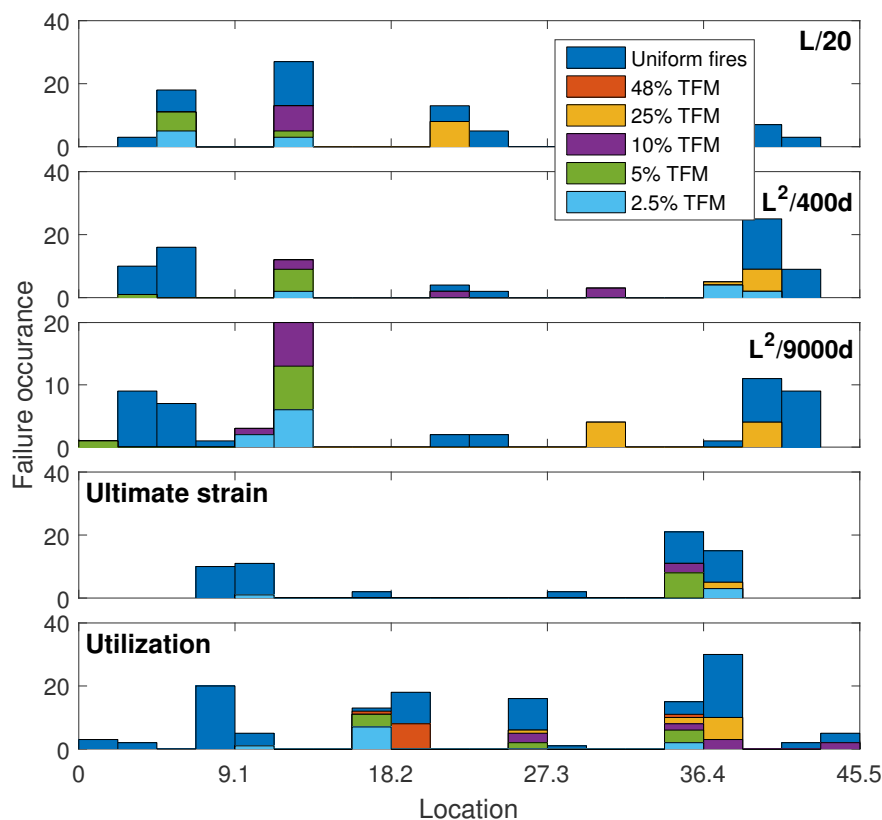
Figure 5.19: Comparison of the number of failure occurrences along the fire path for ultimate strain and deflection failure criteria and locations of the peak utilization in the compartment. Uniform fires include ISO, SFPE, and EC LC fires.

and end bays towards the end of fire path (25% TFM). The ultimate strain criterion in most cases is exceeded in members connected to column C2 and C5. They are close to the end columns and after the pull-in of these columns large bending moments are generated around columns C2 and C5. The locations of the highest utilization for uniform fires are concentrated around the latter columns as well. For travelling fires they are located close to columns C3, C4, and C5 where higher peak temperatures are reached in the members. In general, these results indicate that the location of peak temperature in the compartment could likely be used to identify critical structural members in the compartment for the structural ultimate strain criterion. However, further studies considering different geometries and 3D effects need to be conducted to confirm this.

5.4 Conclusions

Limiting temperature criteria is widely used in the probabilistic assessment of structures subjected to fire. However, it is unclear how representative it is of the actual structural failure, particularly when non-uniform fires such as travelling fires are considered. In this chapter, the effect of fire exposure (uniform and travelling fires) and fire floor location on load-bearing capacity, utilization, beam mid-span deflection, and limiting temperature limit states of the multi-storey steel frame have been investigated. Corresponding element temperatures at failure have been analysed and compared for each failure state.

In terms of overall frame utilization long uniform fires in this study are found to result in the highest average utilization (i.e. 100th percentile), while 48% TFM and short-hot parametric fires result in the lowest utilization. However, the results indicate that for TFM fires in comparison to uniform fires a higher percentage of members is under higher peak utilization. In addition, travelling fires result in significantly increased utilization of internal columns by up to approx. 40% while under uniform fires it increases by up to 5% only.

Critical fire scenarios based on utilization analysis and the failure times for ultimate strain and deflection criteria are found to occur on the upper levels of the building where column section reduces in size. This indicates that column section sizes and their change on different levels of the frame are important in defining the weakest floors. For the investigated frame, the most severe fire scenarios in the terms of failure time have been found to be 25% travelling fire (deflection and ultimate strain) and long-cool parametric fire (ultimate strain). However, failure based on the ultimate strain criterion under the latter fire scenarios only occurs on the upper weaker floors of the frame. In addition, results show that ultimate strain failure tends to occur close to the location of peak temperature in the compartment. On the lower floors of the frame small travelling fires become more onerous and lead to failure during fire in the larger number of cases.

The results indicate that there is no single fire scenario which would represent the

worst case. For different fire exposures, failure occurs on different floors subjected to fire. In most travelling fire scenarios failure occurs during the heating, but for small TFM ultimate strain failure occurs during cooling. Moreover, the results reveal that there is no relationship between the time to reach the critical structural member temperature in the compartment and the failure time. Nevertheless, results show that the critical member temperature in the compartment could be safely used as the conservative failure criterion in the assessments of generic steel framed buildings without any particularly unusual characteristics when subjected to both uniform and non-uniform fires.

Acknowledgements

References

[1] J. Stern-Gottfried and G. Rein, "Travelling fires for structural designPart I: Literature review," *Fire Safety Journal*, vol. 54, pp. 74–85, nov 2012.

[2] J. Stern-Gottfried and G. Rein, "Travelling fires for structural design-Part II: Design methodology," *Fire Safety Journal*, vol. 54, pp. 96–112, nov 2012.

[3] A. Law, N. Butterworth, J. Stern-gottfried, and Y. Wong, "Structural fire design: many components, one approach," in *The 1st international conference on performance based and life cycle structural engineering*, no. December, (Hong Kong), 2012.

[4] A. Law, J. Stern-Gottfried, and N. Butterworth, "A Risk Based Framework for Time Equivalence and Fire Resistance," *Fire Technology*, vol. 51, pp. 771–784, jul 2015.

[5] F. M. Block and T.-S. Kho, "Engineering an Icon or the Probabilistic-based Structural Fire Engineering of the Battersea Power Station," in *Proceedings of the 9th International Conference on Structures in Fire* (M. E. M. Garlock and V. K. R. Kodur, eds.), (Princeton, NJ), pp. 901–908, DEStech Publications, 2016.

[6] T. Gernay, N. Elhami Khorasani, and M. Garlock, "Fire fragility curves for steel buildings in a community context: A methodology," *Engineering Structures*, vol. 113, pp. 259–276, apr 2016.

[7] A. Law, P. Kotsovinos, and N. Butterworth, "Engineering geometrically bi-linear columns to deliver fire resistance: Standard heating," *Engineering Structures*, vol. 100, pp. 590–598, oct 2015.

[8] G. Flint, S. Lamont, B. Lane, H. Sarrazin, L. Lim, D. Rini, and C. Röben, "Recent Lessons Learned in Structural Fire Engineering for Composite Steel Structures," *Fire Technology*, vol. 49, pp. 767–792, jul 2013.

[9] J. Bono, "New Criteria for Fire Endurance Tests. in Fire Test Performance, ASTM STP 464," in *Fire Test Performance, ASTM STP 464*, (Union City, N. J.), pp. 106–126, American Society for Testing and Materials, 1970.

[10] CEN, "EN 1993-1-2:2005 - Eurocode 3. Design of steel structures. General rules. Structural fire design," 2005.

[11] Y. Z. Yin and Y. C. Wang, "Numerical simulations of the effects of non-uniform temperature distributions on lateral torsional buckling resistance of steel I-beams," *Journal of Constructional Steel Research*, vol. 59, pp. 1009–1033, aug 2003.

[12] É. Maia, C. Couto, P. Vila Real, and N. Lopes, "Critical temperatures of class 4 cross-sections," *Journal of Constructional Steel Research*, vol. 121, pp. 370–382, jun 2016.

[13] W. Skowronski, "Load capacity and deflection of fire-resistant steel beams," *Fire Technology*, vol. 26, pp. 310–328, nov 1990.

[14] A. Law, J. Stern-Gottfried, M. Gillie, and G. Rein, "The influence of travelling fires on a concrete frame," *Engineering Structures*, vol. 33, pp. 1635–1642, may 2011.

[15] J. Stern-gottfried, A. Law, G. Rein, M. Gillie, and J. L. Torero, "A Performance Based Methodology Using Travelling Fires for Structural Analysis," in *8th International Conference on Performance-Based Codes and Fire Safety Design Methods*, (Lund, Sweden), Society of Fire Protection Engineers (SFPE), 2010.

[16] CEN, "EN 1991-1-2:2002 - Eurocode 1. Actions on structures. General actions. Actions on structures exposed to fire," 2002.

[17] C. Röben, *The effect of cooling and non-uniform fires on structural behaviour*. Phd, The University of Edinburgh, 2009.

[18] A. Law, *The Assessment and Response of Concrete Structures Subject to Fire*. Doctor of philosophy, The University of Edinburgh, 2010.

[19] F. H. Rezvani and H. R. Ronagh, "Structural response of a MRF exposed to travelling fire," *Proceedings of the Institution of Civil Engineers - Structures and Buildings*, vol. 168, no. 9, pp. 619–635, 2015.

[20] H.-X. Yu, X.-Q. Sun, and K. Wong, "Resistance of steel space frames subjected to localized travelling fire," in *Proceedings of the 8th International Conference on Structures in Fire* (G.-Q. Li, V. K. R. Kodur, S.-C. Jiang, J. Jiang, S.-W. Chen, and G.-B. Lou, eds.), (Shanghai, China), pp. 1121–1128, Tongji University Press, 2014.

[21] P. Kotsovinos, *Analysis of the structural response of tall buildings under multifloor and travelling fires*. Doctor of philosophy, The University of Edinburgh, 2013.

[22] F. Sadek, J. A. Main, H. S. Lew, S. D. Robert, V. P. Chiarito, and S. El-Tawil, "NIST Technical Note 1669. An Experimental and Computational Study of Steel Moment Connections under a Column Removal Scenario," tech. rep., National Institute of Standards and Technology (NIST), 2010.

[23] S. E. Quiel and M. E. M. Garlock, "3-D versus 2-D modeling of a high-rise steel framed building under fire," in *Proceedings of the 5th International Conference on Structures in Fire (SiF'08)* (K. H. Tan, V. K. R. Kodur, and T. H. Tan, eds.), (Singapore), pp. 278–289, 2008.

[24] G. Flint, *Fire Induced Collapse of Tall Buildings*. Doctor of philosophy, University of Edinburgh, 2005.

[25] BSI, "BS ISO 834-10:2014 Fire resistance tests. Elements of building construction. Specific requirements to determine the contribution of applied fire protection materials to structural steel elements," 2014.

[26] SFPE, "SFPE Engineering Standard on Calculating Fire Exposures to Structures . SFPE S.01 2012.," 2011.

[27] B. Meacham, H. Park, M. Engelhardt, A. Kirk, V. Kodur, I. van Straalen, J. Maljaars, K. van Weeren, R. de Feijter, and K. Both, "Fire and Collapse , Faculty of Architecture Building , Delft University of Technology: Data Collection and Preliminary Analyses," in *Proceedings of the 8th International Conference on Perfomance-Based Codes and Fire Safety Design Methods*, (Lund, Sweden), 2010.

[28] S. Lamont, A. S. Usmani, and M. Gillie, "Behaviour of a small composite steel frame structure in a "long-cool" and a "short-hot" fire," *Fire Safety Journal*, vol. 39, pp. 327–357, jul 2004.

[29] R. L. Alpert, "Calculation of response time of ceiling-mounted fire detectors," *Fire Technology*, vol. 8, pp. 181–195, aug 1972.

[30] A. H. Buchanan, *Structural Design for Fire Safety*. John Wiley & Sons, Ltd, 2001.

[31] ECCS, "Design Manual on the European Recommendations for the Fire Safety of Steel Structures," tech. rep., European Convention for Constructional Steelwork - Technical Committee 3 - Fire Safety of Steel Structures, 1985.

[32] B. R. Kirby, "Recent developments and applications in structural fire engineering designA review," *Fire Safety Journal*, vol. 11, pp. 141–179, dec 1986.

[33] HMGovernment, "Fire safety: Approved Document B. Volume 2 - Buildings other than dwelling houses," 2006.

[34] K. H. Tan and W. F. Yuan, "Buckling of elastically restrained steel columns under longitudinal non-uniform temperature distribution," *Journal of Constructional Steel Research*, vol. 64, no. 1, pp. 51–61, 2008.

[35] S. A. Kilic and S. Selamet, "Symmetric and Asymmetric Collapse Mechanisms of a Multi-Story Steel Structure subjected to Gravity and Fire," in *Structures Congress 2013*, (Reston, VA), pp. 2545–2554, American Society of Civil Engineers, apr 2013.

[36] J. O. Hallquist, *LS-DYNA theory manual*. Livermore Software Technology Corporation, 2006.

[37] R. M. Lawson and S. J. Hicks, "Design of composite beams with large web openings (P355)," tech. rep., SCI, 2011.

[38] CEN, "EN 1993-1-1:2005 - Eurocode 3. Design of steel structures. General rules and rules for buildings," 2005.

[39] J. V. Ryan and E. W. Bender, "Fire endurance of open-web steel-joist floors with concrete slabs and gypsum ceilings, NBS Building Materials and Structures Report 141," tech. rep., 1954.

[40] A. H. Gustaferro, "Temperature Criteria at Failure," in *Fire Test Performance, ASTM STP 464*, (Union City, N. J.), pp. 68–84, American Society for Testing and Materials, 1970.

[41] V. Babrauskas and R. B. Williamson, "The historical basis of fire resistance testing - Part II," *Fire Technology*, vol. 14, pp. 304–316, 1978.

[42] J. V. Ryan and A. F. Robertson, "Proposed criteria for defining load failure of beams, floors, and roof constructions during fire tests," *Journal of Research of the National Bureau of Standards, Section C: Engineering and Instrumentation*, vol. 63C, no. 2, p. 121, 1959.

[43] BSI, "Fire tests on building materials and structures. Part 10. Guide to the principles, selection, role and application of fire testing and their outputs," 2008.

[44] ISO, "Fire-resistance tests - Elements of building construction. Part 1: General requirements," 1999.

[45] ASTM Committee E05, "Standard test methods for fire tests of building construction and materials," 2016.

[46] S. Lamont, B. Lane, G. Flint, and A. Usmani, "Behavior of Structures in Fire and Real Design - A Case Study," vol. 16, no. February 2006, 2007.

[47] ECCS Technical Committee 3, "European Recommendations for the fire safety of steel structures," tech. rep., 1983.

[48] A. S. Usmani, J. M. Rotter, S. Lamont, A. M. Sanad, and M. Gillie, "Fundamental principles of structural behaviour under thermal effects," 2001.

[49] M. E. Garlock and S. E. Quiel, "Plastic Axial Load and Moment Interaction Curves for Fire-Exposed Steel Sections with Thermal Gradients," *Journal of Structural Engineering*, vol. 134, pp. 874–880, jun 2008.

Appendices

5.A Effect of fire protection and beam section size

The effect of different level of fire protection of the steel beams and columns and the increased beam section size, i.e. sectional capacity, on the failure time, the corresponding temperature of the failed element and the frame utilization are shown in Figs. 5.A1 and 5.A2. The frame with both beams and columns designed for 120 min of the ISO fire resistance (B120 C120) only fails when subjected to the SFPE and ISO fire scenarios after 150 min of exposure. It indicates a 3 times higher fire resistance than for a frame with B60 C120. In the majority of the cases, the frames with the columns with the lower level of fire protection (B60 C60) and larger beam cross-section (B60 C120 - LC) tend to reach failure at earlier and later times, respectively, in comparison to B60 C120 but within a similar range (up to approx. 20 min differences). However, there are cases where lower column protection leads to an improved fire resistance (e.g. 2.5% - 10% TFM - deflection criteria, ISO - all criteria), and larger beam section leads to earlier failure time (e.g. 25% TFM - $L^2/9000d$). It should be noted that members with a larger section could result in increased thermally induced forces which in some scenarios could prove more critical in comparison with a smaller section. The most significant differences in failure time occur for 2.5 - 10% TFM (up to 200 min or even 370 min - 2.5% TFM). The critical temperatures of the failed elements in comparison to the B60 C120 are either higher or

lower irrespective of the level of fire protection, section size or failure criteria. They range between 350°C and 750°C. The maximum differences are up to 130°C. In most cases, the increased beam section size, protection and decreased column protection result in higher element temperatures at the time of failure.
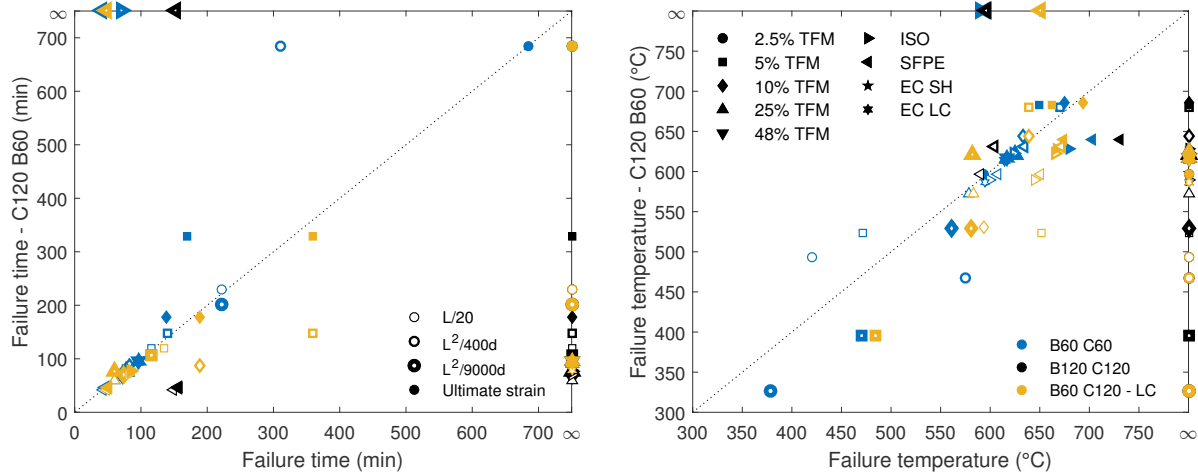

Figure 5.A1: Comparison of failure times (left) and corresponding failed element web temperatures (right) for the cases with different levels of protection assumed for beam and columns and larger beam cross-sections with the base case (C120 B60).

.

The CDF of the maximum at any time mean and peak utilization of the members in the frame, which are shown in Fig. 5.A2, indicate that the increased beam section size results in the highest improvement of frame utilization. This is followed by the increased beam protection (B120 C120), but the difference is relatively small. B60 C60 result in the most severe utilization rates for uniform fires but for travelling fires utilization of the frame is similar to that with increase member fire resistance. For the 5% TFM, the 25% TFM and the EC SH, the frame with increased column protection even shows slightly higher maximum frame utilization. The reason for this, is most likely the higher rigidity of the columns with the higher protection resulting in higher axial restraint and, thus, axial forces that develop within heated beams. Therefore, depending on the fire scenario a higher level of fire protection for different members within the frame will either typically lead to an enhanced or sometimes reduced fire resistance.

5.B Supporting Data

Fig. 5.B1 shows a comparison of the average temperatures of the structural member (beam or column) where failed elements are located at the time of failure according to different failure criteria. Failure criteria include ultimate strain failure and deflection related failure criteria of $L/20$, $L^2/400d$, and rate of $L^2/9000d$ over 1 min. Fig.5.B1 is presented here in reference to Fig. 5.12 and is referred to in Section 5.3.3 of this chapter. Fig. 5.B1 shows that the difference between the average member temperatures,
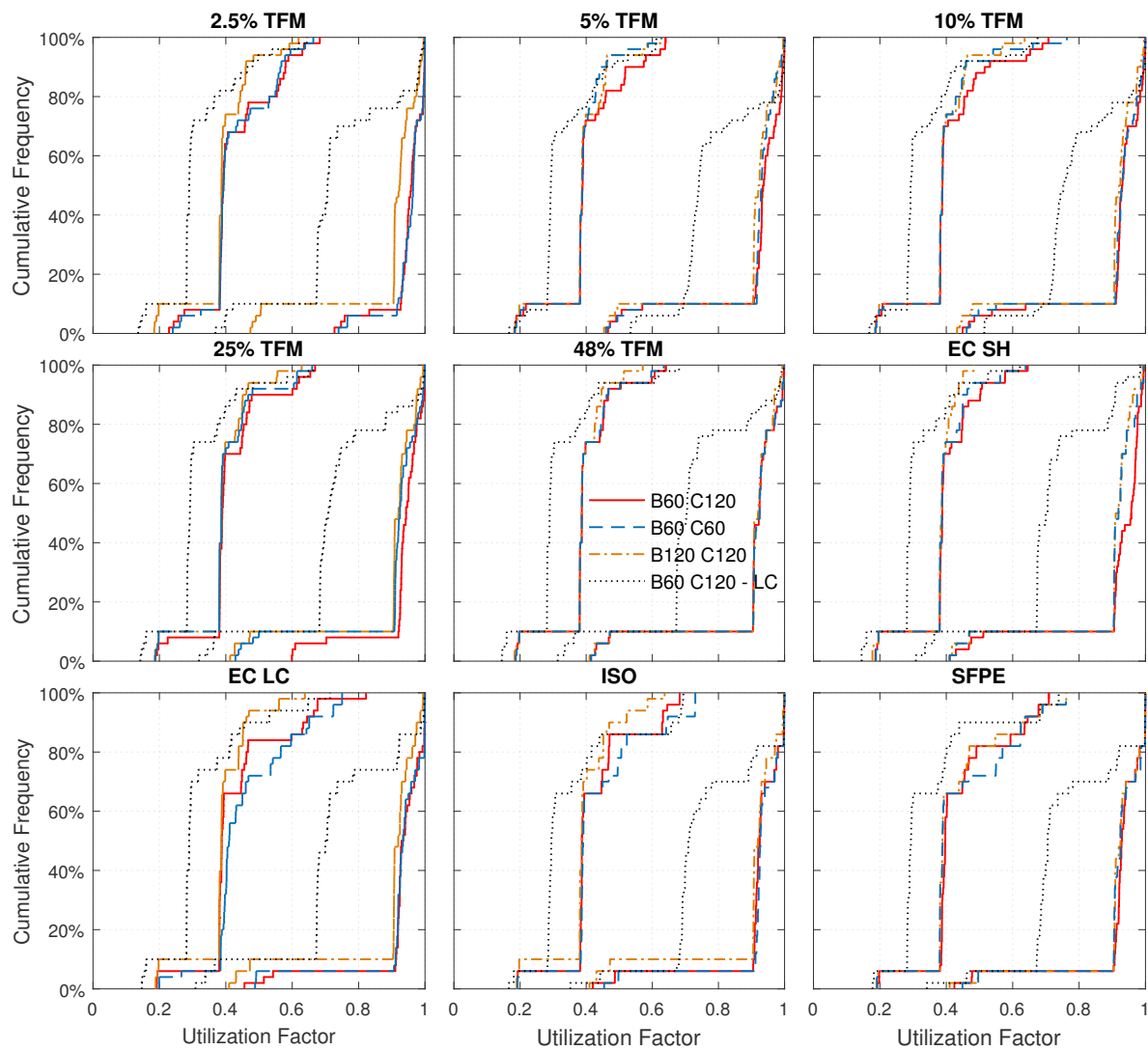
Figure 5.A2: The effects of level of fire protection and beam section size on the CDF of maximum at any time average (lower bound) and peak (upper bound) utilization of members in the frame.

.

where failure occurred, at failure for the fires occurring on the same floors is very small and ranges between 0.04 to 6.8°C. The difference of the localized temperatures of the failed elements ranges between 2 and 33°C (Fig. 5.13). For travelling fires the difference between the average structural member temperatures is up to 500°C.
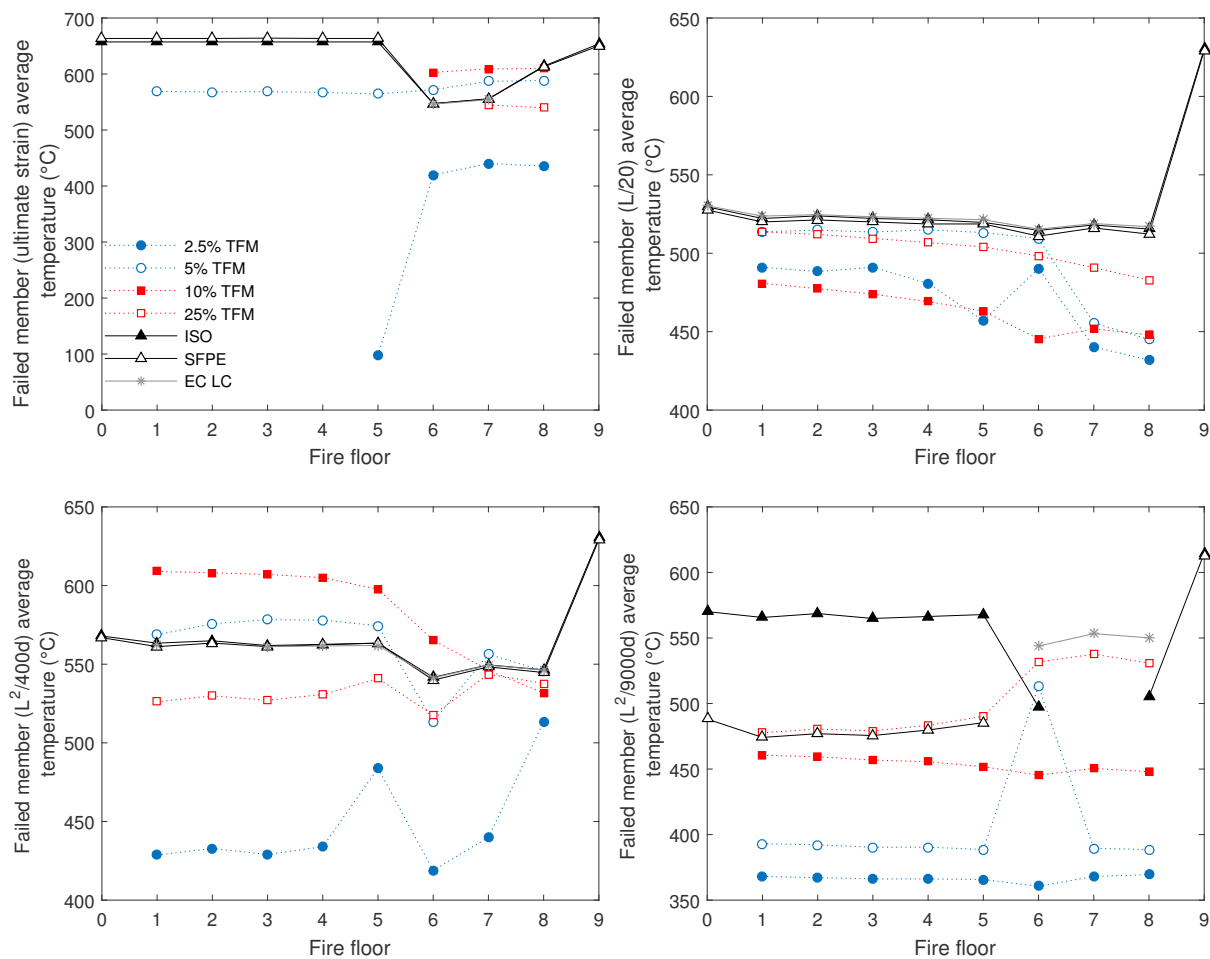
Figure 5.B1: Corresponding average temperatures of the structural member where failed elements are located for different failure criteria (ultimate strain, $L/20$, $L^2/400d$, and $L^2/9000d$ over 1 min) and for all fire scenarios.

Chapter 6

Structural Response of a Steel-Frame Building to Horizontal and Vertical Travelling Fires in Multiple Floors

Summary [1]

During previous fire events such as the World Trade Centre Towers (WTC) 1, 2 & 7 in New York (2001), the Windsor Tower in Madrid (2005) and the Plasco building in Iran (2017), flames were observed to travel horizontally across the floor plate and vertically to different floors. Such fires are not considered as part of the traditional prescriptive structural design for fire. Recently, the Travelling Fires Methodology (TFM) has been developed to account for such travelling nature. A dozen of studies have investigated the structural response of steel, concrete, and composite structures to a single-floor travelling fire. 5 out of 6 of the vertically travelling fire studies have been limited to the structures with long span composite truss system as in WTC Towers. The aim of this chapter is to investigate the response of a substantially different structural system, i.e. a generic multi-storey steel frame, subjected to travelling fires in multiple floors, and varying the number of fire floors, including horizontal and vertical fire spread. A two-dimensional 10-storey 5-bay steel frame is modelled in the finite element software LS-DYNA. The number of multiple fire floors is varied between 1 and 10, and for each of these scenarios, 5 different fire types are investigated. They include four travelling fire scenarios and the standard fire. In total, 51 fire simulations are considered. The development of deflections, axial forces, bending moments and frame utilization are analysed. Results show that the largest stresses develop in the fire floors adjacent to cool floors, and their behaviour is independent of the number of fire floors. Results indicate that both the fire type and the number of fire floors have a significant effect on the failure time (i.e. exceeded element load carrying capacity) and the type of collapse mechanism. In the cases with

---

a low number of fire floors (1 to 3) failure is dominated by the loss of material strength, while in the cases with larger number of fire floors (5 to 10) failure is dominated by thermal expansion. Collapse is mainly initiated by the pull-in of external columns (1 to 3-floor fires; 1 to 9-floor fires for 2.5% TFM) or swaying of the frame to the side of fire origin (5 to 10-floor fires). This chapter assesses a different structural form compared to previous literature under an extensive range of multiple floor travelling fire scenarios. It is found that although vertically travelling fires result in larger beam axial forces and initial deflections, simultaneous travelling fires result in shorter failure times and represent a more onerous scenario for the steel frame investigated.

6.1   Introduction

The understanding of the fundamental mechanics of a whole building behaviour in fire has significantly increased in the last decades, especially following the Broadgate fire in London in 1990 [1, 2], which took place in a 14-storey steel framed building under construction. Even though the majority of steelwork was unprotected and active fire protection methods were not functional, the building showed robust behaviour and did not collapse. Following this accident, full-scale tests of various multi-storey buildings were carried out in Cardington between 1994 and 1999 [3]. The Broadgate fire and Cardington tests showed that steel framed buildings as a whole performed better in fire than indicated by the prescriptive design of individual members. Therefore, prescriptive design approaches were believed to be conservative [2].

However, the prescriptive design was challenged and concerns were raised after the collapse of the World Trade Centre Towers 1, 2 & 7 in New York (2001) [4] and Windsor Tower fire in Madrid (2005). Firstly, the collapse of the buildings during these accidents showed that for buildings with non-conventional structural layout (unlike in Broadgate fire and Cardington tests) the prescriptive guidance assuming single elements can be non-conservative [5]. Secondly, during these events, fires were observed to travel horizontally across the floor plate and vertically between different floors. Such fires were not considered in the traditional prescriptive design at the time. Design codes and, thus, most of the understanding of the structural behaviour in fire were based on the assumption of uniform fires in a compartment. Recent work [6, 7] has shown that, while the uniform fire assumption may be suitable for small enclosures, the large, open-plan compartments typical of modern architecture, do not burn simultaneously throughout the whole enclosure. Instead, these fires, as observed in the accidents, tend to burn over a limited area and move across floor plates as flames spread with time. They are referred to as travelling fires. To account for this travelling nature, the Travelling Fires Methodology (TFM) was developed by Stern-Gottfried et al. [6, 7]. In Chapter 2, the TFM has been improved to account for more realistic fire dynamics and range of fire sizes and is referred to as iTFM. Unlike traditional design methods, this methodology accounts for non-uniform temper-

ature distributions and long-fire durations observed in the aforementioned travelling fire incidents. The methodology has been applied to investigate the thermal and structural response of steel [7, 8], concrete [9, 10] and composite structures [11, 12]. In most of these studies it was concluded that the consideration of more realistic fire exposure such as travelling fires is important for the structural response and that a uniform fire assumption is not the most conservative. However, most of this work has been limited to single-storey travelling fires.

Following the 9/11 events, a lot of research has been carried out on the structural response of structural arrangements similar to WTC Towers (long-span composite truss system) subjected to multiple floor fires [2, 5, 13–15]. Usmani et al. [2] and Flint et al. [5] carried out computational analysis on the collapse mechanisms of the WTC Towers. The number of simultaneously heated floors and the maximum fire temperature were varied. A generalised exponential curve was used to represent the fire. Collapse was found to primarily be a result of geometric changes (i.e. inward pull-in of the external columns) and occurred at temperatures as low as 400°C. Based on the latter work Lange et al. [14] identified two main collapse mechanisms (strong floor and weak floor) and proposed a design methodology. These collapse mechanisms were further examined by Kotsovinos and Usmani [15]. The authors performed parametric studies and established the criteria on the occurrence of strong and weak floor collapse mechanisms.

Röben et al. [13] carried out computational analysis on the steel-concrete composite structure exposed to vertically travelling fires with inter-floor time delay. The fires on each floor were represented by exponential curves adopted from the aforementioned studies. The results indicated cyclic deflection patterns of columns which were not observed previously for simultaneous multi-floor fires. The authors concluded that both simultaneous and vertically travelling fires result in different structural responses and either of them can be more onerous. One of the first studies which considered multiple floor horizontally and vertically travelling fires was conducted by Kotsovinos [12]. Fire type (i.e. uniform and travelling), size and inter-floor time delay were varied. To represent the horizontally travelling fire, the TFM [7] was used. In this study, uniform fires were found to result in higher stresses in the floor in comparison to travelling fires. Similarly to the study by Röben et al. [13], cyclic displacement patterns were observed for the cases with vertically travelling fire. In addition, results showed that small inter-floor time delay (300 s) did not have a significant effect on the structural performance.

In all of the previously identified studies significant and extensive work has been carried out to understand the structural response of high-rise structures subjected to simultaneous, horizontally and vertically travelling fire scenarios. However, most of this work on multiple floor fires is limited to structures with a long span composite truss system like in the WTC Towers. Furthermore, the focus of most of the work in [2, 5, 13, 14] was on the collapse of the WTC, and thus the authors did not draw any generic conclusions on the effect on the structural response of the number of storeys subjected to

fire. In these studies collapse was mainly associated with the stiffness of the structural members. The effect of the number of fire floors subjected to fire was only considered in the work by Kotsovinos and Usmani [15].

In this chapter, the response of a substantially different structural system, i.e. generic multi-storey steel frame, subjected to multiple floor travelling fires and varying number of simultaneously heated fire floors is investigated. Additionally, this chapter investigates how the structural response of the frame changes with inter-floor time delay, upward and downward fire spread, and opposing fire spread on different floors.

6.2 Computational model & domain

6.2.1 The structure

The multi-storey steel frame considered in this analysis is the same as in Chapter 4 and is based on the moment resistant frame published by NIST [16]. It is a 10-storey 5-bay frame representative of a generic office building with a floor layout of 45.5 m × 30.5 m. It is designed according to the ASCE 7-02 standard. The plan layout and elevation of the building are shown in Fig. 6.1. In this study the structural fire response of a 2D internal frame with the longest beam span of 9.1 m is investigated. For more details the reader is referred to Chapter 4, Section 4.2.1 of this thesis.
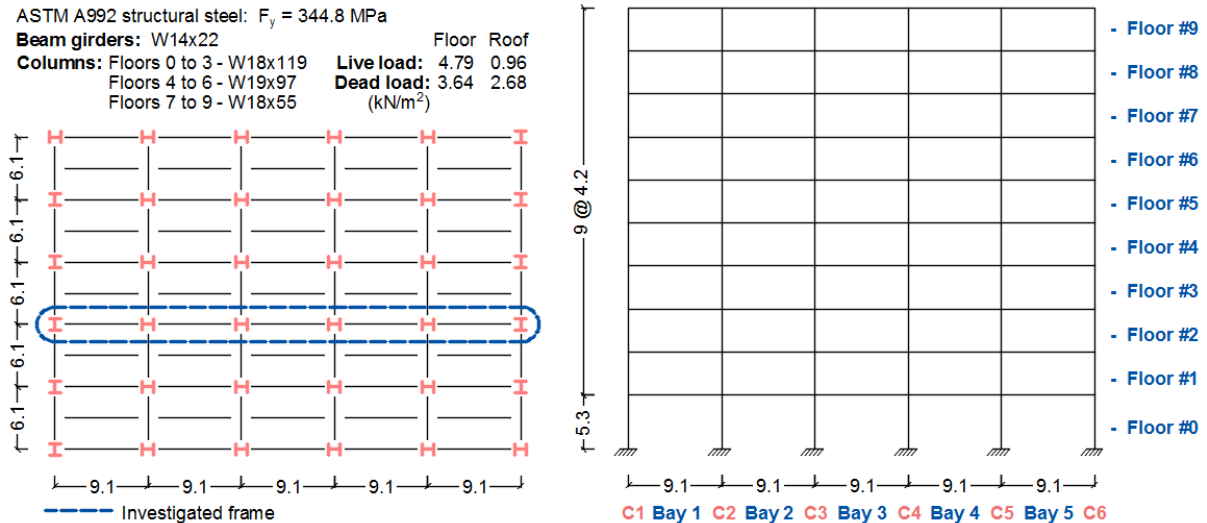
Figure 6.1: Plan layout (left), elevation (right) and structural member details of the investigated frame [16]. Frame dimension units are in meters.

6.2.2 Fire scenarios

The structural response of the frame subjected to TFM (Chapter 2) and the standard fire (ISO) [19] is investigated. The number of floors subjected to fire simultaneously is varied between 1 and 10 (i.e. a whole frame). In addition, two-floor vertically travelling

fire scenarios are considered to analyse the effect of time delay due to upward and downward fire spread between floors and opposing horizontal fire spread on multiple floors. Vertical fire spread delay between floors is assumed to be 10 min and 25 min. Similar values were used in the study by Röben et al. [13] and, as identified in the latter study, are within the estimated vertical fire spread rates of 6 and 30 min based on the Windsor Tower fire in Madrid (2005). In total, 51 different fire scenarios are investigated as shown in Table 6.1.

Table 6.1: Details of the investigated fire scenarios.

Fire scenario	Fire floors (#)	Fire type	Time delay between floors
Horizontal (simultaneous)	5 4 & 5 4, 5, & 6 3, 4, 5, 6, & 7 2, 3, 4, 5, 6, 7, & 8 1, 2, 3, 4, 5, 6, 7, 8, & 9 0, 1, 2, 3, 4, 5, 6, 7, 8, & 9	2.5% TFM, 10% TFM, 25% TFM, 48% TFM, and ISO	0 min
Opposing (simultaneous)	4 ($\rightarrow$) & 5 ($\leftarrow$) [a] 4 ($\leftarrow$) & 5 ($\rightarrow$) [a]	10% TFM and 25% TFM	0 min
Vertically travelling	From 4 to 5 ($\uparrow$) [a] From 5 to 4 ($\downarrow$) [a]	10% TFM, 25% TFM, and ISO	10 & 25 min

a. Arrows indicate horizontal and vertical fire spread directions on and between different floors.

To represent a travelling fire exposure, iTFM presented in Chapter 2 is used. An illustration of a travelling fire is shown in Fig. 6.2. Each floor of the frame in this study is subjected to four TFM scenarios: fire sizes of 2.5%, 10%, 25%, and 48% of the floor area. The correlation to represent the standard fire (referred to as the ISO standard fire in this chapter) is taken from the Eurocode [19]. The standard fire has its origins in the early 20th century and forms the basis of fire resistance rating and standards worldwide. The same fire scenarios were considered and more details on the parameters used to generate the curves are given in Chapter 4, Section 4.2.2. Illustration of the gas temperatures for all fire scenarios at the mid-span of Bay 2 is shown in Fig. 6.3.

6.2.3 Heat transfer

Beams and columns are designed for 60 min and 120 min standard fire resistance respectively with a limiting temperature of 550°C using Eq. (6.1) [7, 20]. At 550°C steel maintains only 60% of its ambient temperature strength because of the thermal degradation of its mechanical properties and, thus, it is commonly accepted as the critical
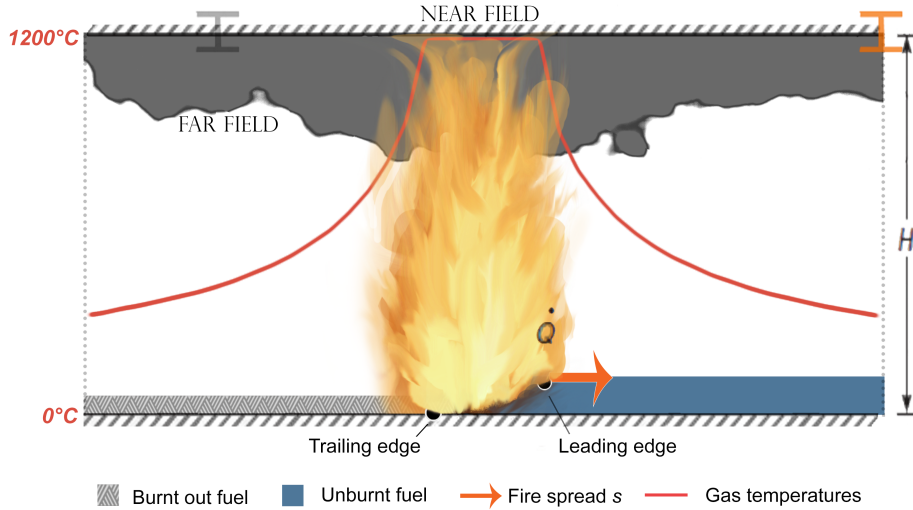
Figure 6.2: Illustration of a travelling fire and distribution of gas temperatures in the near-field and far-field.
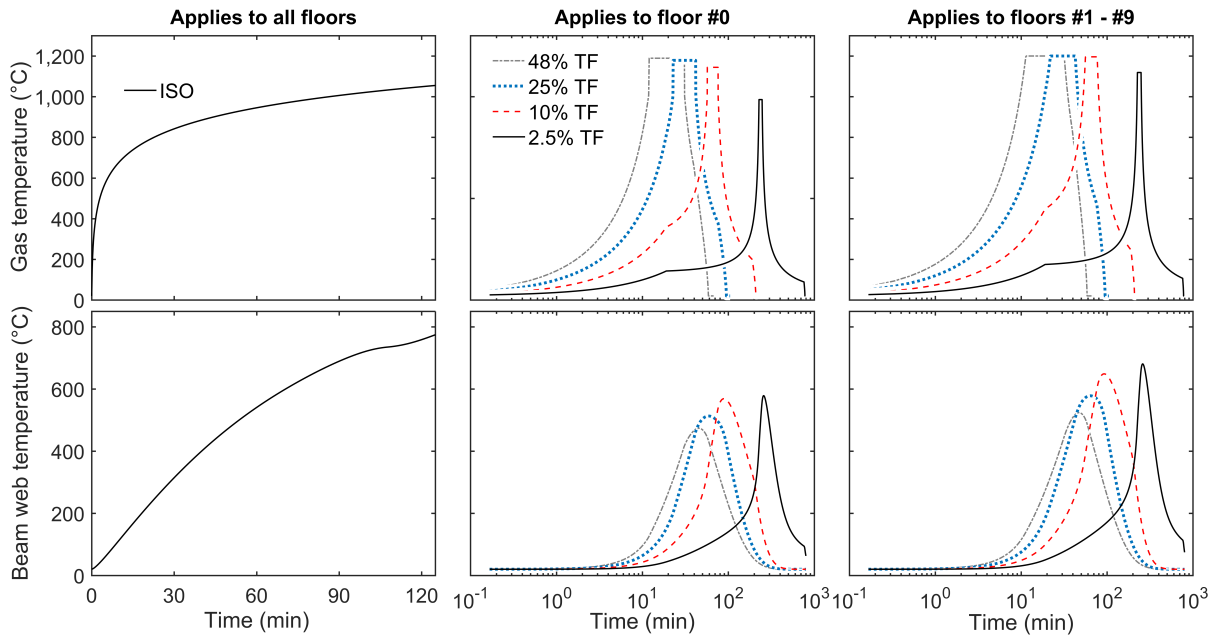
Figure 6.3: Gas temperatures (top) and corresponding steel beam web temperatures (bottom) for the considered fire scenarios.

temperature for steel in traditional design [21].

$$\Delta T_s = \frac{H_p}{A}\frac{k_i}{d_i\rho_s c_s}\frac{\rho_s c_s}{[\rho_s c_s + (H_p/A)d_i\rho_i c_i/2]}(T_g - T_s)\Delta t \tag{6.1}$$

where H_p is the heated perimeter of the beam or column (m), A is the cross-section area of the beam or column (m^2), T_s is the steel temperature (K), T_g is the gas temperature (K), d_i is the thickness of the insulation (m), ρ_s is the density of steel (kg/m^3), c_s is the temperature dependent specific heat of steel taken from [22] (J/kg.K), and Δt is the time step (s). Heat transfer to the structural members using Eq. (6.1) is carried out assuming

lumped capacitance for separate parts of the cross-section (i.e. web and flanges) as in Chapter 4. For more details, see Section 4.2.3.

An illustration of temperature development in the beam sections at the mid-span of Bay 2 is shown in Fig. 6.3. It shows that at the indicated location, beams subjected to small travelling fires (e.g. 5% TF) reach higher temperatures in comparison to large travelling fires (e.g. 48% TFM) by up to approx. 160°C. Even though large travelling fires may have higher near-field temperatures than small travelling fires, their durations and the time it takes to reach those temperatures are significantly different. 48% TFM travels along the compartment in 1 h, while 5% TFM takes up to 13 h.

6.2.4 LS-DYNA model

The multi-storey steel frame is modelled using the general purpose finite element software LS-DYNA (Release 7.1.1) explicit solver. The LS-DYNA model used was the same as in Chapter 4 and, therefore, all the details are given and the reader is referred to Chapter 4, Section 4.2.4 for more information. All of the parameters for the model were chosen based on mesh density and parameter sensitivity convergence studies (Appendix C). Table 6.2 shows mesh density convergence results for the frame exposed to the ISO fire on Floor #2. The aim of this study is the investigation of the global structural response, and, thus, no attempt was made to capture localized failures in the beams, columns, or in the beam-to-column connections.

**Table 6.2**: Mesh density convergence.

Beam element length (m)	Kinetic energy/ Internal energy (%)	Average relative error (%) - Bay 1 Floor #2			CPU time (s)
		Displacement	Bending Moment	Axial force	
0.0625	3×10^{-3}	-	-	-	26506
0.125	4×10^{-4}	1.72	0.71	5.34	44190
0.25	5×10^{-4}	5.22	1.65	8.71	5847
0.5	3×10^{-3}	10.98	2.68	19.37	1774
1	7×10^{-3}	17.99	3.76	27.87	556

6.3 Results and discussion

6.3.1 Multiple-floor fires

The development of the beam mid-span displacements, axial forces, bending moments and column lateral displacements in 5 bays on Floor #5 for a 25% travelling fire scenario is shown in Fig. 6.4, where comparison is made between a single floor and 5-floor fire scenarios. The results show that under multiple floor fires the structural response is significantly different compared to a single floor fire. In the multiple-floor fire scenario initial (i.e. within the first 50 min) peak beam mid-span displacements and bending

moments are lower by up to 270 mm and 63 kNm, respectively, in comparison to the single-floor fire scenario. However, column lateral displacements are larger and indicate the swaying of the frame in the direction of the fire origin until failure occurs at 53 min. In addition, the beams in Floor #5 in the multiple 5-floor fire are under tension rather than compression as in the single floor fire. The reason for that is that during the multiple floor fire scenario the beams in Floor #5, which is the central fire floor, have lower axial restraint to thermal expansion from the adjacent floors in comparison to a single floor fire. This is because the adjacent floors in the former case are expanding as well. Thus, thermal bowing and moment redistribution dominate the behaviour and the heated beams are subject to tension.
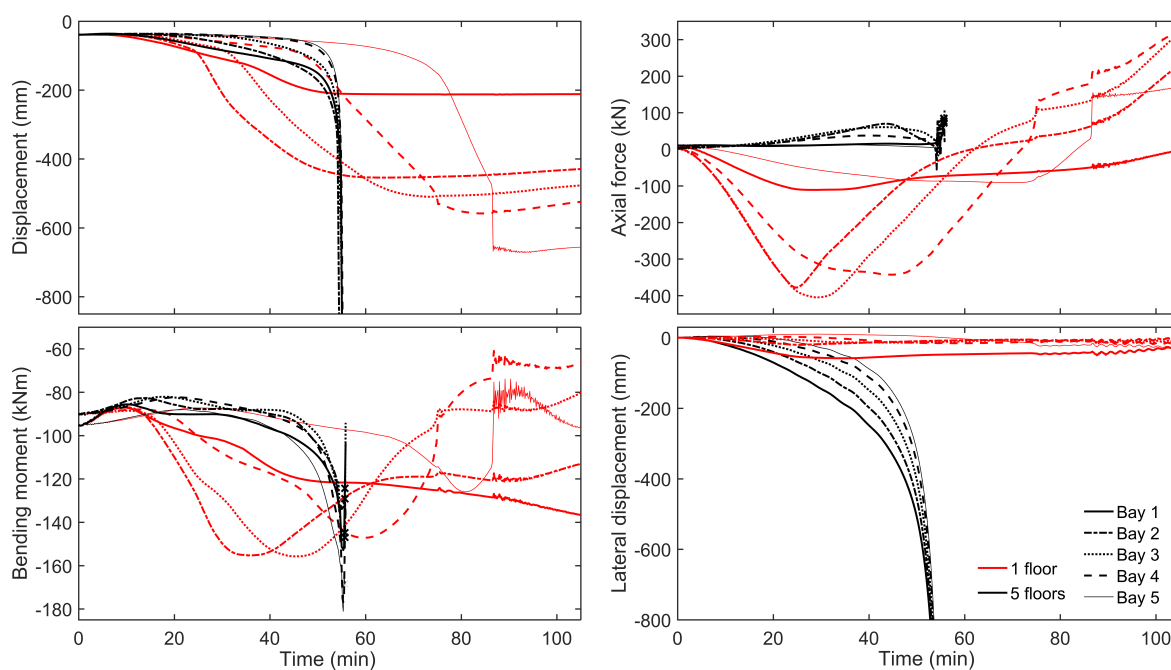
Figure 6.4: Comparison of Floor #5 beam mid-span displacement, axial force, bending moment and column lateral displacement development for a frame exposed to the 25% TFM on 1 floor and 5 floors.

In general, if there is sufficient axial restraint from the surrounding structure, at the beginning of fire exposure beams are under compression due to the restrained thermal expansion until yielding or buckling occurs. Yielding takes place when compressive axial force begins to decrease followed by elasto-plastic response and a sudden increase in deflection [26]. This can be clearly seen for a single floor fire scenario. Although not shown in Fig. 6.4, axial force development patterns are similar in fire floors adjacent to cool floors irrespective of the number of fire floors because of the stiff surrounding structure. Thus, the highest axial forces develop within these floors. This is illustrated in Fig. 6.5, which shows the peak compressive or tensile axial forces which develop during the fire exposure for different fire scenarios (travelling fires and ISO fire) and different number of multiple floors on fire. Positive and negative values indicate tension and

compression, respectively. The results show that, as identified previously, the highest compressive axial forces develop in the fire floors adjacent to the cool floors. As a result, due to stress redistribution the highest tensile stresses develop within the latter (i.e. cool floors). Due to thermal expansion of multiple floors and, thus, lack of axial restraint to thermal expansion, axial forces that develop in interior fire floors are significantly smaller. They are between 0.1 and 102 kN. That is 0.03 - 53% of the compressive axial forces (181 - 335 kN) in the fire floors adjacent to cool floors.
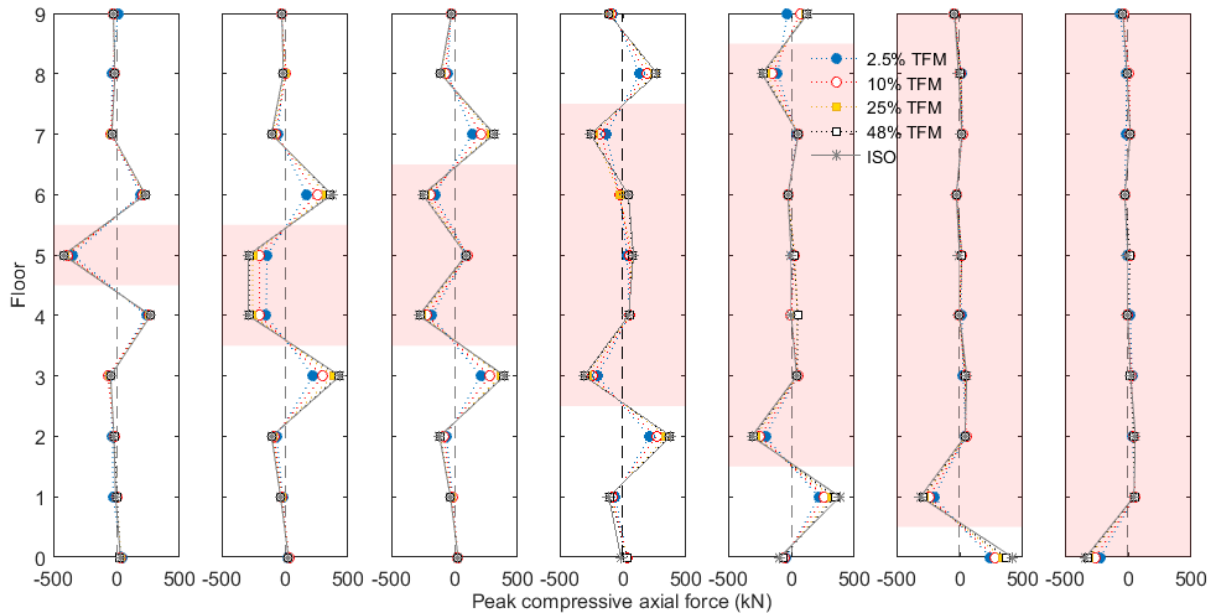
Figure 6.5: Peak beam axial forces which develop during the fire exposure on different levels of the building. Shaded area represents the fire floors.

The variation of the peak compressive axial forces which develop in beams and the time to reach it with the number of floors exposed to fire is shown in Fig. 6.6. The highest axial forces develop earliest for the 25% and 48% TFM and ISO fires irrespective of the number of floors exposed to simultaneous fire. This is because under uniform (ISO) and large TFM fire scenarios thermal expansion of beams in the heated floors is larger in comparison to localised smaller (2.5% and 10%) TFM scenarios. A similar observation was made in Chapter 4 on the analysis of the effect of travelling fires and uniform fires on the structural response of the same frame. In terms of the number of fire floors the highest axial forces develop for the single floor fire scenario. In this case, the unheated structure provides a higher axial restraint in comparison to intermediate cases where the number of cool floors is reduced. The lowest axial forces develop for the 2-floor and 3-floor fire scenarios. This is likely due to the fact that column section sizes in the fire floors adjacent to the cooler structure are smaller than in the other cases and, therefore, result in a lower level of axial restraint. However, the structural response in fire can be influenced by many different factors. They include but are not limited to, for example, material non-linearity, geometric non-linearity, restraint conditions, stress redistribution,
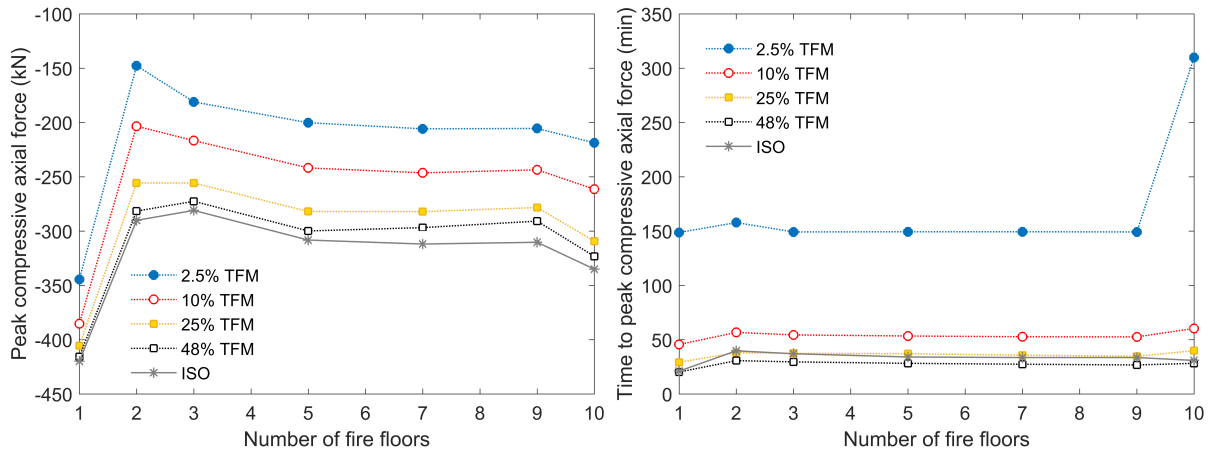
Figure 6.6: Peak heated beam compressive axial force variation (left) and time to reach it (right) with fire scenario and number of floors simultaneously exposed to fire.

thermal bowing, restrained thermal expansion, etc. Different combinations of various factors in some cases may lead to very similar results. Therefore, further studies varying the location of the fires and column sizes should be conducted to confirm this. Time to reach the peak axial force in general follows similar trends as the axial forces and is lowest for the 48% TFM.

The failure time and corresponding web temperatures of the element that failed for different fire scenarios are shown in Fig. 6.7. Failure is defined as the exceeded element load carrying capacity (i.e. ultimate strain) and indicates the local collapse. The results indicate that with the increasing number of simultaneously heated fire floors failure time decreases as expected. This is primarily because of the larger loss of stiffness of the frame as the larger number of the floors is heated. For the cases where the whole frame is exposed to the TFM scenarios there is a slight increase in time in comparison to the 9-floor fire scenarios and for 2.5% TFM failure does not occur. This is likely due to the slightly reduced rigidity of the frame and consequently axial forces and bending moments as the whole frame is expanding simultaneously. Also, high axial forces only develop in ground floor beams (see Fig. 6.5). In Chapter 5 it was observed that depending on the structural metric examined, either travelling fires or uniform fires can lead to failure and be the worst case scenario. Similarly, this study shows that for 1-floor to 3-floor fires ISO results in the earliest failure time, while for the larger number multiple fire floors 25% and 48% TFM indicate an earlier failure time. In addition, no failure is reported for the single floor fire for the latter fire scenarios. It shows that it is important to consider multiple floor fires in the structural design as the single floor fire scenario might not always capture the probable failure.

The web temperatures of the failed element indicate that for smaller and longer in duration TFM scenarios (2.5% and 10%) failure occurs when elements reach temperatures between 500 and 700°C. These values are within the expected range and are around the temperature of 550°C, which indicates a loss of material strength of 40%. However, for
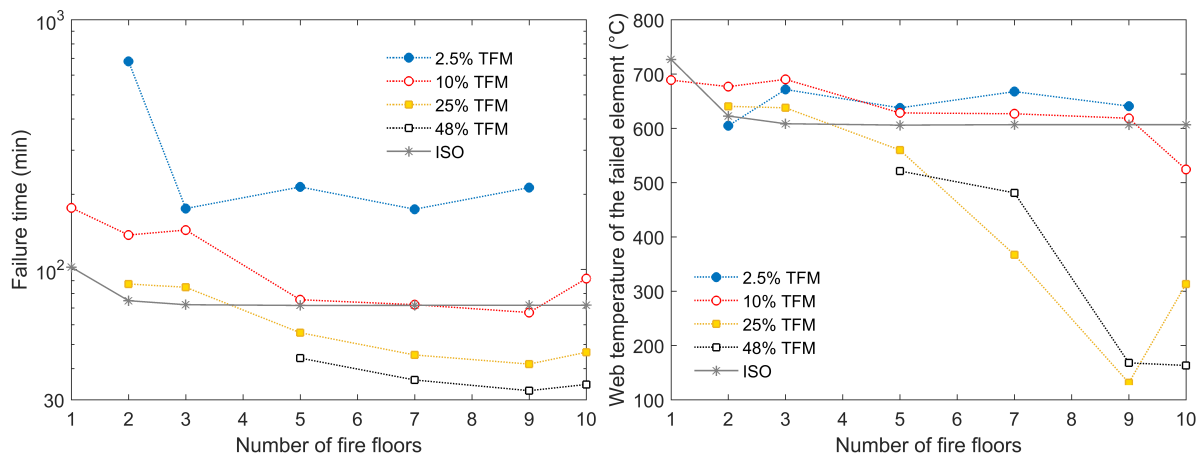
Figure 6.7: Variation of the failure time (left) and corresponding web temperature of the element that failed (right) with different fire scenarios and number of s simultaneously exposed to fire.

large TFM scenarios (25% and 48%) and ISO fire with the number of multiple fire floors larger than 5 failure occurs within members with temperatures as low as 125°C. Due to relatively uniform temperature distribution and large overall thermal expansion in these cases the frame sways towards the fire origin initiating the failure. Similar failure mechanism occurs for all fire scenarios with 5 or more floors exposed to simultaneous fires except for the 2.5% TFM. Illustration of the typical deflected shapes close to failure is shown in Fig. 6.8. For the cases with up to 3 heated fire floors and all 2.5% scenarios failure is a result of pull-in of external columns at the fire origin or towards the end of the fire path. It is similar to the weak-floor and strong-floor collapse mechanisms reported in [14, 15]. For the travelling fire scenarios, cooler beams subjected to the far-field heating or cooling and adjacent cool floors provide a large axial restraint and path for stress redistribution similarly to the concrete core in the latter studies.

Weak-floor collapse mechanism is identified as the initiation of collapse due to the buckling of the floor below the fire floors [14, 15]. For the strong-floor collapse mechanism failure is a result of the plastic collapse and formation of three hinges [14, 15]. For the travelling fire scenarios occurring in the multi-bay frame as in this study both mechanisms or a mix of them are observed. For the 3-floor 10% TFM and 5-floor 2.5% TFM results in Bay 2 indicate deflected shape patterns similar to the weak-floor collapse. In the other TFM and ISO scenarios deflected patters and pull-in of the columns is similar to the strong-floor or a mixed collapse mechanism. For the multi-storey and multi-bay frame analysed in this study failure type seems to be a result of not only the relative stiffness of the member at room temperature and number of fire floors as in [15], but also the travelling fire scenario considered.

Analysis of the axial force and bending moment separately within different members may give an indication of stresses which develop within these members but not of the actual member utilization. Utilization is the factor of the load carried by the member
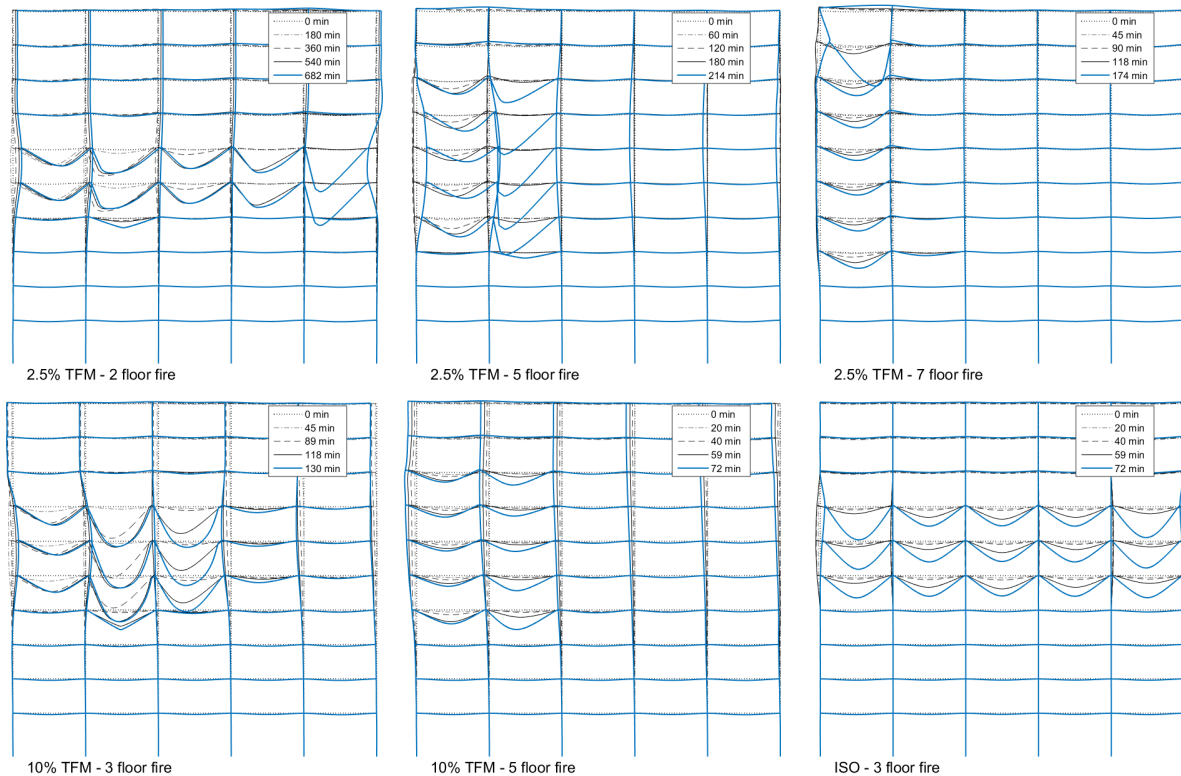
Figure 6.8: Illustration of typical deflected shapes of the frame close to failure for 2.5% TFM, 10% TFM and ISO fires and varying number of fire floors. Displacement scale factor is 5.

and its load carrying capacity. Two members may have similar peak axial forces developing within them and have significantly different temperature distributions at that time. With increasing temperature, the cross-section load carrying capacity decreases and thus utilization of these members and how close to failure they are might be very different. Therefore, to account for this the results are also analysed in the terms of the utilization of the members. Plastic axial load and moment (P-M) interaction curves are calculated according to [27]. Temperature dependent yield strength reduction factors are taken from the Eurocode [22]. Illustration of P-M curves at ambient temperature and during the 25% 2-floor and 9-floor travelling fire is shown in Fig. 6.9. P-M curves are shown for the elements that failed first, i.e. beam for 25% TFM 2-floor fire and column for 25% 9-floor fire. One curve is shown for the column, because it reaches a temperature of 130°C only. At this temperature steel still maintains all of its strength. The utilization of the member is found based on these curves, axial forces, and bending moments in different members at every time step. Cumulative density functions (CDF) of frame utilization at failure or the end of fire exposure for all fire scenarios are shown in Fig. 6.10. CDF shows what percentage of the members in the frame is under the utilization equal to or lower than the specified value. The lower and upper bounds in Fig. 6.10 show the average and peak utilization, respectively, of different members (i.e. beams and columns). It should

be noted that even at ambient temperature utilization of the frame is relatively high.

The results indicate that the frame experiences the highest average and peak utilization in the fire scenarios with 5 or more simultaneously heated fire floors. In general, frame utilization is highest in fire scenarios with the highest failure times. Considering the scenarios for which failure did not occur, results indicate the highest post-fire utilization for the 2.5% TFM 1-floor fire scenarios Average member utilization is between 18 and 80%. For other scenarios (2.5% 10-floor, 25% TFM 1-floor, and 48% 1 to 3-floor fires) it is lower and between 17 and 67%. For all scenarios more members are under higher utilization with increasing number of floors on fire. However, the maximum average utilization within the frame is highest for the single floor ISO fire scenario.

6.3.2 Opposing and vertically travelling fires

Comparisons of heated beam mid-span displacement, axial forces, bending moments and column lateral displacement for simultaneous, opposite and vertically travelling 2-floor 25% TFM are shown in Fig. 6.11. Development of beam mid-span displacement for all fire scenarios follows a similar trend. Peak displacements develop in Bay 3 and are the lowest in the bay of fire origin. The only difference is that for the vertically travelling fire scenario development in the upper fire floor is delayed. The magnitude of the deflections in both heated fire floors are almost identical. Even in the opposing fire spread scenario development of beam deflections in respect to the fire origin location is similar. That is, deflections on Floor #4 Bay 1 are the same as on the upper floor Bay 5, where the fire is spreading in the opposite direction. Though, the peak beam displacement values are slightly higher (up to 90 mm) in simultaneous and opposite fire scenarios than in the vertically travelling fire scenario. This could be due to a higher axial restraint to thermal expansion (beams in the upper floor remain cool for 25 min) and larger amount
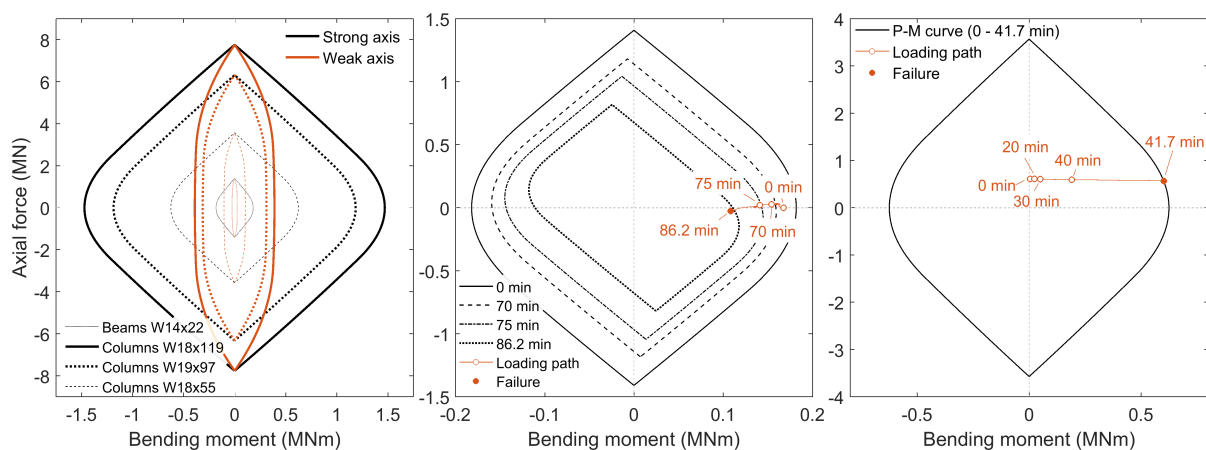
Figure 6.9: Illustration of P-M interaction curves for frame elements at room temperature (left); during the 25% TFM 2-floor (middle) and 9-floor (right) fire scenarios for the elements that failed and their utilization.
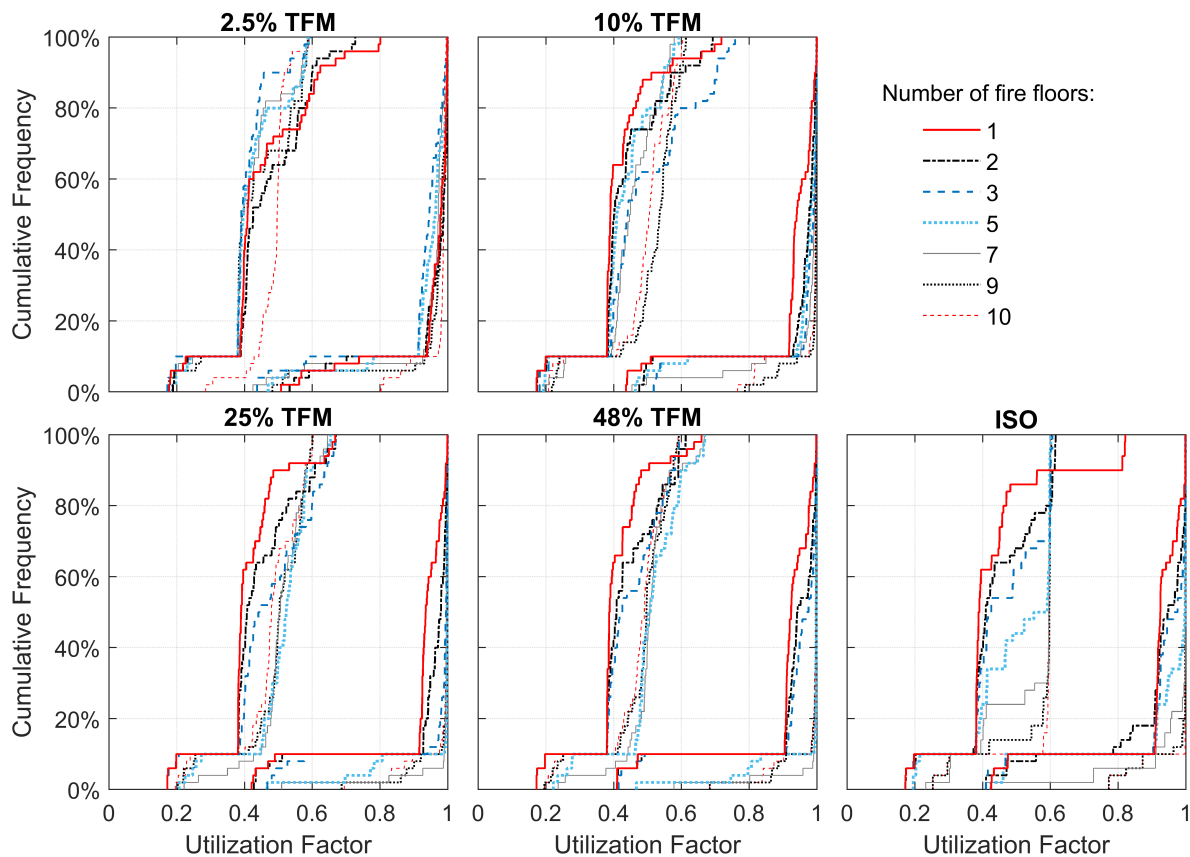
Figure 6.10: Cumulative frequency function of frame utilization at failure or the end of fire exposure for all fire scenarios.

of thermal stresses contributing to the compressive axial force development instead. However, the initial deflections larger than 200 mm develop earlier in the vertically travelling fire scenario.

Unlike beam mid-span deflections, the effect of different fire spread scenarios is more significant on the development of beam axial forces, bending moments, and column lateral displacements. Due to higher axial restraint, as identified previously, the highest axial forces in heated beams develop for the vertically travelling fire scenario. They are higher by up to 120 kN and 150 kN than in simultaneous and opposite fire scenarios, respectively. Similarly, the highest bending moments develop in the vertically travelling fire scenario as well. In addition, for the simultaneous fire, all beams on the heated floors during the heating are in compression while for the opposing fire scenario beams in the bay of origin are in tension.

Column lateral displacements attain the largest values for the simultaneous fire scenario (by up to 20 mm). This is because of the higher combined thermal expansion across the frame and lower thermal restraint. In other scenarios different members either experience near-field temperatures in the opposite sides of the bay or on the same side but after a thermal delay. The largest displacements develop in the bay of the fire origin. Lateral column displacement results in increased eccentricity of the load acting on the
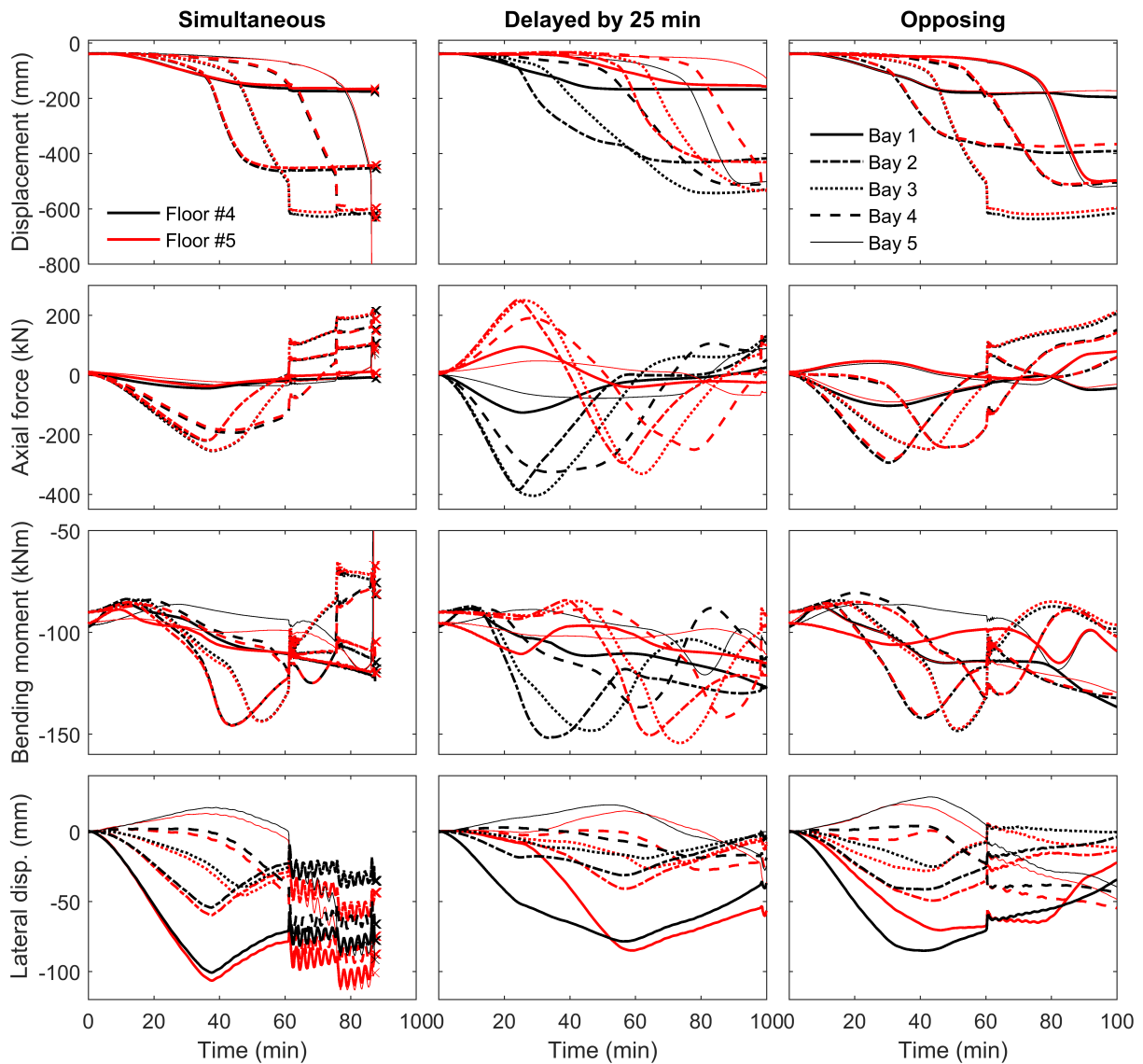
Figure 6.11: Comparison of beam mid-span displacement, axial force, bending moment and column lateral displacement development for a frame exposed to the 25% TFM on Floors #4 and #5 and varying fire spread (simultaneous, vertically travelling and opposing).

columns and, therefore, larger bending moments. Once the heated beams go into tension, column displacement reverses and they are pulled in inwards. This leads to the initiation of failure for the simultaneous multiple-floor fire scenario. No failure is reported for the vertically travelling and opposing fire scenarios. Unlike in previous studies on vertical travelling fires [12, 13], no significant oscillations in the lateral column displacement due to the vertical fire spread are observed in this study. This could be due to the different number of fire floors, different beam span length (9.1 m vs. approx. 18 m), stiffness of the beams and the surrounding structure or fire scenario used and needs further investigation to draw any definite conclusions.

Comparison of the CDF of the average and peak utilization of different floor members
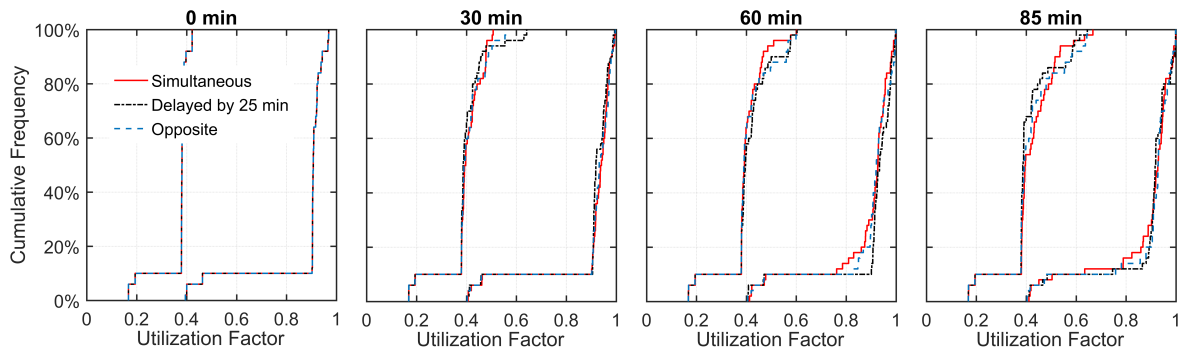
Figure 6.12: Cumulative frequency function of frame utilization at 0, 30, 60, and 85 min for simultaneous, vertically travelling and opposing fire spread scenarios.

at 0, 30, 60 and 85 min for different fire spread scenarios is shown in Fig. 6.12. The results show that the level of frame utilization for different fire scenarios is very similar, particularly for the first 30 min. Even for the simultaneous fire scenario close to failure (at 85 min) the average utilization of the frame is higher by only 2.1%. Similar overall stress and displacement development trends are observed for the other investigated fire scenarios (10% TFM and ISO fire, and vertically travelling fire with a delay of 10 min). In general, similarly to the work by Röben et al. [13] results indicate that depending on the structural metric of interest (displacements, utilization, or structural failure) either of the fire scenarios can represent the worst case scenario.

6.4 Conclusions

In this chapter, the structural response of a generic steel frame exposed to multiple-floor travelling fires and standard fire has been investigated. Results show that the highest stresses develop in the fire floors adjacent to the cool floors while in the intermediate fire floors the stresses are significantly smaller (i.e. axial forces by up to 47-99.97%). Peak compressive and tensile axial forces develop in the fire floors adjacent to the cool floors and in the cool floors, respectively. With increasing number of fire floors (from 2 to 10) and travelling fire size, the peak beam compressive axial forces rise by 41-71 kN (15-48%) and 70-134 kN (20-90%), respectively. However, the highest axial forces develop for fire scenarios with only one fire floor.

Results indicate that for the investigated frame the failure time and collapse mechanism are affected by both the fire type and the number of fire floors. For the cases with 1 to 3 fire floors failure is mostly dominated by the loss of material strength with temperature and occurs at the temperatures between 600 and 730°C. Failure is initiated by the pull-in of external columns. On the other hand, for the cases with 5 or more fire floors failure is dominated by the thermal expansion and geometric effects and occurs at temperatures as low as 130°C. The frame fails by swaying to the side of the fire origin. Failure time decreases with increasing travelling fire size. ISO fire is more onerous for

the cases with 1 to 3 fire floors. For the cases with 5 and more fire floors 25% and 48% travelling fires indicate earlier failure even though no failure occurs for the 48% TFM with lower number of fire floors.

In addition to varying the fire type and number of simultaneously heated fire floors the effect of opposing and vertically travelling two-floor fires has been investigated. In general, the patterns of stress and deflection development are similar irrespective of fire spread direction. The results show that vertically travelling fires result in higher beam axial forces and deflections early during the fire exposure. However, simultaneous fires lead to shorter times to failure and could be used to represent the worst case scenario. Also, unlike in the published literature on the structures with long span composite truss systems, results show no significant cyclic movement of columns for vertically travelling fires. This could be due to a different structural system or a small number of fire floors and further studies varying the number of fire floors for vertically travelling fires need to be conducted.

Results show that fire type (travelling or a standard fire) and number of fire floors have a significant effect on the failure time and type of collapse mechanism. One single worst case fire scenario cannot be readily identified, especially considering the uncertainty in the number of fire floors likely to occur in a real fire.

Acknowledgements

References

[1] British Steel, "The Behaviour of Multi-Storey Steel Framed Buildings in Fire," tech. rep., British Steel, Rotherham, 1999.

[2] A. S. Usmani, Y. C. Chung, and J. L. Torero, "How did the WTC towers collapse: a new theory," *Fire Safety Journal*, vol. 38, pp. 501–533, oct 2003.

[3] B. R. Kirby, "The Behaviour of a Multi-storey Steel Framed Building Subjected to Fire Attack Experimental Data," tech. rep., Rotherham, 1998.

[4] R. G. Gann, A. Hamins, K. McGrattan, H. E. Nelson, T. J. Ohlemiller, K. R. Prasad, and W. M. Pitts, "Reconstruction of the Fires and Thermal Environment in World Trade Center Buildings 1, 2, and 7," *Fire Technology*, vol. 49, pp. 679–707, jul 2013.

[5] G. Flint, A. Usmani, S. Lamont, B. Lane, and J. Torero, "Structural Response of Tall Buildings to Multiple Floor Fires," *Journal of Structural Engineering*, vol. 133, pp. 1719–1732, dec 2007.

[6] J. Stern-Gottfried and G. Rein, "Travelling fires for structural designPart I: Literature review," *Fire Safety Journal*, vol. 54, pp. 74–85, nov 2012.

[7] J. Stern-Gottfried and G. Rein, "Travelling fires for structural design-Part II: Design methodology," *Fire Safety Journal*, vol. 54, pp. 96–112, nov 2012.

[8] F. H. Rezvani and H. R. Ronagh, "Structural response of a MRF exposed to travelling fire," *Proceedings of the Institution of Civil Engineers - Structures and Buildings*, vol. 168, no. 9, pp. 619–635, 2015.

[9] A. Law, J. Stern-Gottfried, M. Gillie, and G. Rein, "The influence of travelling fires on a concrete frame," *Engineering Structures*, vol. 33, pp. 1635–1642, may 2011.

[10] A. Law, *The Assessment and Response of Concrete Structures Subject to Fire*. Doctor of philosophy, The University of Edinburgh, 2010.

[11] C. Röben, *The effect of cooling and non-uniform fires on structural behaviour*. Phd, The University of Edinburgh, 2009.

[12] P. Kotsovinos, *Analysis of the structural response of tall buildings under multifloor and travelling fires*. Doctor of philosophy, The University of Edinburgh, 2013.

[13] C. Röben, M. Gillie, and J. L. Torero, "Structural behaviour during a vertically travelling fire," *Journal of Constructional Steel Research*, vol. 66, pp. 191–197, feb 2010.

[14] D. Lange, C. Röben, and A. Usmani, "Tall building collapse mechanisms initiated by fire: Mechanisms and design methodology," *Engineering Structures*, vol. 36, pp. 90–103, mar 2012.

[15] P. Kotsovinos and A. Usmani, "The World Trade Center 9/11 Disaster and Progressive Collapse of Tall Buildings," *Fire Technology*, vol. 49, no. 3, pp. 741–765, 2013.

[16] F. Sadek, J. A. Main, H. S. Lew, S. D. Robert, V. P. Chiarito, and S. El-Tawil, "NIST Technical Note 1669. An Experimental and Computational Study of Steel Moment Connections under a Column Removal Scenario," tech. rep., National Institute of Standards and Technology (NIST), 2010.

[17] S. E. Quiel and M. E. M. Garlock, "3-D versus 2-D modeling of a high-rise steel framed building under fire," in *Proceedings of the 5th International Conference on Structures in Fire (SiF'08)* (K. H. Tan, V. K. R. Kodur, and T. H. Tan, eds.), (Singapore), pp. 278–289, 2008.

[18] G. Flint, *Fire Induced Collapse of Tall Buildings*. Doctor of philosophy, University of Edinburgh, 2005.

[19] CEN, "EN 1991-1-2:2002 - Eurocode 1. Actions on structures. General actions. Actions on structures exposed to fire," 2002.

[20] A. H. Buchanan, *Structural Design for Fire Safety*. John Wiley & Sons, Ltd, 2001.

[21] B. R. Kirby, "Recent developments and applications in structural fire engineering designA review," *Fire Safety Journal*, vol. 11, pp. 141–179, dec 1986.

[22] CEN, "EN 1993-1-2:2005 - Eurocode 3. Design of steel structures. General rules. Structural fire design," 2005.

[23] F. Incropera, D. DeWitt, T. Bergman, and A. Lavine, *Fundamentals of Heat and Mass Transfer*. John Wiley & Sons, Ltd, 2007.

[24] J. O. Hallquist, *LS-DYNA theory manual.* Livermore Software Technology Corporation, 2006.

[25] CEN, "EN 1993-1-1:2005 - Eurocode 3. Design of steel structures. General rules and rules for buildings," 2005.

[26] M. M. S. Dwaikat and V. K. R. Kodur, "A performance based methodology for fire design of restrained steel beams," *Journal of Constructional Steel Research*, vol. 67, pp. 510–524, mar 2011.

[27] M. E. Garlock and S. E. Quiel, "Plastic Axial Load and Moment Interaction Curves for Fire-Exposed Steel Sections with Thermal Gradients," *Journal of Structural Engineering*, vol. 134, pp. 874–880, jun 2008.

Chapter 7

Structural Analyses of Initiation of Collapse Mechanisms of Generic Multi-Storey Steel Frames subjected to Travelling Fires

Summary

In recent years, there have been several fire accidents, e.g. the Plasco building fire in Tehran (2017), which led to either partial or complete collapse of the structures. To ensure that fire induced collapse of a building is prevented, it is important to understand the robustness and initiation of collapse of structures subjected to fire. In this chapter, the initiation of collapse mechanisms of generic multi-storey steel frames subjected to vertical and horizontal travelling fires (i.e. cases presented in Chapters 4-6) are analysed computationally by tracking the formation of plastic hinges in the frame and generation of fire induced loads. Both uniform and travelling fires are considered. For the particular frame examined with a simple and generic structural arrangement and higher applied fire protection to the columns, the results indicate that collapse mechanisms for singe floor and multiple floor fires can be each split into two main groups. For single floor fires (fires taking place in the upper floors of the frame), collapse is initiated by the pull-in of external columns when heated beams in end bays go into catenary action. For single floor fires occurring on the lower floors, failure is initiated (i.e. ultimate strain of the material is exceeded) after the local beam collapse. Failure in both groups is governed by the generation of high loads due to restrained thermal expansion and the loss of material strength. For multiple floor fires with a low number of fire floors (1 to 3), failure is dominated by the loss of material strength and collapse is mainly initiated by the pull-in of external columns. For the cases with larger number of fire floors (5 to 10), failure is dominated by thermal expansion and collapse is mainly initiated by swaying of the frame to the side of fire origin. The results illustrate that for the investigated frame initiation of collapse mechanisms are affected by the fire type, the number of fire floors, and the location of the fire floor. The findings of this study could be of use to designers of buildings when developing fire protection strategies or when assessing the initiation of

collapse for steel framed buildings under single floor or multiple floor fires.

7.1   Introduction

In recent years, there have been several large fire accidents which led to either partial or complete collapse of the structures. They include, for example, the WTC Tower 1, 2, & 7 fires in New York (2001), Windsor Tower fire in Madrid (2005), Faculty of Architecture building fire at TU Delft in Netherlands (2008), and the Plasco building fire in Tehran (2017). To ensure that such accidents are prevented, it is important to understand the robustness and initiation of collapse of structures subjected to fire.

Many studies have been conducted recently to gain a better understanding of mechanisms of collapse of structures subjected to fire [1–14] and the effectives of various bracing systems in preventing the collapse [15, 16]. When structural steel members are heated, they expand and experience large deformations. This thermal expansion is typically restrained by the adjacent cooler structure and differential relative expansion resulting in generation of high axial forces and bending moments within the heated members. Additional axial forces are small, if, for example, all the columns on the same floor are heated, because there is no differential relative elongation between these columns [1]. Heated and expanding structural members result in the generation and shedding of additional loading to the adjacent structure as well. In BRE tests [2, 3] and computational analysis of 2D steel frames [2, 4], the results showed generation of large bending moments in the columns, which were pushed by expanding connected beams. These additional forces generated in a structure due to a fire can result in a local failure of a structural member initiating partial or complete global collapse.

Research on various steel framed structures [2, 5, 6] in which columns were left unprotected or had the same level of protection as beams have indicated columns to be the critical members. In these studies collapse was initiated by the buckling of columns. In the cases where columns were assumed to be protected and have a higher level of protection than beams, failure was governed by large beam deflections [5] and pull-in of external columns [7, 8]. After local beam or column failure, the loads are redistributed to adjacent cooler and stiffer structure. Generally, in research studies [7, 9] global collapse was found to occur due to the inability of structure to shed/transfer the load after local failure.

Flint et al., Lange et al., and Kotsovinos and Usmani [7, 10, 11] have identified and studied two main types of collapse mechanisms, i.e. weak-floor and strong-floor, of tall structures with long-span composite truss system. The weak-floor and strong-floor collapse mechanisms were identified as the initiation of collapse due to the buckling of the floor below the fire floors and due to the plastic collapse and formation of three hinges, respectively. Ali et al [12] identified two collapse modes of single-storey steel frames depending on the location of fire. In the first mode, the frame collapsed inward

due to the catenary action in beams, while in the second mode, when the fire was located close to the edge column, the frame collapsed outward due to the loss of strength of columns. In the second mode, extent of heated portion of the beam was not sufficient to cause catenary force [12]. In 2015, Porcari et al [8] carried out an extensive literature review on the progressive collapse of steel structures subjected to fire and devised two extreme possible structural response scenarios of unprotected steel structures. The two scenarios were related to the slenderness of the structural members, load ratio, presence of the lateral bracing, and weak-floor and strong-floor collapse mechanisms identified in [7, 10, 11].

Collapse mechanisms of buildings subjected to travelling fires have only been studied by Kotsovinos and Usmani [11] for tall structures with long span composite truss system. In this chapter, initiation of collapse mechanisms of a different structure, i.e. generic multi-storey steel frame, subjected to vertical and horizontal travelling fires (i.e. cases presented in Chapters 4-6) are analysed. Location of the single fire floor in the frame and number of simultaneously heated fire floors are varied.

7.2 Cases Considered

The cases considered include single floor and multiple floor uniform (ISO, SFPE, and EC LC) and travelling fire scenarios (2.5%, 10%, 25%, and 48% TFM) for which failure occurred during the fire exposure as reported in Chapters 5 & 6. ISO, SFPE, EC LC, and TFM correspond to a standard fire, constant uniform temperature of 1200C from the SFPE standard, Eurocode long-cool fire, and travelling fire as in Chapters 4 - 6. In total 58 different cases are summarised and overviewed (see Table 7.1). Initiation of failure and collapse is analysed by tracking the formation of plastic hinges in the frame, and generation of axial forces and bending moments in different structural members (analysed in Chapters 4 and 6). In this chapter, failure refers to the local element failure when ultimate strain of the material is exceeded, while 'collapse' refers to the initiation of the global failure of the frame. For both single floor and simultaneous multiple floors fires, different cases are grouped and presented based on the similarities in the initiation of collapse mechanism. This study only analyses the initiation of collapse in the terms of global structural response. That is, as identified in Chapters 4 - 6, local phenomena such as connection failure or local buckling of flanges or web of structural members are not included in the model and, therefore, not considered in the analyses, although they may govern during the progression of collapse.

It should be noted that it is recognised that a number of fully developed fire scenarios involving multiple floors simultaneously are assessed in this work which is not common design practice due to the intent of the requirements in fire safety regulation, other fire safety measures generally provided in buildings, the time required for vertical fire spread and fire to develop within a particular floor plate. It is not implied that all buildings need

to be assessed under any or all these scenarios (noting that for tall buildings a multiple floor fire has been considered for additional robustness by some designers). However, for the purposes of this work, despite some of these scenarios being potentially academic in nature, they have been considered in order to establish the trends in fire induced collapse mechanisms.

Table 7.1: Details of the fire scenarios considered in the study.

| Fire type	Single floor fires (Chapters 4 & 5): fire floors (#)	Simultaneous multiple floor fires (Chapter 6): number of fire floors
ISO	#0, #1, #2, #3, #4, #5, #6, #7, #8, #9	2, 3, 5, 7, 9, 10
SFPE	#0, #1, #2, #3, #4, #5, #6, #7, #8, #9	-
EC LC	#6, #7	-
2.5% TFM	#5, #6, #7, #8	2, 3, 5, 7, 9
10% TFM	#6, #7, #8	2, 3, 5, 7, 9, 10
25% TFM	#7, #8	2, 3, 5, 7, 9, 10
48% TFM	-	5, 7, 9, 10

7.3 Results

7.3.1 Single floor fires
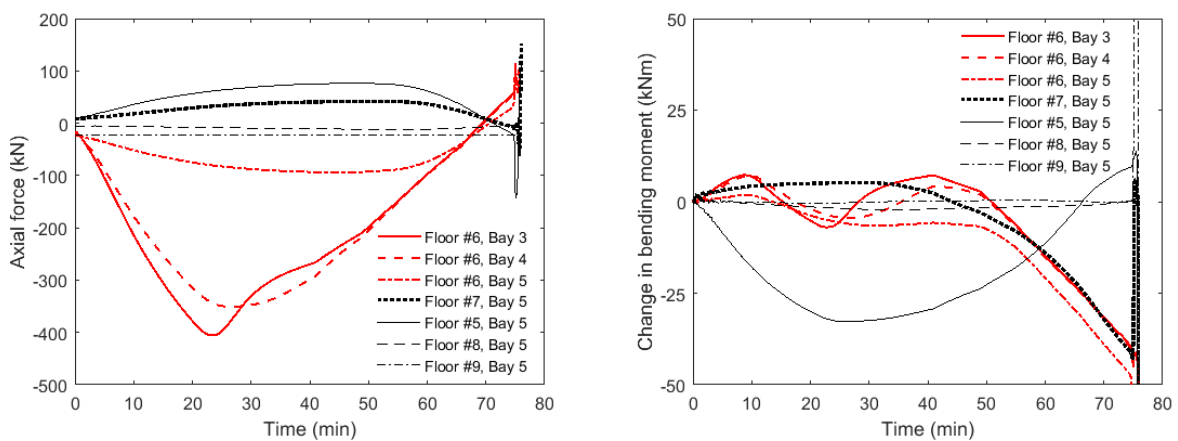
Uniform fires, Floors #6-#9

The illustration of the deflected shape, generation of plastic hinges and change in bending moments with time for a steel frame exposed to ISO fire on Floor #6 are shown in Figs. 7.1 and 7.2. As identified in Chapter 5, frame even at ambient temperature is under a high level of utilization, particularly the beams. At ambient temperature, beams in Bays 1 & 5 and upper floors of the frame experience the highest bending moments (by 5 kNm higher in Floor #7 than in Floor #6). Therefore, as the heated beams begin to expand and generate additional axial forces due to restrained thermal expansion in the heated floors and floors above and below the fire (see Chapter 4), yielding first takes place in the unheated beams on Floor #7 at 11 min. Then, beam in Bay 3 yields due to the development of large axial forces and bending moments because of high axial restraint from the surrounding structure. It is followed by yielding of beams in Bays 2 & 4, and Bays 1 & 5.

Loads generated during the fire are redistributed to the adjacent cool structure. This results into the generation of high bending moments and thus yielding of the unheated end beams in Floor #5. A significant reduction in the bending moments in Floor #6 and increase in Floor #5 after all the beams on the heated Floor #6 have yielded can be observed in Fig. 7.2. Following this, initiation of collapse begins, when the subjected

to fire beams in Bay 5 experience catenary action and pull-in the external columns. As the catenary action begins (i.e. tensile forces are generated), the loads are shed to the beams directly below and above the fire floor, which then yield. The results indicate the beginning of the plastic collapse mechanism when all the beams in Bay 5 above the fire floor have yielded, i.e. the structure is no longer able to redistribute the load. This is followed by the ultimate strain failure in subjected to fire Floor #6 Bay 5. Similar collapse and failure mechanism was observed for the cases where the frame has been subjected to ISO and SFPE fire on Floors #6 - #9 and Eurocode LC fire on Floors #6 and #7.
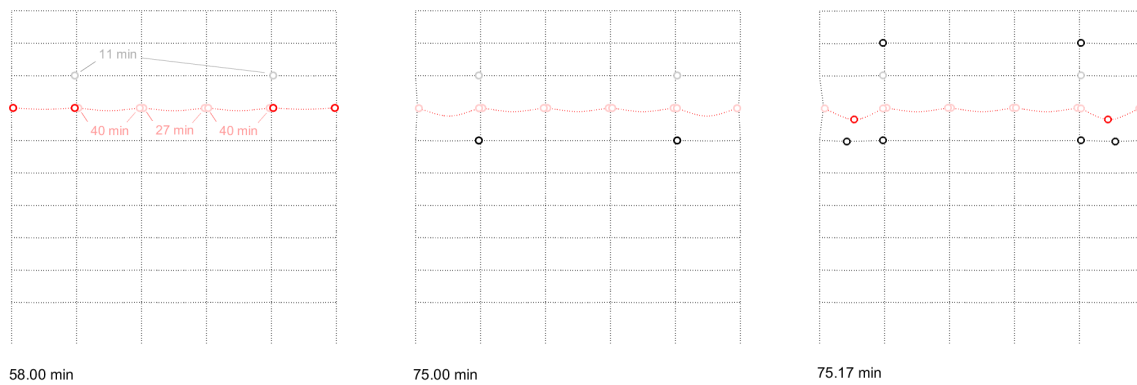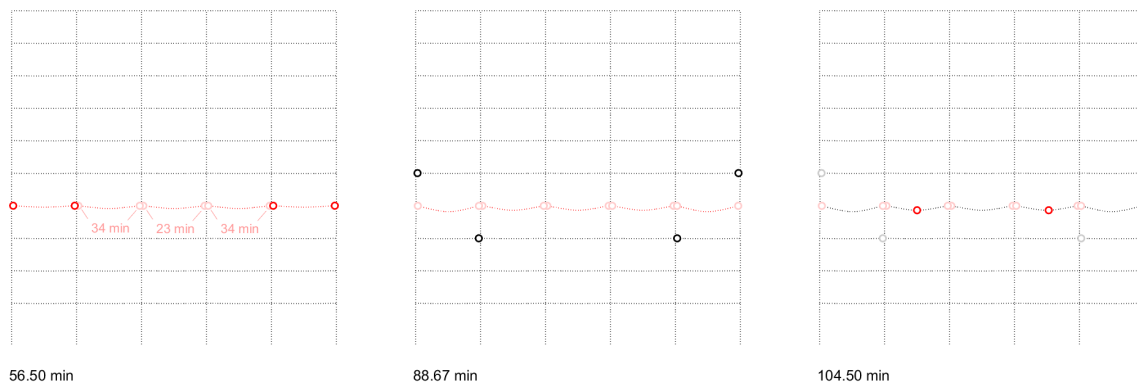

Figure 7.1: Deflected shape of the frame and formation of yielding points and plastic hinges (circles) at different times of fire exposure for a steel frame subjected to ISO fire on Floor #6. Red colour indicates the floor subjected to fire.
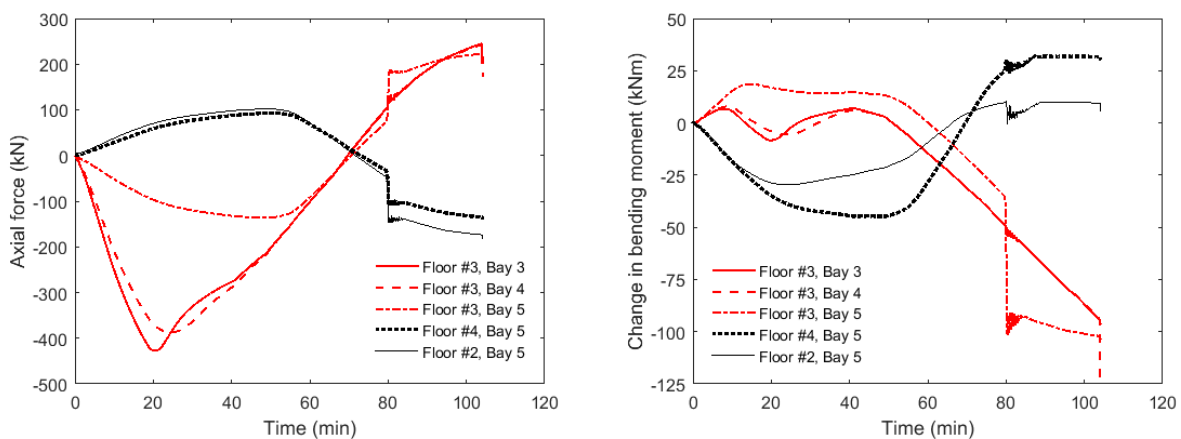

Figure 7.2: Generation of bending moments near connections and axial forces with time for selected beams in the frame subjected to ISO fire on Floor #6. Red colour indicates the floor subjected to fire.

Uniform fires, Floors #0-#5

The illustration of the deflected shape, generation of plastic hinges and change in bending moments and axial forces with time for a steel frame exposed to ISO fire on Floor #3 are shown in Fig. 7.3 and 7.4. Similar to ISO fire occurring on Floor #6, the subjected to fire beams in Bay 3 yield first, followed by Bays 2 & 4, and Bays 1 & 5 due to restrained thermal expansion generated forces. However, cool beams in the floor above the fire only yield after all the beams on the fire floor have yielded, unlike for the cases discussed in the previous section. This is because, bending moments in beams on Floor #4 are lower than on Floor #8 at ambient temperature and additional forces generated at the beginning of fire exposure are not sufficient to cause yielding before the heated beams yield. In this case, fire floor is adjacent to stiffer columns than on the upper floors. These columns are stronger and, therefore, able to resist pull-in and redistribute the load when beams go into catenary action. As a result, collapse is initiated later than for a

Figure 7.3: Deflected shape of the frame and formation of yielding points and plastic hinges (circles) at different times of fire exposure for a steel frame subjected to ISO fire on Floor #3. Red colour indicates the floor subjected to fire.
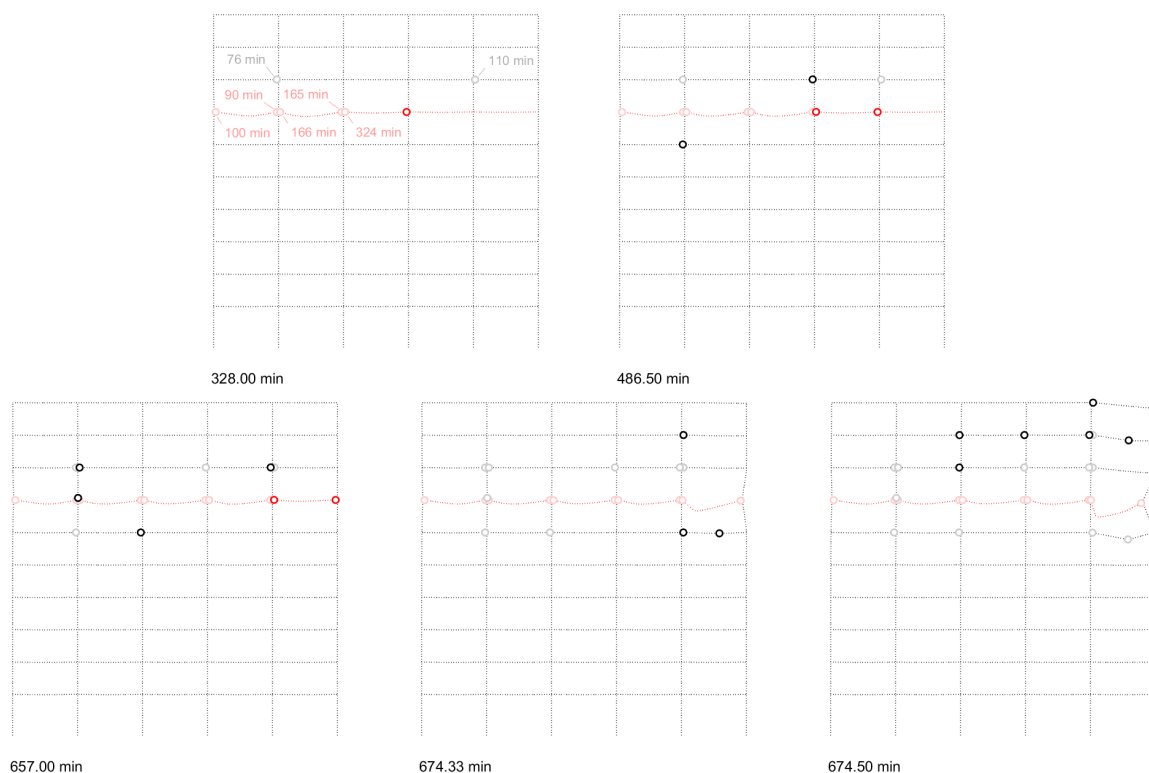

Figure 7.4: Generation of bending moments near connections and axial forces with time for selected beams in the frame subjected to ISO fire on Floor #3. Red colour indicates the floor subjected to fire.

fire on Floor #6 and it is caused by the formation of beam collapse mechanism in the internal subjected to fire Bays #2 and #4. Similar collapse mechanism was observed for the cases where the frame has been subjected to ISO and SFPE fires on Floors #0 - #5.

*Travelling fires, Floors #5-#9*

The illustration of the deflected shape and generation of plastic hinges with time for a steel frame exposed to the 2.5% TFM fire on Floor #6 is shown in Fig. 7.5. As for the ISO fire, yielding first takes place in the cool beam in Bay 1 above the fire floor. It is followed by yielding of beams in the fire floors, as fire travels along the frame generating high loads due to restrained thermal expansion. Due to the redistribution of high loads, members above and below the fire floor yield as well. Collapse is initiated when the fire reaches the far end of the frame (i.e. Bay 5) and the beam goes into catenary action pulling in the end column C6. Fig. 7.6 shows change in bending moments within structural members adjacent to Bay 5. Results indicate that as the heated beam in Bay 5 goes into tension, additional bending moments are generated in the connecting columns, C6. These moments are redistributed to the upper floors causing yielding of unheated members, and reduced robustness of the structure. Once all the beams in Bay 5 above the fire floor yield, plastic collapse mechanism is formed and ultimate strain failure in
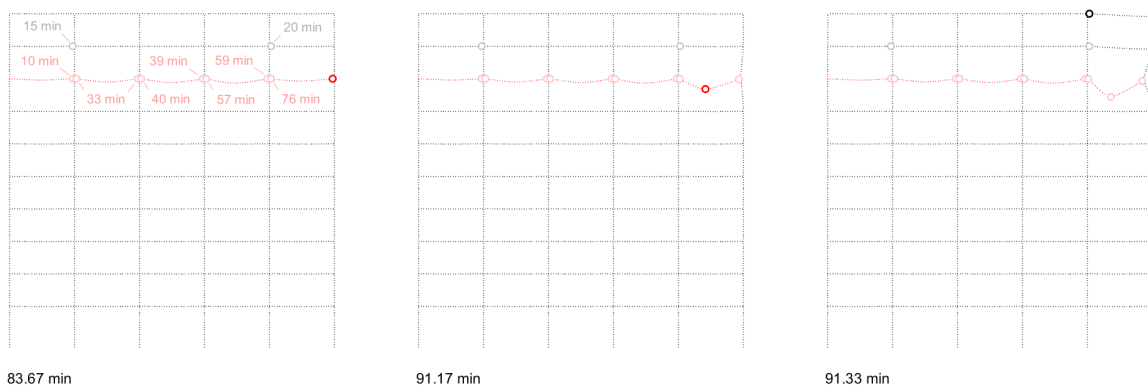

Figure 7.5: Deflected shape of the frame and formation of yielding points and plastic hinges (circles) at different times of fire exposure for a steel frame subjected to 2.5% TFM fire on Floor #6. Red colour indicates the floor subjected to fire.
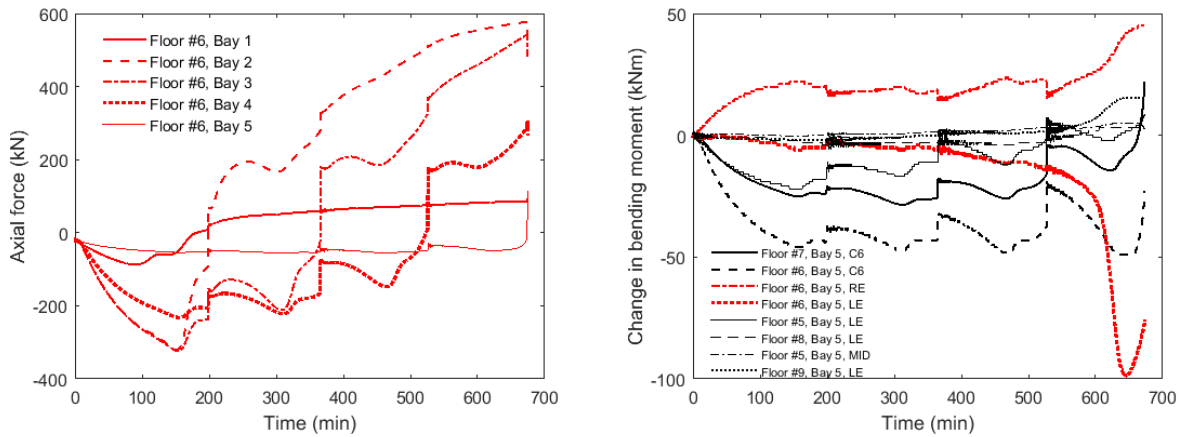
Figure 7.6: Generation of bending moments and axial forces with time for selected structural members of the frame subjected to 2.5% TFM fire on Floor #6. Red colour indicates the floor subjected to fire. C6, RE, LE, and MID refer to Column 6, and right end, left end, and middle of the beam, respectively.
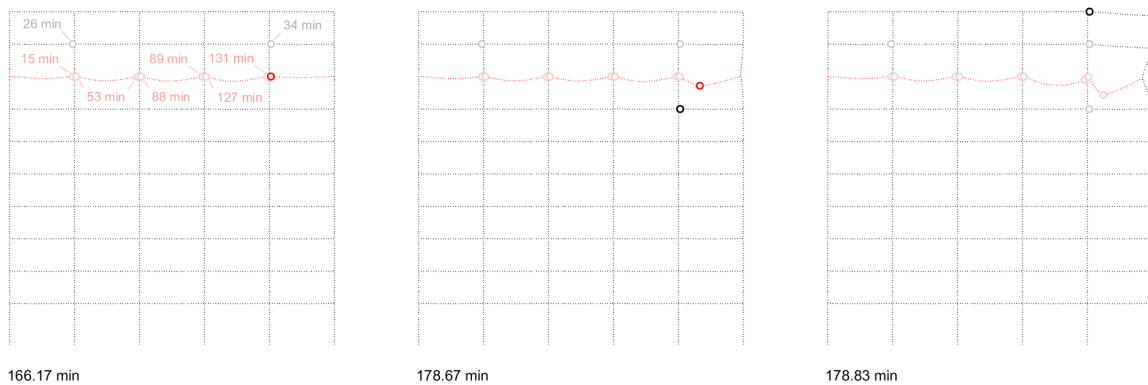
Figure 7.7: Deflected shape of the frame and formation of yielding points and plastic hinges (circles) at different times of fire exposure for a steel frame subjected to 10% TFM fire on Floor #7. Red colour indicates the floor subjected to fire.

Figure 7.8: Deflected shape of the frame and formation of yielding points and plastic hinges (circles) at different times of fire exposure for a steel frame subjected to 25% TFM fire on Floor #7. Red colour indicates the floor subjected to fire.

the heated beam in Bay 5 is reported.

A similar collapse mechanism by pull-in of column C6 and formation of plastic hinges in Bay 5 above the fire floor develops for a frame subjected to 2.5% TFM on Floors #5, #7, and #8; 10% TFM on Floors #6 - #8 (see Fig. 7.7); and 25% TFM on Floors #7 & #8 (see Fig. 7.7). However, for the 10% TFM and the 25% TFM on Floors #7 and #8 beams in the floor below the fire floor do not yield until beams in Bay 5 go into catenary action. This is because, heated beams on these floors are restrained by more slender columns (i.e. less stiff) than on the lower floors of the structure and the additional forces that develop during the fire due to restrained thermal expansion are relatively smaller. For example, axial forces are lower by up to approx. 70-100 kN (10-35%) than in the floors below. For the same reason, beam end in Bay 1 connected to column C1, does not experience yielding.

7.3.2 Multiple floor fires

Standard fire - ISO

Figures 7.9 and Fig. 7.10 illustrate the deflected shape and the generation of plastic hinges with time for a steel frame exposed to ISO fire on 2-floors and 5-floors, respectively. In this case, beams in the cool floors directly above and below the fire floors yield first. This is because axial forces and bending moments generated in these floors due to load redistribution in the fire floors are higher than in the fire floors (see Fig. 7.11). At 30 min axial forces in Floor #3 Bay 1 are higher by 26 kN (40%) than in Bay 1 of the heated Floors #4 and #5. Then, as for the single floor fires, heated beams in the internal bays yield first followed by the end bays. Additional forces that develop in internal bays due to restrained thermal expansion are higher because of the higher axial restraint from the surrounding structure and, therefore, they yield earlier. Fig. 7.11 also shows that axial forces in the lower heated floor, Floor #4, are higher than in the upper heated floor, Floor #5, causing earlier yield times in the lower floor. Collapse is initiated when subjected to fire beams in Bays 1 and 5 go into catenary action and begin to pull-in the columns C1 and C6. Due to the shedding of the load to adjacent structure beams in the upper bays yield as well and the plastic collapse mechanism is initiated. Unlike for ISO fire occurring on a single Floor #4 or #5, frame for a 2-floor fire occurring on the same floors is unable to resist the cumulative load from both fire floors and transfer to the surrounding structure.

For a frame exposed to ISO fire on 5-floors (Fig. 7.10), as for the 2-floor fire, yielding begins in the end bays (Bays 1 and 5) of cool floors directly above and below the fire floors due to high bending moments and axial forces that are generated within these floors. It is then followed by yielding of the beams on the highest (Floor #7) and lowest (Floor #3) heated floors begging at the internal bay. This is because these floors are subjected to the highest axial forces (see Chapter 6 and Fig. 7.11). The load is then redistributed and
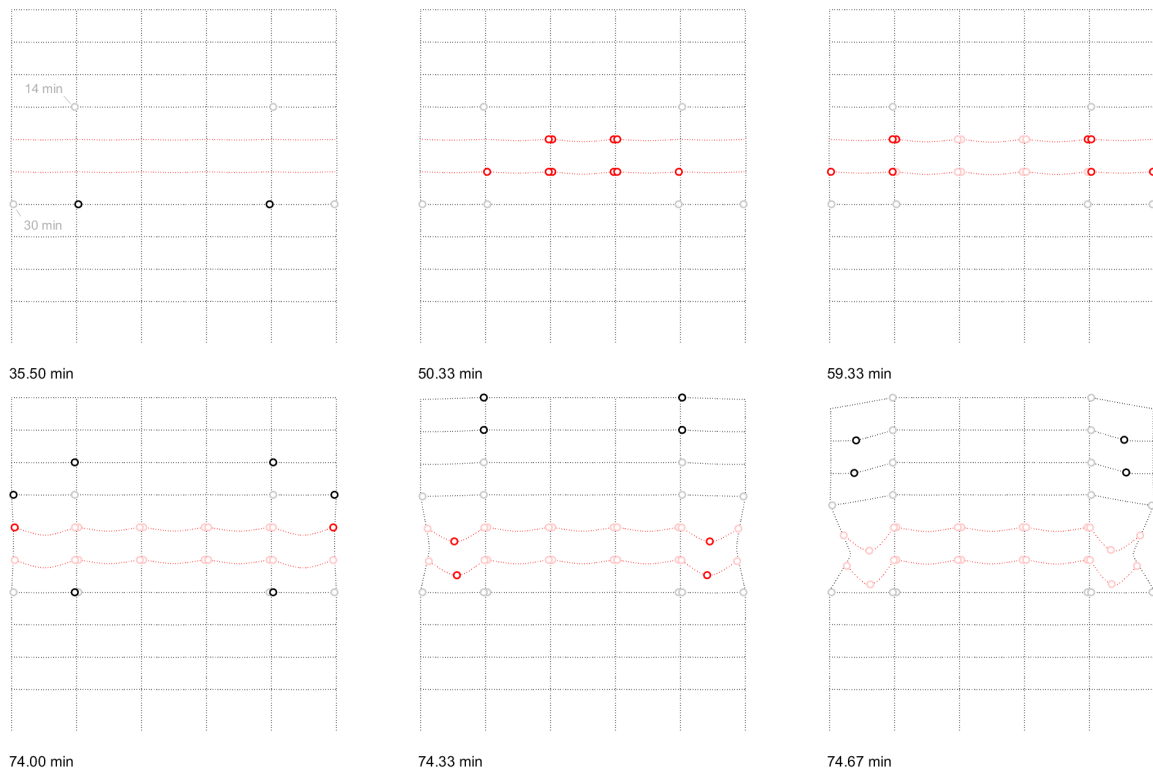
Figure 7.9: Deflected shape of the frame and formation of yielding points and plastic hinges (circles) at different times of fire exposure for a steel frame subjected to ISO fire on 2-floors simultaneously. Red colour indicates the floor subjected to fire.
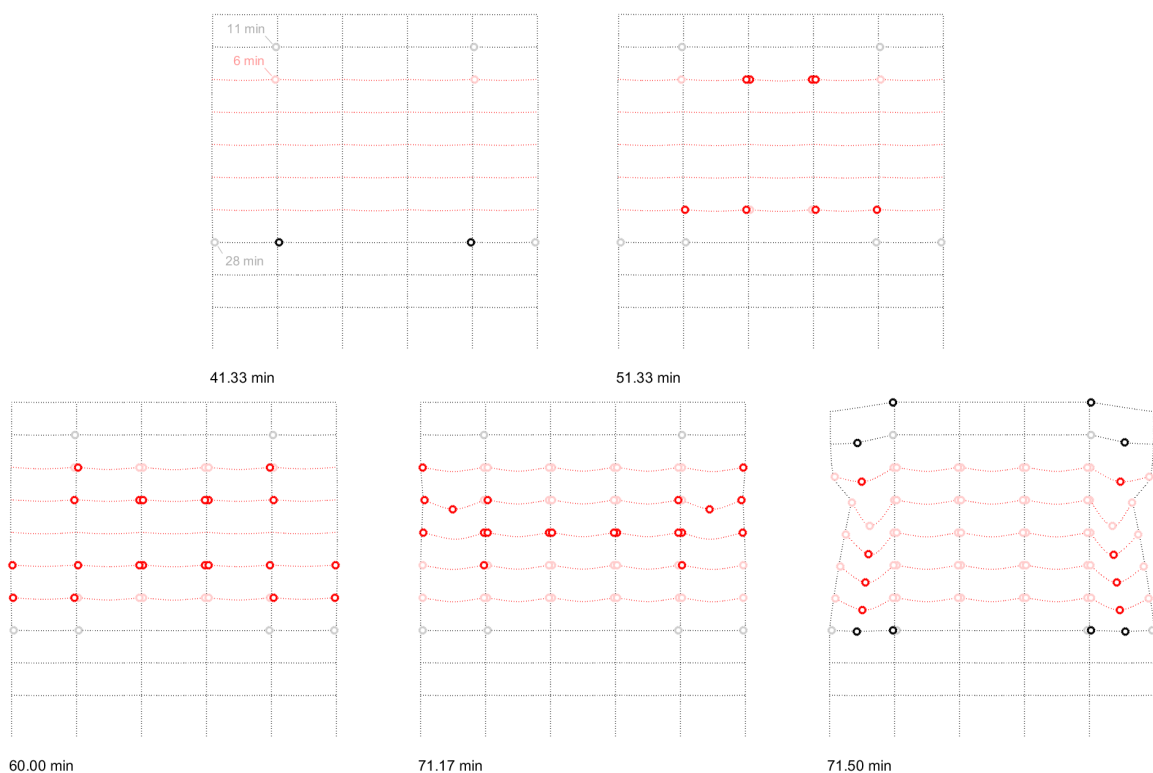
Figure 7.10: Deflected shape of the frame and formation of yielding points and plastic hinges (circles) at different times of fire exposure for a steel frame subjected to ISO fire on 5-floors simultaneously. Red colour indicates the floor subjected to fire.
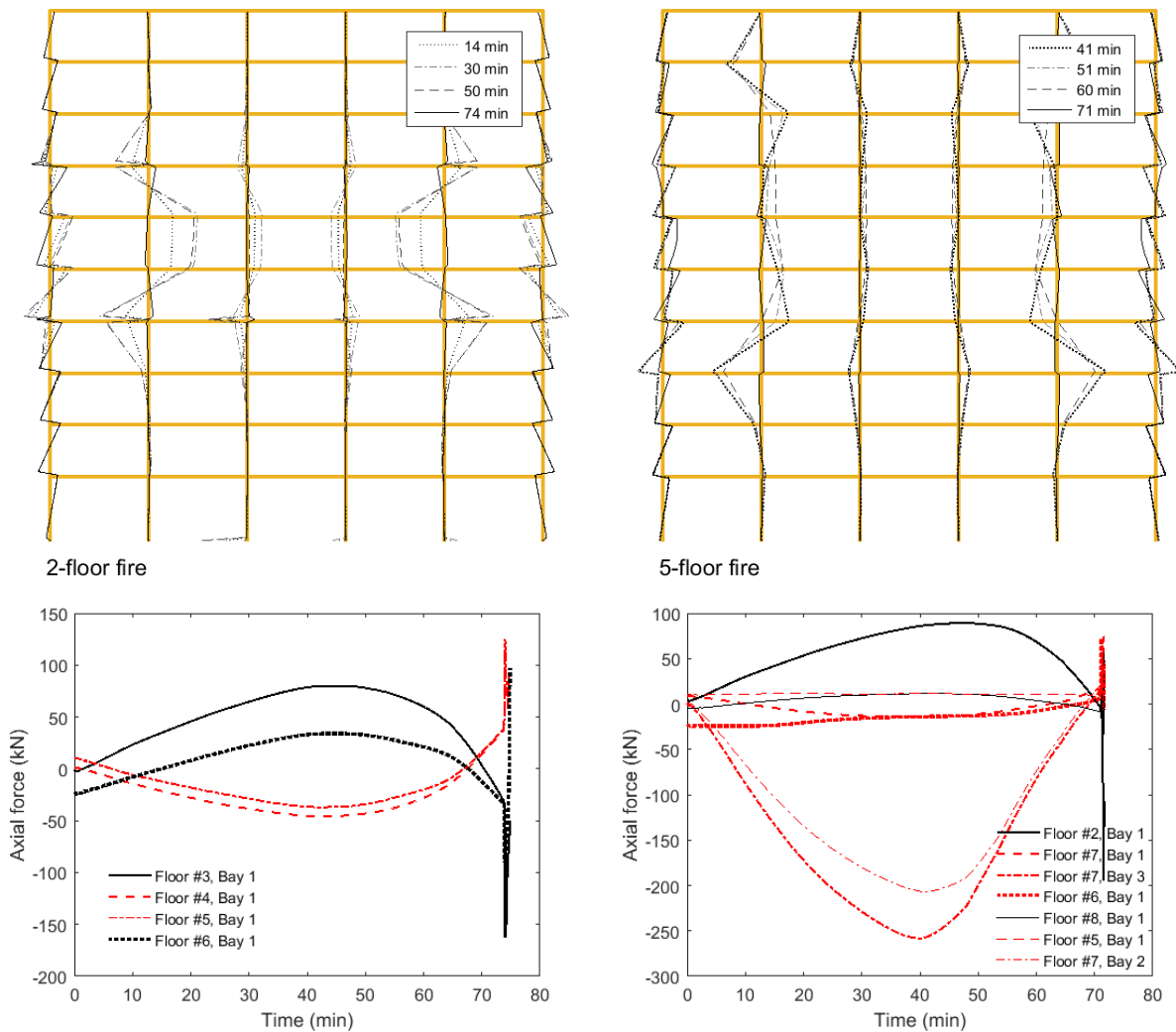
Figure 7.11: Generation of column bending moments (top) and beam axial forces (bottom) with time for selected beams in the frame subjected to ISO fire on 2-floors (left) and 5-floors(right). Red colour indicates the floor subjected to fire.

yielding takes place in intermediate fire floors (Floors #4 and #6) followed by the central fire floor (Floor #5). Collapse is initiated when heated beams go into catenary action. Due to load redistribution, cool beams in end bays of Floor #9 yield allowing for pull-in of external columns, because the frame cannot transfer the load anymore. A plastic collapse mechanism forms. Columns are pulled-in on heated Floors #6 and #7 where column section reduces in size. They have the lowest stiffness to resist the tensile forces in adjacent heated beams and, therefore, are pulled-in first. Similar collapse mechanism was observed for all the cases where the frame has been subjected to ISO fire on multiple floors.
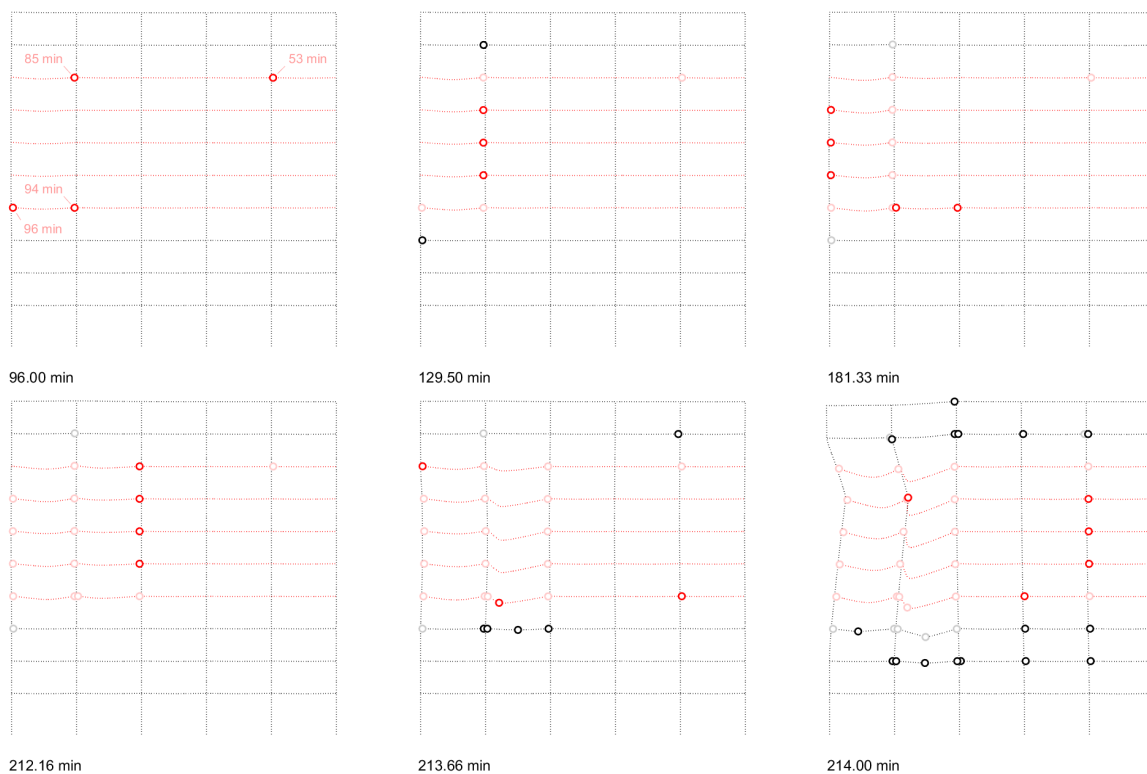
2.5% TFM

The illustration of the deflected shape and the generation of plastic hinges with time for a steel frame exposed to 2.5% TFM fire on 2-floors, 3-floors, and 5-floors simultaneously is shown in Fig. 7.12, Fig. 7.13, and Fig. 7.14, respectively. In all of the cases heated beams in Bay 1 yield first, followed by Bay 2, etc., as the fire travels along the frame. Beams in the highest and lowest subjected to fire floors yield first as they experience higher forces due to restrained thermal expansion (see. Chapter 6 and Fig. 7.15). Then, due to load redistribution, beams in the upper and lower unheated floors yield as well. Redistribution of the bending moments in the frame at different times of fire exposure for 2-floor and 5-floor fires in illustrated in Fig. 7.15. For a 2-floor fire, yielding of the heated beams in Bay 1 causes a decrease in the bending moments and axial forces in those beams and increase in the bending moments in the cool floors (e.g. Floor #8) above. Collapse is initiated when fire reaches Bay 5 and the beams located in that bay go into catenary action pulling end columns (C6) inward. Plastic collapse mechanism forms once all the beams on the floor above the heated floors in Bay 5 have yielded. An increase in the bending moment in Bay 5 Floor #9 just before the mechanism forms and the beam yields can be seen in Fig. 7.15.
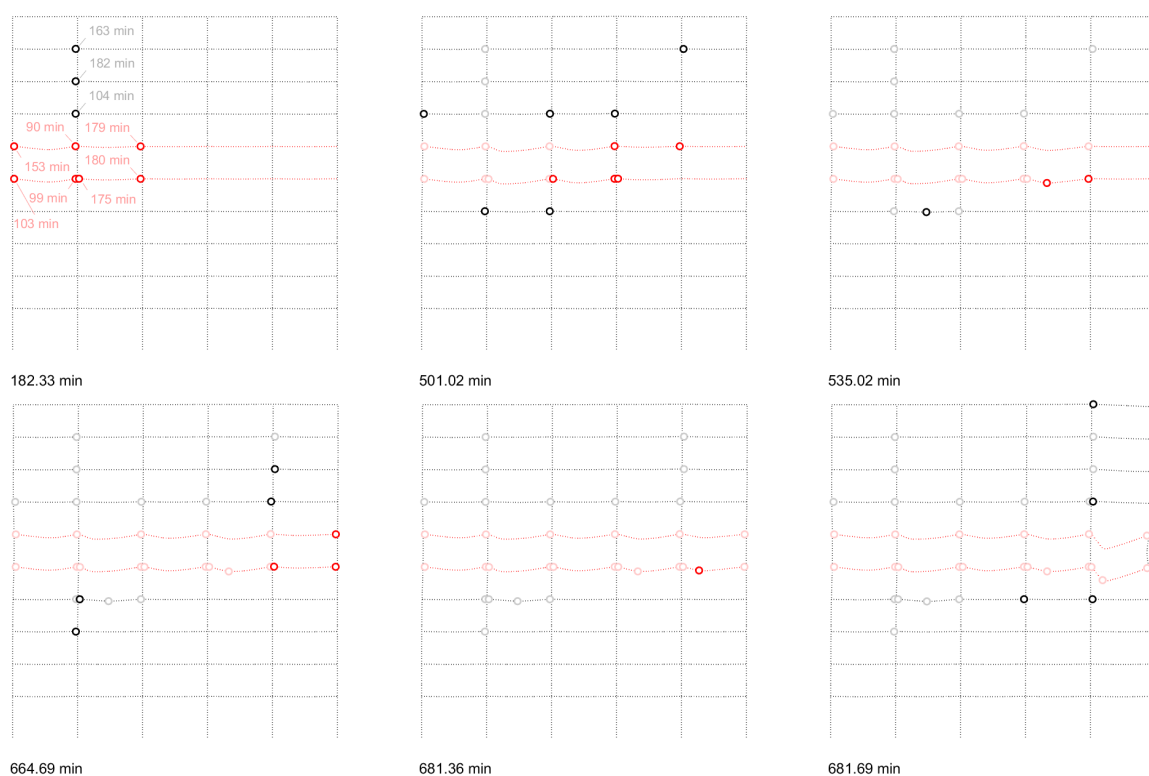
Figure 7.12: Deflected shape of the frame and formation of yielding points and plastic hinges (circles) at different times of fire exposure for a steel frame subjected to 2.5% TFM fire on 2-floors simultaneously. Red colour indicates the floor subjected to fire.
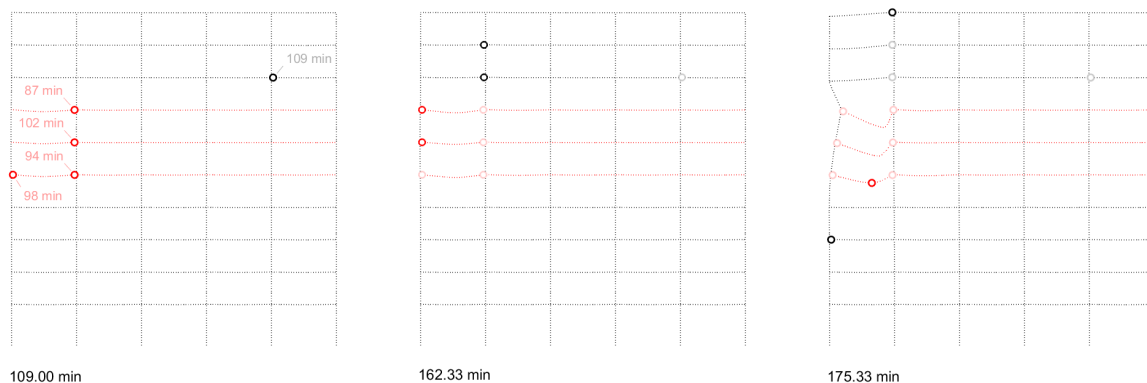
Figure 7.13: Deflected shape of the frame and formation of yielding points and plastic hinges (circles) at different times of fire exposure for a steel frame subjected to 2.5% TFM fire on 3-floors simultaneously. Red colour indicates the floor subjected to fire.

Figure 7.14: Deflected shape of the frame and formation of yielding points and plastic hinges (circles) at different times of fire exposure for a steel frame subjected to 2.5% TFM fire on 5-floors simultaneously. Red colour indicates the floor subjected to fire.

For the cases when the frame is subjected to 2.5% TFM on more than 2 floors, collapse is initiated before fire reaches Bay 2 (3-floor and 7-floor fires) or Bay 3 (5-floor and 9-floor fires). It occurs after beams in Bay 1 yield and go into catenary action. The cumulative tensile axial force on heated columns C1 and redistributed forces in the floors above are large enough to cause yielding of the cool beams and, as a result, pull in of the columns. For a 3-floor fire plastic mechanism forms after all the beams in Bay

1 in the floors above the fire floor have yielded, while for a 5-floor fire it forms when beams below and above the heated floors in Bay 2 have yielded. In the latter case, as in all the other cases, before failure, forces are redistributed through cooler and stronger members. It can be observed by the formation of the plastic hinges in the cool floors and heated beams in Bay 5, which have not reached high temperatures yet (Fig. 7.14). Loads are redistributed/shed through the mechanism similar to the cantilever. For 7-floor and 9-floor fires, initiation of collapse is similar to 3-floor and 5-floor fires, respectively.
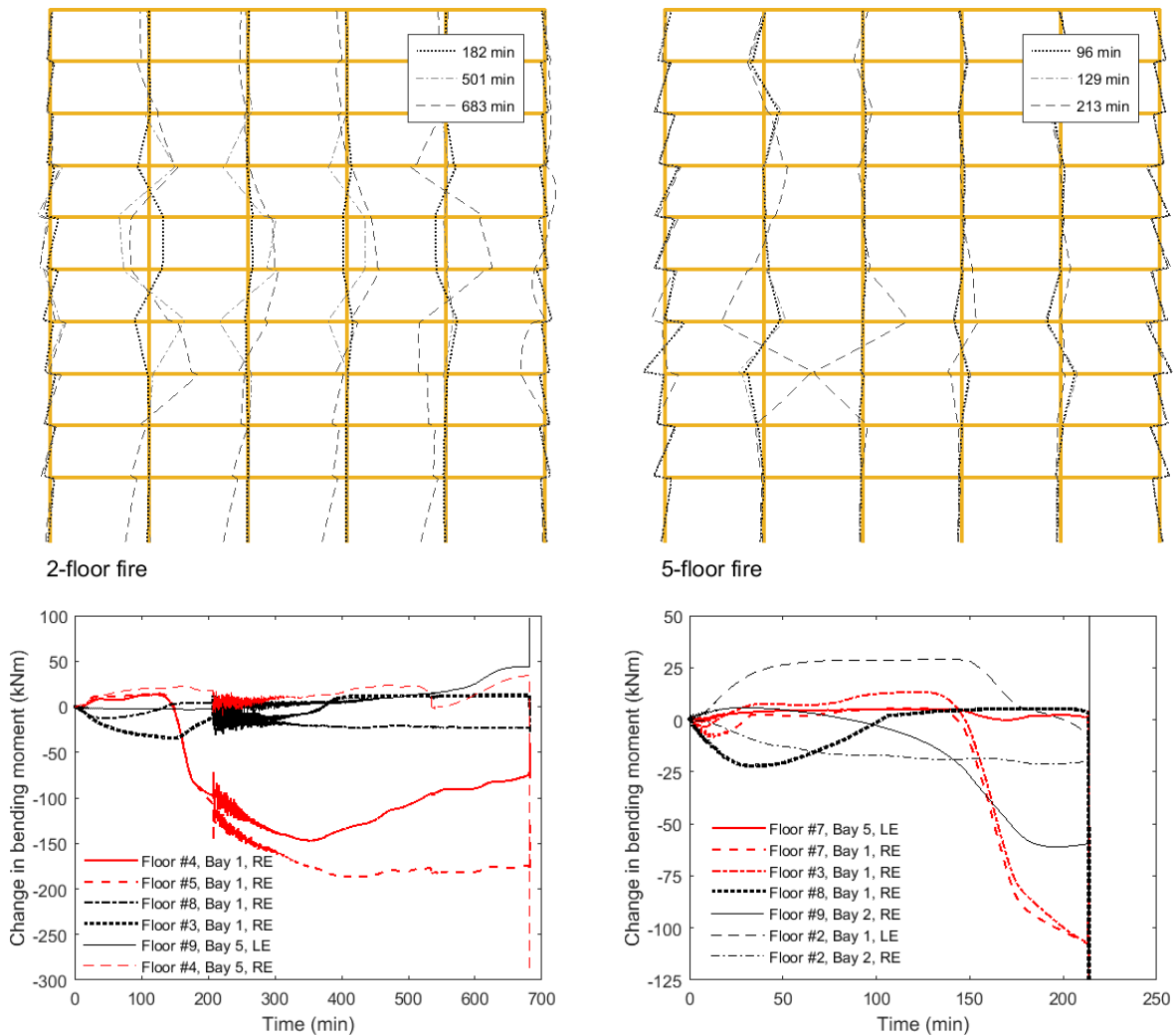
Figure 7.15: Generation of column (top) and beam (bottom) bending moments with time for selected structural members of the frame subjected to 2.5% TFM fire on 2-floors (left) and 5-floors(right). Red colour indicates the floor subjected to fire. RE and LE refer to right end, and left end of the beam, respectively.

10% TFM

The illustration of the deflected shape and the generation of plastic hinges with time for a steel frame exposed to 10%TFM fire on 3-floors, 5-floors, and 9-floors simultaneously

is shown in Fig. 7.16, Fig. 7.17, and Fig. 7.18, respectively. For 3-floor and 5-floor fires beams in Bays 1 and 2 in the lowest heated floors yield first followed by yielding of cool beams directly below or above the fire. However, initiation of collapse mechanisms for the two cases are different. For a 3-floor fire failure is initiated when fire reaches Bay 3 due to heated beam collapse whereas for a 5-floor fire failure is initiated by pull in of columns C1 and C2. In the former case, beam collapse in Bay 3 takes place after all the beams in the floors directly below and above the fire floors have yielded, tensile (catenary) axial forces have generated within the Bay 3 beams and ultimate strain failure has been reached. Redistribution of bending moments along the columns is illustrated in Fig. 7.19. Initiation of collapse for a 5-floor fire is similar to the 2.5% TFM 5-floor fire discussed in a previous section. Collapse is initiated after beam collapse mechanism forms in Bay 2 Floor #2 and all the beams above the heated floors in Bay 2 yield. This is similar to the weak-floor collapse mechanism reported in [7, 9, 10] in which collapse of the frame with long-span composite truss system occurs after buckling the cool floor directly below the fire floors.
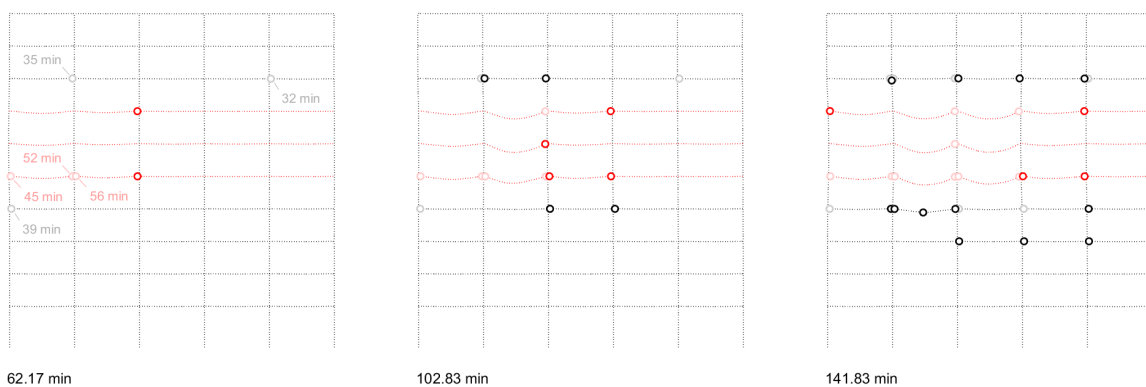
Figure 7.16: Deflected shape of the frame and formation of yielding points and plastic hinges (circles) at different times of fire exposure for a steel frame subjected to 10% TFM fire on 3-floors simultaneously. Red colour indicates the floor subjected to fire.

Figure 7.17: Deflected shape of the frame and formation of yielding points and plastic hinges (circles) at different times of fire exposure for a steel frame subjected to 10% TFM fire on 5-floors simultaneously. Red colour indicates the floor subjected to fire.

Figure 7.18: Deflected shape of the frame and formation of yielding points and plastic hinges (circles) at different times of fire exposure for a steel frame subjected to 10% TFM fire on 9-floors simultaneously. Red colour indicates the floor subjected to fire.
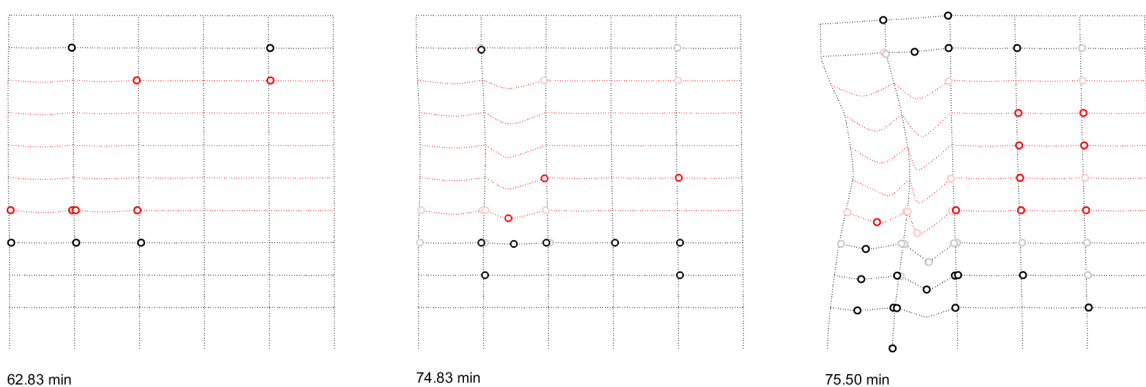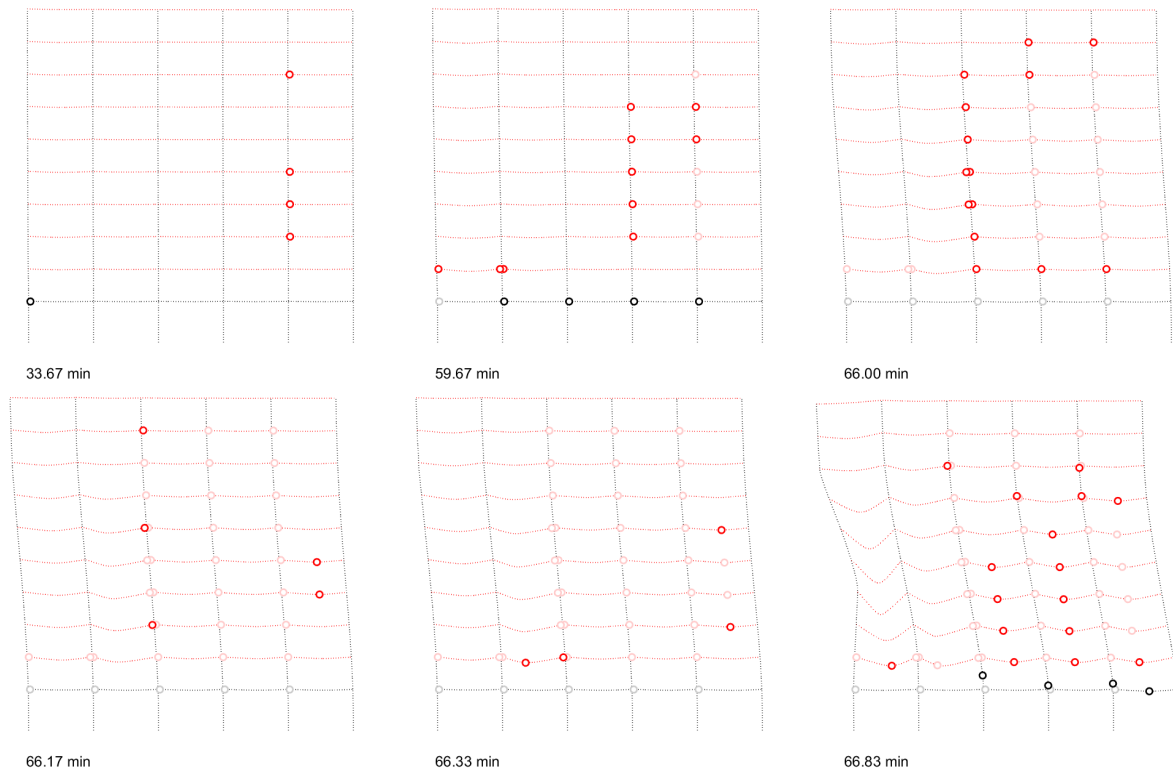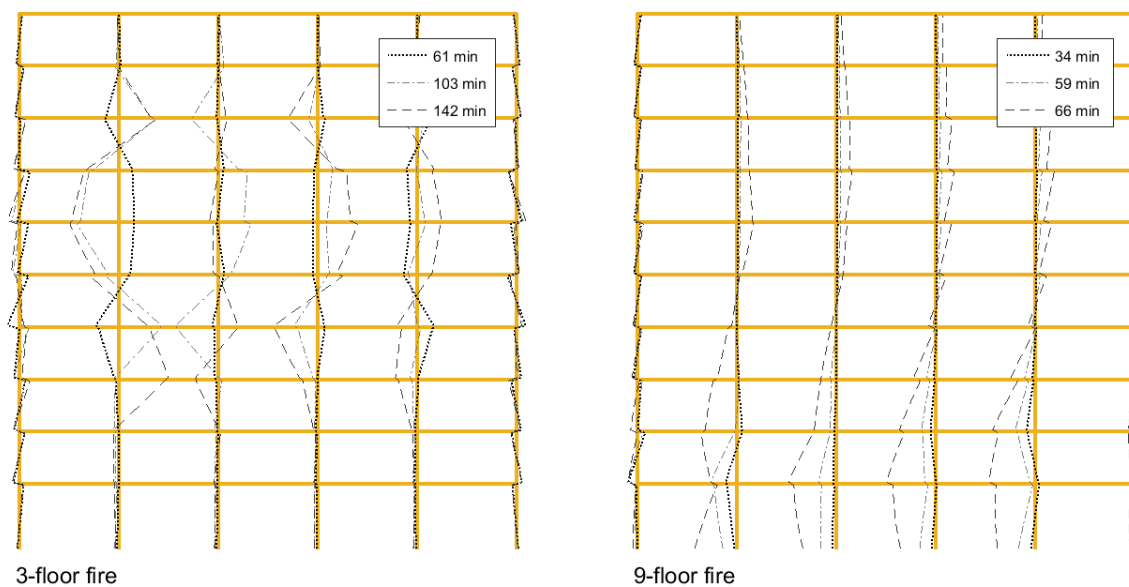

Figure 7.19: Generation of column bending moments with time of the frame subjected to 10% TFM fire on 3-floors (left) and 9-floors(right).

Unlike in the previously discussed fire scenarios, collapse mechanism for a 9-floor fire is dominated by large deformations in the frame rather than loss of material strength.

In this case, expanding beams on Floors #1 to #9 result in large cumulative lateral displacement of columns in Bays 1 and 2. In turn, additional bending moments are generated in Bays 5 followed by Bays 4 and 3 redistributing the load and maintaining stability of the frame. Yielding first occurs in the only cool floor, Floor #0, and Bay 5, where the highest forces are generated (see Chapter 6 and Fig. 7.19). Frame begins to collapse by swaying to the side of the fire origin after all most of the beams in Bays 3 to 5 and columns C3 to C5 on Floor #1 have yielded forming a plastic collapse mechanism. Frame is no longer able to transfer the load to stronger members and maintain stability. For 2-floor, 7-floor, and 10-floor fires, initiation of collapse is similar to 3-floor, 5-floor, and 9-floor fires, respectively.

25% TFM

The illustration of the deflected shape and the generation of plastic hinges with time for a steel frame exposed to 25% TFM fire on 3-floors, 5-floors, and 9-floors simultaneously is shown in Fig. 7.20, Fig. 7.21, and Fig. 7.22, respectively. As in previously discussed cases, yielding occurs first in the beams on the lowest heated floor and cool floors directly above and below the fire floors in Bay 1. This is due to the forces generated as a result of

Figure 7.20: Illustration of the deflected shape of the frame and formation of yielding points and plastic hinges (circles) at different times of fire exposure for a steel frame subjected to 25% TFM fire on 3-floors simultaneously. Red colour indicates the floor subjected to fire.
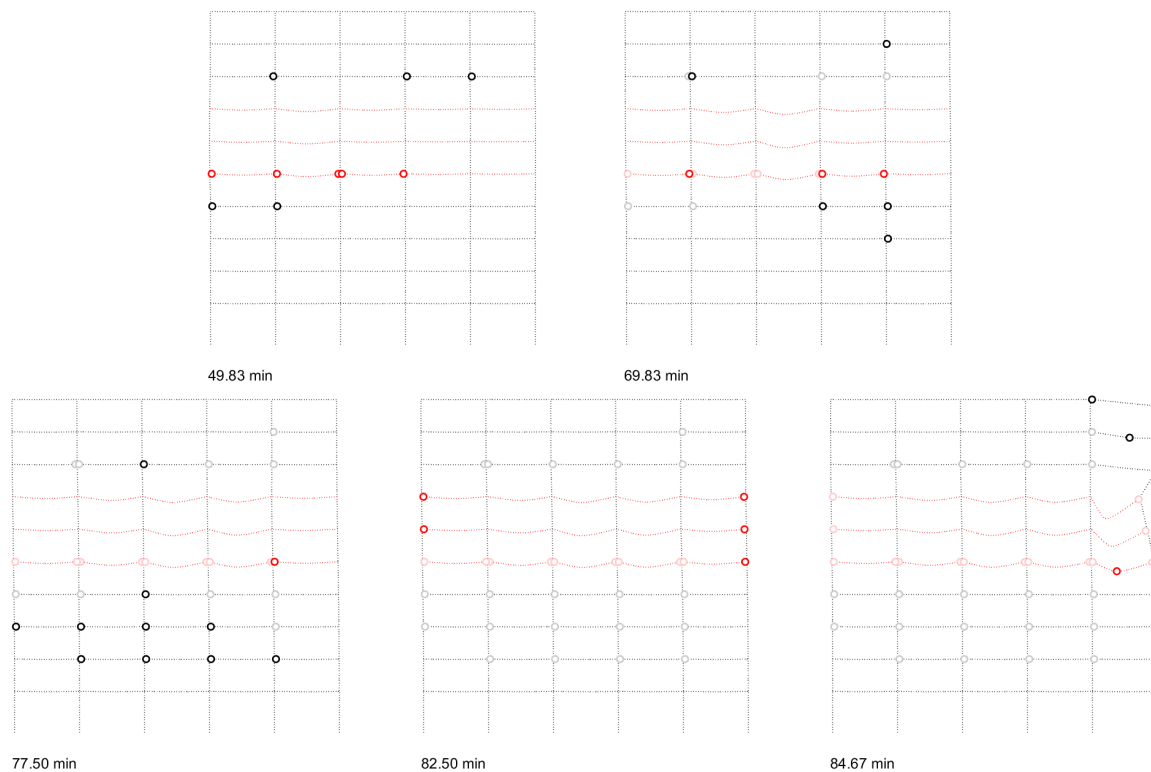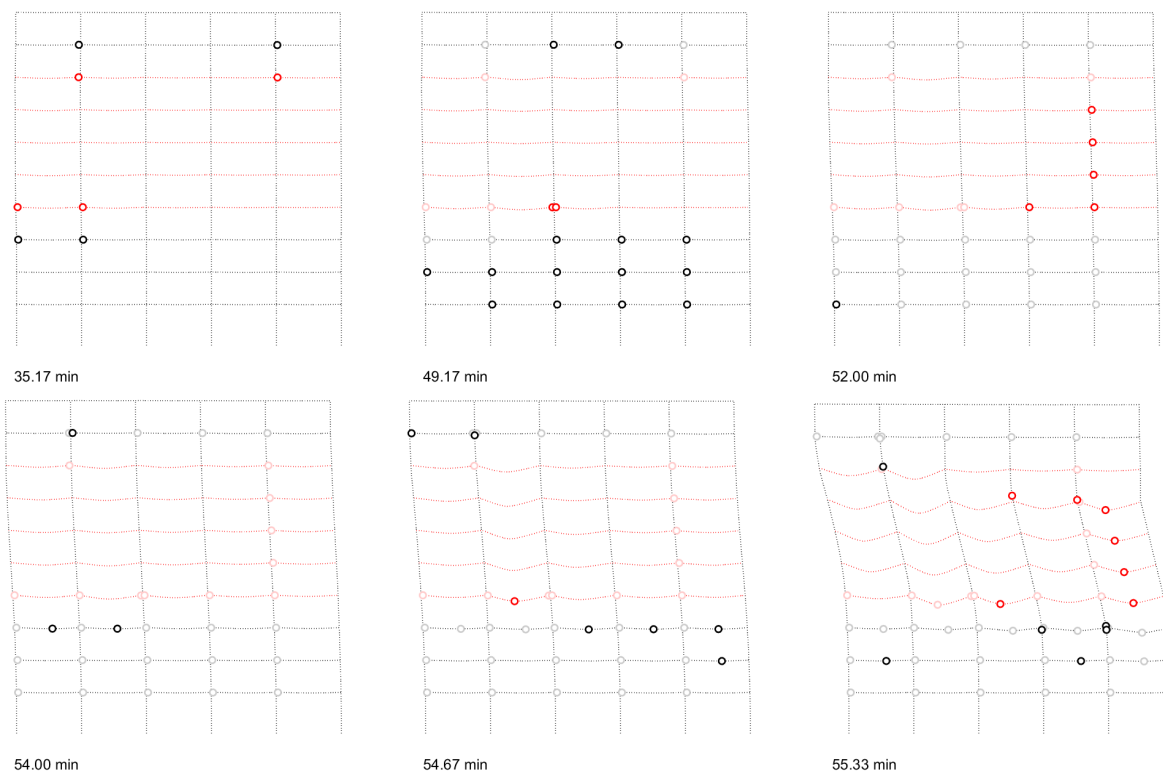
Figure 7.21: Deflected shape of the frame and formation of yielding points and plastic hinges (circles) at different times of fire exposure for a steel frame subjected to 25% TFM fire on 5-floors simultaneously. Red colour indicates the floor subjected to fire.

Figure 7.22: Deflected shape of the frame and formation of yielding points and plastic hinges (circles) at different times of fire exposure for a steel frame subjected to 25% TFM fire on 9-floors simultaneously. Red colour indicates the floor subjected to fire.

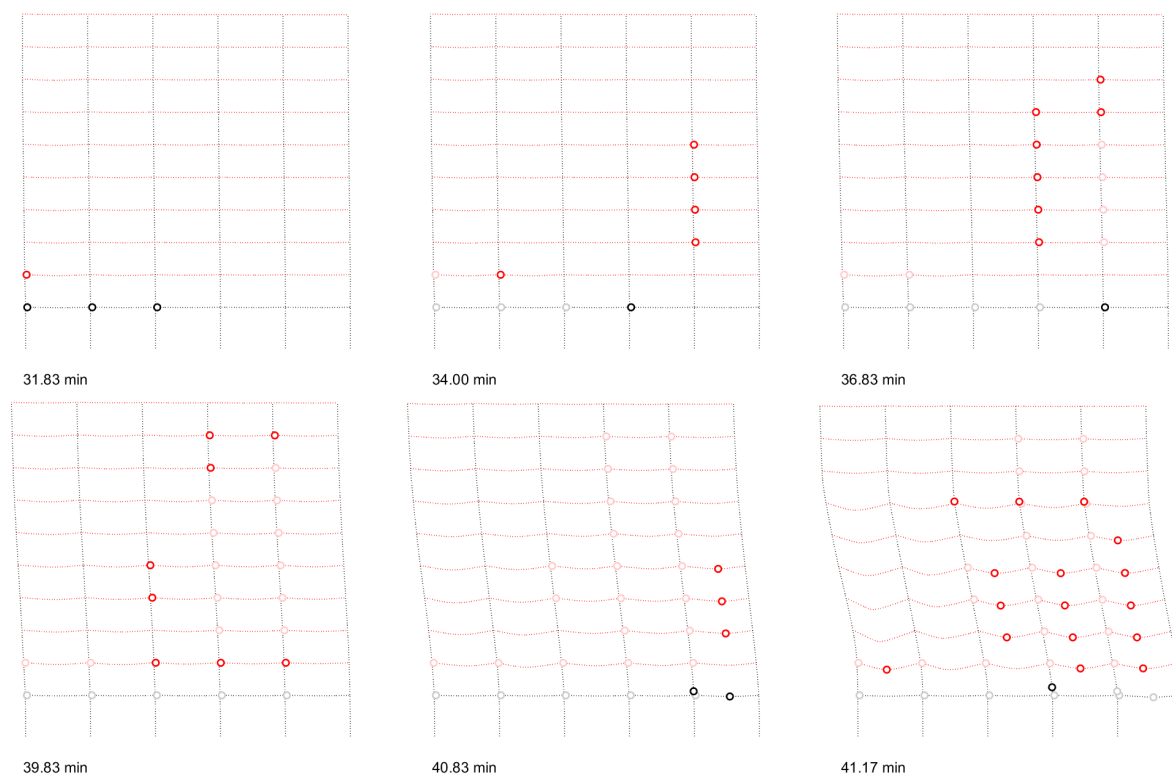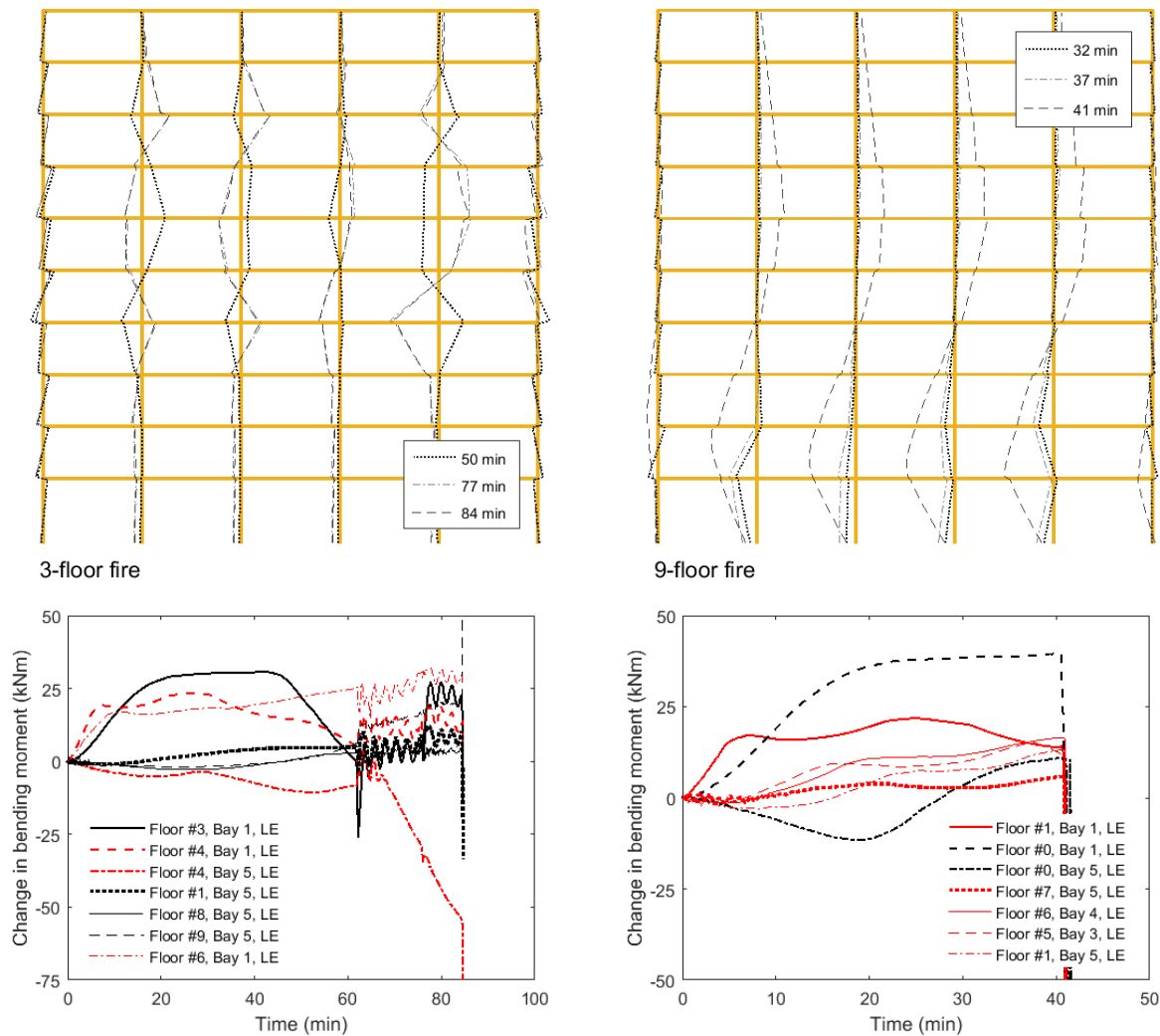**Figure 7.23**: Generation of column (top) and beam (bottom) bending moments with time for selected structural members of the frame subjected to 25% TFM fire on 3-floors (left) and 9-floors(right). Red colour indicates the floor subjected to fire. RE and LE refer to right end, and left end of the beam, respectively.

the restrained thermal expansion. For a 3-floor fire, only the beams on the lowest fire floor yield as the fire travels across the compartment. Fire generated forces are redistributed to the cool floors above and below the fire floor. The extent of the yielded unheated members below the fire floors is higher than for a frame subjected to 2.5% TFM and 10% TFM. This is mainly because collapse is initiated towards the end of fire exposure unlike in the latter cases. 25% TFM fire travels faster across the compartment. Initiation of collapse for a 3-floor fire occurs when the heated beam in Bay 5 Floor #4 goes into catenary action and beam in Bay 5 Floor #9 yields forming a plastic collapse mechanism. Redistribution in bending moments in columns and beams in illustrated in Fig. 7.23.

5-floor and 9-floor initiation of collapse mechanisms are similar. Beams on the fire affected floors expand pushing columns in Bay 1 outward. Significant cumulative column lateral displacement develops due to the heating of a large number of fire floors (more

than 3). This creates a large momentum in the frame generating additional forces in Bay 5 and causing yielding. Therefore, as for the 10% 9-floor fire failure is dominated by large deformations. For a 5-floor fire, frame is unable to maintain stability after all the beams in floors below the fire and heated beams in Bay 5 have yielded. For a 9-floor fire collapse is initiated after yielding of the unheated beams on Floor #0 and heated beams in Bays 3 to 5. It is similar to the collapse mechanism of a frame exposed to a 10% TFM on 9 floors. Fig. 7.23 shows increasing bending moments in Bay 5 to Bay 3 beams as fire spreads along the compartment and generation of high bending moments along the internal columns for a 9-floor fire as the frame begins to sway. For 2-floor,
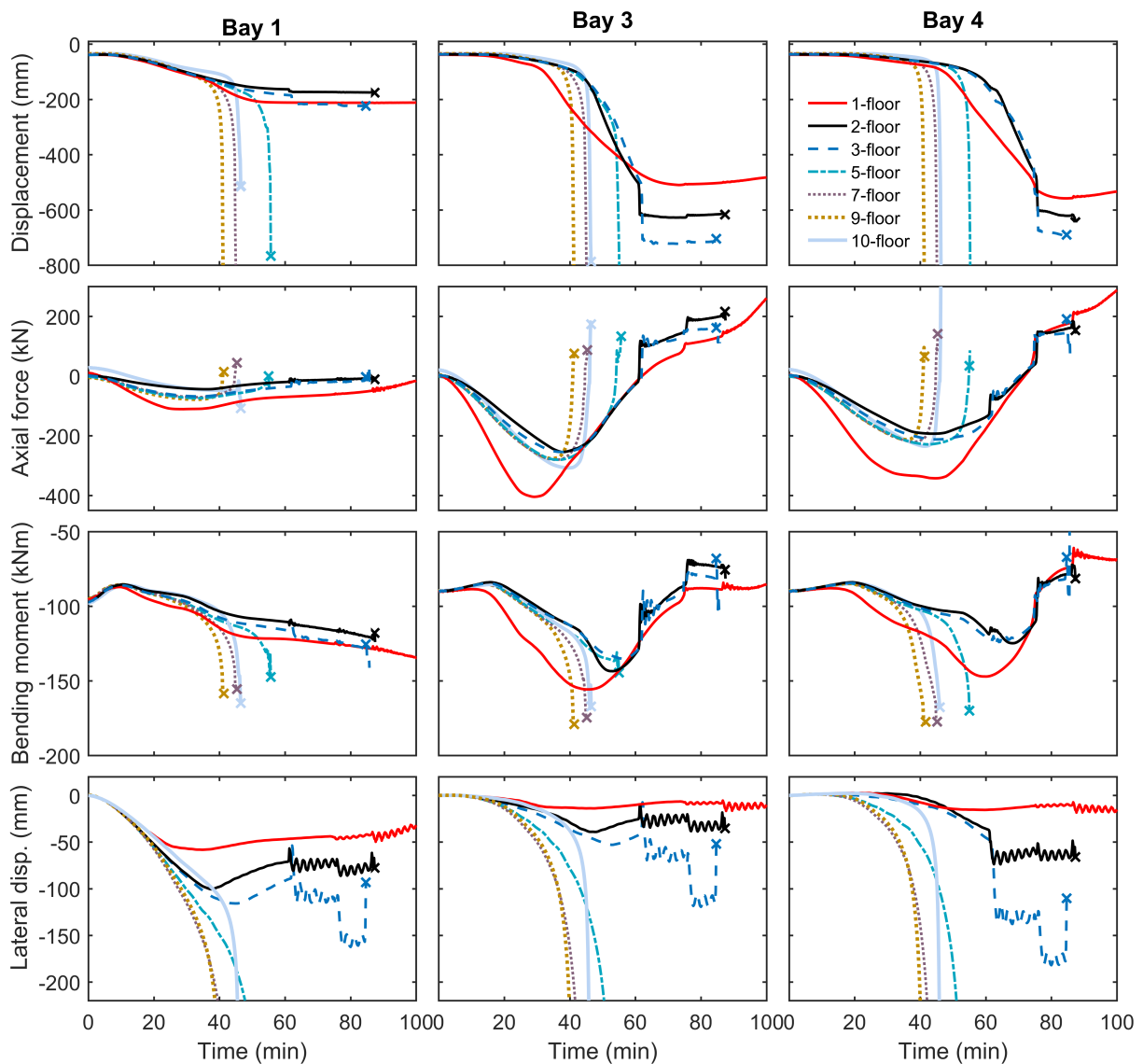

Figure 7.24: Development in time of mid-span deflections, axial forces, and bending moments at each of the beams in the lowest heated floor; and development of lateral displacements at the beam to column nodes on the left hand side of the beam for a varying number of multiple fire floors. Frame is subjected to the 25% TFM.

.

7-floor, and 10-floor fires, initiation of collapse is similar to 3-floor, 5-floor, and 9-floor fires, respectively.

Comparison of effects of the changing number of fire floors on the development of stresses and displacements is illustrated in Fig. 7.24. Results are illustrated for beams in Bay 1, Bay 3 and Bay 4 for 1-floor to 10-floor fires. The highest axial forces and bending moments within heated beams are generated when the frame is subjected to the 25% TFM on 1 floor. This is because beams are axially restrained by columns in the cool floors directly above and below the fire floor and, therefore, differential lateral elongation between beams in the adjacent floors is the largest in comparison to larger number of fire floors. Fig. 7.24 shows, as identified previously, the increasing lateral displacement of columns towards the side of fire origin and increasing bending moments with increasing number of simultaneously heated fire floors.

48% TFM

Fig. 7.25 and Fig 7.26 show the deflected shape and the generation of plastic hinges with time for a steel frame exposed to 48% TFM fire on 5-floors, and 9-floors simultaneously, respectively. The mechanism of collapse is similar to the frame exposed to 25% TFM on 5 floors and 9 floors. It occurs due to large deformations within the frame,
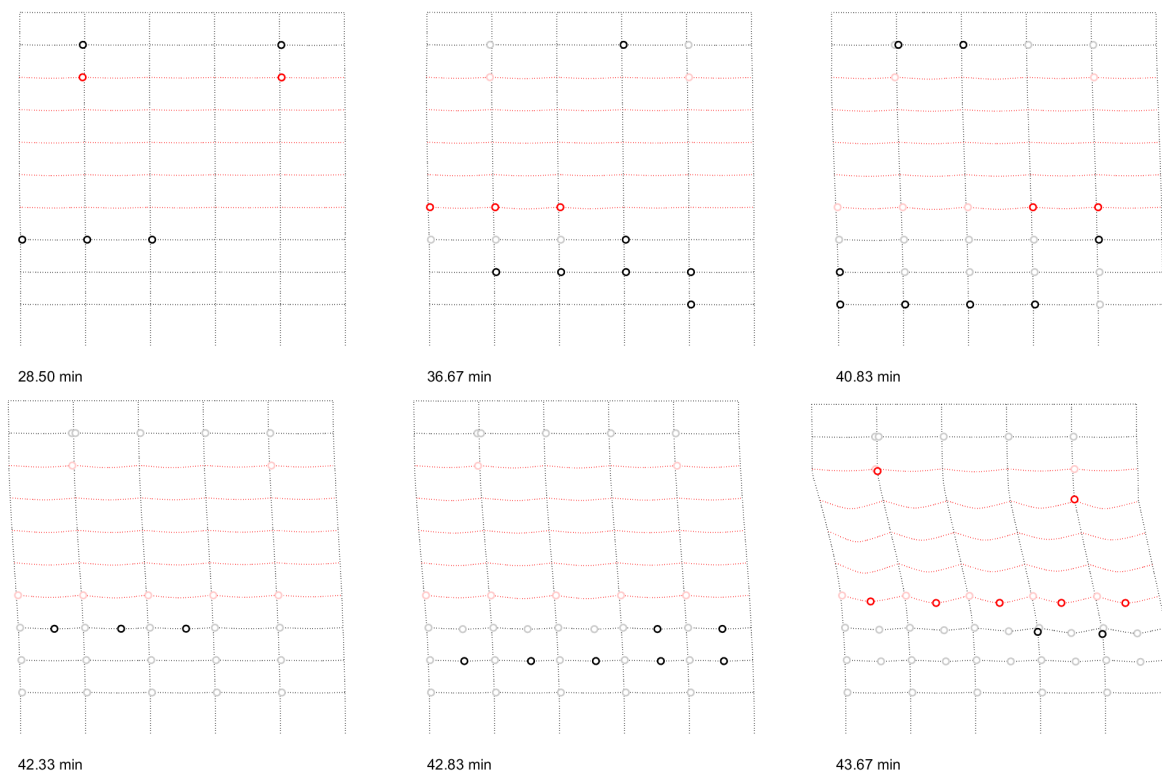
Figure 7.25: Deflected shape of the frame and formation of yielding points and plastic hinges (circles) at different times of fire exposure for a steel frame subjected to 48% TFM fire on 5-floors simultaneously. Red colour indicates the floor subjected to fire.
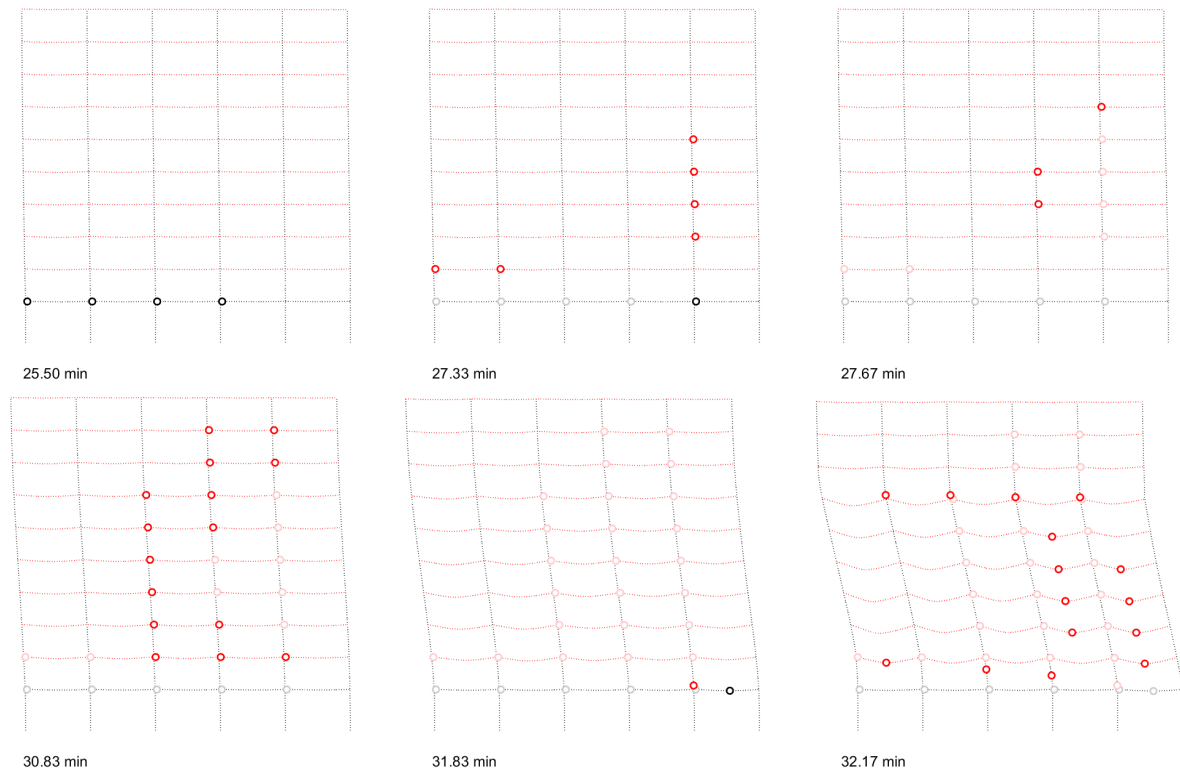
Figure 7.26: Deflected shape of the frame and formation of yielding points and plastic hinges (circles) at different times of fire exposure for a steel frame subjected to 48% TFM fire on 9-floors simultaneously. Red colour indicates the floor subjected to fire.
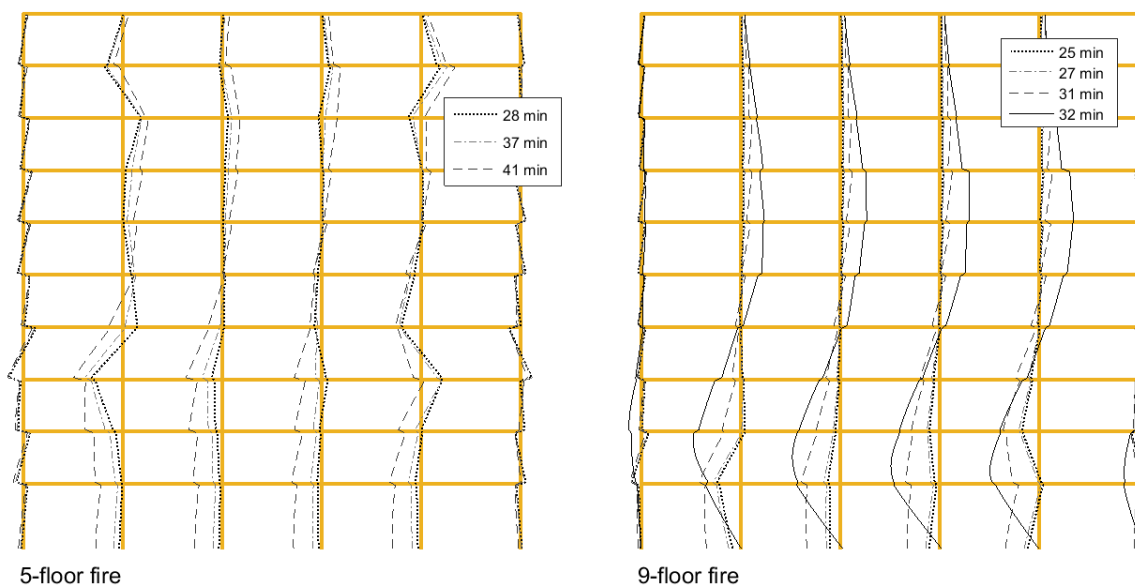
Figure 7.27: Generation of column bending moments with time of the frame subjected to 48% TFM fire on 5-floors (left) and 9-floors (right)

i.e. cumulative lateral displacements of columns, which are being pushed by expanding beams, in Bays 1 and 2. This results in the generation of large bending moments within

the frame, particularly in unheated floors Floor #0 to Floor #2 (3-floor fire) and Floor #0 (9-floor fire) before the initiation of collapse (see Fig. 7.27). Instability and failure takes place when the frame is no longer able to redistribute the forces. For a 5-floor fire stability is mainly maintained by the cool floors below the fire floors and after beams within these floors have yielded frame begins to sway. For a 9-floor fire stability is maintained and loads are redistributed through the beams and columns in Bay 5 followed by Bays 4 and 3 after the unheated beams in Floor #0 have yielded. For 7-floor, and 10-floor fires, initiation of collapse is similar to 5-floor, and 9-floor fires, respectively.

7.4 Conclusions

In this chapter, 58 different cases of a generic steel frame subjected to horizontally and vertically travelling uniform and travelling fires have been considered to investigate the initiation of collapse mechanisms. The frame examined has a simple and generic structural arrangement and higher applied fire protection to the columns compared with the beams.

In most of the analysed cases yielding first occurs in the lowest and highest fire floors and adjacent cool floors close to the connections. This is because the highest axial forces and bending moments due to the restrained thermal expansion are generated within these floors. For uniform fires, beams in the central bay yield first followed by Bays 2 & 4 and Bays 1 & 5, while for travelling fire scenarios yielding of the beams on the heated floors follows the fire spread. Buckling of the columns does not occur in any of the cases likely because they were assumed to have a higher level of protection than beams (i.e. equivalent to 120 min of standard fire exposure). Therefore, columns do not reach sufficiently high temperatures (see Chapter 4) to cause significant thermal expansion and additional axial forces, which could lead to buckling. In addition, the utilization of the columns at ambient temperature is significantly lower than the utilization of beams (by up to 40%). Thus, failure for the frame considered in this study is mainly governed by the thermally induced loads generated as a result of the restrained thermal expansion of the beams as in [5, 7, 8].

For single floor fires, initiation of collapse mechanisms could be split into two general groups depending on the location of the fire floor of the frame. In the first group, collapse is initiated by the pull-in of external columns after heated beams in Bays 1 & 5 (uniform fires) or Bay 5 (travelling fires) go into catenary action. This occurs for fires located in the upper floors of the frame (uniform fires Floors #6-#9 and travelling fires Floors #5-#9). Heated beams on the upper floors are connected to the weaker column sections than in the lower floors and they are unable to transfer and sustain the loads after beams in end bays go into catenary action. In the second group, i.e. fires occurring on the lower floors of the frame, the frame is sufficiently robust to resist the catenary action and maintain stability. In these cases, failure is initiated (i.e. ultimate strain of the material

is exceeded) after the local beam collapse. Failure in both groups is governed by the generation of high loads due to restrained thermal expansion and the loss of material strength.

For multiple floor fires, as already identified in Chapter 5, different fire scenarios can be split into two main groups. In the first group, failure is mostly dominated by the loss of material strength and occurs for the cases with 1 to 3 fire floors and all 2.5% TFM and ISO scenarios. Similarly to group 1 for single floor fires, collapse is initiated by the pull-in of external columns at the fire origin (Bay 1) or towards the end of the fire path (Bay 5). In the second group, failure is dominated by the thermal expansion and geometric effects and collapse is initiated by swaying of the frame to the side of the fire origin. It occurs for the cases with 5 or more fire floors. Moreover, for the 3-floor 10% TFM and 5-floor 2.5% TFM results in Bay 2 indicate deflected shape patterns similar to the weak-floor collapse reported in [7, 10, 11]. In the other scenarios deflected patters and pull-in of the columns is similar to the strong-floor or a mixed collapse mechanism. However, it should be noted that the location of multiple floor fires was not varied in this study. Location of multiple floor fires in the frame could have a significant affect on the collapse mechanism (as for single floor fires) and needs further investigation.

The results indicate that for the investigated frame initiation of collapse mechanisms are affected not only by the fire type but also the number of fire floors and location of the fire floor. The finding of this study could be of use to designers of buildings when developing fire protection strategies or when assessing the initiation of collapse for steel framed buildings.

References

[1] P. Shepherd and I. Burgess, "On the buckling of axially restrained steel columns in fire," *Engineering Structures*, vol. 33, pp. 2832–2838, oct 2011.

[2] C. Bailey, D. Moore, and T. Lennon, "The structural behaviour of steel columns during a compartment fire in a multi-storey braced steel-frame," *Journal of Constructional Steel Research*, vol. 52, pp. 137–157, nov 1999.

[3] Y. Wang, "An analysis of the global structural behaviour of the Cardington steel-framed building during the two BRE fire tests," *Engineering Structures*, vol. 22, pp. 401–412, may 2000.

[4] J. A. El-Rimawi, I. W. Burgess, and R. J. Plank, "Studies of the Behaviour of Steel Subframes with Semi-rigid Connections in Fire," *Journal of Constructional Steel Research*, vol. 49, pp. 83–98, jan 1999.

[5] J. Y. R. Liew, L. K. Tang, T. Holmaas, and Y. S. Choo, "Advanced analysis for the assessment of steel frames in fire," *Journal of Constructional Steel Research*, vol. 47, pp. 19–45, aug 1998.

[6] A. Agarwal and A. H. Varma, "Fire induced progressive collapse of steel building structures: The role of interior gravity columns," *Engineering Structures*, vol. 58, pp. 129–140, jan 2014.

[7] G. Flint, A. Usmani, S. Lamont, B. Lane, and J. Torero, "Structural Response of Tall Buildings to Multiple Floor Fires," *Journal of Structural Engineering*, vol. 133, pp. 1719–1732, dec 2007.

[8] G.-L. F. Porcari, E. Zalok, and W. Mekky, "Fire induced progressive collapse of steel building structures: A review of the mechanisms," *Engineering Structures*, vol. 82, pp. 261–267, jan 2015.

[9] E. Alderighi and W. Salvatore, "Structural fire performance of earthquake-resistant composite steelconcrete frames," *Engineering Structures*, vol. 31, pp. 894–909, apr 2009.

[10] D. Lange, C. Röben, and A. Usmani, "Tall building collapse mechanisms initiated by fire: Mechanisms and design methodology," *Engineering Structures*, vol. 36, pp. 90–103, mar 2012.

[11] P. Kotsovinos and A. Usmani, "The World Trade Center 9/11 Disaster and Progressive Collapse of Tall Buildings," *Fire Technology*, vol. 49, no. 3, pp. 741–765, 2013.

[12] H. M. Ali, P. E. Senseny, and R. L. Alpert, "Lateral displacement and collapse of single-story steel frames in uncontrolled fires," *Engineering Structures*, vol. 26, pp. 593–607, apr 2004.

[13] R. Becker, "Structural behavior of simple steel structures with non-uniform longitudinal temperature distributions under fire conditions," *Fire Safety Journal*, vol. 37, no. 5, pp. 495–515, 2002.

[14] S. A. Kilic and S. Selamet, "Symmetric and Asymmetric Collapse Mechanisms of a Multi-Story Steel Structure subjected to Gravity and Fire," in *Structures Congress 2013*, (Reston, VA), pp. 2545–2554, American Society of Civil Engineers, apr 2013.

[15] R. Sun, Z. Huang, and I. W. Burgess, "The collapse behaviour of braced steel frames exposed to fire," *Journal of Constructional Steel Research*, vol. 72, pp. 130–142, may 2012.

[16] J. Jiang, G.-Q. Li, and A. Usmani, "Effect of Bracing Systems on Fire-Induced Progressive Collapse of Steel Structures Using OpenSees," *Fire Technology*, 2014.

Chapter 8

Conclusions

8.1 Outcomes of the present research

Current design codes invoke gas timetemperature curves which are based on small enclosure fires and assume uniform temperature distributions in the compartments. However, in real buildings, fires have been observed to travel. To account for the travelling nature of fires, Travelling Fires Methodology (TFM) has been developed between 2007 and 2011 at the University of Edinburgh. In Chapter 2 the TFM has been refined based on a better fire model. The limitation on the range of possible fire sizes has been introduced. It reduces the computational time required by eliminating unrealistic fire coverage areas based on fire spread rates observed in experiments and real fires. Analytical correlation, that is independent of grid size and can be easily calculated with any mathematical tool, has been presented for generation of gas timetemperature curves. Flapping term has been introduced that leads to reduced near-field temperatures for smaller fire sizes which cover a range between 800 and 1200°C observed in real building fires. The occurrence of peak member temperatures for fire sizes in the range of 5 to 20% is found to diminish with increasing flapping angle.

Prior to the study of the effects of iTFM on the structural response, finite element software LS-DYNA used for the analyses in Chapters 4-7 has been validated for structural fire analysis (Chapter 3). Four different canonical problems have been modelled in LS-DYNA based on the experimental and numerical studies published in the literature. Results indicate that explicit dynamic solver of LS-DYNA is able to capture the key phenomena of heated structures. For all benchmarks, it is able to predict the development trends of displacements, axial forces, and bending moments with increasing temperature within acceptable level of accuracy. However, during cooling in composite concrete slab model LS-DYNA solution is found to differ from the published results below the temperature of 400°C and is less conservative in predicting tensile axial forces. Time scaling sensitivity study indicates that inertia effects generated during application of thermal load to the system have a more significant influence on the final result in LS-DYNA than preloading due to static loads. High variation in results and kinetic energy with

different parameters, especially for the composite concrete floor slab case, highlights that an extensive parameter sensitivity study has to be carried out for every model to ensure that LS-DYNA solution converges and is quasi-static. In addition, time scaling study shows that a generally applied ad-hoc rule in explicit dynamic analysis that the kinetic to internal energy ratio for the most of the time has to be less than 5% to achieve a quasi-static solution might be too high for structural analysis in case of fire.

The structural response of a generic protected 10-storey steel frame exposed to the improved Travelling Fires Methodology (iTFM) developed in Chapter 2 and uniform fires defined in standards has been studied in Chapters 4-7. Analyses on the effect of the location of the fire floor in the multi-storey steel frame (Chapter 4) has revealed that the development trends of displacements and stresses in beams on each floor is similar, except for fires occurring on the ground floor and the top floor. Higher displacements and lower axial forces are found to develop within beams in the upper floors, where column section reduces in size, due to the reduced level of restraint. In addition, critical fire scenarios, based on utilization and failure criteria analyses (Chapter 5), have been found to occur on the same floors as well. This indicates that column section sizes and their change on different levels of the frame are important in defining the weakest floors. The development of axial forces and bending moments in the floors more than 2 floors away from the fire floor is found to be negligible. This, therefore, indicates that modelling of five floors of the structure (with the fire in the middle floor) could be sufficient to capture the correct structural behaviour and stress redistribution.

Comparing the structural response of the steel frame subjected to travelling fires and uniform fires (Chapter 4), the rate and magnitude of the highest beam mid-span deflections is found to depend mainly on the fire duration and not the fire type (i.e., TFM or uniform fire). Short and hot fires result in faster development of deflections while long and cool fires result in larger peak deflections. On the other hand, the locations where these peak deflections occur are observed to be different for TFM and uniform fire scenarios. For travelling fires the highest deflections initially develop in the edge bays while for uniform fires in the central bay. Also, the displacements under travelling fire exposures are found to be more irregular.

In Chapter 4 uniform fire scenarios are found to result in larger compressive axial forces in comparison to travelling fires, while peak bending moments are in the similar range for both travelling fires and uniform fires. In the terms of overall frame utilization during the fire (Chapter 5) long uniform fires have been found to result in the highest average frame utilization (i.e. 100th percentile), while 48% TFM and short-hot parametric fires resulted in the lowest utilization. However, the results indicate that for TFM fires in comparison to uniform fires a higher percentage of members is under higher peak utilization. In addition, travelling fires result in significantly increased utilization of internal columns by up to approx. 40% while under uniform fires it increases by up to 5% only. In addition, when the frame is subjected to travelling fire scenarios smaller than the width

of the bay irregular oscillations of axial forces, bending moments, lateral displacements and thus member utilization (in the range of 2 - 38%) are observed. This is not the case when the frame is exposed to uniform fires or large size travelling fires.

In Chapter 5 the structural response of the steel frame subjected to various fire scenarios has been assessed in the terms of load-bearing capacity, utilization, beam mid-span deflection, and limiting temperature limit states. The most severe fire scenarios in the terms of failure time have been found to be 25% TFM (deflection and stability) and long-cool parametric fire (stability). However, failure based on the stability criterion under the latter fire scenarios only occurs on the upper weaker floors of the frame. If lower floors of the frame are considered, small travelling fires are found to become more onerous and lead to failure during fire in the larger number of cases.

The location of the peak temperature in the compartment has been studied in Chapter 2 and is found to occur at the end of the fire path. It is observed to be dominated by fire spread rate for small fire sizes up to 30% although it depends on the thickness of fire protection and heat release rate. Total heat release rate becomes more dominant for large fires. The analysis on the location of the peak temperature in the compartment has been carried out with a premise that it may be important for the identification of critical structural members. To investigate whether this is true, locations of the peak temperature have been compared with the critical locations based on the structural analyses (Chapter 5). It was observed that stability failure tends to occur close to the location of peak temperature in the compartment.

In real fire accidents, fires have not only been observed to travel horizontally but also vertically between different floors. The effect of the number of floors on which travelling fires occur simultaneously has been investigated in Chapter 6. Results show that the highest stresses develop in the fire floors adjacent to the cool floors while in the intermediate fire floors the stresses are significantly smaller. However, the highest axial forces are found to develop for fire scenarios with only one fire floor. Results also reveal that, for the investigated frame, the failure time and collapse mechanism are affected not only by the fire type, but also the number of fire floors and the location of the fire floor (Chapter 7). For the cases with 1 to 3 fire floors failure is mostly dominated by the loss of material strength with temperature and occurs at the temperatures between 600 and 730°C. Failure is initiated by the pull-in of external columns. On the other hand, for the cases with 5 or more fire floors failure is dominated by the thermal expansion and geometric effects and occurs at temperatures as low as 130°C. The frame fails by swaying to the side of the fire origin. ISO fire is found to be more onerous for the cases with 1 to 3 fire floors. For the cases with 5 and more fire floors 25% and 48% travelling fires indicate earlier failure even though no failure occurs for the 48% TFM with lower number of fire floors.

In Chapter 6, in addition to varying the fire type and number of simultaneously heated fire floors the effect of opposing and vertically travelling two-floor fires has been

investigated. The patterns of stress and deflection development are found to be similar irrespective of fire spread direction. The results indicate that vertically travelling fires result in higher beam axial forces and deflections early during the fire exposure. However, simultaneous fires are found to lead to shorter times to failure.

Analyses presented in Chapters 4 to 7 highlight that in the structural design for fires it is important to consider more realistic fire scenarios associated with travelling fires as they might trigger previously unnoticed structural mechanisms. Results on the multi-storey steel frame indicate that, depending on the structural metric examined, both travelling fires and uniform fires can be more severe than the other. A single worst case fire scenario under which a structure could be designed and deemed to be safe cannot be established. For different fire exposures failure is found to occur on different range of floors subjected to fire. Therefore, in order to ensure a safe fire resistance design of buildings with large enclosures, a range of different fires including both travelling fires and uniform fires need to be considered.

8.2 Future work

The work presented in this thesis proposes crude changes to the Travelling Fires Methodology and provides an insight on the differences in the structural response of a steel frame exposed to both travelling fires and uniform fires. A large amount of future research could be carried out to improve and validate the travelling fire model and get a better understanding of the structural response to such fires.

8.2.1 Refinement and validation of travelling fires

The proposed changes to the Travelling Fires Methodology represent a simple fire model. Experimental evidence in large compartments is necessary to gain a better understanding of the travelling fire dynamics and in order to validate and improve the iTFM. The experiments should be well designed and instrumented so that a natural fire spread and non-uniform temperature distributions in the compartment could be recorded. Experiments in relatively large compartments approx. 100 m^2) where a travelling nature of fire has been captured are currently limited to Cardington tests [1] and "Tall Building Tests [2].

In this thesis a range of possible fire sizes has been reduced based on the fire spread rates measured in experiments and observations from real fires. However, the lower limit of fire spread rates is still unrealistically low as it is based on very small spread rates from wood crib fires. Further more extensive work could be conducted to limit the range of likely fire sizes even more. Well-designed experiments could be conducted to get a better understanding of, for example, fire spread rates between different office workstation configurations and configurations commonly used in modern structures.

iTFM model presented in this work assumes fires spreading along a linear 1D path. Fire dynamics in large enclosures give a very wide range of possible fire paths which are not currently represented in iTFM. Further work could be conducted to extend the methodology to consider the 2D fire spread along various paths and temperature distributions in the compartment. Initial investigation on the effect of various simplified fire paths (linear, ring inwards and outwards, and clockwise fire spread around the core) on the structural response of the concrete structure has been carried out by Law et al. [3, 4]. He found that different fire paths have a small impact on the structural response. Based on the deflection, hogging and sagging strain, and rebar temperature metrics the differences were up to 10% in comparison to linear fire spread.

The concept of flame flapping has been introduced in this thesis to account for flame fluctuations and to represent more realistic near-field temperatures. The proposed reduced near-field model is a simple approximation of temperatures over the flapping region. Currently, experimental data available is limited to small localised fires in the open or the fire size in respect to the total floor area of the enclosure is not considered. Further experiments could be conducted which would investigate, for example, the effects of the dimensionless heat release rate and compartment dimensions on the near-field temperatures of a localised stationary or travelling fire.

Currently iTFM represents non-uniform temperature distributions along the ceiling only. This is because the structural elements at the ceiling experience the maximum exposure to hot gases [5]. Vertical temperature distributions, i.e. along the structural members such as columns, in the compartment are not considered. In all of the research carried out up to date on the structures exposed to travelling fires columns were either assumed to stay cool or assumed to be subjected to uniform temperatures along the height. In many experiments, particularly on localised fires vertical temperature distributions in the compartment have been recorded to have a high non-uniformity. This could have a significant effect on the structural response. Thus, work to include non-uniform vertical temperature distributions could be undertaken to represent a more realistic fire exposure and to improve iTFM.

8.2.2 Further validation of LS-DYNA and dynamic solvers

In general, LS-DYNA has been found to give good predictions of the structural response to fire in comparison to other software and experiments. However, significant differences in the solutions, particularly development of deflections, were obtained for the composite steel-concrete floor model. It is unknown whether this is because of the inherent assumptions in LS-DYNA or whether it is related to different input used in Abaqus. Further study could be conducted where both LS-DYNA and Abaqus models are prepared using the same assumptions to eliminate any uncertainties in the input.

Response of structures to fire is frequently idealised as a quasi-static problem and modelling it using the real time fire duration would require a significant computational

time. In this thesis a combination of two different approaches has been considered to reduce the computational time associated with the fire duration, i.e. time scaling and damping. Further work could be conducted to investigate the effects of mass scaling, which is a commonly used approach, and how well it compares with the latter two approaches. In addition, it could be interesting to investigate the applicability of time scaling, damping, and mass scaling in the structural fire analyses when creep is considered.

In the validation study of LS-DYNA presented in this thesis, Release 7.1.1 version was used. It could be interesting to investigate whether there are any differences between the solutions obtained using other releases of LS-DYNA and how significant they are (if any).

8.2.3 3D Structural analyses

Structural analyses presented in this thesis has been based on the 2D model of a simple steel frame. Such representation ignores composite action effects between steel beams and concrete slab, and concrete membrane tensile action. Thus, this work could be advanced by carrying out the analyses on the 3D model of the composite structure incorporating the effects of the concrete floor slab. Similar work has only been carried out by Röben [6] on a part of the composite floor plate (2 bay × 2 bay) assuming continuity boundary conditions. It could also be interesting to investigate the differences in the results of the 2D and 3D model exposed to travelling fires. There are very few similar studies on generic structures present in the literature. 2D models offer an important computational advantage and such analyses could help to gain a better understanding on limitations of 2D models and whether they are significant, particularly when larger structures are investigated.

Structural response of the steel frame in this work has been investigated in the terms of the temperature, deflection, and stability failure criteria. However, this analysis has been limited to the 2D model. Further work could be undertaken to investigate these failure criteria on the 3D model and different structural systems. Definition of an appropriate failure criteria is particularly important for probabilistic analyses to assess the safety of structures. In addition, in the present study and other research published in the literature where the structural response to travelling fires has been investigated, beam to column connections were either assumed to be fixed or pinned. In reality, it is likely to be somewhere between the two constrains. Inclusion of more realistic connections in the finite element models (e.g. by representing them as a set of springs) could help to represent a more realistic structural response and capture their failure. In previous work connections have been found to fail prematurely during cooling due to high tensile axial forces. This could be particularly important for structures subjected to small travelling fires.

Unlike in the published literature on the structures with long span composite truss

systems, results presented in this thesis show no significant cyclic movement of columns for vertically travelling fires. This could be due to a different structural system or a small number of fire floors and further studies varying the number of fire floors, structural system, and model complexity (2D vs. 3D) for vertically travelling fires could be conducted. On the other hand, when the frame is subjected to travelling fire scenarios smaller than the width of the bay irregular oscillations of stresses and thus member utilizations are observed within beams. Therefore, it could be interesting to investigate how these oscillations change with, for example, varying level of fire protection to the beams, bay length, direction of the travelling fire, various travelling fire parameters, and inclusion of the concrete slab in the model.

References

[1] B. R. Kirby, D. E. Wainman, L. N. Tomlinson, T. R. Kay, and B. N. Peackok, "Natural fires in large scale compartments - A British Steel technical, Fire Research Station collaborative project," 1994.

[2] J. L. Torero, A. H. Majdalani, C. Abecassis-empis, and A. Cowlard, "Revisiting the Compartment Fire," in *Proceedings of the 11th International Symposium on Fire Safety Science*, (Christchurcch, New Zealand), 2014.

[3] A. Law, *The Assessment and Response of Concrete Structures Subject to Fire.* Doctor of philosophy, The University of Edinburgh, 2010.

[4] A. Law, J. Stern-Gottfried, M. Gillie, and G. Rein, "The influence of travelling fires on a concrete frame," *Engineering Structures*, vol. 33, pp. 1635–1642, may 2011.

[5] J. Stern-Gottfried and G. Rein, "Travelling fires for structural design-Part II: Design methodology," *Fire Safety Journal*, vol. 54, pp. 96–112, nov 2012.

[6] C. Röben, *The effect of cooling and non-uniform fires on structural behaviour.* Phd, The University of Edinburgh, 2009.

Appendix A

Material Properties

This appedix presents the thermal and mechanical properties of steel and concrete used in different chapters of this thesis.

A.1 Steel

Steel material properties at ambient temperature used in different chapters are summarised in Table A.1. Temperature dependent relative elongation and specific heat of steel according to the Eurocode 3 used in Chapters 3-7 and Chapters 2 & 4-7, respectively, are illustrated in Fig. A.1. Figures A.2 and A.3 illustrate temperature dependent mechanical properties of steel according to Gillie [1] (Chapter 3, BM2) and Eurocode 3 [2] (Chapters 3-7), respectively. During cooling steel material properties were assumed to return to original values at ambient temperature unloading along the path with the initial elastic modulus.

Table A.1: Steel material properties at ambient temperature.

	c_p (J/kg.K)	E (GPa)	υ (-)	α ($^\circ$C^{-1})	σ_y (MPa)	Temperature dependent properties
Chapter 2	440	-	-	-	-	Buchanan [3] (Fig. A.1)
Chapter 3:						
BM1	-	210	0.3	1.2×10^{-5}	408	EN1993-1-2 (Figs. A.1 & A.3)
BM2	-	207 [a]	0.3	1.2×10^{-5} [a]	250	Gillie [1] (Fig. A.2)
BM3 (beams)	-	210	0.3	1.35×10^{-5} [a]	300	EN1993-1-2 (Fig. A.3)
BM3 (rebar)	-	210	0.3	1.35×10^{-5} [a]	450	EN1993-1-2 (Fig. A.3)
BM4	-	210	0.3	1.2×10^{-5}	275	EN1993-1-2 (Figs. A.1 & A.3)
Chapters 4-7	440	210	0.3	1.2×10^{-5}	345	EN1993-1-2 (Figs. A.1 & A.3)

a. Material properties taken to be independent of temperature.
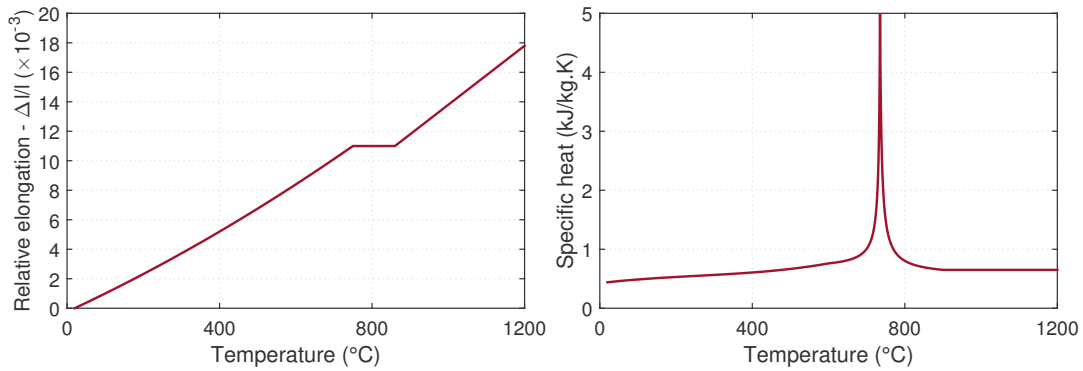
Figure A.1: Temperature dependent relative elongation according to Eurocode 3 [2] (left); and specific heat of steel according to Buchanan [3] and Eurocode 3 [2] (right).
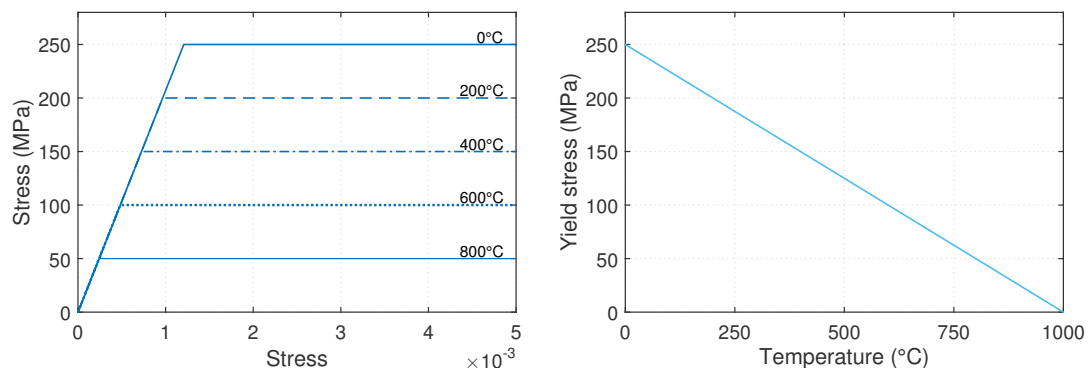
Figure A.2: Stress-strain relationship (left) and yield stress (right) for steel at elevated temperatures used in Chapter 2, BM2 [1].
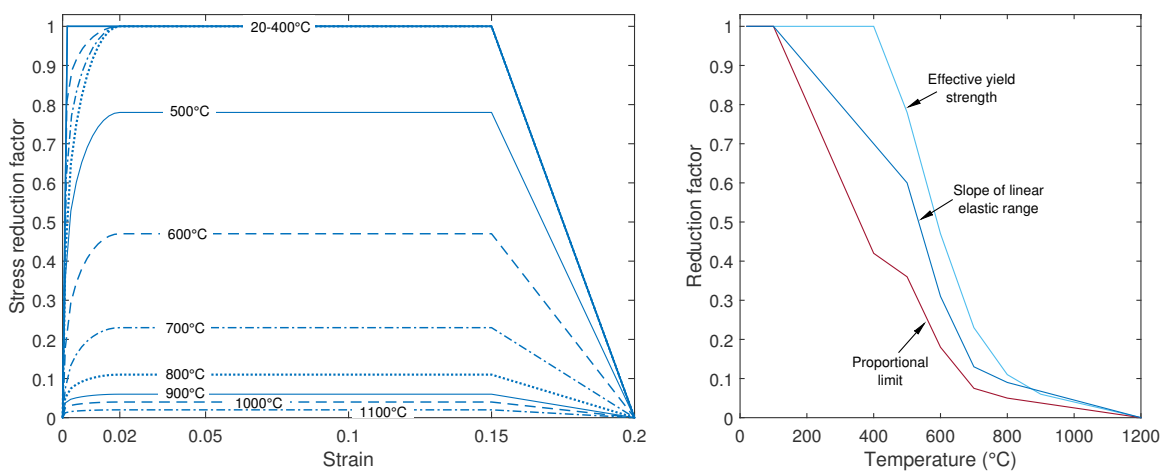
Figure A.3: Reduction factors for stress-strain relationship (left) and effective yield strength, slope of linear elastic range, and proportional limit (right) for steel at elevated temperatures according to Eurocode 3 [2].

A.2 Concrete

Thermal concrete properties used for heat transfer analyses in Chapter 2 were taken from [3, 4] and are given in Table A.2. In the analyses these properties were assumed to be temperature independent. Mechanical concrete material properties at ambient temperature and temperature dependent properties used in Chapter 3 BM3 are shown in Table A.3 and Fig. A.4, respectively. Temperature dependent properties were taken from Eurocode 2 [4]. During cooling concrete material properties were assumed to return to original values at ambient temperature unloading along the path with the initial elastic modulus.

Table A.2: Concrete material properties at ambient temperature used in Chapter 2.

	ρ (kg/m^3)	k (W/m.K)	c_p (J/kg.K)
Chapter 2	2300	1.3	1000

Table A.3: Concrete material properties at ambient temperature used in Chapter 3.

	ρ (kg/m^3)	υ (-)	α (°C^{-1})	σ_u (MPa)	ε_u (-)	Temperature dependent properties
Chapter 3, BM3	2400	0.25	9×10^{-6}	47	0.002	EN1992-1-2 (Fig. A.4)
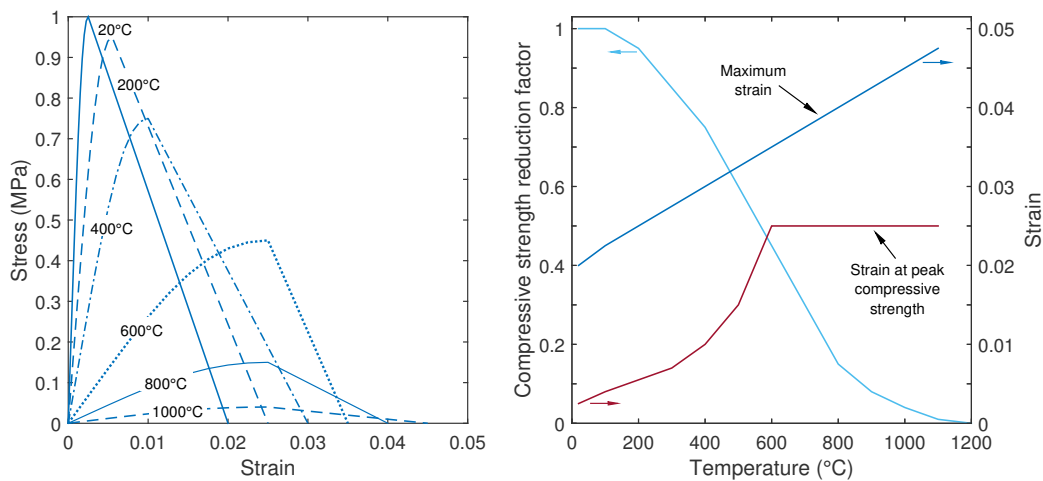
Figure A.4: Reduction factors for stress-strain relationship in compression (left) and compressive strength, maximum strain, and strain at peak compressive strength (right) for concrete at elevated temperatures according to Eurocode 2 [4].

References

[1] M. Gillie, "Analysis of heated structures: Nature and modelling benchmarks," *Fire Safety Journal*, vol. 44, pp. 673–680, jul 2009.

[2] CEN, "EN 1993-1-2:2005 - Eurocode 3. Design of steel structures. General rules. Structural fire design," 2005.

[3] A. H. Buchanan, *Structural Design for Fire Safety.* John Wiley & Sons, Ltd, 2001.

[4] CEN, "EN 1992-1-2:2004 - Eurocode 2. Design of concrete structures. General rules. Structural fire design," 2004.

Appendix B

Reduced Near-Field vs. Moving Average

Travelling Fires Methodology (TFM) considers design fires to be composed of two moving regions: the near-field (flames) and the far-field (smoke). The near-field represents the flames directly impinging on the ceiling and assumes the peak flame temperatures, i.e. 800-1200°C. In chapter 2, near-field has been revised to account for natural lateral fluctuations of the flames on the ceiling by introducing the concept of the flapping angle. Equations to calculate reduced near-field temperature, which approximate temperatures over the flapping length in the near-field region, have been introduced. In addition to that, a calculation using moving average over the temperatures (both near-field and far-field) along the fire path have been considered in the study and is presented in this Appendix.

Similarly to the reduced near-field, moving averages have been calculated by using the flapping length as the subset length of the data set, i.e. gas distributions along the fire path. Illustrative comparison of gas and corresponding steel temperatures along the fire path between different TFM concepts assuming near-field of 1200°C, reduced near-field, and moving average calculation is shown in Fig. B.1. Comparison of the steel temperatures obtained using reduced near-field and moving average concepts (Figs. B.2-B.4) indicates that the differences in the final result between these two concepts are very small. For all scenarios, the 95th percentile error is between 2% and 15% (7 and 50°C). Thus, as calculation using moving averages is more computationally expensive, reduced near-field concept has been chosen for iTFM.
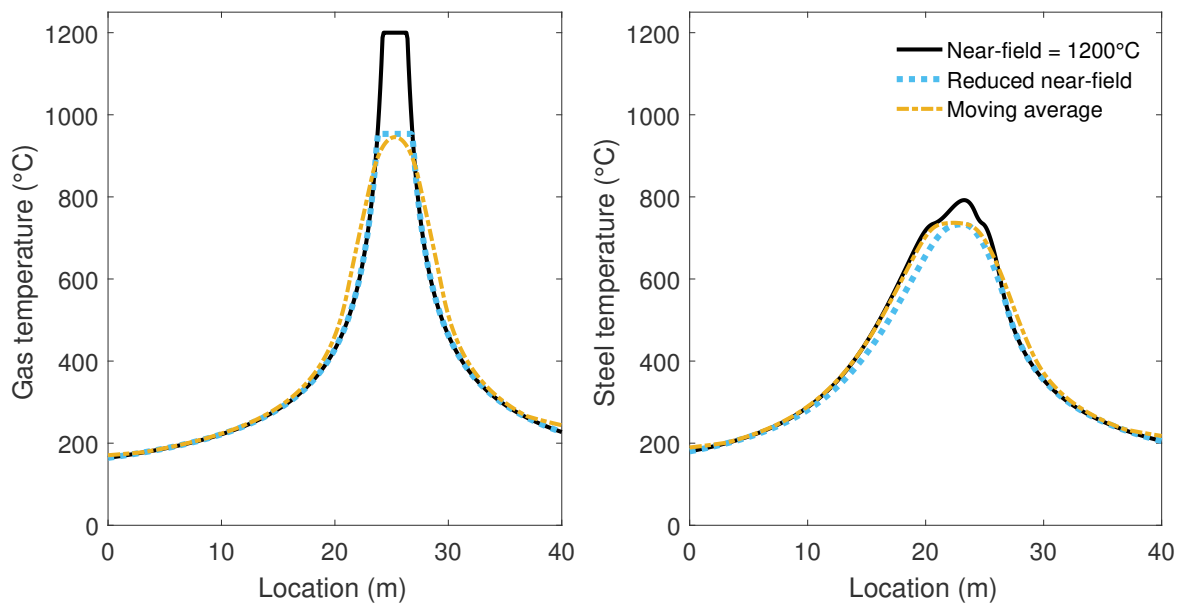
Figure B.1: Gas (left)and corresponding steel (right) temperatures along the fire path for different TFM concepts. Steel beam protection is designed for 60 min standard fire resistance as in Chapter 2.
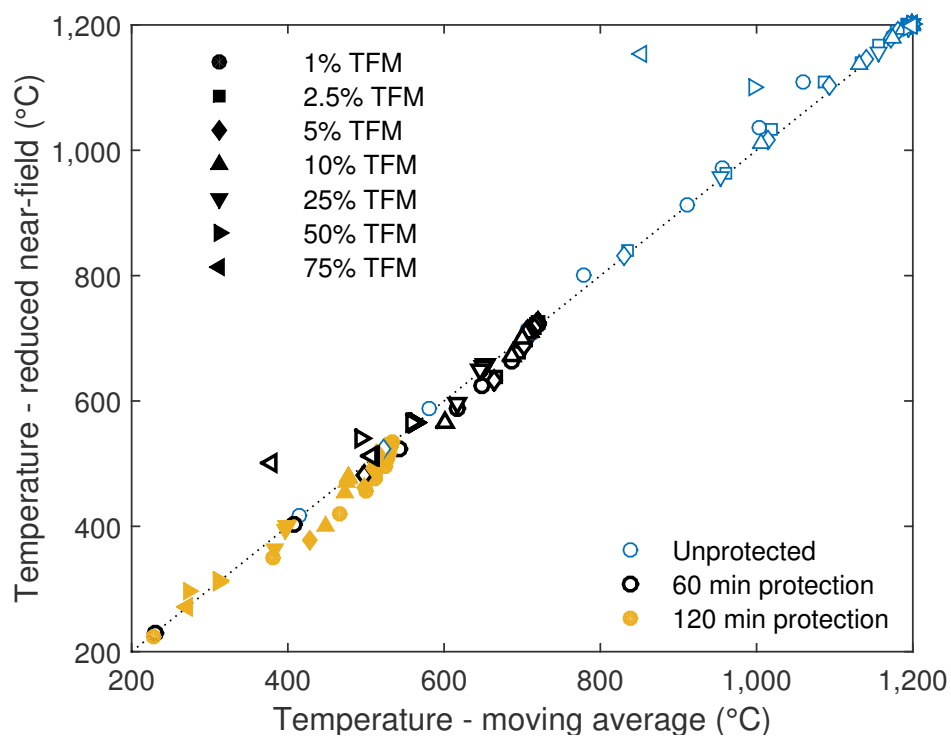
Figure B.2: Comparison of steel temperatures at the middle of the fire path exposed to TFM with reduced near-field and moving average concepts. Flapping angles between 2° and 75° are considered. Steel beam protection corresponds to equivalent standard fire duration.
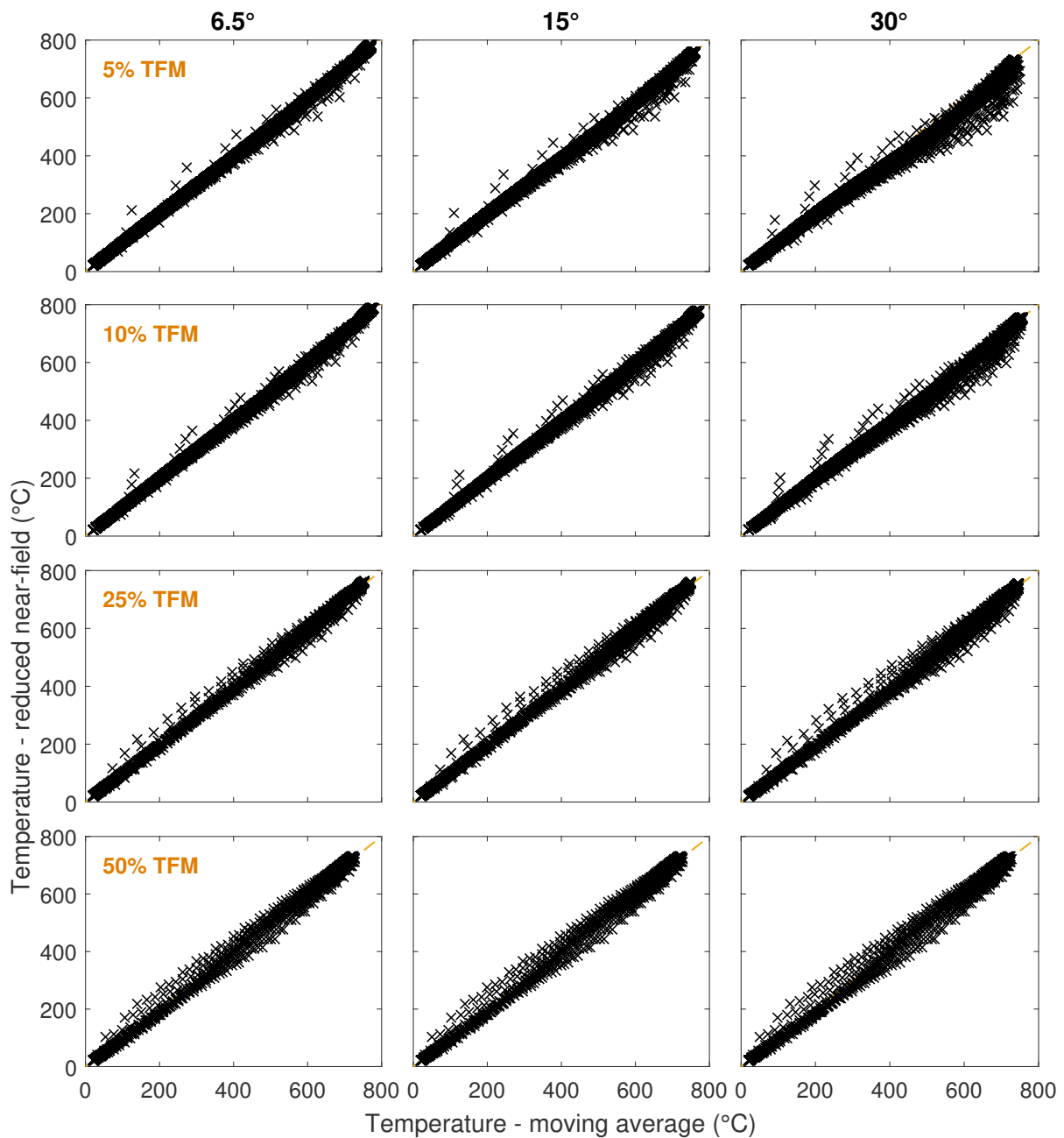
Figure B.3: Comparison of steel beam temperatures exposed to TFM with reduced near-field and moving average cconcepts at every 0.5 m along the fire path and at every 60 s of fire exposure. 5%, 10%, 25%, and 50% travelling fire sizes, and 6.5°, 15°, and 30° flapping angles are considered. Steel beam protection is designed for 60 min standard fire resistance as in Chapter 2.
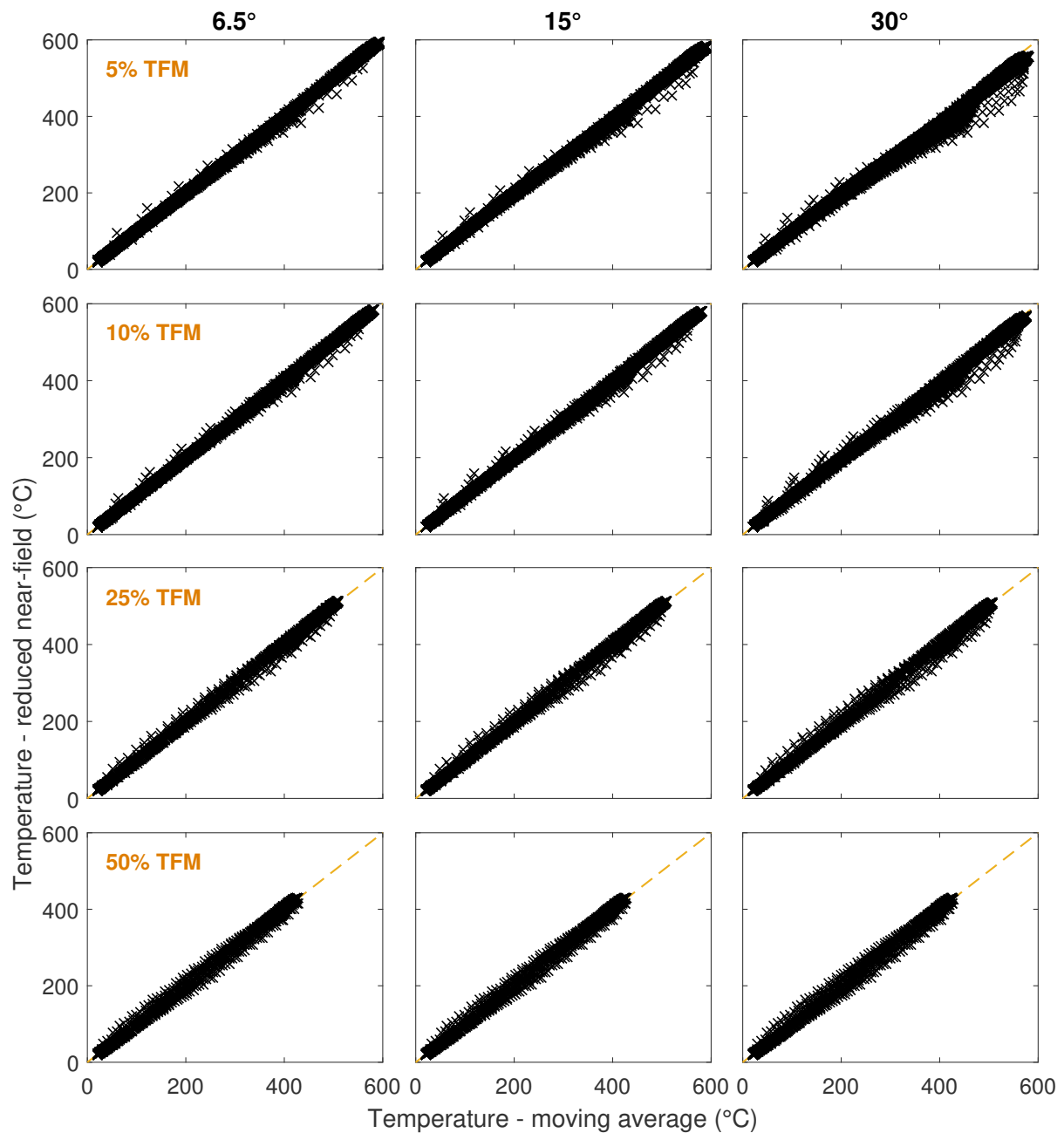
Figure B.4: Comparison of steel beam temperatures exposed to TFM with reduced near-field and moving average concepts at every 0.5 m along the fire path and at every 60 s of fire exposure. Steel beam protection is designed for 120 min standard fire resistance as in Chapter 2.

Appendix C

LS-DYNA Model Parameter Sensitivity Study

In this Chapter, LS-DYNA parameter sensitivity study is presented for the FEM model of the multi-storey steel frame used for the analyses in Chapters 4 to 6. A parameter sensitivity study is carried out in order to determine the optimum balance between accuracy and computational efficiency, and to ensure that a quasi-static solution is obtained. The study presented here is similar to that carried out in Chapter 3. The effect of parameters such as load time scaling, mesh density, and number of beam integration points on the convergence of the solution is investigated. A 25% travelling fire (iTFM, Chapter 2) and a standard fire are considered. The initial model parameters are identified in Table C.1. During the parameter sensitivity study only one parameter is varied at a time. The other model parameters are kept constant as shown in Table C.1. Each parameter is defined and discussed in more detail in Chapter 3. Based on this parameter sensitivity study, the final model parameters were then chosen for the analyses presented in Chapters 4 to 6.

Table **C.1**: Initial model parameters used for parameter sensitivity study.

Preload duration	Time scale factor	Element length	Beam integration refinement factor, k
1 s	100	0.25 m	0

C.1 Effect of preload due to gravity and static load

Preload duration is varied between 1 and 512 s. In addition, application of global damping is considered. Variation of kinetic to internal energy ratio, displacement and axial force at steady-state with preload simulation time is shown in Fig. C.1. Results show, as expected, that kinetic to internal energy ratio decreases with increasing preload time and is very low (between $3 \times 10^{-12}\%$ and $3 \times 7^{-4}\%$). Kinetic to internal energy rations for all pre-load times considered are less than 0.1%, which is a general rule of

thumb for a solution to be considered as steady-state. Some oscillations in the steady-state displacement and axial force can be observed for preload times of 1 to 4 s. However, their amplitudes are very small and could be considered to be negligible (axial force up to ± 0.74 kN, displacement up to ± 0.18 mm).
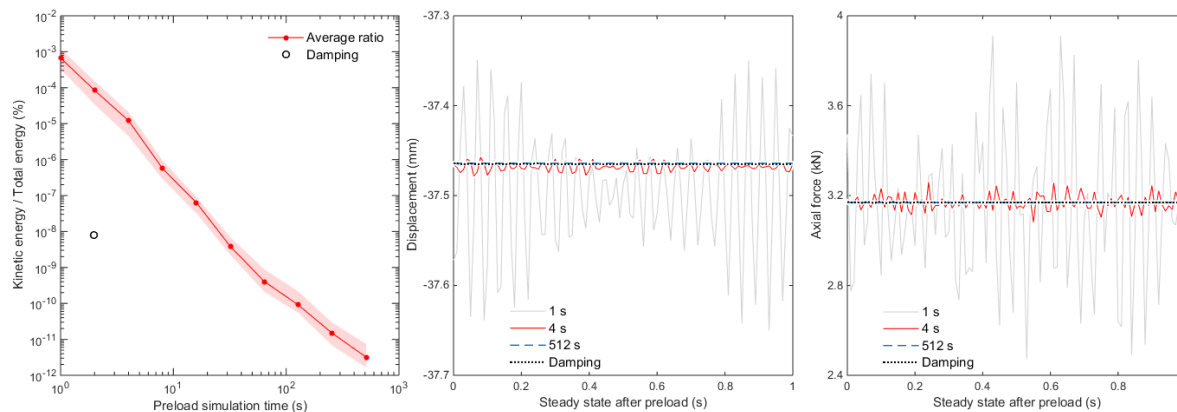
Figure C.1: Variation of the kinetic to total energy ratio with preload application time (left), and the effect of preload application time on displacement (middle), and axial force (right). Displacements and axial forces shown are during 1 s after the preload was applied and kept constant. Shown data is for the beam in Bay 1 Floor #2.

C.2   Effect of thermal load time scaling factor

Three preload durations are considered (1 s, 32 s, and damping) and for each thermal load application duration scaling factor is varied between 1 and 10,000. In addition, a case where damping is applied during the fire exposure is considered as well. Scaling factor only affects the structural response. Heat transfer is carried out prior to LS-DYNA analyses and then final temperature development within members is scaled down. Scaling factor of 1 corresponds to real-time fire duration, while 100 corresponds to thermal load being applied 100 times faster. The preload is applied first and then kept constant for 1 s. Following that once the steady-state solution has been reached, the thermal load is applied. In the cases where damping is applied during preload only, the critical damping factor is reduced to 0 before the application of the thermal load. For this study a 25% travelling fire and standard fire exposures are considered.

Results are shown in Figs. C.2 and C.3. The relative error is based on the results of the case with the longest preload (i.e. 32 s) and smallest scaling factor (i.e. 1 - travelling fire and 10 - standard fire). Results show convergence of the solution and reducing kinetic to internal energy ration in the system with reducing scaling factor, as could be expected. For all solutions, preload application duration has no effect on the final solution and kinetic to internal energy ratio in the system. Therefore, the shortest preload time of 1 s is chosen for the final model. For scaling factors, results show that

there is little effect on the final solution for the scaling factors between 1 and 1000. For these scaling factors relative errors and kinetic to internal energy ratios are below 1% and 0.4%, respectively. A general rule of thumb is that a solution is considered to be quasi-static when the kinetic energy to internal energy ratio in the system for most of the time is less than 5% (see Chapter 3). Therefore, based on the kinetic to internal energy ration, solution convergence, and computational time the scaling factor of 100 is chosen as the most optimal solution for the final model.
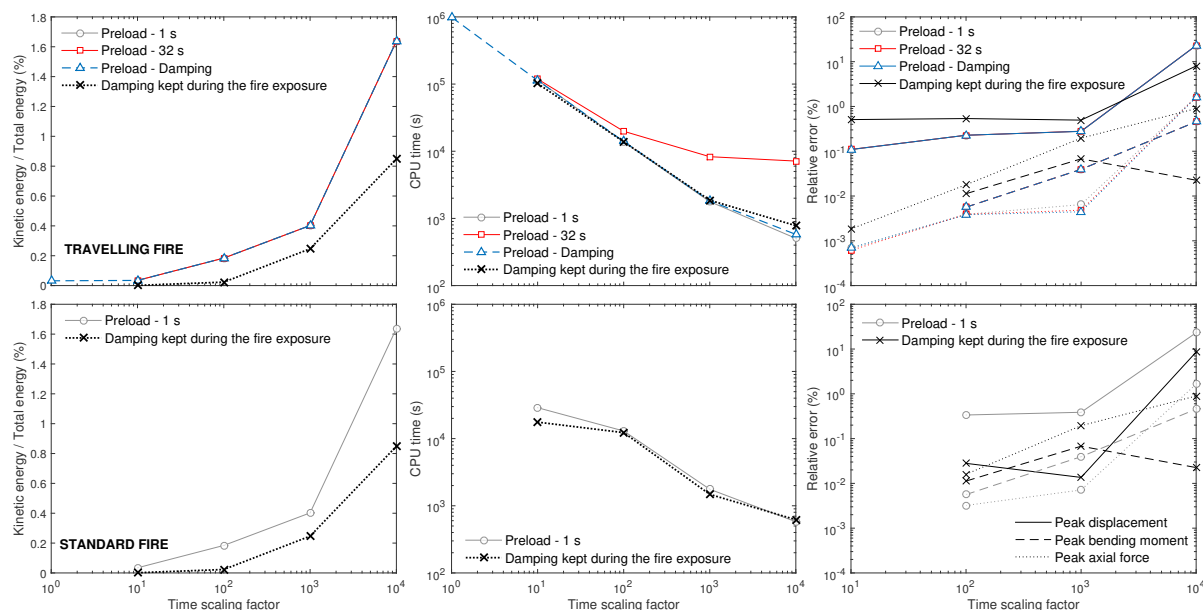
Figure C.2: Variation of kinetic to total energy ratio (left), CPU time (middle), and relative error of peak displacement, peak bending moments and peak axial force (right) with time scaling factor. Floor #2 is exposed to a 25% travelling fire (top) and a standard fire (bottom). Data is shown for the beam in Bay 1 Floor #2.

C.3 Effect of the number of beam element integration points

Beam integration refinement factor, k, is varied between 0 and 11 for a 25% travelling fire exposure. Effect of beam integration refinement factor on the final solution is shown in Fig. C.4. Average relative error is based on the results of the case with the highest integration factor (i.e. 11). Results show a clear convergence in the average relative error with increasing integration refinement factor. The highest error for a factor k of 0 is 10% for axial forces. For bending moment and beam displacement errors are 4% and lower. There is no clear convergence between the kinetic to internal energy ratio with the refinement factor, k. However, for all cases the kinetic to internal energy ratio is below 0.5%. Based on the average relative errors and development of axial forces, bending moments, and displacements the convergence is reached for the beam integration refinement factor $k = 5$. Therefore, this value is chosen for the final model.
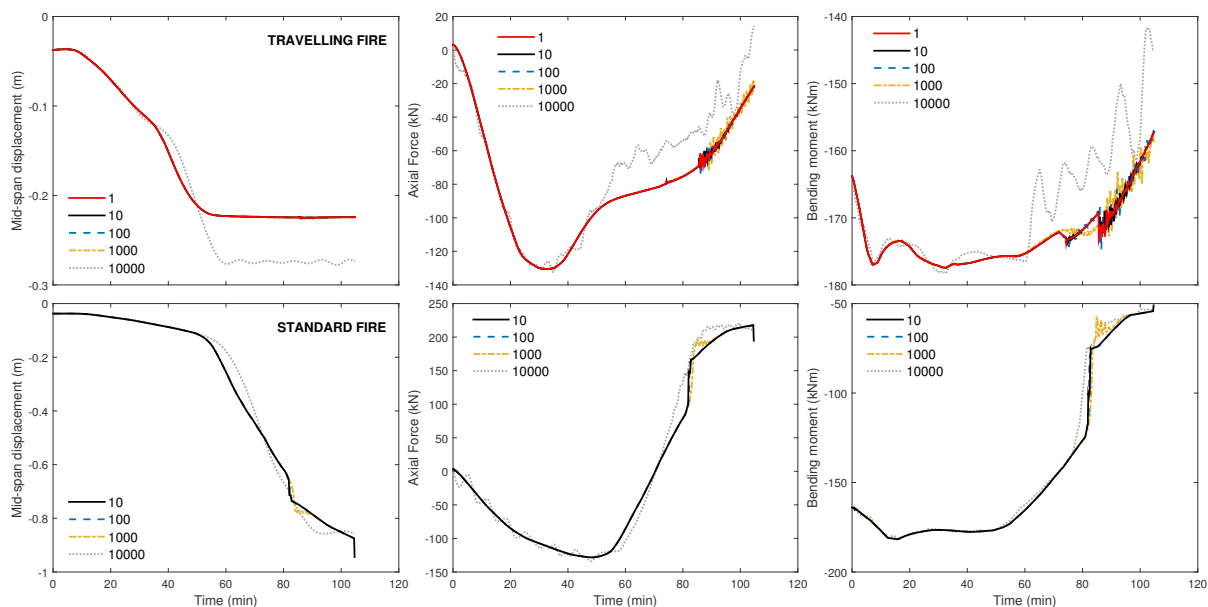
Figure C.3: Variation of beam mid-span displacement (left), axial force (middle), and bending moment (right) with time scaling factor. Floor #2 is exposed to a 25% travelling fire (top) and a standard fire (bottom). Data is shown for the beam in Bay 1 Floor #2.
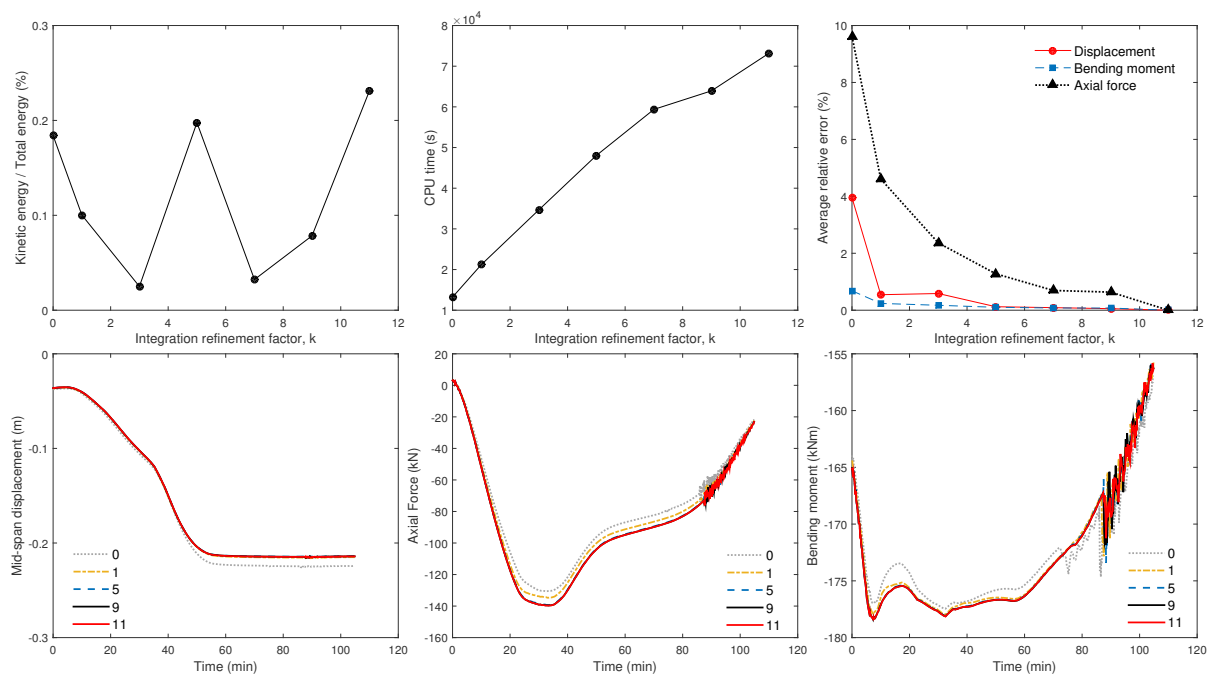

Figure C.4: Variation of kinetic to total energy ratio (top left), CPU time (top middle), average relative error of displacement, bending moments and axial force (top right), beam mid-span displacement (bottom left), axial force (bottom middle) and bending moment (bottom right) with integration refinement factor. Floor #2 is exposed to a 25% travelling fire. Data is shown for the beam in Bay 1 Floor #2.
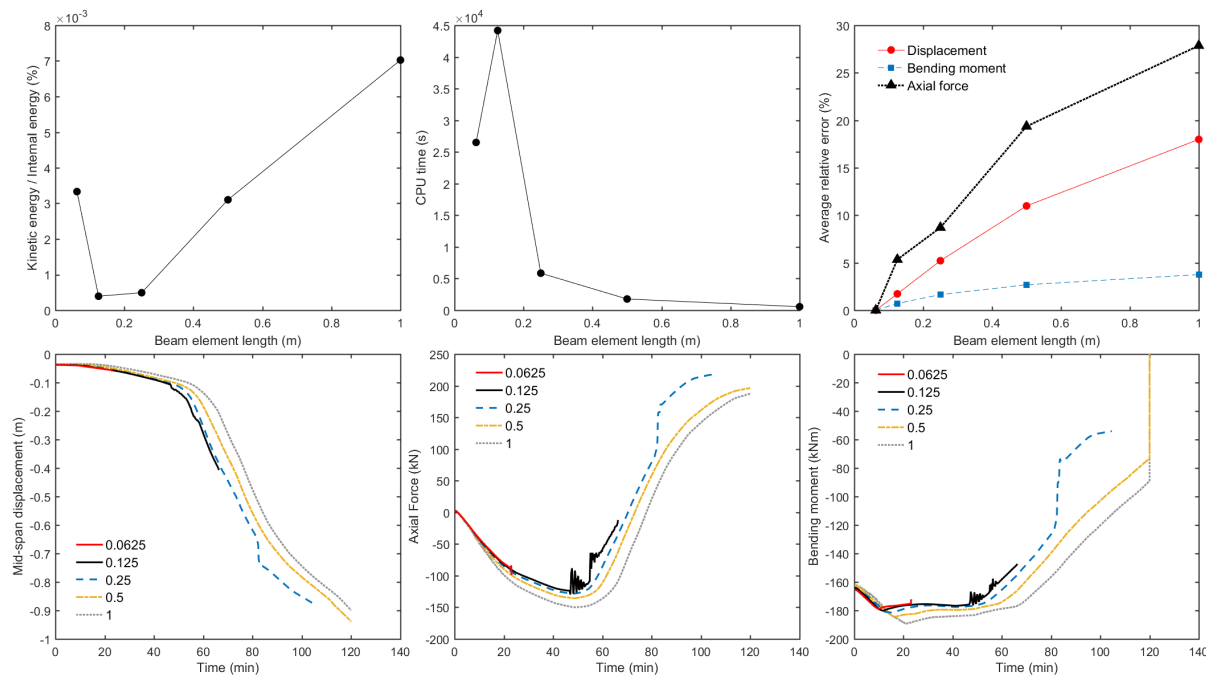
Figure C.5: Variation of the kinetic to internal energy ratio for 95% of the time (top left), CPU time (top middle), average relative error of displacement, bending moment and axial force (top right), beam mid-span displacement (bottom left), axial force (bottom middle) and bending moment (bottom right) with element length. Kinetic to internal energy ratios and average relative errors are calculated for the first 23 min of fire exposure until the model with beam element length of 0.0625 m fails. Floor #2 is exposed to a standard fire. Data is shown for the beam in Bay 1 Floor #2.

C.4 Mesh density convergence

Beam element length is varied between approximately 0.0625 and 1 m. For mesh density convergence a standard fire exposure is considered because, unlike for travelling fires, the final temperatures within beam elements are not beam element length dependent. Results are shown in Fig. C.5. For very small mesh sizes (0.0625 and 0.125 m) numerical instabilities occur early during the fire exposure. Thus, average relative errors are only calculated for the duration until numerical instabilities occur for a solution with beam element length of 0.0625 m, that is 23 min. Similar instabilities have been observed in Chapter 3 (Benchmark #1). Due to the instabilities present in the solutions for the finest mesh densities, the mesh with the beam element length of ~ 0.25 m is selected as the "converged" solution for the final model. In addition, kinetic to internal energy ratio for this mesh size is the lowest $4 \times 10^{-4}\%$.

C.5   Final model parameters

Final model parameters, which have been chosen as optimal based on the accuracy of solution and computational efficiency, used in the analyses presented in Chapters 4 to 6 are summarised in Table C.2.

Table C.2: Final model parameters used in the analyses presented in Chapters 4 to 6.

Preload duration	Time scale factor	Element length	Beam integration refinement factor, k
1 s	100	0.25 m	5

Appendix D

Multiple Floor Fires - Deflected Shape

In Chapter 6, structural response of a multi-storey steel frame exposed to multiple floor fires has been investigated. In this chapter Figs. D.1-D.4 are presented illustrating the deflected shape of the frame for all multiple floor fire scenarios considered in Chapter 6. Different fire exposures include 2.5%, 10%, 25%, and 48% travelling fires (TFM), and a standard fire (ISO). Number of multiple fire floors is varied between 1 and 10 (i.e. a whole frame).
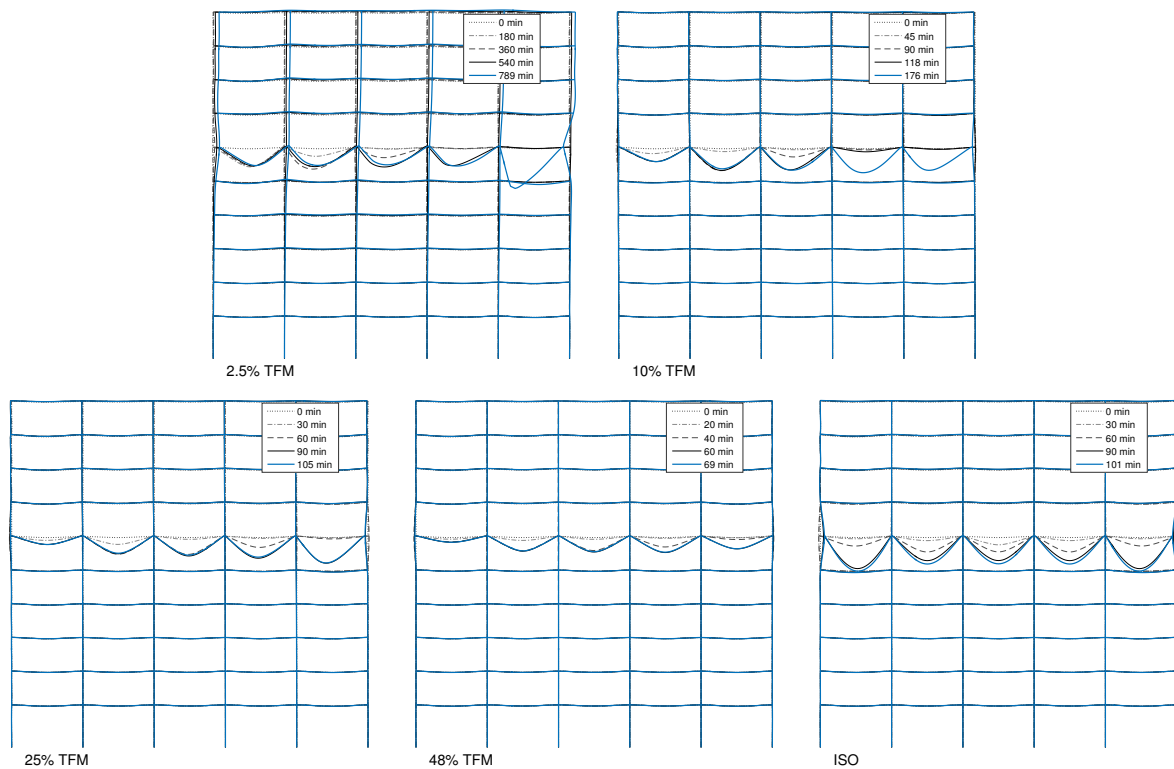
Figure D.1: Deflected shape of the frame for 2.5%, 10%, 25%, and 48% TFM travelling fires, and a standard fire (ISO) occurring on one floor (Floor #5). Displacement scale factor is 5.
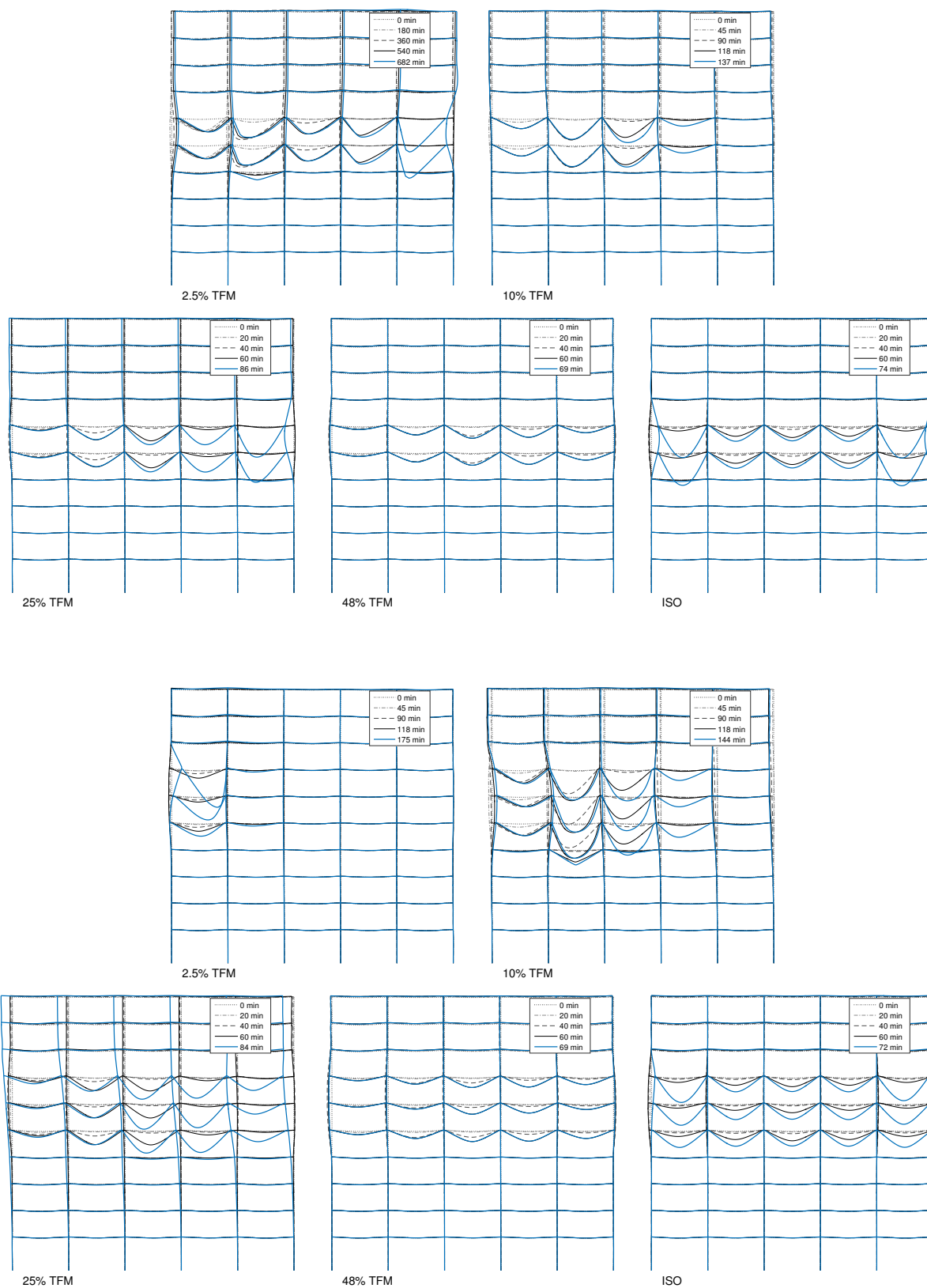
Figure D.2: Deflected shape of the frame for 2.5%, 10%, 25%, and 48% TFM travelling fires, and a standard fire (ISO) occurring on two floors, Floors #4 & #5 (top); and three floors, Floors #4, #5, & #6 (bottom). Displacement scale factor is 5.
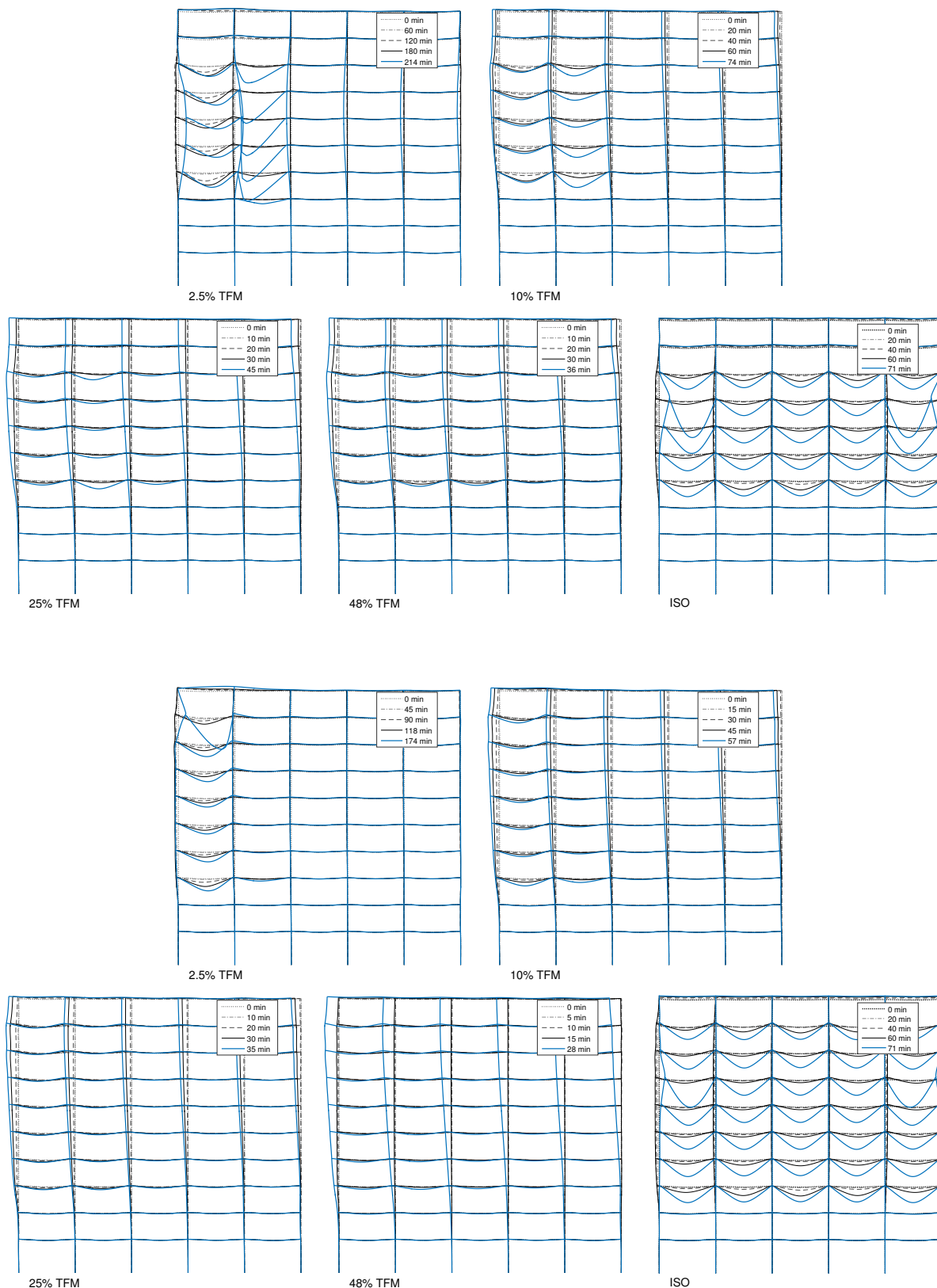
Figure D.3: Deflected shape of the frame for 2.5%, 10%, 25%, and 48% TFM travelling fires, and a standard fire (ISO) occurring on five floors, Floors #3, #4, #5, #6, & #7 (top); and seven floors, Floors #2, #3, #4, #5, #6, #7, & #8 (bottom). Displacement scale factor is 5.
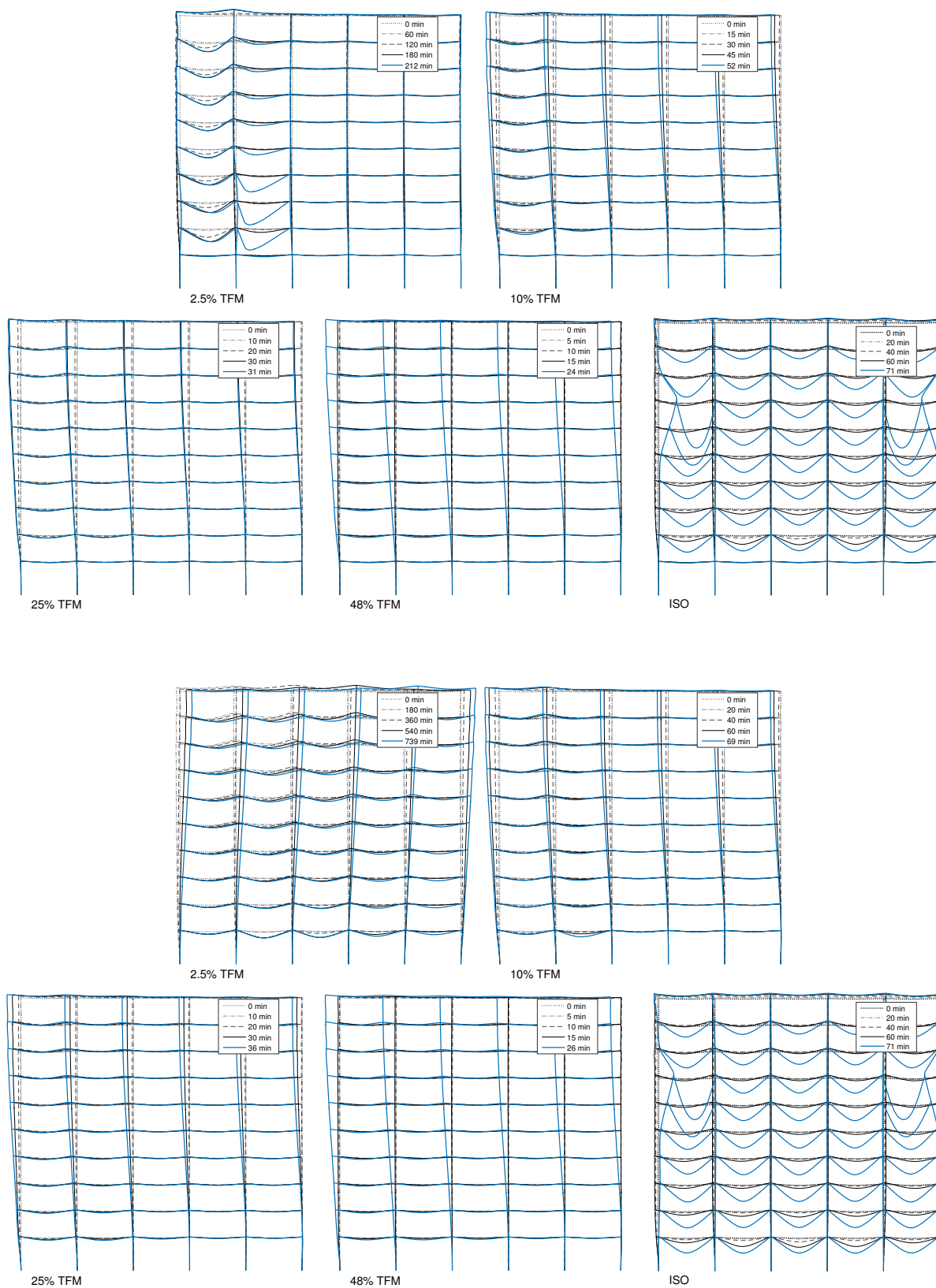
Figure D.4: Deflected shape of the frame for 2.5%, 10%, 25%, and 48% TFM travelling fires, and a standard fire (ISO) occurring on nine floors, Floors #3, #4, #5, #6, & #7 (top); and a whole frame (bottom). Displacement scale factor is 5.

Appendix E

iTFM Code

During the course of research a Matlab code was written for the calculation of travelling fire gas temperatures according to the Improved Travelling Fires Methodology (iTFM), which has been presented in Chapter 2. The code is reproduced below and can be obtained online from https://zenodo.org/collection/user-imperialhazelab under a Creative Commons Attribution license.

```matlab
% iTFM code for calculations of gas temperature in improved formulation of travelling fires
% by Egle Rackauskaite and Guillermo Rein, Imperial College London, UK.
% Based on the journal paper (doi:10.1016/j.istruc.2015.06.001): E Rackauskaite, C Hamel,
% A Law, G Rein, Improved formulation of travelling fires and application to concrete and
% steel structures, Structures, 2015.
% Contact authors at g.rein@imperial.ac.uk and reingu@gmail.com
% Work funded by Engineering and Physical Sciences Research Council and Arup
% Code published under a Creative Commons license CC BY 4.0

clear all
close all
syms R


% % ===================================================================
% % =============================        ==============================
% % =============================  INPUT  ==============================
% % =============================        ==============================
% % ===================================================================

% === ROOM PARAMETERS ===

WIDTH = 18;         % WIDTH OF THE COMPARTMENT (m)
HEIGHT = 3.5;       % HEIGHT OF THE COMPARTMENT (m)
L = 24;             % LENGTH OF THE COMPARTMENT (m) - FIRE PATH

dx = 0.25;          % LENGTH - CALCULATE TEMPERATURES EVERY dx (m)
dt = 10;            % TIME STEP (s)

% === FIRE PARAMETERS ===

FSIZE = 0.1;        % DIMENSIONLESS FIRE SIZE ( = LENGTH OF FIRE / LENGTH OF FIRE PATH)
QII = 500;          % HEAT RELEASE RATE PER UNIT AREA (kW/m2)
QF = 570000;        % FUEL LOAD DENSITY (kJ/m2)
T_ROOM = 20;        % ROOM TEMPERATURE ( C )
T_NF = 1200;        % PEAK FIRE TEMPERATURE ( C )

% === FLAPING ANGLE ===

FANGLE = 6.5;       % FLAPPING ANGLE ( )

% === FIGURES ===

ti = [30 60 120]; % TIMES OF INTEREST (min)
xi = [0 13 20];   % LOCATIONS OF INTEREST (m)

% % ===================================================================
% % =============================        ==============================
% % =============================  PARAMETER CALCULATIONS  =============
```

200

```matlab
% % =================================                          ==========================
% % ===============================================================================

% === FIRE PARAMETERS ===

TB = QF / QII;                          % LOCAL BURNING TIME (s)
TTOTAL = TB * ( 1 / FSIZE + 1 ); % TOTAL FIRE DURATION (s)
LF = L * FSIZE;                         % LENGTH OF THE FIRE (m)
S = LF / TB;                            % SPREAD RATE OF THE FIRE (m/s)
TLIMIT = 1.3 * TTOTAL;                  % DURATION FOR WHICH TEMPERATURES ARE CALCULATED (s)

% === NUMBER OF LOCATIONS OF INTEREST AND TIME STEPS ===

tt = 0:dt:TLIMIT;   % ARRAY OF TIME STEPS (s)
xx = 0:dx:L;        % ARRAY OF LOCATIONS (m)

% % ===============================================================================
% % ==================================          ==========================
% % ==================================   FLAPPING   ==========================
% % ==================================          ==========================
% % ===============================================================================

F = LF + 2 * HEIGHT * tan( FANGLE * pi / 180 ); % FLAPPING LENGTH (m)
Q = WIDTH * LF * QII;                           % TOTAL HEAT RELEASE RATE(kW)
T = 5.38 / HEIGHT * ( Q / R )^(2/3) + T_ROOM;   % ALPERT'S EQUATION (1972) doi: 10.1007/BF02590543

R0 = Q * ( 5.38 / ( HEIGHT * ( T_NF - T_ROOM ) ) )^(3/2); % INTERSECTION POINT OF Tmax (ALPERT'S
    EQUATION) AND T_NF (e.g. 1200 C)
if R0 > F / 2
    T_NEAR_FIELD = T_NF;
else
    RX1 = max( 0 , R0 - LF / 2 );
    RX2 = max( LF / 2 , R0 );
    R2 = F / 2; % DISTANCE FROM THE CENTRE OF THE FIRE TO FLAPPING RANGE EDGE
    T2 = int(T,R,RX2,R2); % SUM OF TEMPERATURE EXCLUDING NEAR-FIELD
    Ttotal = 2 * T2 + 2 * T_NF * RX1 + T_NF * LF; % SUM OF TEMPERATURES OVER FLAPPING LENGTH
    T_NEAR_FIELD = double( Ttotal / F ); % MAX NEAR-FIELD TEMPERATURE INCLUDING FLAPPING
end

% % ===============================================================================
% % ==============================          ==============================
% % ==============================   GAS TEMPERATURES   ==============================
% % ==============================          ==============================
% % ===============================================================================

T_MAX = zeros(numel(xx),numel(tt)); % GAS TEMPERATURE T_MAX(location,time) (C)
for x = 1:numel(xx)
    for t = 1:numel(tt)
        L_TRAILING = S * tt(t);
        if L_TRAILING < L
            Lt = L_TRAILING;                        % TIME DEPENDENT FIRE FRONT (m)
            Ft = min([ FSIZE , L_TRAILING / L ]); % TIME DEPENDENT FIRE SIZE (dimensionless)
        elseif abs( L_TRAILING - L ) < 1e-14       % [L_TRAILING(t) = L] TO ACCOUNT FOR FLOATING POINT
                CALCULATION i.e. 1-1 = 0. 1e-14 = tolerance
            Lt = L_TRAILING;                        % TIME DEPENDENT FIRE FRONT (m)
            Ft = min([ FSIZE , L_TRAILING / L ]); % TIME DEPENDENT FIRE SIZE (dimensionless)
        else
            Lt = L;                                 % TIME DEPENDENT FIRE FRONT (m) when fire reaches
                the end of the fire path
            Ft = 1 + ( LF - L_TRAILING ) / L;       % TIME DEPENDENT FIRE SIZE (dimensionless) when fire
                reaches the end of the fire path
            if abs( 1 + ( LF - L_TRAILING ) / L ) < 1e-14 % TO ACCOUNT FOR FLOATING POINT CALCULATION
                    i.e. 1-1 = 0. 1e-14 = tolerance
                Ft = 0;
            end
        end
        r = abs( xx(x) - Lt + 0.5 * L * Ft ); % DISTANCE FROM FIRE CENTRE

        %============ CALCULATION OF TMAX ====================
        if tt(t) > TTOTAL                   % ROOM TEMPERATURE AT THE END OF FIRE
            T_MAX(x,t) = T_ROOM;
        elseif r < 0.5 * L * Ft           % NEAR-FIELD
            T_MAX(x,t) = T_NEAR_FIELD;
        elseif ( r - 0.5 * L * Ft ) < 1e-14 % [r = 0.5*L*Ft] TO ACCOUNT FOR FLOATING POINT CALCULATION
                i.e. 1-1 = 0. 1e-14 = tolerance
            T_MAX(x,t) = T_NEAR_FIELD;
        else                                % FAR-FIELD
            T_MAX(x,t) = T_ROOM + ( 5.38 / HEIGHT ) * ( L * Ft * WIDTH * QII / r )^(2/3);
            if T_MAX(x,t) > T_NEAR_FIELD
                T_MAX(x,t) = T_NEAR_FIELD;
            end
        end
    end
```

```
        %─ END ════════════════════════════════════════════════
    end
end
```

```
        %─ END ════════════════════════════════════════════════
    end
end
```